

# **Comparative Performance Analysis of Texture Characterization Models in DIRSIG**

**By Captain Neil Scanlan, Canadian Forces**

**B.Sc., Physics and Astronomy, University of Toronto, 1998**

**A thesis submitted in partial fulfillment of the requirements for the Degree of Master  
of Science at the Chester F. Carlson Center for Imaging Science  
Rochester Institute of Technology  
2003**

**Signature of Author: \_\_\_\_\_**

**Neil Scanlan**

**Accepted By: \_\_\_\_\_**

**Graduate Program Coordinator**

**Date**

**CHESTER F. CARLSON CENTER FOR IMAGING SCIENCE  
ROCHESTER INSTITUTE OF TECHNOLOGY  
ROCHESTER, NEW YORK**

---

**M.S. Degree Thesis Paper**

---

The M.S. Thesis Paper of Neil W. Scanlan has been examined and approved by the Thesis Committee as satisfactory for the requirements for the M.S. degree in Imaging Science.

**Signature of Advisor:** \_\_\_\_\_

**Dr. John Schott**

**Thesis Committee Member:** \_\_\_\_\_

**Dr. Richard Hailstone**

**Thesis Committee Member:** \_\_\_\_\_

**Dr. Carl Salvaggio**

**M.S. THESIS PAPER RELEASE PERMISSION  
ROCHESTER INSTITUTE OF TECHNOLOGY  
CHESTER F. CARLSON CENTER FOR IMAGING SCIENCE**

Title of Thesis:

**Comparative Performance Analysis of Texture Characterization Models  
in DIRSIG**

I, Neil W. Scanlan, hereby grant permission to Wallace Memorial Library of R.I.T. to reproduce this thesis paper in whole or in part. Any reproduction will not be for commercial use or profit.

Signature: \_\_\_\_\_

Date

## Acknowledgements

I would like to take this opportunity to extend my utmost gratitude to the following colleagues, faculty members, advisors, acquaintances, collaborators, friends, and family for their efforts in assisting and/or supporting me. Without them, this work would not have come to be. In no particular order, they are hereby recognized:

*Amanda Scanlan, Michael Scanlan, Scott Brown, Emmett Ientilucci, John Schott, Carl Salvaggio, Richard Hailstone, Jim Kelley and the RSI team, Rob Sundberg and the SSI team, Alex Tyrrell, Cindy Schultz, Carloyn Kennedy, Nina Gibson-Raqueno, Rolando Raqueno, Gary DiFrancesco, Alvin Spivey, Bryan Shaw, all other colleagues and faculty members I have worked with, Major Wayne Farrell, and the Canadian Forces for providing this excellent educational opportunity to me.*

## **ABSTRACT**

The analysis and quantitative measurement of image texture is a complex and intriguing problem that has recently received a considerable amount of attention from the diverse fields of computer graphics, human vision, biomedical imaging, computer science, and remote sensing. In particular, textural feature quantification and extraction are crucial tasks for each of these disciplines, and as such numerous techniques have been developed in order to effectively segment or classify images based on textures, as well as for synthesizing textures. However, validation and performance analysis of these texture characterization models has been largely qualitative in nature based on conducting visual inspections of synthetic textures in order to judge the degree of similarity to the original sample texture imagery.

In this work, four fundamentally different texture modeling algorithms have been implemented as necessary into the Digital Imaging and Remote Sensing Synthetic Image Generation (DIRSIG) model. Two of the models tested are variants of a statistical Z-Score selection model, while the remaining two involve a texture synthesis and a spectral end-member fractional abundance map approach, respectively. A detailed validation and comparative performance analysis of each model was then carried out on several texturally significant regions of two counterpart real and synthetic DIRSIG images which contain differing spatial and spectral resolutions. The quantitative assessment of each model utilized a set of four performance metrics that were derived from spatial Gray Level Co-occurrence Matrix (GLCM) analysis, hyperspectral Signal-to-Clutter Ratio (SCR) measures, mean filter (MF) spatial metrics, and a new concept termed the Spectral Co-Occurrence Matrix (SCM) metric which permits the simultaneous measurement of spatial and spectral texture. These performance measures in combination attempt to determine which texture characterization model best captures the correct statistical and radiometric attributes of the corresponding real image textures in both the spatial and spectral domains. The motivation for this work is to refine our understanding of the complexities of texture phenomena so that an optimal texture characterization model that can accurately account for these complexities can be eventually implemented into a synthetic image generation (SIG) model. Further, conclusions will be drawn regarding which of the existing texture models achieve realistic levels of spatial and spectral clutter, thereby permitting more effective and robust testing of hyperspectral algorithms in synthetic imagery.

## TABLE OF CONTENTS

<b>1. Introduction.....</b>	<b>1</b>
<b>2. Work Statement.....</b>	<b>5</b>
<b>3. Background Theory and Literature Review.....</b>	<b>7</b>
<b>3.1 Image Texture Theory.....</b>	<b>7</b>
3.1.1 Origin, Types, and Descriptions of Texture.....	8
3.1.2 Texture Measurement, Analysis, and Quantification.....	16
3.1.2.1 The GLCM Approach to Texture.....	19
<b>3.2 DIRSIG Introduction.....</b>	<b>24</b>
3.2.1 Why Use Synthetic Image Generation Models?.....	25
3.2.2 The Modular Design of DIRSIG.....	26
<b>3.3 Texture Characterization Models To Be Tested.....</b>	<b>30</b>
3.3.1 Single-Bandpass (SBP) Z-Score Selection Model.....	30
3.3.2 Multiple-Bandpass (MBP) Z-Score Selection Model.....	40
3.3.2.1 Theory.....	40
3.3.2.2 Previous Results.....	43
3.3.3 Texture Synthesis Models.....	46
3.3.3.1 Literature Review.....	47
3.3.3.2 Tyrrell’s Multi/Hyperspectral Texture Synthesis Models.....	54
3.3.3.2.1 The S/P Model.....	54
3.3.3.2.2 The Image Quilting Model.....	59
3.3.3.2.3 Preliminary Results.....	60
3.3.3.2.4 Spectral Expansion Texture Synthesis Model.....	63
3.3.3.3 Texture Synthesis Model Performance Evaluation.....	64
3.3.4 Fraction Map Texture Characterization Model.....	64
<b>4. Experimental Design and Methodology.....</b>	<b>69</b>
<b>4.1 Experimental Design Overview.....</b>	<b>69</b>
<b>4.2 Implementation of Texture Models.....</b>	<b>70</b>
4.2.1 SBP and MBP Models.....	70
4.2.2 Texture Synthesis Models.....	73
4.2.3 FM Model.....	80

<b>4.3 Imagery To Be Rendered.....</b>	<b>83</b>
4.3.1 CitiPix Imagery.....	84
4.3.2 HYDICE ARM Imagery.....	86
<b>4.4 Pre-Processing Considerations.....</b>	<b>87</b>
<b>4.5 Texture Model Performance Metrics.....</b>	<b>90</b>
4.5.1 Spatial Domain.....	90
4.5.1.1 Mean Filter Spatial Metric.....	92
4.5.1.2 GLCM Spatial Metric.....	94
4.5.2 Spectral Domain.....	99
4.5.2.1 Signal-to-Clutter Ratio (SCR) Metric.....	100
4.5.2.2 Spectral Co-Occurrence Matrix (SCM) Metric.....	101
4.5.3 Detailed Methodology.....	104
4.5.3.1 CitiPix Texture Test Regions.....	104
4.5.3.2 HYDICE ARM Texture Test Regions.....	106
<b>5. Results and Analysis.....</b>	<b>109</b>
<b>5.1 CitiPix Imagery Results.....</b>	<b>109</b>
5.1.1 SBP Model.....	110
5.1.2 MBP Model.....	112
5.1.3 Texture Synthesis Model.....	114
5.1.4 FM Model.....	116
<b>5.2 HYDICE ARM Imagery Results.....</b>	<b>117</b>
5.2.1 SBP Model.....	119
5.2.2 MBP Model.....	125
5.2.3 Texture Synthesis Model.....	127
5.2.4 FM Model.....	130
<b>5.3 CitiPix Metric Results.....</b>	<b>132</b>
5.3.1 MF Metric.....	133
5.3.2 GLCM Metric.....	139
5.3.3 SCM Metric.....	148
<b>5.4 HYDICE ARM Metric Results.....</b>	<b>153</b>
5.4.1 MF Metric.....	153
5.4.2 GLCM Metric.....	164
5.4.3 SCR Metric.....	180

5.4.4	SCM Metric.....	183
<b>5.5</b>	<b>Comparative Performance Analysis of Texture Models.....</b>	<b>194</b>
5.5.1	SBP Model.....	195
5.5.2	MBP Model.....	196
5.5.3	Texture Synthesis Model.....	197
5.5.4	FM Model.....	199
5.5.5	Sources of Error.....	201
5.5.6	Comparative Performance Analysis Synopsis.....	205
<b>5.6</b>	<b>Supplementary Results.....</b>	<b>212</b>
5.6.1	CitiPix Scene Rendered Using HYDICE Imaging Spectrometer.....	212
5.6.2	SSI Texture Characterization Model Results.....	216
5.6.2.1	Background Theory.....	216
5.6.2.2	Texture Model Results and Performance Analysis.....	216
<b>6.</b>	<b>Conclusions and Recommendations.....</b>	<b>227</b>
<b>7.</b>	<b>References.....</b>	<b>234</b>

## **LIST OF FIGURES**

- Figure 1:** Areal, Aggregate and Intimate Material Mixture Types
- Figure 2:** VisTex Sample Texture Images
- Figure 3:** Brodatz and Binary Sample Texture Images
- Figure 4:** VisTex Sample Texture from Structural Approach to Texture Description
- Figure 5:** Sample GLCM computation
- Figure 6:** Scene Geometry Submodel of DIRSIG
- Figure 7:** Ray Tracing Submodel of DIRSIG
- Figure 8:** Geometric Distortion Introduced by DIRSIG Sensor Submodel
- Figure 9:** Sample DIRSIG Synthetic Image and Real Counterpart Image
- Figure 10:** Sample DIRSIG Synthetic Image Before and After Texture Characterization
- Figure 11:** Tiered Approach to Texture Characterization in DIRSIG
- Figure 12:** Mean, Standard Deviation, and Z-Score Computations from Sample Texture Image
- Figure 13:** Illustration of Single-Bandpass Texture Characterization Model
- Figure 14:** Texture Characterization With and Without Expanded Database of Transition Curves
- Figure 15:** Illustration of Multiple-Bandpass Texture Characterization Model
- Figure 16:** Multiple Bandpass (MBP) Model Example: Texture Images
- Figure 17:** Multiple Bandpass (MBP) Model Example: Sample Reflectance Curves
- Figure 18:** Illustration of Spatial Texture as a Stationary Ergodic Random Process
- Figure 19:** Illustration of Nonstationarity of Spectral Correlation
- Figure 20:** Illustration of Markov Random Field Theory Models
- Figure 21:** Differing Textures with Identical Marginal Statistics
- Figure 22:** Example of a Complex Steerable Filter Bank
- Figure 23:** Real Part of Complex Steerable Filters at Four Orientations
- Figure 24:** Imaginary Part of Complex Steerable Filters at Four Orientations
- Figure 25:** Steerable Pyramid Decomposition of Brodatz Presscloth Texture Image
- Figure 26:** Synthesis and Analysis Sides of Steerable Pyramid Resampling Technique
- Figure 27:** Steerable Pyramid System Design
- Figure 28:** Diagram of S/P Texture Synthesis Algorithm
- Figures 29-32:** Tyrrell's Image Quilting Preliminary Results
- Figure 33:** Tyrrell's S/P Model Preliminary Results
- Figure 34:** Extraction of End-Member Fractional Abundance Maps from HSI Texture Image
- Figure 35:** Illustration of FM Texture Model
- Figure 36:** Experimental Design Summary

**Figure 37:** Multimodal Texture Map Suggesting Usage of Masked Texture Images

**Figure 38:** GML-Derived Material Map for HYDICE ARM Data

**Figure 39:** Sample Masked Texture Map for HYDICE ARM Image

**Figure 40:** Example of Repetitive Artifacts Arising From Mirroring Utility for Texture Synthesis Model

**Figure 41:** GML-Derived Material Map for CitiPix Data

**Figure 42:** Incorporation of Texture Synthesis Model into DIRSIG Using Reflectance Maps

**Figure 43:** Sample HYDICE ARM Fractional Abundance Maps

**Figure 44:** Sample CitiPix Fractional Abundance Maps

**Figure 45:** Subset of Kodak CitiPix Image Over Rochester, NY

**Figure 46:** Portion of CitiPix Data (Red Channel) To Be Rendered in DIRSIG

**Figure 47:** Subset of HYDICE ARM Run 29 Data To Be Rendered in DIRSIG

**Figure 48:** Illustration of Pre-Processing Necessity

**Figure 49:** Empirical Line Method (ELM) Calibration Methodology for CitiPix and HYDICE ARM Imagery

**Figure 50:** Sample MF Metric Output Imagery for HYDICE ARM Data

**Figure 51:** Sample ENVI GLCM Computation

**Figure 52:** Sample GLCM Metric Texture Features – Contrast and Correlation

**Figure 53:** Sample SCM Metric Texture Features for Two Spectral Band Pairs – Contrast and Correlation

**Figure 54:** CitiPix Texture Test Region Locations

**Figure 55:** HYDICE ARM Texture Test Region Locations

**Figure 56:** Performance Metric Methodology

**Figure 57:** Real CitiPix Imagery – Red, Green, and Blue Channels

**Figure 58:** CitiPix DIRSIG Imagery Using SBP Texture Model

**Figure 59:** CitiPix DIRSIG Imagery Using MBP Texture Model

**Figure 60:** CitiPix DIRSIG Imagery Using Texture Synthesis Model

**Figure 61:** CitiPix DIRSIG Imagery Using FM Texture Model

**Figure 62:** Real HYDICE ARM Imagery – Bands 22, 32, 65, 95, 115, 157, 184, and 195

**Figure 63:** Dependence of SBP and MBP Models on Quality of Ground Truth Data

**Figure 64:** HYDICE ARM DIRSIG Imagery Using SBP Texture Model

**Figure 65:** HYDICE ARM DIRSIG Imagery Using MBP Texture Model

**Figure 66:** HYDICE ARM DIRSIG Imagery Using Texture Synthesis Model

**Figure 67:** HYDICE ARM DIRSIG Imagery Using FM Texture Model

**Figure 68:** CitiPix Scene Simulation Using HYDICE Sensor Platform and SBP Texture Model

**Figure 69:** CitiPix Scene Simulation Using HYDICE Sensor Platform and MBP Texture Model

**Figure 70:** CitiPix Scene Simulation Using HYDICE Sensor Platform and FM Texture Model

**Figure 71:** HYDICE ARM DIRSIG Imagery Using SSI Texture Model

## **List of Tables**

- Table 1:** Texture Test Regions for CitiPix Data
- Table 2:** Texture Test Regions for HYDICE ARM Data
- Table 3:** 8 Representative Spectral Bands of HYDICE Data Used In Metric Analysis and Band Center Values
- Table 4:** Mean and Standard Deviation Statistics for Ground Truth and Image-Derived Data
- Table 5:** Sample Mean and Standard Deviation Statistics of Corresponding HYDICE and TS Model Imagery
- Tables 6-8:** CitiPix MF Metric – Average Values of Absolute Difference Images – R, G, B
- Tables 9-11:** CitiPix MF Metric – Percentage of Outliers from Variance Threshold – R, G, B
- Tables 12-14:** CitiPix GLCM Contrast Metric – Average Values of Absolute Difference Images – R, G, B
- Tables 15-17:** CitiPix GLCM Contrast Metric – Percentage of Outliers from Variance Threshold – R, G, B
- Tables 18-20:** CitiPix GLCM Correlation Metric – Average Values of Absolute Difference Images – R, G, B
- Table 21:** CitiPix SCM Contrast Metric – Average Values of Absolute Difference Images – R-B Channels
- Table 22:** CitiPix SCM Contrast Metric – Percentage of Outliers from Variance Threshold – R-B Channels
- Table 23:** CitiPix SCM Correlation Metric – Percentage of Outliers from Variance Threshold – R-B Channels
- Table 24:** CitiPix Average Values from All Metrics and Spectral Bands (AVG and % Outliers)
- Table 25:** MF Metric for HYDICE Imagery – Average Values of Absolute Difference Images
- Table 26:** MF Metric for HYDICE Imagery – Percentage of Outliers from Variance Threshold
- Table 27:** GLCM Contrast Metric for HYDICE Imagery – Average Values of Absolute Difference Images
- Table 28:** GLCM Contrast Metric for HYDICE Imagery – Percentage of Outliers from Variance Threshold
- Table 29:** GLCM Correlation Metric for HYDICE Imagery - Percentage of Outliers from Variance Threshold
- Table 30:** SCR Metric Values for HYDICE Imagery
- Table 31:** SCM Contrast Values for 4 Spectral Band Pairs - Average Values of Absolute Difference Images
- Table 32:** SCM Contrast Values for 4 Spectral Band Pairs - Percentage of Outliers from Variance Threshold
- Table 33:** SCM Correlation Values - Percentage of Outliers from Variance Threshold
- Table 34:** HYDICE Average Values from All Metrics and Spectral Bands (AVG, % Outliers, and Rankings)
- Table 35:** Texture Model Rankings of CitiPix DIRSIG Output Imagery
- Table 36:** Texture Model Rankings of HYDICE ARM DIRSIG Output Imagery
- Table 37:** The Use of Metric Weights in Order to Determine Overall Spatial-Spectral Performance
- Table 38:** Final Ranking of Texture Characterization Models Based on Nature of Imagery to be Rendered
- Table 39:** Synopsis of the Conditions and Limitations for Optimal Texture Model Performance
- Table 40:** MF Metric Results for Sampling of Bands of SSI DIRSIG HYDICE ARM Imagery
- Table 41:** GLCM Contrast Metric Results for Sampling of Bands of SSI DIRSIG HYDICE ARM Imagery

**Table 42:** GLCM Correlation Metric (Number of Outliers) for SSI Model Results

**Table 43:** SCR Values for Five Texture Test Regions of SSI DIRSIG HYDICE ARM Imagery

**Table 44:** SCM Contrast Metric for SSI Model Results

**Table 45:** SCM Correlation Metric (Percentage of Outliers from Variance Threshold) for SSI model results

**Table 46:** Final Rankings of Texture Characterization Models Based on Nature of Imagery to be Rendered

## 1. Introduction

Texture has become one of the most important yet astoundingly complex properties of digital images over the past twenty-five years. This is evidenced by its wide variety of applications, ranging from the fields of computer vision and graphics for texture synthesis, analysis and characterization, to the biomedical community for cellular microtexture analysis, to the remote sensing and image processing community for image classification, feature extraction, target detection, and synthetic image generation (SIG) models. While texture is indeed an intuitive concept, it nonetheless has an elusive formal definition; in fact, there *is* no single universally accepted definition of the term “texture.” Instead, it seems to depend heavily on the particular application, such as those listed above.

For example, even in the broadest sense, a definition of texture as either a surface or an image property has not been adequately formulated, so even in our everyday language, one would likely be challenged to describe the meaning of texture. Webster’s dictionary defines texture in two contexts as “a distinctive, complex, underlying pattern or structure” and “the quality of a surface of woven material” [Webster’s, 1986]. Clearly these are referring to texture as a physical surface property. In terms of remote sensing applications, it can be said that image texture describes the structure of the variation in brightness within an object of interest [Schott, 1997], or at larger scales, between objects of interest (i.e., transition regions). These textures often arise from variations in target reflectance, since most targets are composed of heterogeneous mixtures of several materials from a family of spectral reflectance curves. Further affecting the appearance of image texture is topographic effects such as sun-target angles and variations in insolation (shadowing).

In the texture synthesis literature, the concept of image texture tends to stray from material spectral properties, since synthesis models are concerned with mathematically modeling texture as a random process, where the goal is to produce synthetic textures that appear to have been generated from the same underlying process [De Bonet & Viola, 1998]. This leads to the concept of “visual texture” which has been defined as “a set of repeating structural elements subject to randomness in location, size, color, and orientation”

[Simoncelli and Portilla, 1998] or “the visual effect which is produced by a spatial distribution of tonal variations over relatively small areas” [Baraldi and Parmiggiani, 1995]. Essentially, textures are viewed in this field as structures composed of a large number of more or less ordered similar elements or patterns, characterized by primitives and placement rules, where if the primitives contain a high level of gray-level variation in a small region, it is known as a microtexture [Ganesan and Bhattacharyya, 1995]. Most texture synthesis models are concerned with modeling such microtextures, usually only in a single band or in RGB space. Only recently have there been efforts to produce multispectral or hyperspectral texture synthesis models, and some variants of these models will be among those tested in this work.

The above discussion serves as a preliminary illustration of the complexity and challenges of texture characterization. For instance, if we cannot adequately describe texture even in terms of our own vocabulary, then how does one suppose that we can train a computer to quantify or even produce it? Further, while most texture synthesis algorithms aim to produce textures that are perceptually similar to the human eye, a major problem lies in the fact that the mechanism of the human visual system (HVS) for texture discrimination is not very well understood. However, producing realistic and visually similar synthetic texture is only the first challenge. There is an additional need for a robust, quantitative method of measuring how well synthetic textures are represented in relation to their truth counterparts. Unfortunately, there has not been much work performed exclusively on this aspect other than the use of human subjects to judge whether real and synthetic textures are perceptually similar, which roughly equates to the mere matching of first-order statistics, which do not solely suffice for adequate texture description [Van de Wouwer et al., 1999, Simoncelli & Portilla, 1998]. Measurement and quantification of texture is a challenging task in itself, not to mention the difficulties in establishing mathematically how well a synthetic texture is represented compared to a real image.

In this work, four different texture characterization models (described in the following sections) will be implemented as necessary into the Digital Imaging and Remote

Sensing Synthetic Image Generation (DIRSIG) model, and subsequently tested on several regions of two synthetic images and compared with their truth image counterparts. The models to be tested cover traditional and ad hoc statistical z-score based methods already available in DIRSIG, as well as a texture synthesis statistical model, and an approach which utilizes end-member fractional abundance maps to create synthetic texture. Each of the models will require variable implementation efforts, since some models currently reside within DIRSIG capabilities, while others have never been used in the DIRSIG environment. This comparative performance analysis will require the use of quantitative methods to determine how well each model characterizes texture within a given material type, as well as at transition regions between material types, in both spatial and spectral dimensions. Much of the testing methodology is derived from classification literature based on the use of Gray Level Co-Occurrence Matrices (GLCMs), since this method has consistently been shown to achieve the best results for discriminative power between texture features.

This research attempts to indicate how well we currently understand how to model texture in synthetic imagery, and more importantly determine how to improve synthetic texture in DIRSIG imagery. The importance of modeling texture that is both visually and statistically accurate cannot be overstated. For instance, when dealing with spectrally similar materials in classification situations, textures often become crucial criteria for class discrimination. Also, since textures are a fundamental component of human recognition of real-world targets, realistic looking synthetic targets are essential, especially for analyst training situations. Lastly, since many multi/hyperspectral algorithms seek to exploit spatial and spectral patterns simultaneously, it is of paramount importance that fidelity in both dimensions is preserved in the synthetic image generation process. To illustrate this importance, consider a scene in which the mean brightness levels of two image regions representing samples of forest and water respectively are identical for a certain spectral band. If the spatial texture is not well characterized such that these two materials cannot be differentiated, then classification algorithms run on the SIG image will likely fail, while target detection algorithms will produce an unacceptable false alarm rate. On the other hand, if the

background clutter is unrealistically benign, overly optimistic estimates of detection performance may result. Hence the necessity of characterizing textures correctly in a mathematical and statistical sense, both spatially and spectrally. One of the most powerful advantages offered through the use of synthetic imagery is the ability to test hyperspectral algorithms with great flexibility. But in order to reap the benefits of synthetic imagery for algorithm testing and development, realistic levels of spatial and spectral clutter must be achieved so that we can reliably estimate how these algorithms will perform on real-world imagery. One must keep in mind that the purpose of mathematically modeling texture (or any phenomenon for that matter), is not to simplify the problem, but rather to be able to understand and include in the model the very complexities that make texture such a challenging problem.

## 2. Work Statement

The following section details the specific objectives of this research:

1. Incorporate and/or implement four different texture modeling algorithms (as necessary) into the DIRSIG environment. The four texture characterization models to be tested in this research are:
  - a. The Single-Bandpass (SBP) Z-Score Selection Model;
  - b. The Multiple-Bandpass (MBP) Z-Score Selection Model;
  - c. A Statistical Texture Synthesis (TS) Model; and
  - d. A Fraction Map (FM) Texture Characterization Model.
2. Construct DIRSIG synthetic imagery using each of the four texture models. These simulated scenes will be rendered at differing spatial and spectral resolutions in order to more robustly test the texture models. The real imagery sets to be used for DIRSIG scene construction are:
  - a. Kodak CitiPix imagery with GSD of 0.45 m, and spectral coverage of 400 – 700 nm and;
  - b. Hyperspectral Digital Imagery Collection Experiment Atmospheric and Radiation Measurement (HYDICE ARM) imagery with GSD of 1.7375 m and spectral coverage of 400 nm – 2,500 nm.
3. Application of a series of four texture performance metrics on all of the resultant DIRSIG imagery. The following performance metrics will in combination assess how well both spatial and spectral texture is characterized in the DIRSIG scenes as compared with the corresponding real imagery:
  - a. Mean Filter (MF) Spatial Metric;
  - b. Gray-Level Co-Occurrence Matrix (GLCM) Spatial Metric;
  - c. Signal-to-Clutter Ratio (SCR) Spectral Metric and;
  - d. Spectral Co-Occurrence Matrix (SCM) combined spatial-spectral metric.

4. Conduct a quantitative comparative performance analysis of all four texture models by analyzing the results of the four performance metrics. A qualitative visual analysis will also be included. The assessment of each model will focus on:
  - a. Which models perform better overall;
  - b. Why some models perform better or worse than others, including how each of the models can be improved;
  - c. How we can improve our understanding of texture phenomena and how to model statistically and radiometrically correct synthetic image texture;
  - d. If model performance depends on different types of texture, and if certain models perform better for homogeneous (within-material class) or transition (between material class) textures;
  - e. If model performance depends on the spatial or spectral resolution at which the texture is being modeled and;
  - f. How the models perform in terms of fidelity in both the spatial and spectral domains.

### 3. Background and Literature Review

This section will detail several theoretical aspects of this research. First, some background theory on texture phenomena, analysis, and quantification is presented as a review of the prominent methods relevant to this work. Next, an introductory discussion on the general design of DIRSIG, as well as the texture characterization models currently available for use in DIRSIG are described. Some results of previous work with analysis of these texture models are also discussed. Thereafter, a brief literature review of the basic theory and evolution of several ad hoc texture synthesis algorithms is introduced, leading to a more detailed overview of Tyrrell's S/P, Quilting, and Spectral Expansion texture synthesis models that will be tested in this research. Lastly, a theoretical description of an end-member Fraction Map (FM) approach to texture characterization is presented.

#### 3.1 Image Texture Theory

As mentioned in Section 1, there are many existing definitions of texture, and its interpretation depends on the particular application. Despite this controversy in attempting to provide both qualitative and quantitative meanings to texture, all disciplines seem to agree on two aspects: first, that there is indeed a significant variation between nearby pixels with respect to intensity levels observed in digital images, and secondly that texture is a homogeneous property at some spatial scale larger than the resolution of the image.

Since texture is a familiar, intuitive, and naturally occurring phenomenon in images, it has been an active field of study dating back to early studies of textural perception and discrimination [Julesz, 1962]. The Julesz conjecture focused on the measure of perceptual closeness of texture images, relying on the assumption that the HVS preattentively distinguishes between textures with different first- and second-order probability distributions. As such, this work was the foundation for much more extensive research on texture synthesis models which have evolved significantly in their ability to capture both stochastic and ordered textures, and accordingly have grown with respect to mathematical and computational complexity. Meanwhile, pioneering work by Haralick [1973, 1979] took a

different approach to quantifying texture through both statistical and structural methods, from which most modern literature on texture-based feature extraction, classification, and measurement was derived. Over the years, numerous variants of texture analysis and quantification were spawned, ranging from Gray Level Co-Occurrence Matrices (GLCMs), texture vectors [Berger, 1998], texture spectra [Wang, 1990], and texture metrics based in the frequency domain [Stromberg & Farr, 1986]. Many ad hoc techniques were later developed for more effective and computationally efficient classification methods that utilized spatial texture features. One method that has shown great resilience and consistently excellent results is the GLCM approach, and this will be the main focus of section 3.1.2 on texture quantification since it is most applicable to the work reported here. First, however, we present an introduction to the terminology used to describe some of the prominent types of naturally-occurring textures that are often used as sample templates in order to synthesize textures.

### **3.1.1 Origin, Types, and Descriptions of Texture**

A review of the semantics involved with describing different types of textures will be useful in several capacities of this work. For instance, when applying any of the texture performance metrics to use in the quantitative assessment of its characterization in a synthetic image, one must consider the type of texture that is present in order to determine the parameters to use in its measurement. This is the case in particular for GLCM texture measurements. Also, the quantification of how well a texture synthesis model performs often depends on the type of texture being modeled. As we will see in section 3.3.3 on texture synthesis models, fundamentally different texture models tend to reproduce certain texture types better than others. Therefore, some examples of texture types will be introduced here so that the reader is familiar with the terminology.

As mentioned previously, the phenomenon of textures in an image are due in large part to the variability in spectral reflectance of different material types, as well as shadowing and topographic effects. These instances tend to refer to variability within single material

classes. However, at larger scales textures are often the result of mixtures of different materials, whether areal, aggregate, or intimate with respect to mixture properties. Figure 1 shows an example of each of these three classes of material mixtures for a 50% mix of sand and clay.

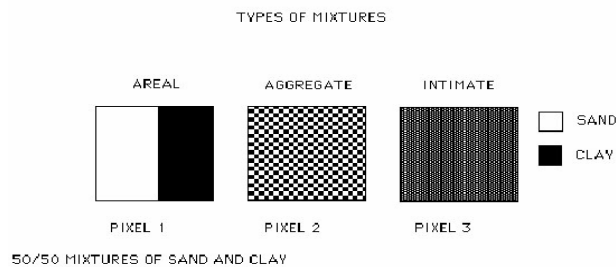


Figure 1: Illustration of the areal, aggregate, and intimate types of material mixtures often observed in digital images.

In this work, texture analysis will be performed for both single-material class “homogeneous” textures (such as the above aggregate and intimate material mixtures), as well as for transition regions between material classes (such as the areal mixture) in both real and synthetic images. An entire taxonomy of different texture types has evolved within the literature based on their visual appearance in both natural and texture images. A popular collection of sample texture images that is consistently cited especially in the texture synthesis and visual texture literature is the Brodatz texture database [Brodatz, 1966], which is featured on several academic websites. This collection is considered to be one of the most complete representations of texture types in existence. Although the emphasis within this database is heavier on monochrome (and some RGB) microtextures that would be more applicable in biomedical cellular imaging, there are nonetheless many textures that are applicable to remote sensing imagery. There are also other more recently developed databases with more interesting RGB textures, such as the Visual Texture (VisTex) database

created at MIT with the intention of providing a large set of high quality textures for computer vision applications. The goal of VisTex is to provide texture images that are representative of real world conditions, and while VisTex can serve as a replacement for traditional texture collections, it also includes examples of many non-traditional textures. As mentioned, most texture synthesis models, including the S/P and Quilting models [Tyrrell, 2002] to be tested in this work, have extensively used these sample texture images to test their models and validate the results.

The first and most basic level of texture nomenclature is that which simply applies semantic meaning to its appearance, and refers to the observable physical properties of the texture. Some typical examples are natural, artificial, stochastic, directional, grainy, coarse, periodic, pseudo-periodic, aperiodic, extended, regular, homogeneous, and mixture. Some textures are adequately described by one or more of these descriptors. These adjectives are clearly descriptive in nature and not at all mathematical, but they do offer the advantage of matching our intuition. One must also keep in mind that visual descriptions of texture such as these depend on the resolution of the texture image. For example, heterogeneous textures can appear very homogeneous at larger scales. Some VisTex examples are shown in Figures 2 (a) - (k), while traditional Brodatz binary textures are shown in Figures 3 (a) – (d). These latter figures show the results of a texture synthesis-by-analysis technique used by Jacovitti et al [1998], with the smaller sample binary texture random fields on the left and their synthetic realizations on the right. One will also find sample Brodatz textures and some preliminary texture synthesis results using S/P and Quilting models in Figures 29-33.



Figure 2 (a): Periodic, coarse texture.



Figure 2 (b): Grainy texture.



Figure 2 (c): Coarse, structural texture.



Figure 2 (d): Directional, aperiodic texture.



Figure 2 (e): Pseudo-Periodic texture.



Figure 2 (f): Stochastic texture.



Figure 2 (g): Natural texture.



Figure 2 (h): Pseudo-Periodic, structural texture.



Figure 2 (i): Aperiodic texture.



Figure 2 (j): Mixed texture.



Figure 2 (k): Stochastic, mixed texture.

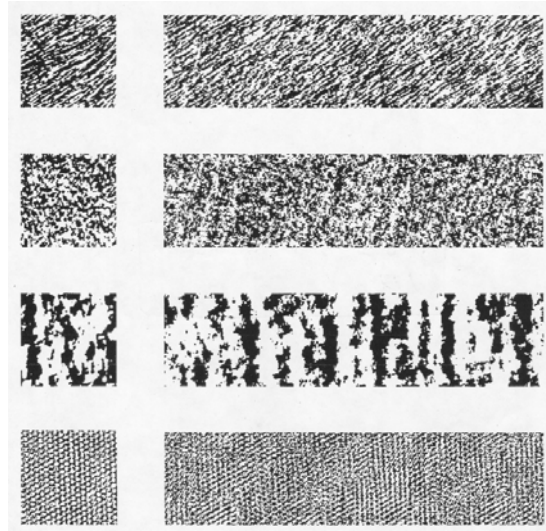


Figure 3(a) – (d): Sample binary texture images and their corresponding synthesis-by-analysis results. The sample textures are (from top to bottom) directional, grainy, coarse, and near-regular).

The subjectivity in describing these textures in this manner is evident, and often this qualitative nomenclature depends on the interpretation of the observer.

There are also more concise definitions of texture types that refer to the detailed content of the texture. This second level of texture nomenclature is still mostly descriptive, but it is often used to subdivide semantically similar texture types. Haralick [1979] first introduced this terminology based on the concept of texture being composed of two basic dimensions. The first dimension is concerned with tonal primitives or local properties, while the second dimension is a description of the spatial dependence or interaction between the primitives. He postulated that texture is described by the number and types of its primitives and their spatial organization or layout. Being dissatisfied with adjective-based texture description, he first attempted to map semantic meaning into precise properties of tonal primitives and their spatial distribution properties. He also introduced texture and tone as independent concepts. For example, when a small image patch has little variation of tonal primitives, the dominant property of that area is tone; whereas if the patch has wide variation of tonal primitives, the dominant property is texture.

Among the many semi-quantitative second-level texture descriptors, there are four key terms that are relevant to this work, which serve to differentiate fine versus coarse textures, as well as weak versus strong textures. A fine texture results when the spatial pattern in the tonal primitives is random and the gray tone variation between primitives is wide, and these are generally characterized by smaller primitives and higher spatial frequencies. On the other hand, as the spatial pattern becomes more definite and the tonal regions involve larger primitives with lower spatial frequencies, a coarse texture results.

Weak textures are those which have little spatial interaction between primitives and can be described and/or differentiated by determining the frequency at which various primitives occur in some local neighborhood. Strong textures are defined as those in which the primitives are somewhat regular with nonrandom spatial interactions. These are described by the frequency of co-occurrence of primitive pairs in a specified spatial relationship.

Note that these texture primitives may be as simple as single pixel gray levels, or they may consist of simple patterns from which more complicated ones can be built (this latter interpretation is commonly used in computer vision and texture synthesis fields, and may also refer to this basic texture unit as a “texture element” or “texel”). There are numerous published methods for defining the primitives and their spatial relationships, but this is far beyond the scope of this work. The texture types and descriptors introduced above provide the foundation for much more quantitative texture measurement and analysis which are presented in the next subsection.

### **3.1.2 Texture Measurement, Analysis, and Quantification**

In the literature, there are three main ways that textures are used in imaging applications. These are:

- a. To segment an image based on textures;
- b. To classify a segmented image by using texture features either exclusively or as supplemental info to spectral content; and

c. To produce descriptions in order to synthesize textures.

In addition, there are three common texture analysis methods that are used for each of these tasks. These are *structural*, *spectral*, and *statistical* approaches. These methods can also be thought of as the third level of texture nomenclature in the form of mathematical texture descriptors, since they each have their own quantifiable measure of texture features largely derived from the second level descriptors. Since this research will focus on more of a statistical method of texture quantification, this approach will be the main focus of this section, while the other methods will merely be briefly introduced. Also, all three of these basic approaches to texture contain numerous variants of mathematical methods for quantifying and analyzing textures. A description of these methods is well beyond the scope of this paper, since only the methods pursued in this research will be reviewed.

Structural approaches to descriptions and models of texture are based on the view that textures are made up of primitives which appear in near regular repetitive spatial patterns. In order to describe the particular texture, a primitive must be defined with a prescribed placement rule. This effectively defines a “grammar” for the way that the pattern of the texture produces structure. This methodology forms the basis of much texture synthesis work, and tends to be used in tandem with statistical models in most texture synthesis-by-analysis research (see Section 3.3.3). An image of a brick wall is a prime example suited to this approach (see Figure 4).



Figure 4: VisTex sample texture image well-suited for structural approach to texture description.

An alternative method is to use Fourier spectrum analysis in order to provide information on texture frequency (eg. low or high energy along a particular radius) and its orientation (eg. low or high energy along a particular angle). This method is most advantageous for periodic textures or for extracting edge features, but is not always effective with other texture types such as those introduced above which are important in remote sensing imagery.

Since textures often tend to be random in nature, but with certain consistent properties, a very effective method for describing and quantifying textures is through their statistical properties. At its most fundamental level, this would involve measurements using the image histogram and computing the moments of intensity such as mean, variance, skew, and kurtosis. Of course, these measures alone do not consider the position of pixels, and only provides information as to the coarseness of the texture. The aim of the statistical approach is to characterize the stochastic properties of the spatial distribution of gray levels in an image. As such, it became apparent that there was a need to obtain a simultaneous parametric measure of spatial relationships between pixel gray levels. This motivation is what led to Haralick's development of the Gray Level Co-Occurrence Matrix (GLCM). Although the GLCM method of texture measurement is sometimes considered to be a purely statistical approach, it can also be viewed as a combined statistical-structural approach to texture description due to its ability to parametrically account for pixel gray-level spatial arrangements.

The GLCM approach rapidly became a prominent tool for applications such as texture feature extraction, image segmentation, image classification [Yang & Hung, 2002; Wikantika et al., 2000], and even texture analysis and synthesis [Lohmann, 1995]. All of these methods have found great success with the GLCM tool compared with the performance of other methods. In fact, Lohmann found that while the structural approach describes spatial relationships between larger primitives, such as "blobs" or "dots", the statistical method offers the advantage of producing spatial relationship measures between individual pixels. As such, statistical measures such as the GLCM tend to work ideally for

finer textures, which are the prominent texture features observed in remote sensing satellite and aerial imagery. Although there are numerous more mathematically complex statistical methods of texture segmentation and description methods, such as Markov Random Field models [Cross & Jain, 1983], textural energy filters [Laws, 1985], and fractal-based approaches [Keller & Chen, 1989], comparative studies have demonstrated the power of the GLCM approach as the most consistent performer among texture quantification tools over a broad range of texture types. There have also been several ad hoc methods which attempt to improve the computational efficiency of the GLCM method when applied image wide for classification, such as linked lists [Clausi and Jernigan, 1998] and hybrid structures [Clausi and Zhao, 2002], however these extensions of the GLCM will not be discussed here since the GLCM will be used in its traditional form for this work. The reason for adopting the conventional method is because increased-efficiency algorithms tend to sacrifice information for computational speed or improved sorting and data storage usually through quantization of pixel gray levels to reduce dimensionality of the analysis. In this research, the proposed GLCM analysis will not be image wide, and will be over smaller subimage regions likely consisting of a small portion of the possible dynamic range of digital images. The following section will detail the basic theory behind GLCMs and subsequently describe the GLCM-derived statistics used in the literature for texture feature discrimination and/or quantification.

### **3.1.2.1 The GLCM Approach to Texture**

As mentioned, the GLCM approach is, in its simplest form, a statistical method to capture the spatial structure of an image in a given bandpass by statistically sampling the way that certain gray levels occur in relation to other gray levels. In Haralick's GLCM method, the probability density function (PDF) of various gray levels is computed at different directions ( $\alpha$ ) with different distances (d) between the gray levels, and is represented in the form of matrices. The technique involves first finding the probability of co-occurrence between two gray levels  $i$  and  $j$  at a given orientation and distance, for all possible co-

occurring pairs in an image window. The GLCM stores these probabilities and is thus dimensioned to the number of gray levels available in the window. The values may be either in integer form, or they may be normalized by the number of gray levels in the window to form a true PDF so that the entries only take on values between 0 and 1. The next step is to calculate the texture features by applying selected statistics to the resulting GLCM. Several of these GLCM-derived statistics known as texture features are discussed later. For most image segmentation applications, these texture features are assumed to belong to the center pixel of the window. Also, for most textural property description considerations, distances of one pixel and angles of 0, 45, 90, and 135 degrees are used. For example, the  $(d = 1, \alpha = 0)$ -pixel pairs are horizontally adjacent, the  $(d = 1, \alpha = 90)$ -pixel pairs are vertically adjacent, the  $(d = 1, \alpha = 45)$ -pixel pairs are right-diagonal neighbors, and the  $(d = 1, \alpha = 135)$ -pixel pairs are left-diagonal neighbors. If we let  $m$  denote the number of gray levels in the window, then the  $(d, \alpha)$  co-occurrence matrix  $C$  is an  $(m \times m)$  matrix, where an entry  $c_{ij}$  of  $C$  denotes the number of pairs of pixels separated by distance  $d$  at angle  $\alpha$ , which have gray values  $i$  and  $j$ . Note that a convention of  $(\Delta x, \Delta y)$  is also sometimes used.

Under this convention, the entries  $c_{ij}$  of a  $C(i, j, 1, 0)$  GLCM record the number of horizontal co-occurrences of gray values  $i$  and  $j$ , while that for a  $C(i, j, 1, 90)$  GLCM record the number of their vertical co-occurrences, and so forth. Lohmann also contends that in most cases, GLCMs are used in small neighborhoods of  $s \times s$  pixels, where typically  $5 < s < 15$  for the purpose of analyzing textures. The following example of the computation of GLCMs will be sufficiently demonstrative that we can avoid the cumbersome mathematical notation involved with a theoretical definition in set notation.

Consider Figure 5(a), which represents a  $4 \times 4$  subimage with four gray levels, ranging from 0 to 3. The general form of the GLCM is depicted in Figure 5(b), which describes which entries are placed into the matrix, in its un-normalized form.

0	0	1	1
0	0	1	1
0	2	2	2
2	2	3	3

Figure 5(a): 4 x 4 subimage for GLCM computation example.

		Gray Levels			
		0	1	2	3
Gray Levels	0	#(0,0)	#(0,1)	#(0,2)	#(0,3)
	1	#(1,0)	#(1,1)	#(1,2)	#(1,3)
	2	#(2,0)	#(2,1)	#(2,2)	#(2,3)
	3	#(3,0)	#(3,1)	#(3,2)	#(3,3)

Figure 5(b): General form of GLCM.

The corresponding spatial co-occurrence calculations for  $d = 1$  and angles of 0, 45, 90, and 135 degrees are as follows:

$$C(i, j, 1, 0) = \begin{bmatrix} 4 & 2 & 1 & 0 \\ 2 & 4 & 0 & 0 \\ 1 & 0 & 6 & 1 \\ 0 & 0 & 1 & 2 \end{bmatrix} \quad C(i, j, 1, 90) = \begin{bmatrix} 6 & 0 & 2 & 0 \\ 0 & 4 & 2 & 0 \\ 2 & 2 & 2 & 2 \\ 0 & 0 & 2 & 0 \end{bmatrix}$$

$$C(i, j, 1, 45) = \begin{bmatrix} 4 & 1 & 0 & 0 \\ 1 & 2 & 2 & 0 \\ 0 & 2 & 4 & 1 \\ 0 & 0 & 1 & 0 \end{bmatrix} \quad C(i, j, 1, 135) = \begin{bmatrix} 2 & 1 & 3 & 0 \\ 1 & 2 & 1 & 0 \\ 3 & 1 & 0 & 2 \\ 0 & 0 & 2 & 0 \end{bmatrix}$$

Haralick went on to define 14 texture features derived from GLCMs, which are essentially statistical measures, some of which are correlated to other measures, and some being better texture measures than others. Much of the literature has been devoted to narrowing down these features into manageable sizes, so that just a few measures in combination optimally capture the spatial structure of the texture through their statistics [eg. Zucker et al, 1980]. The original fourteen features, which can be categorized into four different classes [Gotlieb & Kreyszig, 1990], are as follows:

- a. Visual Textural Characteristics: Energy/Angular Second Moment/Uniformity/Homogeneity (f1), Contrast (f2), and Correlation (f3);
- b. Statistics-Based: Variance (f4), Inverse Difference Moment (f5), Sum Average (f6), Sum Variance (f7), and Difference Variance (f10);
- c. Information Theory- Based: Sum Entropy (f8), Entropy (f9), and Difference Entropy (f10); and
- d. Information Measures of Correlation (IMC): IMC I (f12), IMC II (f13), and Maximal Correlation Coefficient (f14).

There have since been several other variants in addition to the above list, but they are beyond the scope of this work, and unnecessary to introduce due to their redundancy. Six of these fourteen GLCM-derived statistical parameters are arguably considered to be the most relevant for best texture discrimination results: Energy (also known as Angular Second Moment or Uniformity or Homogeneity), Contrast, Variance, Correlation, Entropy, and Inverse Difference Moment. These statistical parameters are listed in mathematical form below [Haralick, 1973, 1979; Rosenblum, Salvaggio, & Schott, 1990]. As introduced earlier,  $m$  is the number of gray levels in the region under consideration, while  $C(i,j)$  is the  $(i,j)$ th entry of the un-normalized GLCM and  $c(i,j)$  is the  $(i,j)$ th entry of the normalized GLCM, so that we have  $c(i,j) = (C(i,j)/m)$  and

$$c(i, j) = \sum_{j=1}^m C(i, j) \quad (1)$$

which leads to the formal definitions of these eight main features:

a. Energy/Angular Second Moment/Uniformity/Homogeneity

$$f1 = \sum_{i=1}^m \sum_{j=1}^m [c(i, j)]^2 \quad (2)$$

b. Contrast

$$f2 = \sum_{n=0}^{m-1} n^2 \left[ \sum_{i=1}^m \sum_{j=1}^m c(i, j) \right] \quad (3)$$

for  $|i - j| = n$ , or more commonly:

$$f2 = \sum_{i=1}^m \sum_{j=1}^m c(i, j)(i - j)^2$$

c. Correlation

$$f3 = \frac{\left[ \sum_{i=1}^m \sum_{j=1}^m (i, j)c(i, j) - \mu_x \mu_y \right]}{\sigma_x \sigma_y} \quad (4)$$

d. Variance

$$f4 = \sum_{i=1}^m \sum_{j=1}^m (i - \mu)^2 c(i, j) \quad (5)$$

e. Inverse Difference Moment

$$f5 = \sum_{i=1}^m \sum_{j=1}^m \left[ \frac{c(i, j)}{1 + (i - j)^2} \right] \quad (6)$$

f. Entropy

$$f9 = - \sum_{i=1}^m \sum_{j=1}^m c(i, j) \log[c(i, j)] \quad (7)$$

where  $\mu_x$ ,  $\mu_y$ ,  $\sigma_x$ , and  $\sigma_y$  are the means and standard deviations of the rows and columns of C, respectively. ENVI also produces the statistic of *Dissimilarity*, which is quite similar to Contrast, except  $|i - j|$  replaces the  $(i - j)^2$  term. Gotlieb & Kreyszig evaluated the performance of texture classification using these six features (f1, f2, f3, f4, f5, and f9) in

different combinations, and found that usually combinations of three to four features produced the best results for texture discrimination. Some other authors [Hauta-Kasari et al., 1999] also contend that, as long as there are a low number of gray levels in a small image window, then a sparse GLCM can itself be used as a feature for adequate texture description. Baraldi and Parmiggiani [1995] also attempted to investigate the statistical meaning of the same six features by associating a textural interpretation to each of them. This work is important because it serves to relate theoretical meaning to the visual appearance of each parameter. This can theoretically allow for the use of certain GLCM-related statistical measures to advertently capture certain types of scene-dependent texture in both real and synthetic imagery. What this also means is that it is theoretically possible to compare these measures from corresponding real and synthetic textures in order to determine which real texture features are not captured in the synthetic image (or vice versa in the case that the synthetic image contains artifact textures not present in the original texture) based on mismatch of these statistics. Thus, these features can be used to gauge similarity between real and synthetic textures. This obvious power and flexibility of using the GLCM approach to texture feature quantification and discrimination is the main reason why this method has been selected for this work. While some authors cite the GLCM approach as cumbersome for image-wide classification considerations due to the large number of parameters and computations involved, it is the very availability of these parameters that makes this method adaptive and flexible enough to employ as a detailed texture feature descriptor for comparing real and synthetic textures in local neighborhoods, and for the comparative performance analysis of texture modeling algorithms. One final note is that this method has the potential to be extended to describe spectral information, as will be described in Section 4.

### **3.2 DIRSIG Introduction**

This section is intended to acquaint the reader with the fundamental design and functions of DIRSIG, which will prepare the reader for a theoretical discussion of the traditional texture characterization methods that are used to produce realistic-looking scenes,

which will be presented in section 3.3. This will include the original Single-Bandpass (SBP) Z-Score Selection model, as well as the augmented model which uses Multiple Bandpass (MBP) regions in the selection of spectral reflectance curves for a given pixel. First, however a brief discussion ensues on the purpose, motivation, and challenges involved in producing synthetic imagery.

### **3.2.1 Why Use Synthetic Image Generation Models?**

Synthetic image generation (SIG) has quickly become a popular and powerful tool in the remote sensing community and beyond. While this process of modeling the world in order to mimic real images demands a detailed knowledge of the entire image chain, it also serves as one of the most useful tools in obtaining such an understanding by helping to visualize each aspect of the image chain. If properly implemented, synthetic image generation offers the advantage of merging the radiometric, spatial, and spectral aspects of the image chain in a way that can very closely resemble the actual process, which would be otherwise impossible to gain such an accurate systems perspective. It must be kept in mind however, that as valuable as these tools are, they will only perform as well as our understanding of the process that we are studying, and accordingly the SIG models should be treated as approximations of the actual process, and not as completely accurate representations.

There are many advantages of synthetic image generation in its applications to the study of imaging systems and image analysis. The most attractive aspect is that synthetic images can be produced over a range of spatial, spectral, and radiometric performance specifications, providing versatility in constructing realistic scenes. In particular, synthetic images are commonly used for the testing and development of algorithms on scenes containing a target of interest over widely varying scenarios, scene components, and acquisition conditions. Further, since SIG models are often highly modularized and are composed of submodels, the identification of weak links in the chain is thus made easier by isolating each major component of the imaging chain and analyzing the level of accuracy and fidelity produced at each step. As such, these models can provide diagnoses as to whether

simplifying assumptions made along the chain were valid, or if certain aspects have been completely overlooked.

As detailed by Schott [1997], synthetic images are often flat in appearance relative to real imagery and they tend to lack exquisite detail often because of the inability to reproduce the complexities of naturally varying texture in many material classes (such as with the case of DIRSIG, as described in the next section). However, it is not always the case of a lack of understanding or the inability to adequately describe detailed textural features in synthetic images that produces this flat appearance; in fact, this flatness can be considered satisfactory as long as the crucial elements of the scene under study are well represented and if the statistics and radiometry are deemed reasonably close to what is observed in real imagery. In applications where more structural detail is required, one frequently encounters the “textural dilemma” of synthetic image generation, which essentially is a trade-off between the immense time and effort involved in building models to great levels of detail and the negative impact this has on unpalatably long simulation run times, which often deems the extra effort unjustifiable. Despite this dilemma, it has always been highly desirable to be able to construct synthetic images with detailed textural features so as to attain optimal quality and fidelity, while having the ability to quantify how well it represents a real scene. It is also appealing to be able to determine whether improved textural feature representations by way of the use of different texture characterization models (of varying sophistication) in synthetic images will have a significant impact on the overall image chain. This is ultimately what will be investigated in this study.

### **3.2.2 The Modular Design of DIRSIG**

The Digital Imaging and Remote Sensing Image Generation (DIRSIG) Model is an integrated collection of independent first principles based submodels which work in conjunction to produce radiance field images with high radiometric fidelity in the 0.3 – 20 micron region of the electromagnetic spectrum. It is comprised of five main submodels which are designed to allow for a high degree of flexibility and interchangeability within the

DIRSIG model, as well as to diagnose and improve the model by isolating and analyzing each submodel. The submodels are as follows:

- a. Scene Geometry Submodel: This provides the mechanism through which collections of three-dimensional targets are incorporated into the synthetic image generation environment, usually in the form of three-dimensional wire frame models. They are generated either in an AutoCad environment or by use of a computer graphics software package called Rhinoceros, after which the object facets are attributed and placed into the synthetic scene using a locally produced program called Bulldozer. This submodel also establishes the relative positions of the sensor, targets, and other aspects of the scene, as pictured in Figure 6;

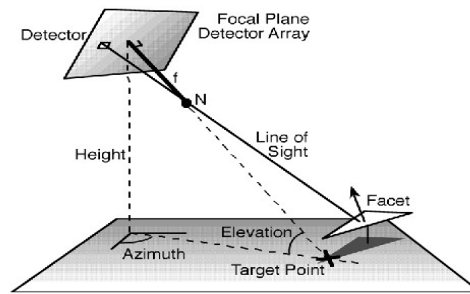


Figure 6: The relative geometry of the sensor and the scene being constructed is established using the scene geometry submodel in DIRSIG (illustrations courtesy of the DIRSIG homepage).

- b. Ray Tracing Submodel: Searches the database produced by the scene geometry submodel in order to generate lists of objects and other facets that intersect rays corresponding to a given pixel. For a given pixel, the facets encountered may be either opaque or obscuring transmissive bodies such as clouds or plumes. The DIRSIG ray tracer utilizes a non-uniform spatial subdivision method called an octree, as illustrated in Figure 7.

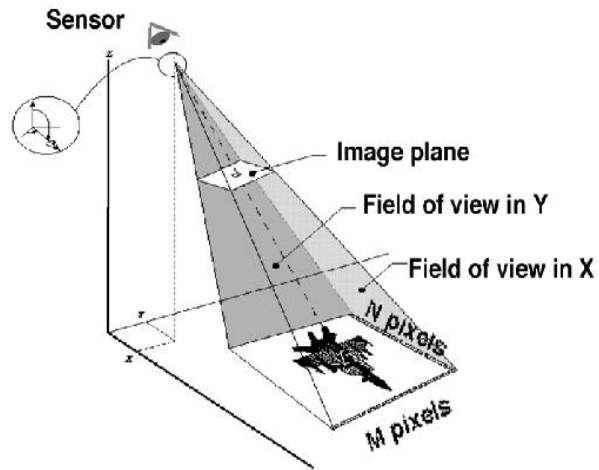


Figure 7: The ray tracing submodel determines which object facets contribute to the radiance for a given pixel.

The ray tracer also establishes solar shadowing histories for temperature predictions and background contributions for radiometry computations at diffuse surfaces. This in turn is used by the radiometry submodel for radiance computations;

- c. Thermal Submodel: Uses a forward chaining differential model called THERM in order to account for thermal material properties, meteorological histories, and solar shadow histories. The output imagery of this submodel is highly characteristic of that seen in actual MWIR and LWIR imagery;
- d. Radiometry Submodel: Makes use of the MODTRAN radiation propagation model for exoatmospheric irradiance, emitted and scattered radiances, and path transmission predictions at varying resolutions. This submodel utilizes bidirectional reflectance data, accounts for specular and diffuse background contributions, as well as emission and path length dependent extinction for thermally transmissive objects; and
- e. Sensor Submodel: This submodel is able to account for detailed descriptions of the type of sensor being modeled, as well as its spectral characteristics, and thus directs the computations made for each pixel in the aforementioned

submodels. The user is able to design several types of imaging focal planes, including line, pushbroom, and whiskbroom scanner geometries. This ties all other submodel outputs together in that it completes the computation by convolving the radiometric output with the sensor's modeled spectral response. For example, DIRSIG imagery with the use of a line scanner geometry is able to replicate the geometric distortions characteristic of the sensor type, such as the tangent effects seen in Figure 8.

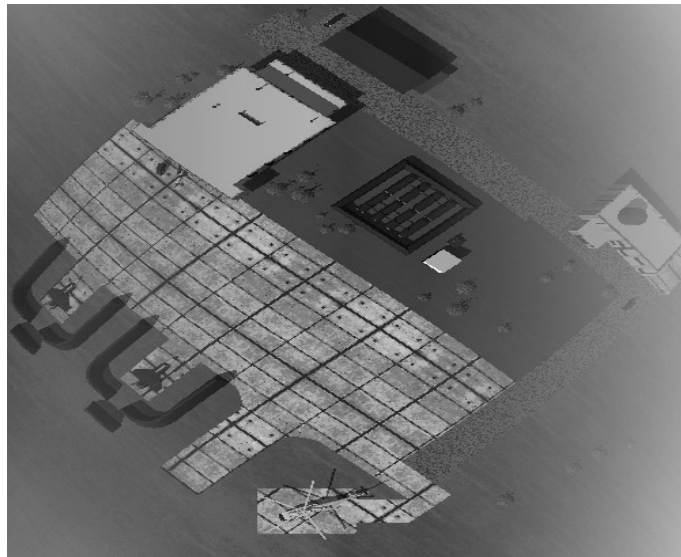


Figure 8: Illustration of geometric distortion in DIRSIG imagery through the use of the sensor submodel.

This subsection has merely served as an introduction to the modular design of DIRSIG, including details of the five main submodels. There is an immense amount of theory behind the generation of DIRSIG scenes, and the reader is encouraged to refer to the latest version of the DIRSIG Users' Manual for supplemental information [Brown, 2001]. Nonetheless, the information presented above is sufficient to understand the basic process of DIRSIG scene generation at a rudimentary level. The important aspects to be covered here are those relating to the current methodology involved in characterizing texture in DIRSIG imagery,

which is detailed in the proceeding section. An example of the relative appearance of real and DIRSIG imagery is shown in Figure 9.



Figure 9: Example of appearance of DIRSIG imagery compared to corresponding truth image.

### 3.3 Texture Characterization Models To Be Tested

This section will describe in great detail each of the four texture characterization models to be tested in this research. The models presented here are as follows:

- a. Single-Bandpass (SBP) Z-Score Selection Model;
- b. Multiple-Bandpass (MBP) Z-Score Selection Model;
- c. Texture Synthesis Models and;
- d. Fraction Map (FM) Texture Model.

#### 3.3.1 Single-Bandpass (SBP) Z\_Score Selection Model

Before describing the algorithm used to apply texture to DIRSIG scenes, a brief discussion about some of the preceding steps in the scene building and rendering process are in order here. As mentioned above, objects to be placed in DIRSIG scenes are usually created using a graphics software package called Rhinoceros [Becker, 1999], after which the objects' facets are attributed in a locally produced program named Bulldozer. The baseline process described in the above section on DIRSIG's modular design generates bland images

in that brightness variation within a material would only be introduced by solar irradiance variations due to slope, shadowing effects, and other BRDF-induced variations. An example of a DIRSIG image before and after traditional texture application is shown in Figure 10.



Figure 10: Sample DIRSIG image before (left) and after (right) texture characterization.

The spatial variability in the spectral character both within an object and at the boundaries between objects is a fundamentally important feature used for most multi/hyperspectral exploitation algorithms. In order for DIRSIG to be used to support the development and evaluation of these algorithms, it must adequately represent the spatial-spectral structure within and at the transition between material types. In order to do so, a two-tiered tool for incorporation of texture, material transition, and aggregate mixtures of materials has been developed [Schott et al, 1995, Schott & Brown, 1998]. The first tier accounts for material type variations within a facet or group of facets, and the second tier considers variations within a material type associated with reflectance/emissivity/transmissivity variations.

The initial steps of the first tier involves the generation of a material map made up of an image material identification look-up table (LUT). This material map is usually generated

with the terrain classifier method that produces the optimal separability between material types. For the images rendered in this research, it was found that the best material classes distinction was achieved using the Gaussian Maximum Likelihood (GML) classifier. During this stage, only one spectral reflectance curve is chosen for a given material class in the synthetic image, since it is the second tier of the model will later apply texture to each pixel spectrally. Before that, the transition regions between material types are modeled more closely. The user assigns to a group of facets a high level object identification, after which the material map LUT is projected onto these high level facets such that any point of a given facet that is “hit” by a ray can also be assigned to a lower level material type, such as grass, soil, or asphalt. This is done by determining which material type is projected onto that point from the high level material map associated with that object. This effectively produces transition regions that can possess various spatial mixtures of materials such as asphalt, gravel, soil, and vegetation. This turns out to be a convenient method of generating spatial mixtures of materials without having to reconstruct them on a pixel-by-pixel basis. This first tier is illustrated in the material map portion of Figure 11.

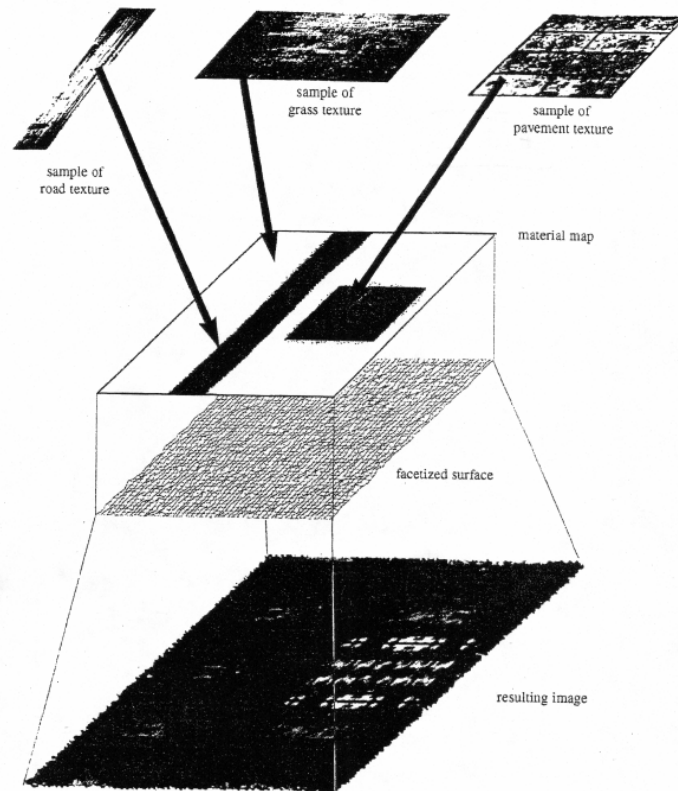


Figure 11: Illustration of tiered approach to texture characterization in DIRSIG.

The second tier of the model includes the use of a texture map. This is a vital aspect of texture characterization since it introduces the realistic-looking variability within material types by introducing both spatial and spectral structure. For each classified region representing a material class in the material map, a texture map is applied. The texture map or “texture image” is essentially an image of how the brightness varies for a material type in one spectral band. It can either be extracted from real data or from some form of texture model. The use of real data is more common for DIRSIG applications, and this data can be either extracted directly from the real image counterpart to the scene being constructed, from an alternate scene with similar material class content, or from several sample images of material types to be rendered in the scene being constructed. These single-bandpass texture

maps are used in conjunction with ground truth spectral reflectance curves in order to apply spatial and spectral structure on a per-pixel basis. The importance of accurate and robust spectral reflectance measurements cannot be overstated, since the spectra heavily depend on the atmospheric conditions and even the time of day that the measurements are taken. If it is not practical to have ground truth data collected at the exact site of the scene at the same time of day that the scene was imaged, then application of these spectral reflectance curves can potentially cause discrepancies between textures observed in real and synthetic images. One way to safeguard against such effects is to ensure that the true variability in the target reflectance is captured in the measurements, otherwise undesirable quantization and “blotchy” textures can result. This phenomenon will be demonstrated in Section 5.

This second tier of the model is the heart of the approach, as it aims to preserve the spatial/spectral correlation of materials in the synthetic image by using a texture image from a single bandpass (hence the name of the model) to drive the selection of a reflectance curve from a large family of curves, usually obtained via field measurement data as described above, or from actual imagery of the specific land cover class. The method applies texture to each pixel spectrally, and the curve selected using the *Single-Bandpass (SBP) Z-score algorithm approach* uses the selected spectral reflectance curve for that pixel across all bandpasses.

The ultimate goal of this texture characterization model is to somehow link the gray value in the sample texture image to a given spectral curve from a large database of possible curves. The mechanism used to do so with this approach utilizes the statistical relationship between the variance of the pixels in the texture image and the variance of the reflectance curves in the texture image bandpass, and the sequence is repeated for each value in the first-tier material map. The reflectance curves in the database are ranked so as to match the z-score of the selected reflectance curve in the texture image bandpass with the z-score of the texture image itself using the following algorithm:

First, the mean spectral reflectance of all of the curves for the specific land cover class is computed:

$$\rho_{avg,i} = \frac{\sum_{\lambda=\lambda_{min}}^{\lambda_{max}} \rho_{\lambda,i}}{n_i} \quad (8)$$

for the  $i = 1, \dots, N$  curves of the particular material type, where  $\rho_{avg,i}$  is the average reflectance over the bandpass for the  $i$ th curve,  $\rho_{\lambda,i}$  is the spectral reflectance for the  $i$ th curve at a given wavelength in the bandpass, and  $n_i$  is the number of points across the bandpass for the  $i$ th curve. The mean and standard deviation for the bandpass averages are then computed as:

$$\rho_{avg} = \frac{\sum_{i=1}^N \rho_{avg,i}}{N} \quad (9)$$

and

$$\sigma_{\rho} = \sqrt{\frac{\sum_{i=1}^N (\rho_{avg,i} - \rho_{avg})^2}{N-1}} \quad (10)$$

Each of the  $N$  curves is then ranked using a z-score measure as follows:

$$z_i = \frac{\rho_{avg,i} - \rho_{avg}}{\sigma_{\rho}} \quad (11)$$

During the scene generation process, for a given pixel in the texture image, the z-score is also computed using the mean and standard deviation of the entire texture image (see Figure 12):

$$z_{texture} = \frac{DC_{i,j} - \mu_{texture}}{\sigma_{texture}} \quad (12)$$

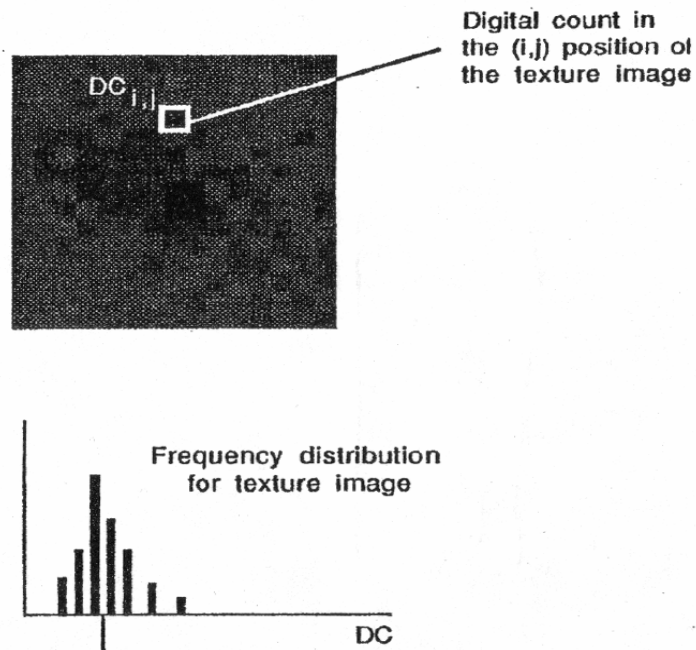


Figure 12: Mean and standard deviation are computed from sample texture images in DIRSIG. The z-score for the pixel at position (i,j) is then determined from the texture image frequency distribution.

The process of using the single-bandpass z-score ranking method is illustrated in Figure 13.

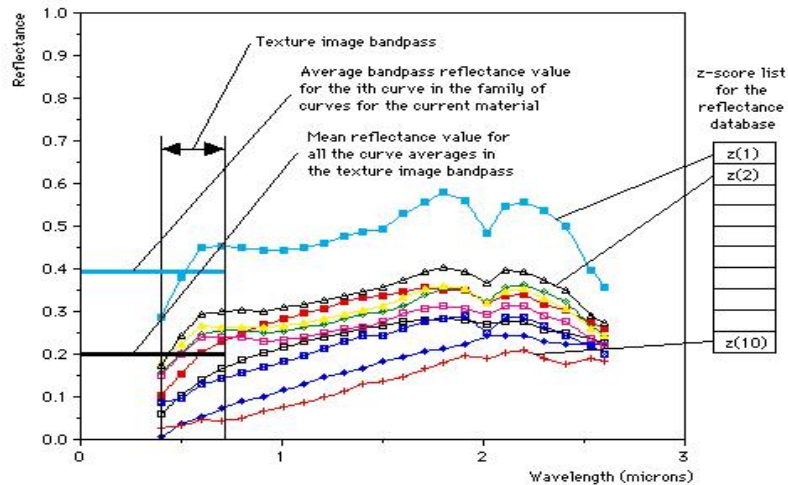


Figure 13: Single-Bandpass (SBP) Z-Score ranking method for texture characterization.

As alluded to earlier, a practical issue arises in that a sufficiently large family of reflectance curves is often not available for this technique, which may result in an unrealistic looking, overly-quantized and non-continuous appearance to the synthetic image, especially at transition regions. In answer to this, Schott et al. [1995] detail a method to produce an arbitrary number of spectral curves from a smaller set of curves that contain the desired multivariate statistics for the given land cover class. This technique, which has now evolved into a utility within DIRSIG called “expand emissivity file”, essentially consists of the generation of uniformly distributed random samples in a spectrally non-correlated space through the use of eigenvalues of the variables in this space, to define the standard deviation for each sample set vector. These vectors are then back-transformed into a spectrally correlated space where they exhibit the same spectral characteristics as the basis set of vectors (curves). For further details on this technique, see [Schott et al., 1995].

An example of a similar application occurred in the modeling of transition regions for the DIRSIG Megascene, which is a current synthetic image effort that will be described in more detail in Section 4. Figure 14 shows some interim results obtained by accounting for the lack of a sufficient number of reflectance curves to represent true variability by using a similar technique as that described above. Figure 14(a) shows the original truth image, while Figure 14(b) shows the original basis set of curves and the corresponding preliminary result of texture characterization. By expanding the set of curves to account for transition regions and thus for more variability, one can obtain much more realistic-looking results, even in the preliminary stages of texture characterization as shown here (Figure 14(c)).



Figure 14a: Original CitiPix truth image.

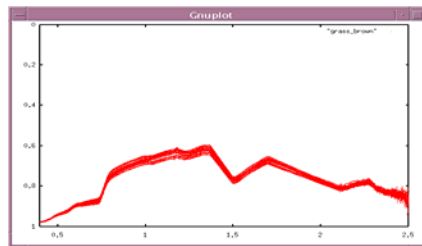


Figure 14b: Preliminary texture characterization without the use of transition curves.

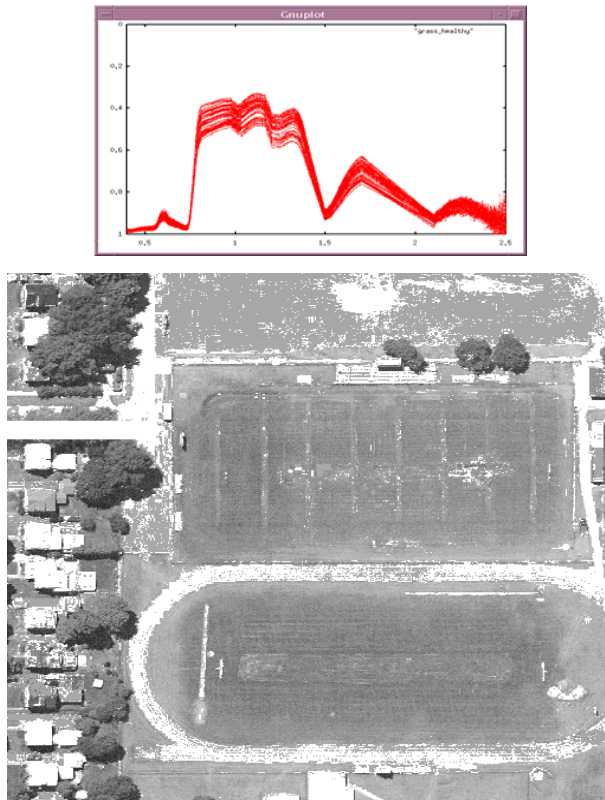


Figure 14c: Preliminary texture characterization with an expanded database of transition curves.

One obvious drawback of the SBP Z-Score Selection technique is that it uses only the bandpass of the texture image to match the spectral reflectance curves for the synthetic texture. This means that the curve with the closest z-score in the specified bandpass is used to describe the entire reflectance spectrum for that pixel, over the entire range of wavelengths in the scene. Clearly, problems will arise in the case that the chosen reflectance curve to represent that pixel departs significantly from the reflectance for the pixel in other non-correlated bandpasses. This SBP Z-Score texture characterization model will be the first model to be tested in this work. The next subsection will review some of the previous work that has been done in assessing this method, which led to the logical extension of it by employing multiple bandpasses to drive the selection of the spectral reflectance curve for each pixel.

### 3.3.2 Multiple-Bandpass (MBP) Z-Score Selection Model

#### 3.3.2.1 Theory

The concept behind the MBP Z-Score texture model is largely based on the SBP model discussed above. As its name suggests, the difference between the models lies in its mechanism in choosing spectral reflectance curves for a given pixel in the DIRSIG image. This model is designed to allow the user to select multiple (and ideally uncorrelated) bandpasses so that the spectral character of the pixel can be represented with more fidelity in all spectral bands. This obviously possesses a theoretical advantage over the SBP model, since it will be less likely that a reflectance curve will be chosen that exhibits significantly different global behavior than that in the bandpasses from which the curve has been selected. Figure 15 illustrates how a composite weighted z-score is calculated using texture images in three bandpasses. Ideally, the additional bandpasses used should be selected such that they are not well-correlated with the original single bandpass used in the SBP model.

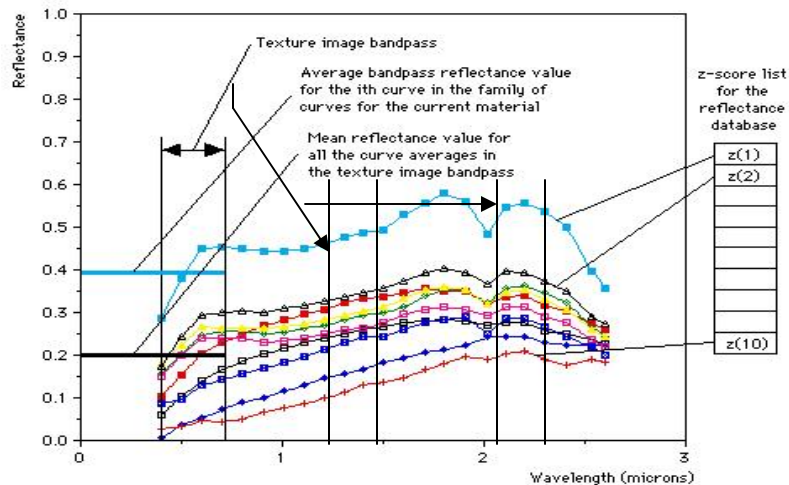


Figure 15: The MBP Texture Model uses multiple texture image bandpasses in order to calculate a composite weighted z-score for each curve (column list, right) and compares these scores to each of the texture image pixel composite z-scores. The curve with the z-score value closest to that of each pixel in the texture image is selected to characterize the spectral behavior of that pixel for the entire spectral extent of the image.

This model can be implemented in DIRSIG by making some relatively simple changes in the input DIRSIG configuration files for each scene to be rendered. A simple illustrative example follows, which will demonstrate how the algorithm works: Consider the case of using three bandpasses to drive the selection of each pixel's reflectance curve. This means that there are three input monochrome texture images (named Tex1.pgm, Tex2.pgm, and Tex3.pgm) to be used for this process, in corresponding bands B1, B2, and B3, as illustrated in Figure 16.

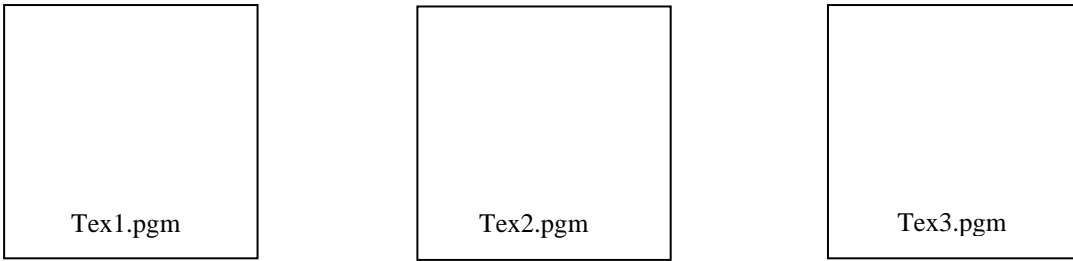


Figure 16: Three texture images are used as input texture maps with the MBP model. As with the SBP model, the z-scores are then computed for each of the texture images:

$$z_{t1} = \frac{DC_{i,j} - \mu_{t1}}{\sigma_{t1}} \quad (13)$$

$$z_{t2} = \frac{DC_{i,j} - \mu_{t2}}{\sigma_{t2}} \quad (14)$$

$$z_{t3} = \frac{DC_{i,j} - \mu_{t3}}{\sigma_{t3}} \quad (15)$$

For the sake of this example, say that these values are  $z_{t1} = 5$ ,  $z_{t2} = 6$ , and  $z_{t3} = 8$ . Although not a realistic situation, consider the case that we have three spectral reflectance curves to choose from for a given pixel, as illustrated in Figure 17.

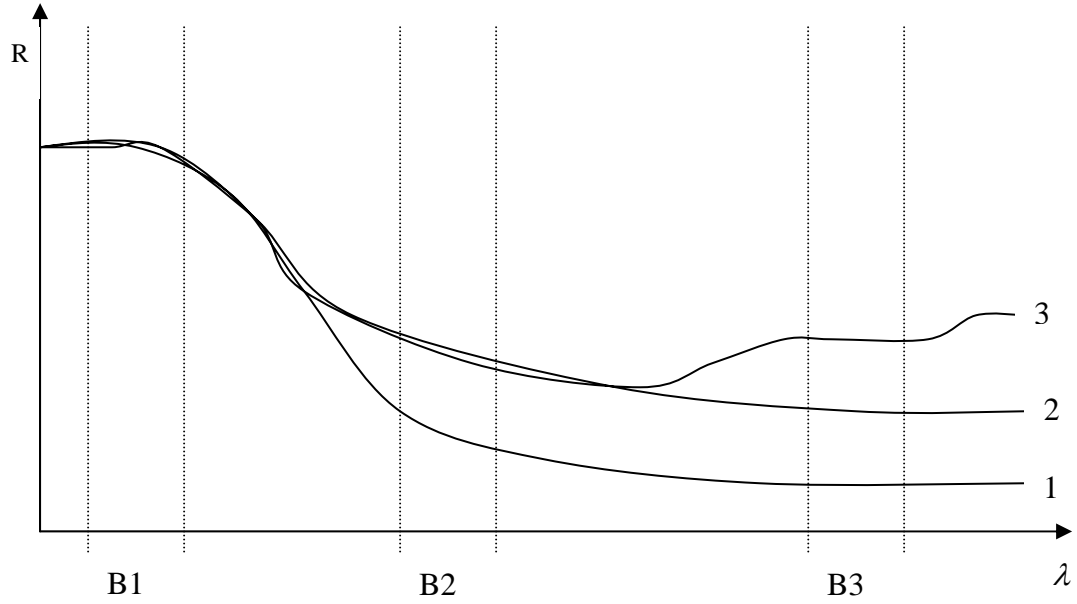


Figure 17: Three sample reflectance curves to choose from in MBP model. Z-Scores are calculated from the mean and standard deviation of all 3 curves in each specified bandpass in the same manner as with the SBP model.

For each specified bandpass, the z-scores are calculated using the mean and standard deviation of all 3 curves in the given bandpass. As with the SBP case, these z-scores will be compared against the z-score values computed above for each of the texture images. In this example, assume that in bandpass B1 we have found that the z-scores for each of the 3 curves are equal, i.e.,  $z_{11} = 8$ ,  $z_{21} = 8$ , and  $z_{31} = 8$ . In B2, we have  $z_{12} = 9$ ,  $z_{22} = 7$ , and  $z_{32} = 7$ , while for B3 it is found that  $z_{13} = 6$ ,  $z_{23} = 7$ , and  $z_{33} = 8$ . The deciding factor for choosing the optimal curve in the MBP model is the error metric, which computes the absolute difference between the z-score values for the texture image and reflectance curves in each bandpass. For B1, we find that:

$$\varepsilon_{11} = |8 - 5| = 3$$

$$\varepsilon_{21} = |8 - 5| = 3$$

$$\varepsilon_{31} = |8 - 5| = 3$$

This means that if we were using just one bandpass to select the reflectance curve, then we can theoretically choose any curve of the three, since the error metrics are equal. When we look at B2 as well, we obtain:

$$\mathcal{E}_{12} = |8 - 5| + |9 - 6| = 6$$

$$\mathcal{E}_{22} = |8 - 5| + |7 - 6| = 4$$

$$\mathcal{E}_{32} = |8 - 5| + |7 - 6| = 4$$

At this point then, using only B1 and B2, either curve 2 or 3 should be chosen. If we add the third bandpass B3, then we find:

$$\mathcal{E}_{13} = |8 - 5| + |9 - 6| + |8 - 6| = 8$$

$$\mathcal{E}_{23} = |8 - 5| + |7 - 6| + |7 - 8| = 5$$

$$\mathcal{E}_{33} = |8 - 5| + |7 - 6| + |8 - 8| = 4$$

Thus the MBP model will choose curve 3 for the pixel under consideration in this example. Note the improved accuracy of curve selection due to the use of multiple bandpasses. For example, in the SBP case, if only B1 was used, then curves 1 or 2 could also have been chosen, which clearly do not exhibit the same spectral character as curve 3 in B3. In this example, more accuracy was attainable by using additional texture bandpasses, and this model can theoretically be extended to any number of bandpasses. However, if one were to go to the extreme of using all bandpasses of the input real image (or alternate texture image), then it is possible to over-constrain the problem, especially in hyperspectral imagery. The algorithm would likely become confused, and many z-score values will be equal. This would deem the extra effort of using potentially hundreds of spectral bandpasses unprofitable. However, the theoretical advantage offered by the MBP model over the SBP model is undeniable, and the results presented in Section 5 will further illustrate this improvement.

### 3.3.2.2 Previous Results

Burtner (2001) incorporated a modified algorithm that uses more than a single bandpass in the selection of the reflectance curve for a given pixel in the synthetic image.

This research focused on the effect of using both two and three bandpasses, and compared the results with the traditional SBP method introduced above. This work also involved increasing the number of spectral reflectance curves using the “expand emissivity file” utility in DIRSIG. This study was only conducted for small samples of grass texture from two different types of imagery: a Modular Imaging Spectrometer Instrument (MISI) image and a Hyperspectral Digital Imagery Collection Experiment (HYDICE) image. The analysis of the generated spatial and spectral texture was largely qualitative in nature. It was concluded that the use of additional reflectance curves slightly improved the results of the synthetic image in most cases, and that the fidelity of the synthetic image seemed to improve with the addition of the second bandpass, while adding a third bandpass was inconsistent in that it did not always significantly improve the results over that obtained with using two bandpasses. The extent of quantitative analysis performed in this research involved the use of the Principal Components Analysis (PCA) utility available in ENVI. Of course, this is a rudimentary measure of fidelity in that it only measures the amount of information contained in the synthetic image as compared with the real image, since the PCA fundamental assumption is that information content equates with variability. It is not surprising that Burtner found that there was a significant gap between the real and synthetic data, since there was only a finite sample of reflectance curves in the database, and because grass is a highly variable material that would require extensive measurements to capture its true inherent variability. This research indicated the requirement for a robust, quantitative measure for texture modeling performance analysis, and that other material types and transition regions need to be studied further in terms of their spatial and spectral fidelity, possibly with the use of different texture characterization models.

Kennedy (2002) used a somewhat more quantitative method in assessing both the SBP and MBP texture models. The quality of the synthetic images was measured using a Composite RMS Error Metric (CREM) that provided a single-valued average performance measure of the model in question. The metric used for the SBP model simply computes the difference in pixel values between the original texture image and the synthetic image:

$$\varepsilon_1 = \frac{1}{n \cdot m} \sqrt{\sum_{i=0}^{n-1} \sum_{j=0}^{m-1} (x1_{i,j} - x2_{i,j})^2} \quad (16)$$

where  $n \times m$  is the size in pixels of the subimage under study,  $x1$  is the pixel value for the texture image, and  $x2$  is the corresponding pixel value in the synthetic image. Similarly, the composite RMS error metric computes the average number of digital counts that each pixel in the synthetic image varies from the corresponding pixel in the original image, in the following manner:

$$\varepsilon = \frac{1}{n \cdot m} \sqrt{\sum_{i=0}^{n-1} \sum_{j=0}^{m-1} (x1_{i,j} - x2_{i,j})^2 + (y1_{i,j} - y2_{i,j})^2 + (z1_{i,j} - z2_{i,j})^2} \quad (17)$$

where  $y1$ ,  $y2$ ,  $z1$ , and  $z2$  are accordingly similar pixel values in the second and third texture bands.

Kennedy expanded on Burtner's results by testing the traditional SBP method, as well as both the two- and three-bandpass models on sample materials of grass, dirt, asphalt, and gravel. The results show that texture characterization using multiple bands with an expanded database of spectral curves does show improved texture in SIG images. However, the results were material-specific. For example, the number of spectral curves in the database required for adequate representation of materials such as asphalt and gravel was considerably less than that required for grass, since grass tends to have more inherent variability and a more complex spectral shape and thus a larger dynamic range. As such, the addition of a third texture band did not significantly improve results for the asphalt and gravel material types, while it was found that the RMS error metric declined more significantly when the third band was added for grass, indicating better results as long as the number of spectral curves in the database for grass was accordingly larger. This requirement of having a larger number of reflectance curves is owing to the fact that, when rendering in multiple bands, one is often faced with the problem of undersampling, especially if the material type exhibits a wide dynamic range. In particular, it was found that if  $N$  curves are required for SBP rendering, then in order to capture the variability and to add significant,

independent information for MBP rendering (using P bands), the number of required spectral reflectance curves would be  $N^P$ .

This augmented MBP texture characterization technique will be the second method to be tested in this research. Also, the CREM was the inspiration for the first of the four texture performance metrics used in this research, the Mean Filter (MF) spatial metric. Neither Burtner nor Kennedy focused on measures of spatial and spectral structure and correlation when assessing the quality of DIRSIG synthetic textures, nor did either of them extend their analyses out to 2,500 nm. In this research, the combination of simple and complex spatial and spectral performance metrics will be used to investigate the behavior of the SBP and MBP models out to such spectral extents, and at different spatial and spectral resolutions in a much more quantitative and thorough manner. More details on this aspect are presented in Section 4.

### **3.3.3 Texture Synthesis Models**

As mentioned previously, most of the work to be found in the texture synthesis literature is concerned with monochrome or RGB texture synthesis techniques. Since the multi/hyperspectral texture synthesis models to be tested in this work are extensions of these simpler models, a brief literature review on the basic concepts and previous work with various types of texture synthesis models will be presented here. The mathematical framework for each of the numerous models is too involved to be discussed in detail in this section; therefore the emphasis will be on the Simoncelli & Portilla (S/P) technique and the Image Quilting method of texture synthesis, which will be two of the synthesis methods under investigation in this research. A third ad-hoc reincarnation of these methods termed the Spectral Expansion texture synthesis model will also be discussed and tested in this work. There are also concluding remarks in this section regarding the sparse typical methods of performance evaluation that have traditionally been used for most texture synthesis models, and the resulting requirement for sound, quantitative measures of model performance.

### 3.3.3.1 Literature Review

Texture synthesis is often described as a realization of a random process defined over an ensemble of all possible texture images. Although each realization is indeed unique, the ultimate goal is to have the synthetic texture appear as if it were generated from the same underlying process as the counterpart real texture. In general, most texture synthesis models aim to model texture as a stationary random process, since the spatial correlation in textures is typically local in nature; that is, the assumption is that all of the relevant spatial information for a given texture is contained locally. This is an advantageous property that most monochrome texture synthesis models employ in order to create much larger regions of texture from sample textures of small size, which leads to the popular application of extrapolating exemplar textures to cover much larger spatial extents, based on the statistics of the monochrome sample texture.

An additional complexity is introduced when modeling color and multi/hyperspectral textures, since both the spatial and spectral components' correlation must be captured simultaneously. As mentioned, monochrome texture is adequately assumed to be stationary and ergodic (where sample averages approach ensemble averages for large sample sizes) in nature, which allows for the use of a limited amount of spatial texture to be used to reliably estimate a model from which an infinite spatial extent of texture can be generated (see Figure 18). Unfortunately, spectral correlation cannot be modeled as a stationary random process, since each spectral band in a multispectral texture image contains global information that must be preserved by the model. Correlation across bands is not relative, and thus each spectral band pair may well have a distinct dependency. Also, since the spectra of an image have a finite extent, there are no repeating dependencies from which to generate an infinite amount of information through a causal model (see Figure 19). It is clear then, that simply extending monochrome techniques would introduce an enormous computational burden, and thus it was found that a technique was required

that could exploit the power of monochrome texture synthesis by extending the information in a single band over the entire spectral image cube.

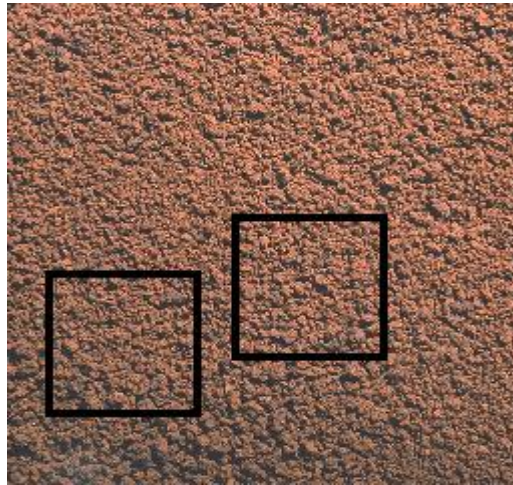


Figure 18: Because the outlined areas exhibit similar spatial correlation that tends to repeat within the image, it is intuitively clear that spatial texture can be modeled as a stationary ergodic process.

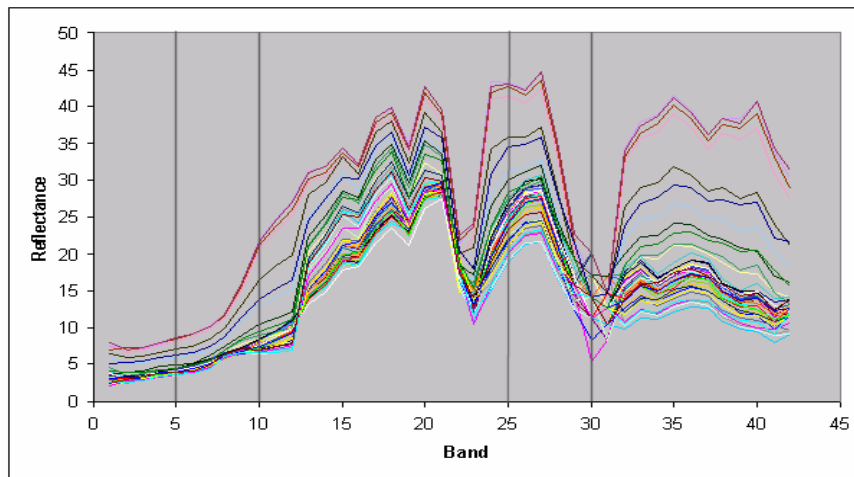


Figure 19: These two pairs of spectral bands demonstrate that spectral correlation cannot be modeled as a stationary ergodic process.

There are many fundamentally different models that have been used throughout the texture synthesis literature that have achieved varying measures of success depending on the type of texture being modeled. What follows is a brief account of some of the most popular methods that have emerged over the past twenty years and some of the strengths and weaknesses of these models, leading up to the methods that have been chosen for testing as possible texture characterization models in DIRSIG. Although there are many specialized and somewhat obscure methods existing in the computer vision and graphics literature, such as those based on syntactic grammars [Lu & Fu, 1978], reaction-diffusion and partial differential equations [Witkin & Kass, 1991], and fractal-based models [Cross & Jain, 1983], the emphasis here will be more on the statistical models of texture synthesis.

Julesz (1962) pioneered the statistical characterization of textures by proposing that the  $n$ th order statistics (for some unspecified  $n$ ) of texture pixels, when considered as samples of a stationary source, could suffice to partition textures into classes that are indistinguishable to human observers. Since then, many models have extensively utilized first- and second-order statistics of pixels and/or coefficients in a fixed linear basis to describe and synthesize textures [Cross & Jain, 1983; Hassner & Sklansky, 1980]. Adaptive linear representations have also been used, which essentially adjust the basis set of vectors in a Gabor wavelet function representation according to the image statistics. This can be performed either by tuning the appropriate 2-D Gabor filters to the dominant frequencies of the image [Dunn et al., 1994; Teuner et al., 1995], or in a more flexible approach employing adaptive filter bandwidths [Portilla et al., 1996]. It was unanimously found that mere second-order statistical approaches failed to capture many significant structures that occur in many textures.

Several directions for texture synthesis models then ensued, however most models had mutual agreement with respect to some of the formal assumptions made in order to formulate their respective models. In particular, several successful models rely upon Markov Random Field (MRF) theory as part of the synthesis framework, and although the mathematical details of MRF theory are quite involved and too lengthy to reproduce here,

MRFs provide an illustrative theoretical view of the great complexities of statistical texture modeling (the reader is directed to Tyrrell [2002] for a more detailed discussion on Markov chains and the basics of MRF theory as it pertains to texture synthesis). The parameters of a MRF are conditional probability estimates for an event based on those surrounding it, which means that there is no causal restriction on the nature of influence between events. This makes the problem potentially overwhelming when one considers the following scenario: Consider a set of pixels on a 2-D grid, where the occurrence of a given pixel across the grid is not statistically independent from every other pixel in the grid (Figure 20). In this case, the neighbors of a central pixel must provide information as to its value, and thus influences from pixels in all directions must be considered. Therefore, there exists a mutual and simultaneous influence between an event (eg. pixel intensity level) and those surrounding it spatially, making it impossible to determine causality.

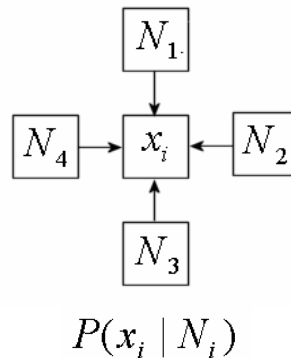


Figure 20: MRFs possess dependencies from all directions simultaneously; MRF model parameters are conditional PDFs of  $x_i$  given the occurrence of its neighbors.

To address this dilemma, many algorithms have surfaced for the purpose of sampling a MRF, most of which involve combinatorial solutions over the space of all  $n^2 \times n^2!$  ways of determining causality over an  $n \times n$  field. Needless to say, many of these predictive models are immensely complex and require unpalatably long convergence times unless a sound and efficient resampling technique is utilized. These methods range from pixel-by-pixel resampling and moving average filter techniques to multiresolution steerable pyramid

resampling techniques [De Bonet & Viola, 1998; Heeger & Bergen, 1995]. A variant of this latter technique will be described in more detail in the next section, since it is the one used in Tyrrell's S/P synthesis model.

A more recent direction that has been taken that has achieved some of the best results in the literature, are models using image wavelet subbands. The advantage of this method of multiresolution image decomposition is that these subbands have been observed to possess non-Gaussian PDFs with long tails, and sharp peaks at zero due to image texture that consists of smooth areas interspersed with occasional edges or other features. Heeger and Bergen (1995) extended on the results of other work where texture was represented by the marginal statistics of the responses of a set of filters. This was performed by using an over-complete (i.e., not orthogonal) fixed linear basis to synthesize textures by iteratively alternating between matching subband and pixel histograms, a method similar to projection onto convex sets (POCS). While this method was effective in capturing the random features of several natural textures and the dominant scales and orientations, it failed to represent extended structural elements such as straight or curved contours and edges, as well as other highly regular patterns. Another sampling technique introduced by Zhu et al. [1997] used Gibbs sampling to match marginal statistics with those estimated from wavelet subbands of the sample texture image. These filters were chosen adaptively so as to consistently minimize entropy, and their results, while able to reproduce a wide variety of textures, were computationally expensive. It was soon thereafter found that the set of marginal statistics of a fixed finite linear basis alone were often unable to capture long-range structures and pseudo-periodic patterns, while second-order textures tended not to be well-represented. An example of such a case where images with identical marginal statistics in a wavelet decomposition representation do not contain similar textural patterns is shown in Figure 21.

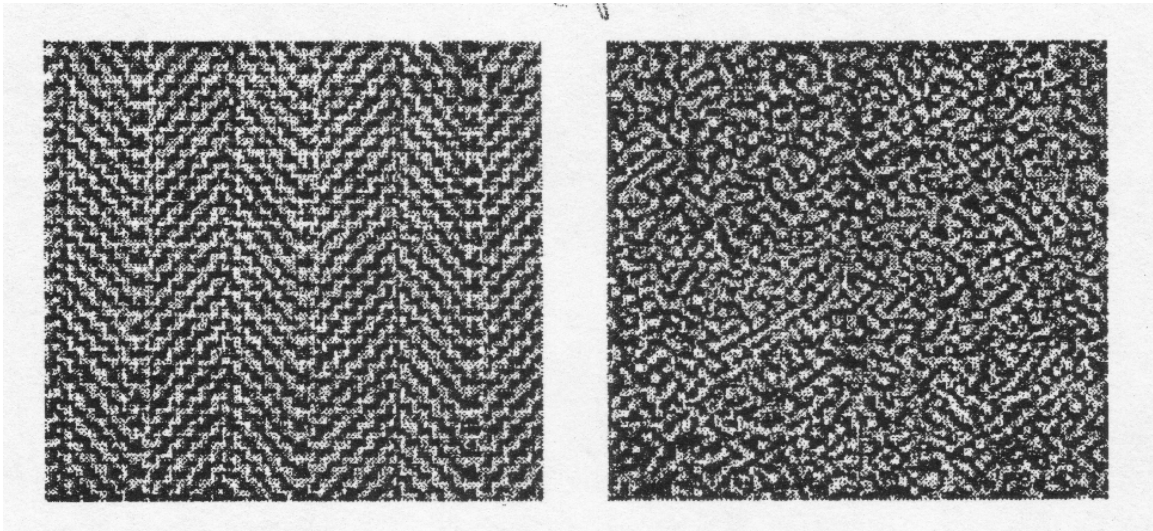


Figure 21: Differing textures with identical marginal statistics.

For this reason, recent works by Simoncelli and Portilla have proposed the additional use of joint statistics of wavelet coefficients, with particular emphasis on the joint histograms of pairs of wavelet coefficient magnitudes at adjacent spatial locations, orientations, and scales of an orthonormal wavelet basis. This method proved to be effective in capturing structural patterns in texture, since it was able to reproduce the observed phenomenon in real images where features tend to produce large coefficients in local spatial neighborhoods. One of the keys to the success of the S/P model is that it differs from most other models in that while both spatial locality and stationarity are assumed, Gaussian behavior is not assumed, and is therefore less restrictive. For example, this method works well on textures such as the classic Brodatz texture of the herringbone (Figure 21, left) which contains a set of locally oriented patterns arranged spatially. One of the most recent variants of the S/P model is one that is capable of characterizing both structural and random aspects of textures in terms of a set of statistical measurements on a complex analytic wavelet representation. This is done by synthesizing images subject to four specific constraints via iterative projection onto solution sets. The statistical constraints enforced in the S/P technique are:

- a. The local spatial correlation of coefficients within each subband;
- b. The local spatial correlation of coefficient magnitudes;

- c. The cross-correlation between coefficient magnitudes at adjacent scales and all orientations; and
- d. The first four moments of the pixel histogram.

More details of this synthesis-by-analysis technique are presented in the next subsection as it pertains to Tyrrell's multi/hyperspectral extension of the S/P model. The relatively new technique of image quilting is also discussed thereafter, followed by a discussion of the Spectral Expansion texture synthesis model that was derived from the S/P model by Tyrrell. The Spectral Expansion model offers the most flexibility of all texture models presented here in terms of its potential as an incorporated texture model in the DIRSIG environment. As such, the three models presented in the following sections (S/P, Quilting, and Spectral Expansion) were coalesced into one nominal "Texture Synthesis model" instead of being tested separately. More details on how the Texture Synthesis model has been incorporated into DIRSIG will be presented in Section 4.2. The above section has introduced the great complexity involved in the field of texture synthesis, with an accompanying review of recent works and the results that were obtained. The reader is directed to the references cited above for more details on any specific texture synthesis algorithm.

### 3.3.3.2 Tyrrell's Multi/Hyperspectral Texture Synthesis Models

#### 3.3.3.2.1 The S/P Model

As mentioned above, the S/P method is a synthesis-by-analysis technique that iteratively enforces a set of statistical constraints over the output of a complex analytic filter bank by extracting multiresolution scale and space information from a sample monochrome texture. Figure 22 shows an example of such a complex steerable filter bank. The filters are typically oriented versions of a common function that form a complex Hilbert Transform pair. Figures 23 and 24 show the real and imaginary parts of these filters at four orientations.

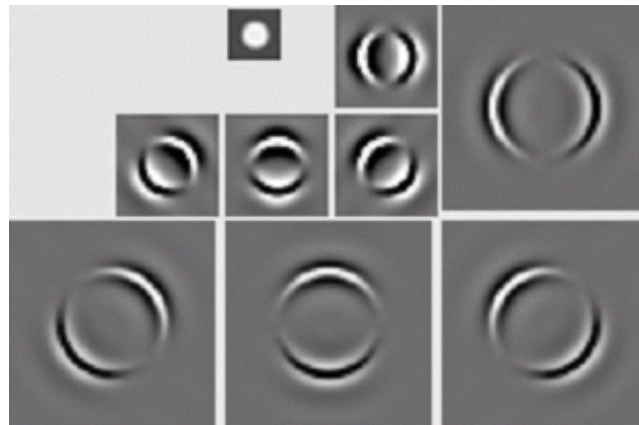


Figure 22: Example of a complex steerable filter bank.

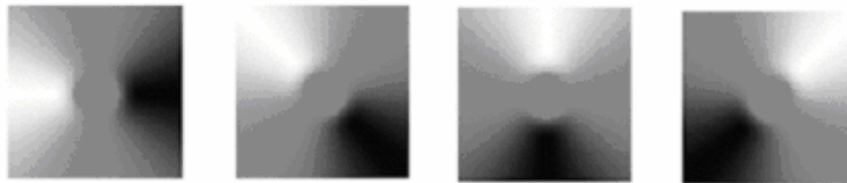


Figure 23: Real part of above complex steerable filters at four orientations.



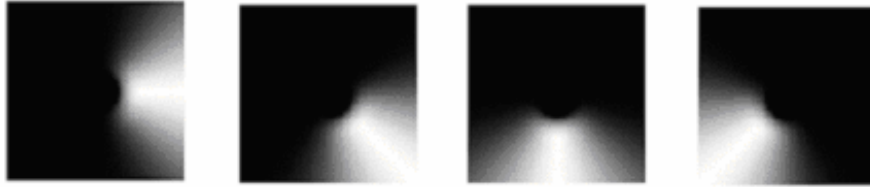


Figure 24: Imaginary part of above complex steerable filters at four orientations.

The algorithm begins with a white noise image, and iteratively coerces it to converge into the form of the desired output synthesized texture through the above statistical constraints. This method proceeds in an iterative, coarse-to-fine fashion over a variant of the steerable pyramid. This resampling technique has the added efficiency that a compact multiresolution representation is used to analyze the sample texture, by using a set of four oriented complex analytic filters at each level of the pyramid so that local phase information can be used to detect the polarity of edges and boundary transitions. The overall purpose of the steerable pyramid is to capture locally oriented structure at each scale within the decomposition, thereby extracting most meaningful features from the input texture image. An example of a steerable pyramid decomposition on the Brodatz presscloth texture image is shown in Figure 25.

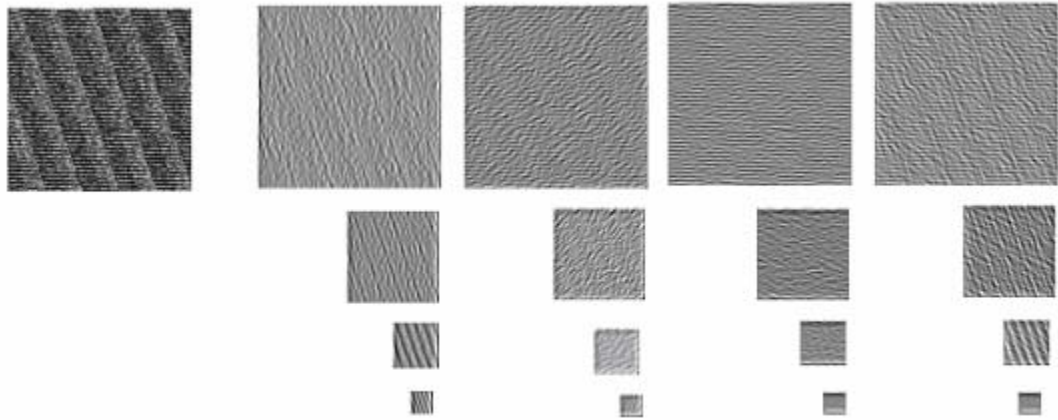


Figure 25: Steerable pyramid decomposition of Brodatz presscloth texture image.

This steerable pyramid technique contains both a synthesis side and an analysis side in order to identify similar neighborhoods, and ultimately to copy information from the analysis side to synthesize the desired texture (Figure 26).

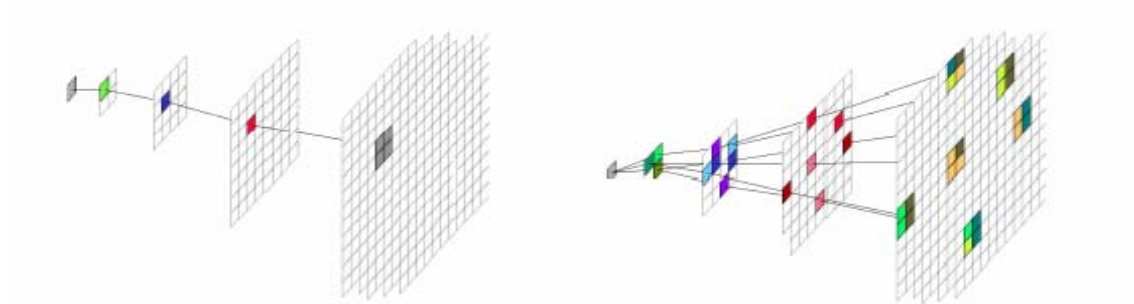


Figure 26: The hierarchical structure of the steerable pyramid used to identify similar neighborhoods. Information from the analysis side (right) is copied in a coarse-to-fine fashion onto the synthesis side (left).

The input white noise image is initially split into high- and lowpass bands, as shown in Figure 27. The lowpass band is then further split into a lower-frequency band and a set of oriented subbands. The recursive reconstruction of a pyramid is achieved by inserting a copy of the shaded region of Figure 27 at the location of the lowpass branch, indicated by

the solid circle. This consists of an additional lowpass operation, downsampling by a factor of two in both directions, and then repeating the process in a recursive fashion.

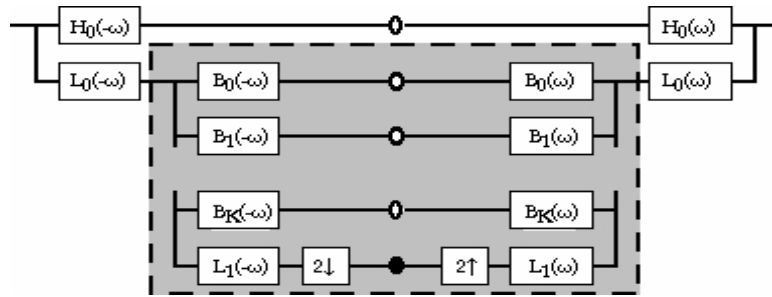


Figure 27: System diagram for the steerable pyramid.

This merely outlines the basic structure of the S/P algorithm in its traditional form for monochrome texture synthesis. For more details, see both papers by Simoncelli and Portilla listed in Section 8. A summarizing diagram of this algorithm is shown in Figure 28.

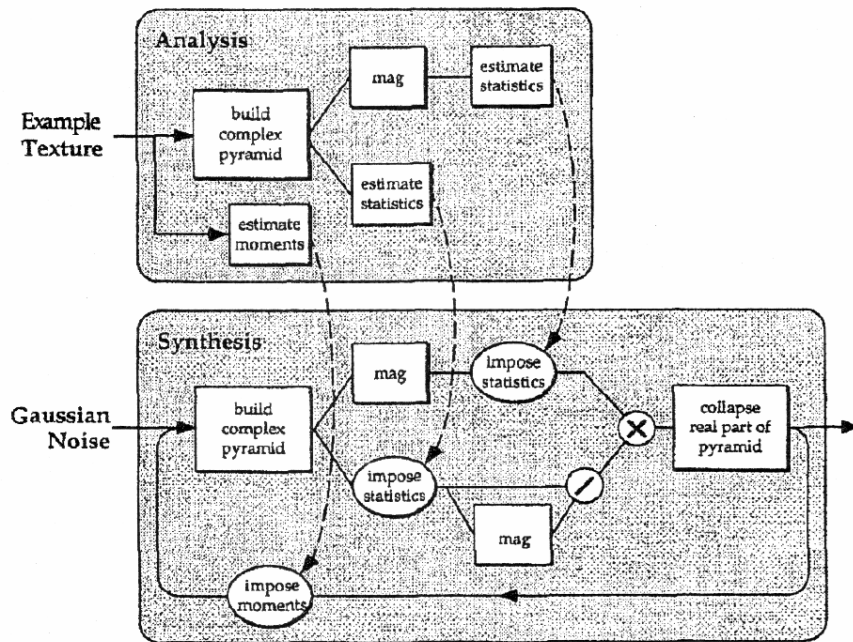


Figure 28: Diagram of S/P texture synthesis algorithm. This illustrates the order of constraint enforcement used with this technique.

Tyrrell extended the S/P model in order to generate multi/ hyperspectral synthetic textures. This method works by first synthesizing texture in a single band, and then using a Markov Random Field (MRF) ideology to select spectral curves conditioned on a local context neighborhood from that band. The key is to choose the single dominant band such that the spatial information is maximized over the entire image cube. This is achieved using the Independent Components Analysis (ICA) transform, which is essentially the same as the familiar Principal Components Analysis (PCA) transform, except that it allows for spatial and spectral domains to be processed separately and makes use of higher-order statistics [Manduchi & Portilla, 1999; Liang, Simoncelli, & Lei, 2000; Tyrrell, 2002]. This is closely related to the statistical principles of the blind source separation problem [Cardoso, 1998] where independent sources are assumed to be mixed by a linear transform such as  $\mathbf{Y} = \mathbf{M}\mathbf{X}$ , and the aim is to determine the matrix  $\mathbf{M}$  via statistical estimation methods. Ultimately,  $\mathbf{M}$  is inverted and used to minimize the mutual information between sources by rendering them statistically independent. For more on this very interesting technique, consult the above-cited references.

Once the dominant band is determined, a modified version of the S/P texture synthesis technique synthesizes a new principal band, after which a non-parametric search is used to find similar neighborhoods between real “source” images and the synthetic images. Lastly, the remaining spectral information is copied from these neighborhoods by means of random sampling. Before proceeding, some more details on the multiresolution resampling technique for generating spectral information is in order. A multiresolution approach is convenient in that it provides a natural representation of textural features, since textures often consist of varying scales. Also, this method relieves the user of having to somehow choose an appropriately sized spatial neighborhood for different texture types. This offers the advantage of inherently increasing the probability of the synthesized texture to generalize well over a wide range of texture types. Tyrrell utilized a Laplacian pyramid multiresolution decomposition in order to define the local context. This model is a simple band-passed decomposition of an image that uses a collection of scaled difference of Gaussian (DOG)

filters. Another advantage of Tyrrell's S/P model is that all spectral information can be generated in parallel, leading to a significant reduction in run time even for a large number of spectral bands. The current version of Tyrrell's S/P technique requires very few user inputs, and usually converges within five iterations of the code.

A final important note on Tyrrell's S/P texture synthesis model is that the output of the model produces the exact spectral extent and spectral resolution as the input texture image. Therefore, when rendering DIRSIG scenes using this texture model, we cannot obtain a spectral resolution that is finer than the input spectral resolution of the real image. This is a limitation that is encountered for both the S/P and the Quilting models of texture synthesis, whereas this is not a factor for the other three texture models to be tested.

#### **3.3.3.2.2 The Image Quilting Model**

The second method in Tyrrell's texture synthesis model uses the technique of Image Quilting. This is a relatively new and simple graphics based approach that literally "quilts" together regions of texture from a sample texture image. This method has been presented both in the context of texture synthesis and texture transfer, where an object is rendered with a texture taken from a different object [Efros & Freeman, 2001]. This latter approach is more applicable to computer graphics, and thus will not be investigated here. Tyrrell chose this method as an alternative to the S/P model since it handles high spectral dimensionality well, and because it is a relatively fast and simple technique that nonetheless demonstrates very good texture synthesis results. This method draws upon the fact that, in the case of pixel-by-pixel resampling, it is very likely that a given pixel's immediate neighbors are the best candidates for the next synthesis step. Quilting therefore saves time by using a compact set of neighbors carried over at each synthesis step, known as a "quilting region" of which the user can specify the size. Each new region is selected from the sample image based on border overlap at neighboring sites, where similar context neighborhoods between the sample and synthetic images must be found by efficient resampling techniques. This resampling must also account for apparent discontinuities between blocks, since the initial placement of quilting regions will likely not match exactly over their boundaries. As for the

spectral information, it can be carried along as each texture block is quilted instead of merely retaining single pixel values. This is another factor that makes quilting much faster, since spatial and spectral information can be determined simultaneously.

There are many resampling methods that have been used for quilting applications, such as the pyramidal operations described above. However, much simpler methods have been used which obtain roughly the same results. Tyrrell has adopted two different resampling methods into his model. The first method is called “alpha blending” (AB), which is a simple technique of literally blending the boundaries of each quilting block together. The main drawback of this approach is that this blending process has the potential to introduce anomalous spectral curves. The other resampling method used by Tyrrell is the minimum boundary error cut, or simply the “minimum-cut” (MC) technique. This is a more detailed procedure whereby the optimal boundary between blocks is more carefully chosen by expressing the boundary error as a cost function. This cost function is defined as:

$$C_{i,j} = |S_{i,j} - B_{i,j}| \quad (18)$$

where  $C$  is the cost,  $S$  is the synthesis region, and  $B$  is the current block region. The minimum-cut technique is analogous to the familiar single source-shortest path problem in which the distance from a single start node to each node in a graph structure is determined. Tyrrell has adopted a multi/hyperspectral variant of an algorithm that solves this problem called Dijkstra’s algorithm, which is presented in detail in Tyrrell [2002]. Note that for both of these methods, the blending or cutting is propagated over all spectral bands.

### 3.3.3.2.3 Preliminary Results

Some preliminary results have been obtained with both the S/P and Quilting techniques using Brodatz sample textures. Note that these results were obtained by running Tyrrell’s raw S/P and Quilting codes on false textures, before the incorporation of Tyrrell’s Texture Synthesis model into DIRSIG. The examples shown below extend 128x128-pixel ASCII Portable Gray Map (PGM) and Portable Pixel Map (PPM) sample textures into 256x256-pixel synthetic textures. Note how the quilting boundaries are visible in some

cases, especially in Figure 32. The default quilting region size of 16x16 pixels was used for these examples.

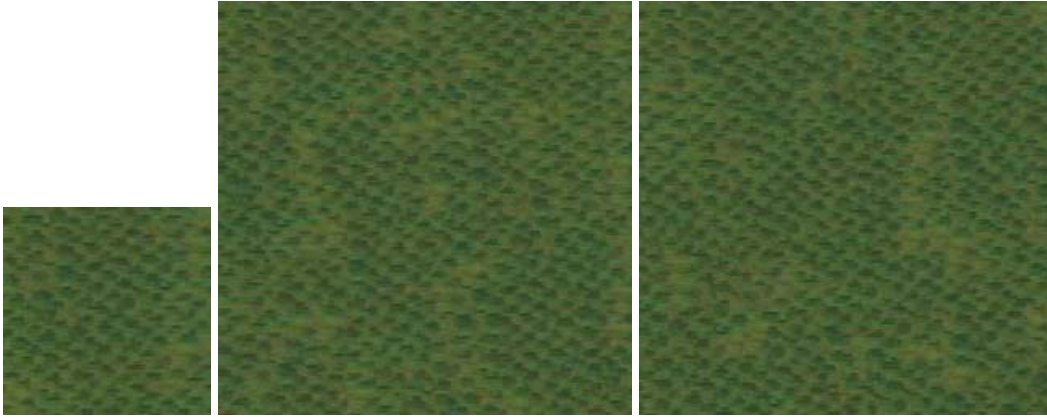


Figure 29: (left to right): Sample image (patches), AB quilting, MC quilting.

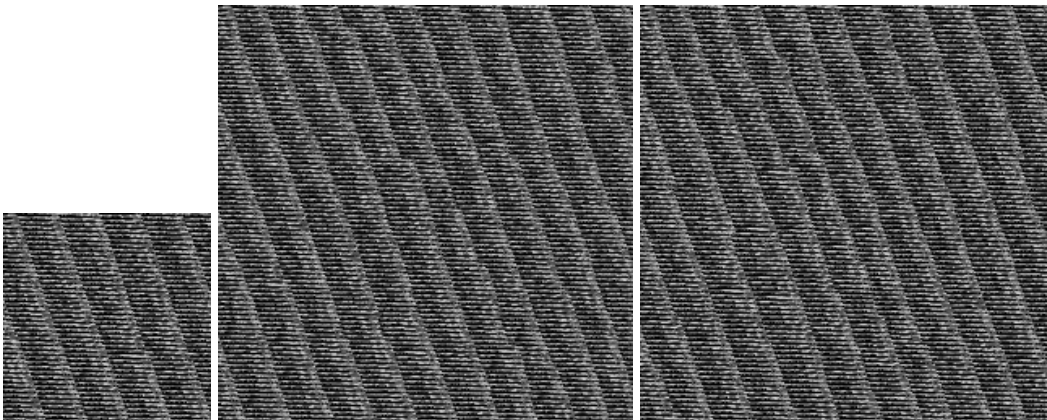


Figure 30: (left to right): Sample image (presscloth), AB quilting, MC quilting.



Figure 31: (left to right): Sample image (trees), AB quilting, MC quilting.

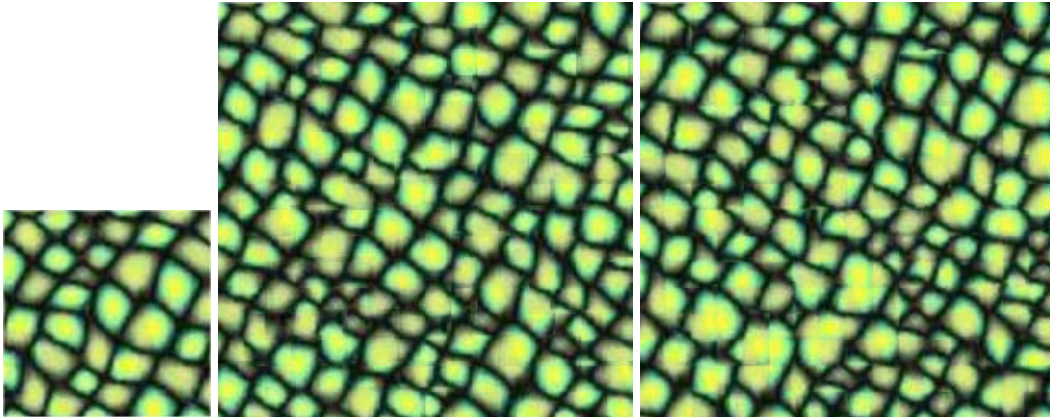


Figure 32: (left to right): Sample image (reptile), AB quilting, MC quilting.

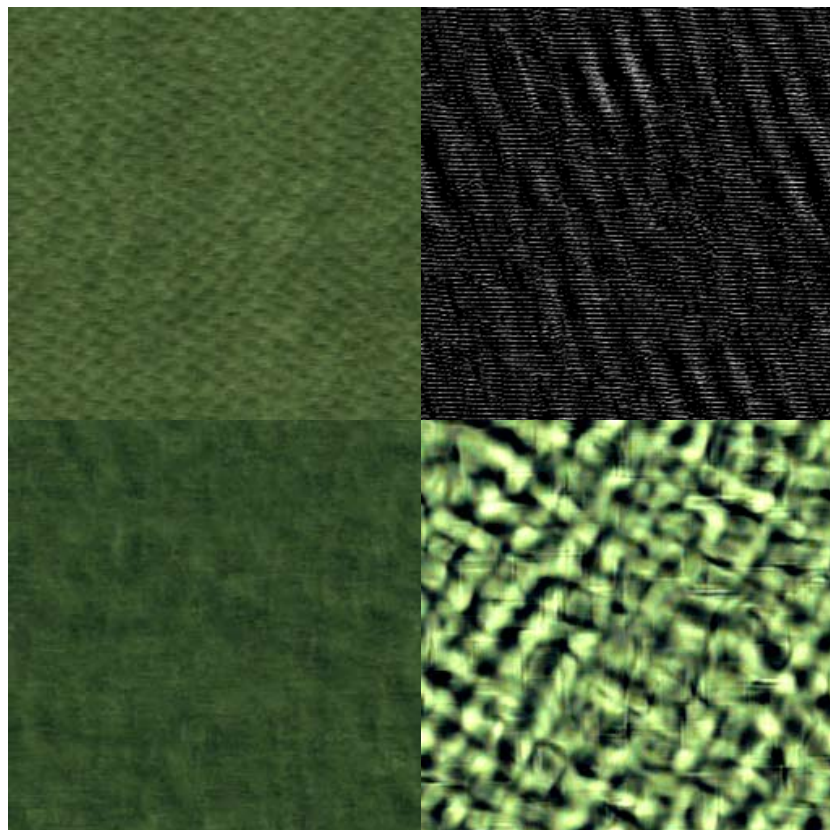


Figure 33: Results from Tyrrell's S/P model for the same sample textures as Figures 29-32.

It is clear from these examples that the S/P model is able to handle natural textures such as the trees and patches much better, while the presscloth and reptile textures, which contain larger repeating structural textures, are not reproduced as well as in the quilting model. Therefore, a rather surprising preliminary result from Tyrrell's synthesis models has been obtained in that, despite the simplicity of the quilting technique, it seems to achieve more visually accurate texture synthesis results over a broad range of textures than the more sophisticated S/P approach. However, these models will be tested in a much more quantitative manner in this work for natural textures occurring in remotely sensed images, so it is not wise to prematurely conclude that quilting will produce better radiometric and statistical results. Further, given the preliminary discussion on the texture synthesis models that has been presented thus far, one might surmise that an immediate advantage of using a texture synthesis model as a texture characterization tool in DIRSIG, is that the aforementioned practical issues involved with obtaining and using large databases of sufficient material spectral reflectance curves (as for the SBP and MBP models) can be avoided and/or augmented by generating synthetic texture directly from sample texture images through the techniques explained above. However, if one opts to create synthetic texture directly from input texture samples while foregoing the use of ground truth reflectance curve databases, then one requires real hyperspectral imagery (HSI) data at the same (or better) spectral resolution and coverage as the output image to be rendered in DIRSIG. Therefore, it would be ideal to be able to use a less restrictive version of the texture synthesis models described above such that more flexibility is offered when constructing DIRSIG scenes. For instance, a model that is capable of reading in ground truth spectral reflectance curves of material types present in the scene to be rendered as supplemental data to a few primary input texture image samples (that do not have to span the entire spectral range of the output DIRSIG image) would be more practical in its DIRSIG-implemented form. This suggestion was made to Tyrrell, and was the motivation for the Spectral Expansion texture synthesis model that is presented in the following section.

#### **3.3.3.2.4 Spectral Expansion Texture Synthesis Model**

This latest incarnation of Tyrrell's texture synthesis models is derived from the S/P model ideology. The Spectral Expansion model has the capability of taking in either a single or a few user-specified spectral bands from the input real texture image. This "principal band (or bands)" is then used in order to create a primary synthesis band of synthetic texture using the S/P model described earlier. However, the method for synthesizing the remaining spectral bands is quite different in this case. Instead of using a complex spectral resampling technique, this model can accept spectral reflectance curves (derived either directly from the input real image or from ground truth measurements), and construct an output synthetic texture image cube by enforcing the spectral covariance statistics of the reflectance curves. Therefore, the output will be at the spectral resolution of the input spectra (or at the resolution of the input image if the entire image is used as the input spectra). It is interesting to note that, due to the nature of the model, the spectral covariance statistics of the output synthetic texture images are guaranteed to be correct, as long as the spectral reflectance curves used by the model are accurate and reliable. The details on how this texture synthesis model has been incorporated into DIRSIG are presented in Section 4.2.

#### **3.3.3.3 Texture Synthesis Model Performance Evaluation**

The problem of quantifying how well a texture model reproduces texture is very complex, and thus most of the literature only judges the quality of the synthesized texture based on perceptual closeness. As stated earlier, this merely equates to the two images having the same first- and (arguably) second-order statistics if the human observer is unable to pre-attentively distinguish between the two. But it has been repeatedly demonstrated that two images can possess the exact same first and second order statistics, as well as other marginal statistics, and still have largely different texture features and patterns. In short, there has been no work focusing on the mathematical and radiometric correctness of synthetic textures in relation to their truth image counterparts, and there is definitely a need

for a robust, quantitative method to do so. This is not even to mention whether spectral fidelity has been preserved; in fact, there is no way to rigorously test both spatial and spectral aspects of synthetic textures without implementing quantitative performance metrics to compare with corresponding real imagery. This necessity is being addressed in this research for texture synthesis of remotely sensed images using the above synthesis techniques and others, through the use of a set of spatial and spectral textural feature statistics and similarity metrics to be described in detail in Section 4.

### **3.3.4 Fraction Map (FM) Texture Characterization Model**

The fourth and final texture characterization model to be tested in this research uses a drastically different approach to creating spatial and spectral variability. It is derived from the concept of unmixing hyperspectral imagery (HSI) through the use of end member selection tools to drive the production of fractional abundance maps for each end member in the particular scene. There are a few well-known algorithms that will perform this task, such as the Pixel Purity Index (PPI) algorithm [Boardman et al., 1995], N-Finder [Winter, 1999], and the Maximum Distance Method (MDM) [Lee, 2002], as well as other simple image-derived methods.

The chosen end-member selection tool for this research was image-derived by defining regions of interest (ROIs) within the ENVI processing environment. This was performed for both the real HYDICE ARM imagery and the CitiPix imagery, despite the fact that the latter is only an RGB image. For each scene, a decision was made regarding the number of principal end-members to keep for the texturing process. This was based on the achievement of “clean”, distinct fractional abundance maps when using the Linear Spectral Unmixing (LSU) tool in ENVI. Once the principal end-members had been chosen, the final fractional abundance maps of each of the end-members were constructed. Note that these steps are specific to the imagery being rendered here, and that any end-member selection tool and unmixing routine can be used to generate the fraction maps when using this texture model (more details of the implementation of this model are presented in Section 4.2).

Theoretically, a linear combination of the principal end-members in accordance with their respective fractional abundance maps will provide a near-complete representation of the original image. This concept is illustrated in Figure 34.

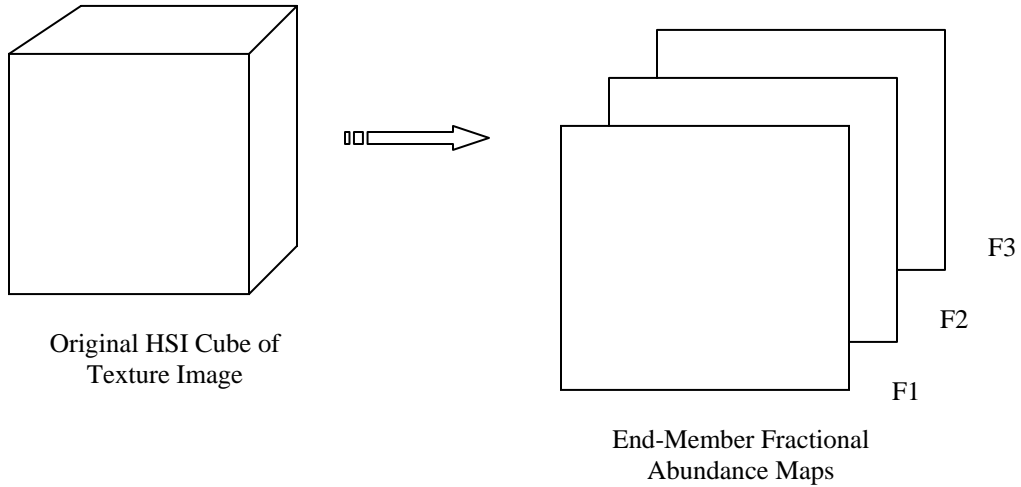


Figure 34: Extraction of end-member fractional abundance maps from original HSI texture image.

Consider the simple case of only three end-members, with corresponding fraction maps  $F_1$ ,  $F_2$ , and  $F_3$ . In this case, the three end-member spectra are considered as basis vectors representing the original image, called  $B_1$ ,  $B_2$ , and  $B_3$ . We can then express a linear combination of these basis vectors, plus a residual error to be the original image  $\mathbf{R}$ :

$$\mathbf{R} = \sum_{i=1}^3 \mathbf{B}_i \mathbf{F}_i + \mathbf{e} \quad (19)$$

where the residual error accounts for the fact that only the principal end-members have been chosen. This error is usually expressed as an RMS error fraction plane in most unmixing programs.

DIRSIG has been modified to have the capability to produce as many end-members as specified in the input fraction maps per pixel in the DIRSIG output image. Therefore, for each of the images to be rendered in DIRSIG, end-member selection and fraction map production in reflectance space must be completed. The input into the construction of

fraction maps can be either the real counterpart image which is to be constructed in DIRSIG, or if one wishes to expand the spectral coverage in the DIRSIG image over that in the input image, then the sensor platform (in the DIRSIG configuration file) can be modified to produce output imagery at user specified spectral bandwidth and extent. This is accomplished by first creating fraction maps using the input imagery that is available. Then, each fraction plane is assigned a nominal reflectance spectrum that is representative of the spectral character of the material type. In order to extend spectral coverage, the ground truth reflectance curves must exceed the coverage of the original input image. Lastly, the sensor's spectral response must be adjusted so that one can obtain the desired spectral extents in the output imagery. This model differs from the SBP and MBP models in that the spatial and spectral variability is not derived from variability within the ground truth data for each material type. Rather, variability is introduced by literally re-mixing the entire set of fraction maps with the nominal reflectance spectrum coupled to each respective end member fraction plane. This model does not use the two-tier system of material and texture maps; the spatial structure is introduced by assigning each pixel with a fraction of each end member that has been calculated in the unmixing process, while spectral structure is provided by the spectrum assigned to each end member. Figure 35 shows an example of the case of three principal end members (and thus three fraction maps). For each pixel in the output DIRSIG image, fractions of each end member are assigned according to the fractions present in the multi-band fraction map image. This can be envisioned as the superposition of the fractional abundance planes being applied on a pixel-by-pixel basis to the output DIRSIG image. This concept is consistent with equation (19), in which a linear combination of the end member fraction maps produces a close approximation to the original image, within residual error factor  $\mathbf{e}$ .

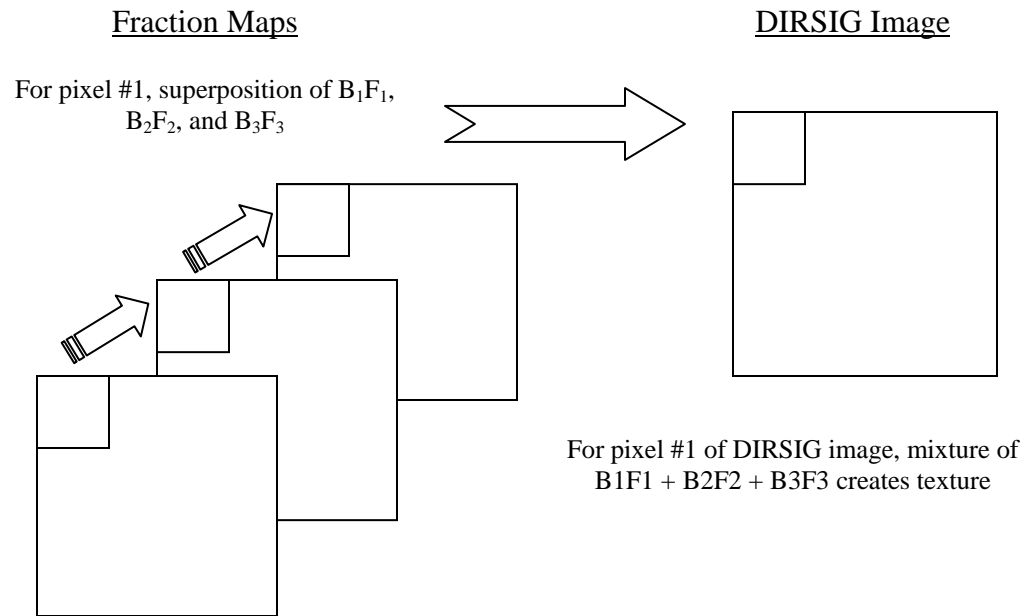


Figure 35: FM Texture Characterization Model. On a pixel-by-pixel basis, the fraction maps corresponding to each end member are re-mixed in order to create spatial and spectral variability in the resultant DIRSIG image.

The above figure illustrates how each pixel in the output DIRSIG image is a linear combination of each of the constructed end member fraction maps, and the weighting of each end member is determined by the fractions in each plane. It is worthy of mention at this point that in the DIRSIG version of the FM model, different mixing models and texture maps can be used for each material map region. In fact, the user has the option of choosing which texture characterization model to use on a per material class basis.

This concludes the background theory and literature review that is necessary to be presented for this research. The following chapters will discuss the experimental design and methodology (in Chapter 4), after which the results and analysis of the performance of each of the four texture models is presented in Chapter 5.

## 4. Experimental Design and Methodology

### 4.1 Experimental Design Overview

The following flowchart provides a summarized view of the experimental design to be followed in this research:

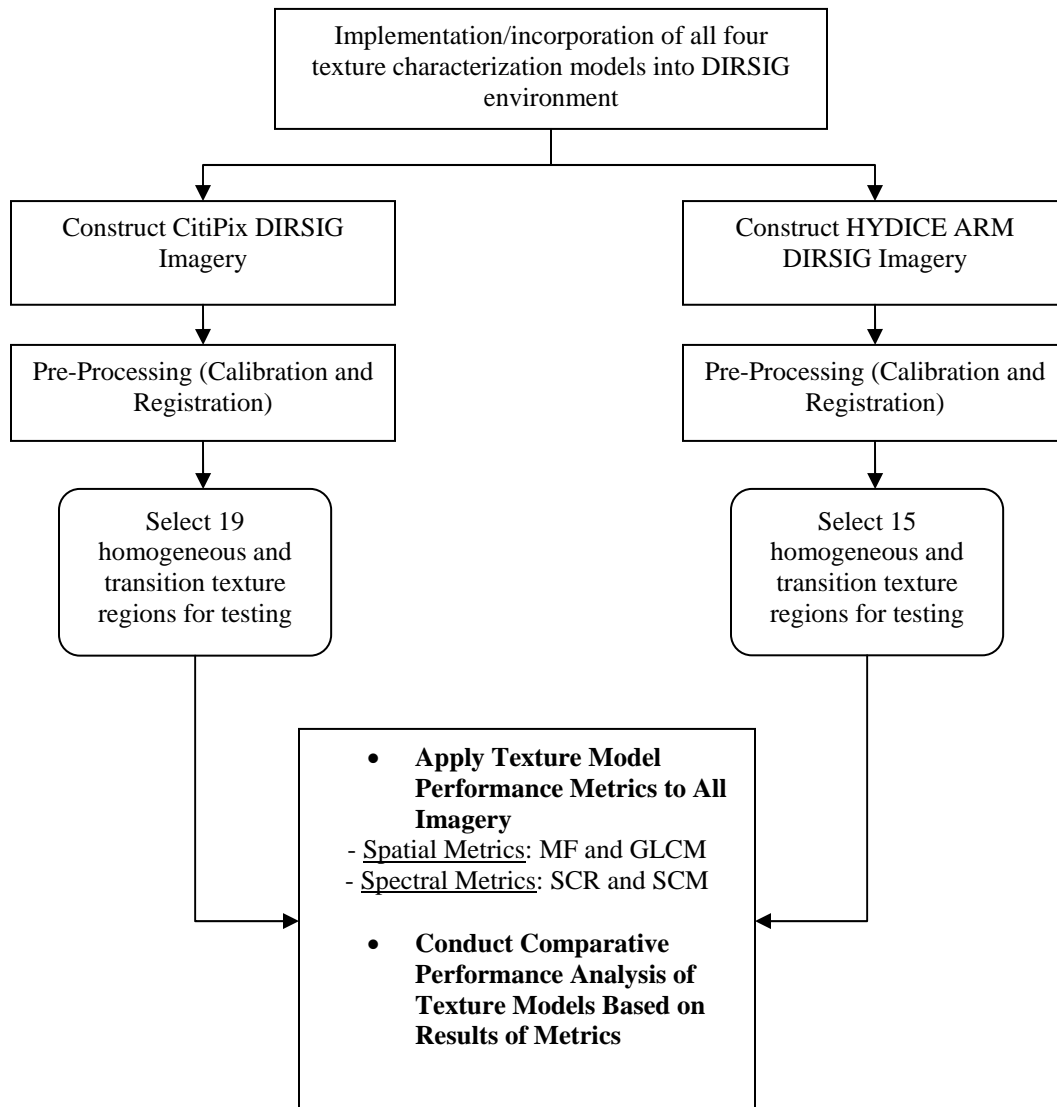


Figure 36: Experimental Design Summary.

## 4.2 Implementation of Texture Models

This section details the practical issues of implementation and/or incorporation of the texture modeling algorithms (as necessary) into the DIRSIG environment. Each model required differing degrees of achieving compatibility with DIRSIG, since some models have been used in the past in similar forms, while others have never been attempted for use within DIRSIG. Details regarding the modifications that have been made to existing DIRSIG texture models are also presented.

### 4.2.1 SBP and MBP Models

Section 3.3.1 presented the SBP model as the default texture characterization model that has been used for the majority of past DIRSIG rendering efforts. Therefore, there was not a requirement for the SBP model to be “incorporated” per se, since it already existed within its data structure. However, two improvements were eventually made over the baseline model in order to overcome apparent shortcomings of the model that were discovered when rendering the HYDICE ARM DIRSIG imagery. These slight modifications are discussed in further detail in Chapter 5, but they are worthwhile to mention here, since these steps have affected the incorporation process for both the SBP and MBP models. The first new capability of the model is useful when the ground truth reflectance curves do not adequately represent the true spatial variability of materials present in the scene to be rendered. A utility was written in order to create image-derived ground truth reflectance curves into the DIRSIG-compatible emissivity file format. These new curves can be used to create more realistic spatial (and spectral) structure, since it effectively extracts data present in the original real scene, and enforces it into the statistics of the synthetic scene. The results of using such data will be illustrated in Chapter 5. Of course, this is only of limited utility since one would need to have real imagery of the same spectral *extent* as the output DIRSIG image; however, it does not necessarily have to be at the same spectral *resolution*, since DIRSIG has the capability to interpolate between wavelength values. The second improvement is more significant and fundamental. It became customary over the past several years to extract a spectral subset of the corresponding real imagery to be

rendered in DIRSIG and use a single band (or multiple bands in the case of the MBP model) as the texture map. The problem with this approach is more apparent when dealing with a scene that has a multimodal distribution. Recall that the SBP and MBP Z-Score Selection algorithms are based on comparing z-scores for the texture maps and reflectance curves for each material class present in the first-tier material map. Since this is performed on a per-material-class basis, then the texture images should ideally be unimodal, or at least exhibit the same type of distribution as the family of reflectance curves for each material type, otherwise the mean and standard deviations that are calculated will skew the z-score computations for the texture map as compared with that of the material reflectance curves. This concept is illustrated in Figure 37.

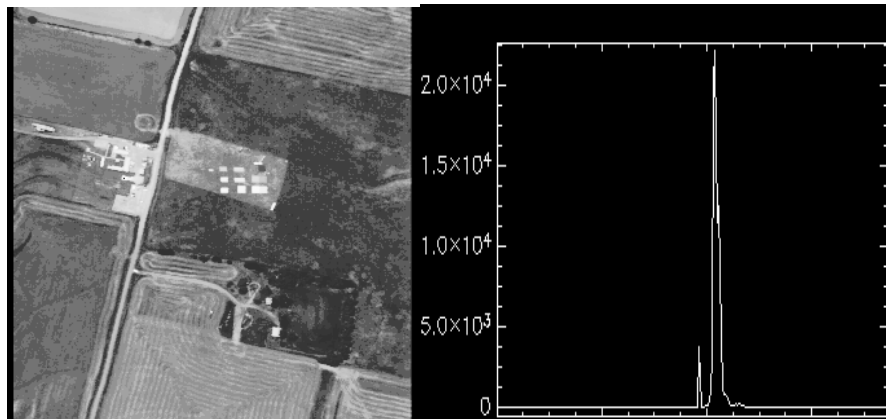


Figure 37: The histogram (right) resulting from using a single-band image as the DIRSIG texture map (left). Bi- or multi-modal distributions can skew the z-score statistics that are integral to the SBP and MBP texture characterization models.

In order to remedy this, the concept of using “masked” texture images was initiated. In this case, one can be more certain that we are comparing “apples with apples” for the z-score comparison step of the algorithm. So for example, if the first-tier material map contains 8 material classes (see Figure 38), then the DIRSIG configuration file for the scene to be rendered will have to be modified to read in 8 separate texture maps, each representing a material class from the material map. These masked texture maps can be constructed by applying precise masks to the single-bandpass texture image, which means that instead of

having just one texture map for the SBP model, there would be 8 texture maps (from the single bandpass) listed in the texture map section of the configuration file in this case. For the MBP model, in the case that one uses three texture image bandpass regions and there are 8 material classes present in the material map, then a series of 24 masked texture maps would have to be used.

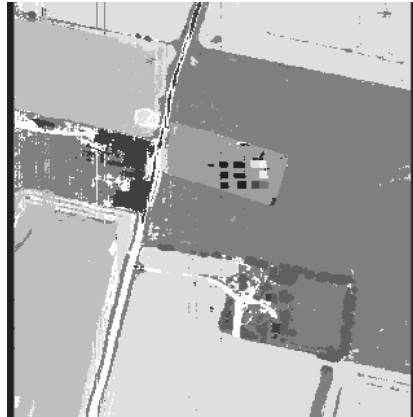


Figure 38: Sample Gaussian Maximum Likelihood (GML)-derived material map image for the HYDICE ARM data.

The option to ignore a user-specified digital count (DC) range has been implemented into DIRSIG so that the masked texture image (such as the one shown in Figure 39) will only have nonzero DC values read by DIRSIG. Therefore, by ignoring the  $DC = 0$  values, the statistics will not be skewed by the masked out regions of the texture image, and thus the mean and standard deviation for each texture image will be based solely on the material type of interest.

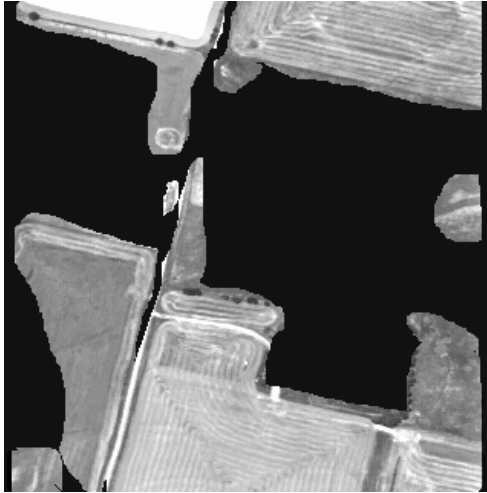


Figure 39: Example of a “masked” texture map for the plowed field region of the HYDICE ARM image. Using this coupled with the “ignore DC range” parameter in the DIRSIG configuration file will permit unimodal distributions and more accurate statistical computations.

In terms of incorporation of the MBP model, it requires only some slight modifications to the DIRSIG configuration file over that of the SBP model. The texture map section requires a list of the texture images and their corresponding bandpass regions to be used when comparing z-scores of the texture maps and reflectance curves for each material class. As discussed in Section 3.3.2, this model has been attempted in the past works by Burtner (2001) and Kennedy (2002), so implementation efforts were relatively simple for the MBP model. The resulting DIRSIG images for both the CitiPix and HYDICE ARM imagery are presented in Sections 5.1 and 5.2 respectively.

#### **4.2.2 Texture Synthesis Models**

As presented in Section 3.3.3, Tyrrell constructed C++ code initially for creating texture synthesis models using the S/P technique and the simpler image quilting technique. Although the results were impressive based on pre-attentive visual analysis, there was a requirement to obtain a more flexible version of these models so that the restrictive necessity of having HSI data at (or finer than) the desired spectral resolution of the output DIRSIG image could be alleviated. The reason for wanting to avoid this situation is because we often

construct SIG images so that we can easily alter spectral properties such as coverage and resolution, and not be confined to the limits of counterpart real data that we use for rendering synthetic scenes. After all, if we could only synthesize out to the extent to which we have real image data, then we may as well simply use the real data itself. The revised model came in the form of the Spectral Expansion Texture Synthesis Model that was introduced in Section 3.3.3.2.4.

The original plan was to test the S/P and Quilting models separately, but due to the concerns explained above, the S/P model was replaced by the Spectral Expansion model, since it uses the same basic synthesis step, and they differ only in the flexibility offered by the latter model for creating expanded spectral coverage to generate the spectral bands of the synthetic texture cube. The Quilting model was also used to generate texture for certain regions of both the CitiPix and HYDICE ARM DIRSIG imagery, since it is able to synthesize textures given smaller input texture image sizes. Thus, both the Spectral Expansion and Quilting models are tested under the umbrella of the “Texture Synthesis” model in this research (note that, however, the Spectral Expansion model was used for most texturing since the utility for long-term use of the Quilting model in DIRSIG is minimal). Chapter 5 will describe in more detail which regions of the Texture Synthesis-derived DIRSIG imagery were textured with either Quilting or Spectral Expansion methods.

As mentioned above, there are limitations for all of the texture synthesis models in terms of the required size of the input texture image required to generate the output synthetic texture images. The S/P and Spectral Expansion models require square input samples of at least 64 x 64 pixels, in increments of powers of 2 (e.g., 128 x 128, 256 x 256, 512 x 512, etc. only), while the Quilting model requires a minimum size of 32 x 32 pixels, with the same dyadic requirement. Of course, one must keep in mind that the synthesized textures tend to exhibit better visual and statistical fidelity when larger input samples are used, since more information about spatial structure can be obtained from a larger spatial sample, and the statistical measures used to synthesize textures are based on a more accurate representative sample from the real counterpart image.

In order to characterize texture in DIRSIG using the Texture Synthesis models, real texture samples were extracted carefully from both the CitiPix and HYDICE ARM imagery. In some cases, it was possible to obtain samples of size 64 x 64 pixels and larger. For these samples, synthetic textures could be generated immediately using the Spectral Expansion model. For reasons that will be discussed shortly, it was essential to have these texture samples in reflectance units, since DIRSIG was to read in the synthetic texture cubes in “reflectance map” mode. Thus, all pre-processing such as calibration of the original imagery had to be completed before these steps were taken (more pre-processing steps are presented in Section 4.4). In cases for which obtaining samples of 64 x 64 pixels directly from the real imagery was not possible, one of two courses of action were taken. First, for the regions to be tested using the Quilting model, it was ensured that the sample size was no smaller than 32 x 32 pixels. If this was the case, then Quilting was used to generate synthetic texture for that material type. If the sample was not large enough for Quilting, then the largest possible sample for the material type was taken (such as for the road and trees in the HYDICE ARM imagery). A utility was then used to “mirror” the texture samples so that the texture samples could be “grown out” to larger spatial sizes, as specified by the user. These regions were expanded to the minimum size of 64 x 64 pixels so that the Spectral Expansion model could be employed to create texture images for these materials. The reason that they were not expanded further is because the mirroring process tended to introduce repetitive artifact patterns that were not present in the original image, and so in order to minimize this effect, the smallest acceptable output size was used. An example of such a case where these artifacts appeared is shown in Figure 40.

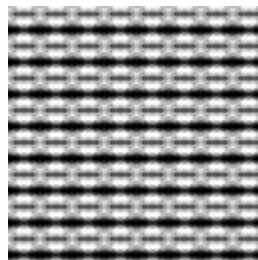


Figure 40: The result of growing out an 8 x 8 region of road to 64 x 64 pixels.

The above example illustrates the worst case of this “artifacting” encountered in this work. Since the road in the HYDICE ARM image is very narrow, the smallest possible sample size was 8 x 8 pixels. Unfortunately, very small portions of the bordering fields were also captured in this sample, which explains the repetitive darker patterns in the above figure. However, this was the best result obtained, even using smaller input sizes for the mirroring process. The results of this anomaly are evident in section 5.2.3, where the results for the HYDICE ARM DIRSIG imagery using the Texture Synthesis model is presented.

The number of synthetic texture cubes to produce for both the CitiPix and HYDICE ARM imagery was determined by the number of material classes present in the GML-generated material map for each image. For example, the HYDICE ARM material map (Figure 38) has 8 material classes:

- a. Plowed field;
- b. Uncut Pasture;
- c. Wheat;
- d. Cut Pasture;
- e. Trailers/Buildings;
- f. Road;
- g. Trees; and
- h. Calibration Panels.

For each of these classes (except for the calibration panels, which were textured using the SBP model so that calibration would be more precise), the best possible input texture sample was extracted from the real image, such that the spatial structure and variability could be captured in the output synthetic image. The calibration panels were much too small to obtain adequate synthetic texture versions, and since calibration to reflectance units is critical

for this work, they were textured using the SBP model for all HYDICE ARM DIRSIG images.

For the CitiPix image, 8 material classes were used (see Figure 41). They are:

- a. Green Grass;
- b. Brown Grass;
- c. Dirt;
- d. Trees;
- e. Asphalt;
- f. Bright Rooftop;
- g. Dark Rooftop; and
- h. Baseball Dirt.

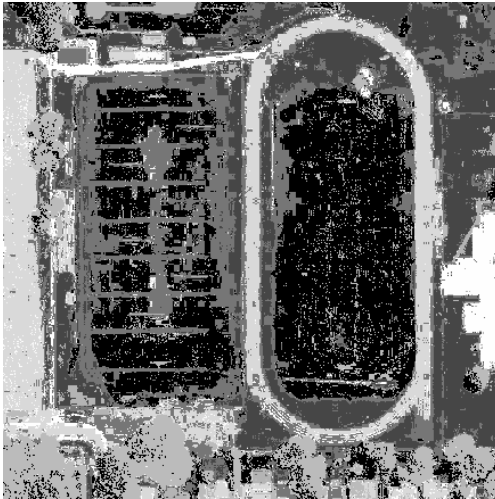


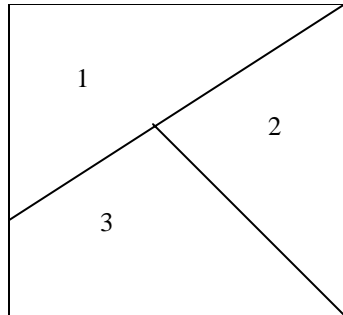
Figure 41: GML-derived material map for CitiPix data.

The reason for including material classes that do not make up significant portions of the image, such as baseball dirt and rooftops, is because they were used for the bright and dark points in the Empirical Line Method (ELM) calibration to reflectance units (more of this is presented in Section 4.4). Since there were no calibration panels present in the CitiPix image to be rendered, in-scene material samples had to be used for ELM calibration. In the same manner as with the HYDICE ARM image, input texture image samples were extracted directly from the CitiPix image in order to create output synthetic textures in RGB-space.

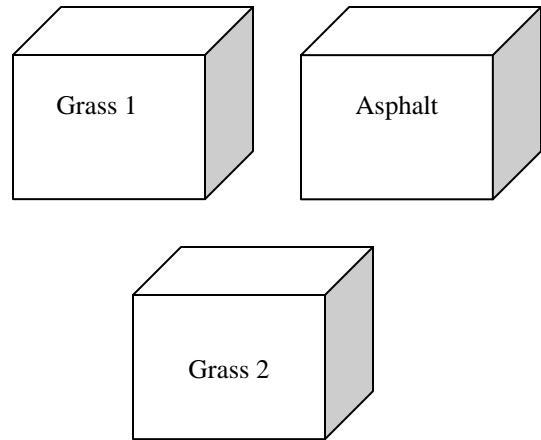
Again, details regarding which of the texture synthesis models were used for which material type are presented in Chapter 5.

As mentioned previously, DIRSIG was able to accept the synthetic reflectance cubes for both the CitiPix and HYDICE ARM imagery as long as the “maps” section of the DIRSIG configuration file was set to work in “reflectance map” mode instead of the more common “texture map” mode that is used for the SBP and MBP models (incidentally, DIRSIG works in “fraction map” mode for the FM model to be discussed in the next section). By working in “reflectance map” mode, the expanded synthetic texture cubes are projected onto the material map via a look-up-table (LUT). This LUT is inserted into the configuration file so that the synthetic reflectance cubes can be paired up with their respective material types present in the material map. The reflectance map algorithm then works essentially as a “cookie-cutting” mechanism by inserting each of the synthetic texture *reflectance maps* into the output DIRSIG image, in accordance with the material map indices assigned to each reflectance map in the LUT. This is illustrated in Figure 42.

Material Map



Texture Synthesis Cubes (not to scale)



LUT:  
1 = Grass 1  
2 = Asphalt  
3 = Grass 2

Output DIRSIG Image:

Each synthetic texture cube is projected onto the material map according to the LUT

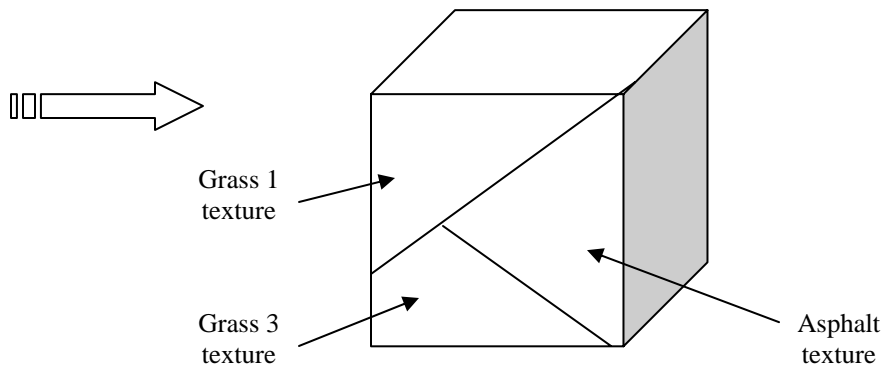
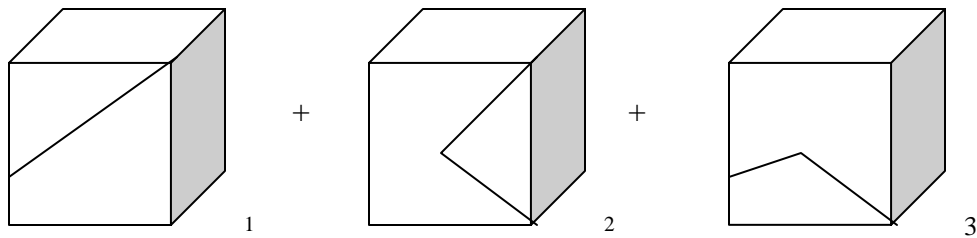


Figure 42: Incorporation of Texture Synthesis model into DIRSIG using reflectance maps.

Figure 42 shows the simple case of 3 material classes in the material map. The three indices in the material map correspond to the material types Grass 1, Asphalt, and Grass 2 as per the LUT in the figure. Each synthetic texture cube is then projected onto the material map in order to texture the DIRSIG image. Only the portions of the synthetic texture reflectance cubes that overlap with its corresponding material index are retained, which effectively creates texture within and between material types. The spectral information is carried along in each synthetic texture cube that was created using either the Spectral Expansion or Image Quilting texture models. The reflectance maps of synthetic textures in this research were constructed such that they exceeded the spatial size of the output DIRSIG image, and the insert point for each of the reflectance maps was carefully chosen so that the best-looking regions of texture would be used for each of the material types, and so that no gaps would occur at transition regions between material classes. The resulting DIRSIG images for the CitiPix and HYDICE ARM imagery are presented in Sections 5.1 and 5.2 respectively.

#### **4.2.3 FM Model**

The basic theory of the FM texture model was presented in Section 3.3.4, where Figure 35 illustrates an intuitive synopsis of how the model works. For both the CitiPix and HYDICE ARM imagery, fractional abundance maps of end members had to be constructed. For the HYDICE ARM image, 7 fraction maps were produced for the following end members:

- a. Cut Pasture;
- b. Plowed Field;
- c. Road;
- d. Trailers/Buildings;
- e. Trees;
- f. Uncut Pasture; and
- g. Wheat.

These end members were defined by defining ENVI Regions of Interest (ROIs) over large representative samples of each end member material type in the real image. Then, the Linear Spectral Unmixing (LSU) algorithm was used to create fraction maps. The decision to use this set of 7 end members and fraction planes was based on the achievement of clean, noise-free, optimally-separated fractional abundance maps with different combinations of spectral end members. Examples of three of the fraction maps are shown in Figure 43.



Figure 43: Sample HYDICE ARM fractional abundance maps. Top left: “Buildings” plane; top right: “cut pasture” plane; bottom: “uncut pasture” plane.

These fraction maps were used by the DIRSIG configuration file by changing the “maps” section to “fraction map” mode. Each fraction map is linked to an average spectrum representing each respective end member in order to ensure that both spatial and spectral re-mixing occur in the output DIRSIG image. These averaged spectra were derived from

regions containing each of the end members within the reflectance-calibrated real HYDICE ARM image. Thus the texture applied to each pixel using the FM model is literally a re-mixing of all seven fraction maps according to the fractional abundance contained in each fraction plane. The results for the HYDICE ARM DIRSIG imagery are presented in Section 5.2.

Since the CitiPix image only contains three spectral bands over the visible region of the electro-magnetic spectrum (in R, G, and B channels), it is not considered to be a hyperspectral image (HSI). Further, spectral unmixing is not always successful for images with so few spectral bands since the process of extracting endmembers can be difficult over well-correlated bands. As such, construction of fractional abundance maps is typically reserved for HSI data. Despite these potential difficulties, fraction maps were nonetheless produced for the CitiPix imagery as well. In this case, the best results for fraction maps resulted when using these four end members:

- a. Green, healthy grass;
- b. Brown, stressed grass;
- c. Asphalt; and
- d. Trees.

The four fractional abundance maps for the CitiPix image using this set of endmembers are shown in Figure 44. The same general methodology as for the HYDICE ARM image was followed in that average spectra were assigned to each fraction plane and re-mixed to create spatial and spectral texture. The results of the FM model for the CitiPix image are presented in Section 5.1.

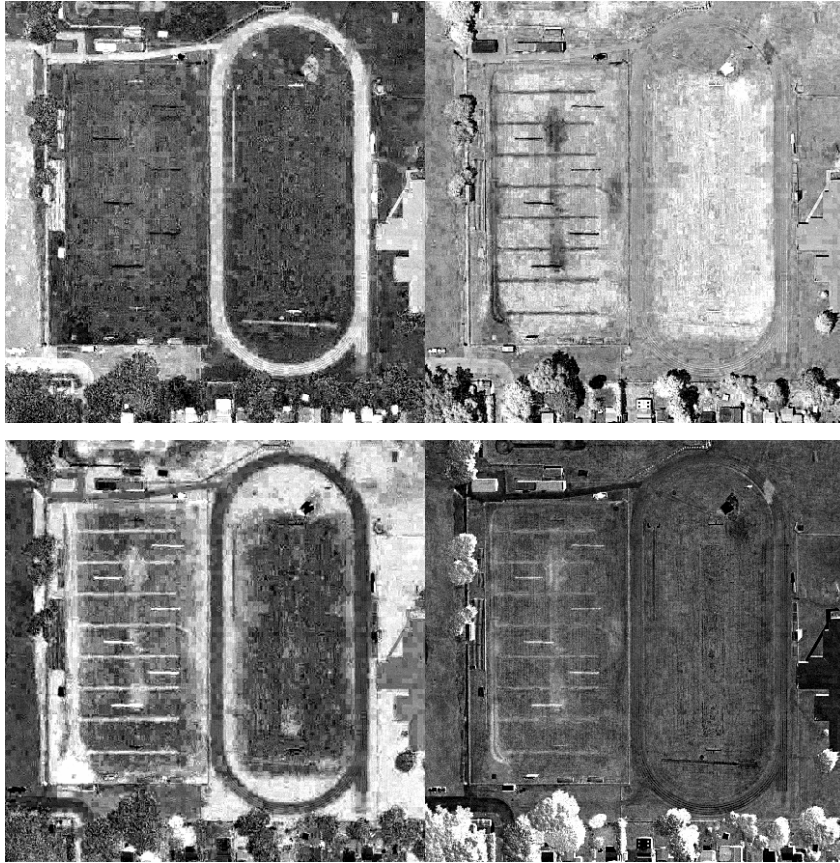


Figure 44: The four fractional abundance maps used for the CitiPix data. Top left: “asphalt/track” plane; top right: “green grass” plane; bottom left: “brown grass” plane; bottom right: “trees” plane.

### 4.3 Imagery To Be Rendered

The four performance metrics will be used to test the four texture characterization models on various homogeneous and transition texture test regions of two sets of imagery. Most texture synthesis models are tested at varying resolutions, as discussed in Section 3.3. This is because some models have been found to perform better at certain spatial resolutions than others. In maintaining this approach, the texture models will be tested at differing spatial *and* spectral resolutions in order to determine if performance depends somehow on either of these factors. As mentioned previously, the first data set to be used in this research is a subset of the Kodak CitiPix imagery over northern Rochester, New York, while the

second is from HYDICE ARM imagery captured over agricultural regions in Lamont, Oklahoma.

#### 4.3.1 CitiPix Imagery

The Kodak CitiPix data to be used in this research is a small subset of a much larger image collection effort over the northern Rochester area. The imagery has been captured using an airborne framing array camera using Kodak film. The images have been digitized into Red, Green, and Blue spectral channels that extend from 400 – 700 nm. The imagery to be used in this work was taken on June 1, 2001 at an altitude of 3.2918 km. The nominal GSD of this imagery is 0.15 m. A larger view of the area to be used in this work is shown below in Figure 45.



Figure 45: Portion of Kodak CitiPix RGB image over northern Rochester, NY.

The central region of the above image, containing two of the fields and the surrounding area, was used in this research as the real CitiPix image to be rendered in DIRSIG. It spans 437 x

437 pixels, and it was degraded to a GSD of 0.45 m, since it was intended to test the texture models' performance at a finer resolution of roughly 0.5 m, and a more coarse resolution of greater than 1 m (which is the case for the HYDICE ARM imagery). The CitiPix region to be used hereafter is shown in Figure 46.

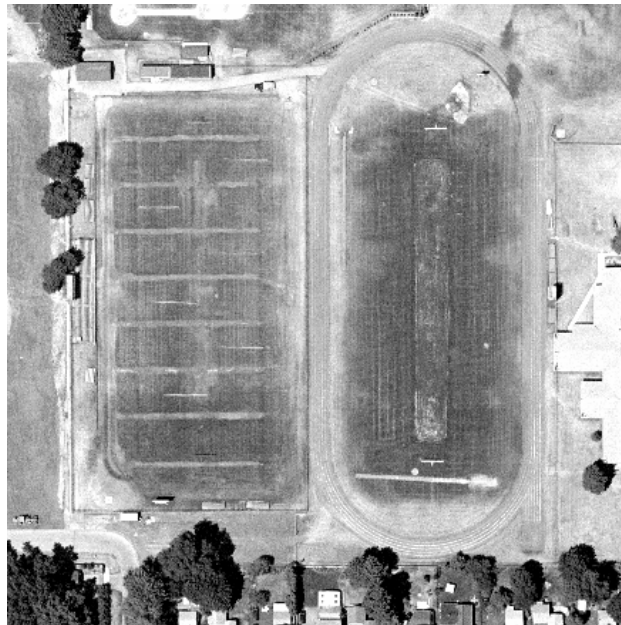


Figure 46: Red Channel of CitiPix image to be used for DIRSIG rendering and texturing using all four texture characterization models in this research.

This image was chosen since it is an ideal candidate for testing of both homogeneous and transition region textures. There are elements of many common textures present in this image including healthy grass, stressed grass, asphalt, trees, rooftops, and many more. As for transitions, there are within-material class transitions such as the lines on the field, the transitions between worn and healthy grass, between the field and the running track, and between the asphalt parking lot and the field. This imagery was used in conjunction with ground truth spectral reflectance data that was gathered by the Digital Imaging and Remote Sensing (DIRS) group at RIT in June 2001 and June 2002. The results of DIRSIG rendering of this scene is presented in Section 5.1, and the 19 texture regions selected for testing the texture models with this imagery are described in detail in Section 4.5.3.

### 4.3.2 HYDICE ARM Imagery

The second set of imagery to be used for this work consists of data with a much larger spectral extent and a different spatial resolution. There are several runs of HYDICE ARM data that were captured in June of 1997, under varying atmospheric conditions. In the past, Run 29 has been used for many studies due to the lack of cloud cover, and the fact that it has calibration panels visible in the image. A subset of Run 29 was used for this work, and it is shown in Figure 47.



Figure 47: Band 20 of HYDICE ARM imagery to be used for DIRSIG rendering and texturing using all four texture characterization models in this research.

This subset is 320 x 320 pixels in size, with a GSD of 1.7375 m. The data was collected using the airborne HYDICE imaging wedge spectrometer flown at an altitude of 3.475 km, which has spectral coverage between 400 – 2,500 nm in 210 spectral bands. This image was chosen for this research due to its simplicity. For example, there are several open regions of cut and uncut pasture, wheat, trees, and plowed field regions that exhibit interesting spatial structure. There are also ideal transition regions to be tested, such as those between cut and uncut pasture, roads and pastures, pastures and plowed fields, wheat and roads, and several

more possibilities. It is also favorable to have the calibration panels present within the image for pre-processing considerations, and for ensuring an accurate ELM calibration to reflectance units for both the real and DIRSIG imagery. This imagery was used in conjunction with ground truth collection data obtained by MTL during overflight [MTL, 1997]. The results of DIRSIG rendering of this scene is presented in Section 5.2, and the 15 texture regions selected for testing the texture models with this imagery are described in detail in Section 4.5.3.

#### **4.4 Pre-Processing Considerations**

There are a few practical considerations that must be addressed before the application of the texture metrics to be used for the comparative performance analysis of the texture characterization models in this study. First, the metrics to be used all assume that the real and synthetic images are at the exact same scales and resolutions, both spatially and spectrally. This is because all four of the metrics are effectively testing on a pixel-to-pixel basis. It is important that corresponding pixels are being compared, or else the results of the metrics will be skewed. For example, the spatial Mean Filter metric literally computes the difference between real and synthetic mean texture filter values, while the GLCM and SCM metrics measure spatial and spectral correlation between specified neighboring pixels. The same applies for the SCR metric, for which the center pixel of the region to be studied is considered as the “signal.” Therefore, in order to be comparing “apples with apples”, it is very important to have the corresponding real and DIRSIG images registered and with the same pixel sizes. The spectral resolution and bandwidth must also be equal between the real and DIRSIG images for these metrics to be meaningful for similar reasons. Further, to ensure that the texture models are tested at varying resolutions, imagery at differing spatial and spectral resolutions have been chosen for use in this study, as detailed in the previous section.

Although the CitiPix and HYDICE ARM DIRSIG scenes that have been constructed simulate the exact same atmospheric and imaging platform parameters as those

in effect at the time of image acquisition, lingering scaling and brightness effects may exist between the corresponding real and synthetic images causing an effective gap between pixel values, even though the spatial structure may appear to be very close to the real image. In order to address this concern, a careful calibration process was necessary in order to ensure that: (a) both images are in the same domain of reflectance units, and (b) that the worst of the atmospheric effects are removed. Theoretically, this will avoid the problem of brightness and scaling effects causing the metrics to give misleadingly poor or false values. For example, consider the following brightness profiles for the real and DIRSIG images, respectively:

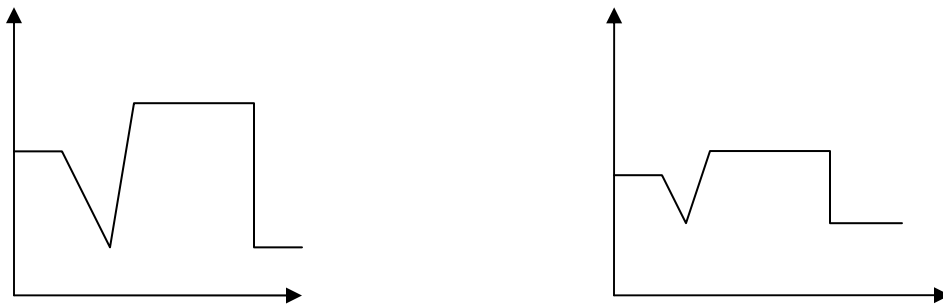


Figure 48: Structurally identical profiles that would be erroneously labeled as dissimilar due to brightness and scaling effects.

In this case, the metrics will likely indicate that the values are quite different for the given pixel, pixel pair, or pixel neighborhood in question. However, it is obvious that the structures of each of the profiles are identical, and that any dissimilarity detected by the metrics is owing to scaling or brightness effects. In order to be consistent, the Empirical Line Method (ELM) of image calibration was used to bring all sets of imagery into the reflectance domain. This alleviates concerns of comparing “apples with oranges”, since DIRSIG images are nominally produced in the radiance domain, while the real imagery used in this study are in raw digital counts (DC). The use of the ELM will require at least two targets (one dark and one bright) of known reflectance value present in both the real and DIRSIG images. A straight line is then fit to the data, thereby scaling both image data sets into the reflectance domain. As discussed in Section 4.3, this was a rather straight-forward

process for the HYDICE ARM imagery since the calibration panels were present in the image being rendered. Of course, reliable and accurate ground truth measurements are essential for the ELM calibration to be successful. The company responsible for ground truth collection for the HYDICE ARM imagery is MTL Systems, Incorporated, and they have provided this data in a very thorough report [MTL Systems, Inc., 1997]. This made the calibration process simpler, and thus produced very good results for ELM calibration using the 6-step grayscale calibration panels of 2, 4, 8, 16, 32, and 64% nominal reflectance values. For the CitiPix data, calibration was performed using in-scene materials for which ground truth data was available. The dark rooftops above the fields and the bright rooftops to the right of the fields, the baseball dirt, and the asphalt were used as calibration sources, due to their invariant nature. An inspection of the calibration factors plot and a visual analysis of scene materials between the real and synthetic imagery indicated a very good calibration result for both HYDICE and CitiPix data. Mean, variance, and standard deviation values were computed on a per-material class basis for all real and synthetic image pairs, and the values were within 2 reflectance units for all models, with some models being much closer than others. This will be discussed further in Chapter 5.

One further note on pre-processing requirements involves the HYDICE ARM data only. There were several noisy spectral bands in this image that were placed on a “bad bands list (BBL)” for all subsequent ENVI processing steps. This was necessary in order to perform a more accurate ELM calibration, and to construct noise-free fractional abundance maps. When all 210 spectral bands were used in the creation of the fraction planes, there would always be at least one plane that consisted mainly of noisy pixels. With the number of bands reduced to 142, the results were much better in terms of end member separability and minimal noise content, and some of these results have already been shown in Figure 43. Once all pre-processing tasks were completed and all 8 DIRSIG images were constructed (representing all 4 texture models on both the CitiPix and HYDICE ARM data), the texture model performance metrics were ready to be applied. To summarize once more, each of the metrics requires that the real and DIRSIG imagery are in the reflectance domain, and that

the corresponding real and DIRSIG imagery are exactly registered at the exact same scales. The following section describes in detail how the four performance metrics were implemented and applied to both the real and DIRSIG imagery in order to assess how well spatial and spectral texture has been characterized by each of the models.

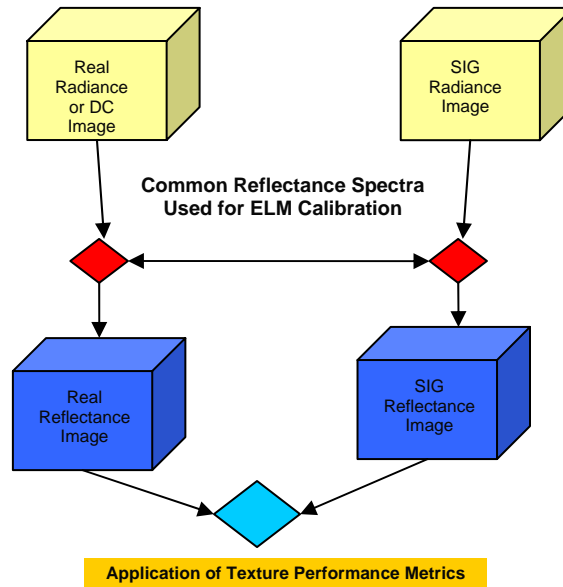


Figure 49: ELM calibration methodology utilized for CitiPix and HYDICE ARM real and synthetic image data.

## 4.5 Texture Model Performance Metrics

### 4.5.1 Spatial Domain

The fundamental hypothesis behind much of the proposed analyses to be conducted in this research is founded upon the results of the GLCM method in quantifying and differentiating image textures. As presented in Section 3.1.2.1, the consistently excellent results obtained by the GLCM approach to texture measurement, and the flexibility offered by the ability to adjust key parameters based on different textural patterns made this method the obvious choice of a quantitative measurement tool in the spatial domain. The conjecture is that, if the GLCM-derived statistics are able to discriminate between textural features such

that the best results are obtained in image segmentation, classification, and target detection applications, then the same method must be sufficient to measure the similarity of texture features between real and synthetic textures in a quantifiable manner. This is a sound argument since much of what DIRSIG synthetic images aim for in terms of fidelity is to be able to support the development and testing of algorithms for such applications, which represent the cornerstone of most remote sensing tasks. Therefore, if the texture measurements for the purpose of performance evaluation of different texture characterization models can achieve the level required for the accurate completion of these tasks that are based on textural features, then it follows that the GLCM approach forms an adequate spatial measurement of textural fidelity in DIRSIG synthetic images. The proposed GLCM testing methodology is described in more detail in Section 4.5.1.2.

Since this detailed GLCM analysis involves a potentially large set of input and output parameters, and because this analysis will be done on a band-by-band basis, the GLCM metric results were not always immediately obvious and thus large volumes of output data had to be sifted in order to produce the desired spatial texture metrics. Therefore, a simpler measure of spatial texture will also be performed. The method chosen for this analysis is the Mean Filter (MF) spatial metric, which was derived from the concept of the Composite RMS Error Metric (CREM) that was introduced in Section 3.3.2 when reviewing previous assessments of the SBP and MBP texture models [Kennedy, 2002], with the improvement being that spatial structure is accounted for using the MF spatial metric, while the CREM simply took the RMS error between pixel values summed over the entire image window. For both the CitiPix and HYDICE ARM real and synthetic data, texture regions to be tested were carefully selected in order to capture both homogeneous and transition region textures. In total, there were 15 regions used for the HYDICE ARM imagery, and 19 regions used for the CitiPix imagery when applying the texture model performance metrics. These regions are described in much more detail in Section 4.5.3.

#### 4.5.1.1 Mean Filter (MF) Spatial Metric

It was originally planned to use the CREM as a simpler spatial metric, since it offered the advantage of producing a single numeric value as its output to assess the overall spatial fidelity of the synthetic texture over the test region under investigation. The intent was to run this metric on all texture regions on a band by band basis, over a subset of representative spectral bands for HYDICE ARM data, and for all three bands of the CitiPix data. However, since this metric only takes the sum of the squared differences between each corresponding pixel in the real and DIRSIG imagery, there is no indication of spatial correlation and structure using this metric. Instead of producing one single output over the entire texture region, it was desired to produce separate outputs for neighborhoods of pixels so that the real and synthetic structural patterns were compared instead of single pixels. This was the initial motivation for using the MF spatial metric instead of the CREM. To further substantiate this decision, it is believed that this metric will not be as biased towards the SBP, MBP, and FM texture models. This is because each of these 3 models applies texture on a pixel-by-pixel basis, while the Texture Synthesis model creates texture by projecting synthetic texture reflectance map cubes onto the material map, which is not a pixel-by-pixel rendering process. Since the CREM only compares single pixels of real and DIRSIG imagery, and not groups of pixels at a time, the CREM would tend to produce misleadingly excellent results for the SBP, MBP, and FM models, while indicating poorer performance of the Texture Synthesis model. Thus the output produced by using the MF spatial metric was deemed to be more useful in discriminating texture model performance in the spatial domain.

Figure 50 illustrates a sample output of the MF spatial metric. The concept is to compare each of the selected texture test regions by passing a 3 x 3 mean filter through both the real and synthetic corresponding regions. The action of this filter is to compute the mean value of the 9 pixels that the 3 x 3 processing window is covering, and apply this value to the center pixel under the window. Therefore, the interim output of the MF metric is an image array that contains information about each 3 x 3 neighborhood as the filter passes through the test region. This retains local spatial structure information that was sacrificed

with the CREM, which merely compared individual pixels and produced a single output value. The output of the MF metric on the corresponding real and synthetic test region pairs were then compared by taking the difference image between the two. This absolute difference image was analyzed in order to determine how close (on average) each 9 pixel neighborhood was between the real and DIRSIG test regions. In addition to examining the *absolute* difference image for each of the texture test regions, a *variance-thresholded* difference image was also used in this analysis. The “acceptable variance” threshold was determined by extracting 2 to 3 additional texture test regions from the real CitiPix and HYDICE ARM imagery that adequately represent the variability observed for each homogeneous and transition region in its immediate vicinity. The variance of the multiple real image samples was then calculated in order to construct a variance threshold image. Finally, the absolute difference image between the real and DIRSIG texture regions was thresholded by the variance image for each texture test region in order to determine the number of outliers and where they were located. Figure 50 shows an example of MF metric outputs for the plowed field texture test region from a single band of the HYDICE ARM data. This illustrative example shows the MF metric result for the real image (left) and the DIRSIG image using the MBP texture model (right).

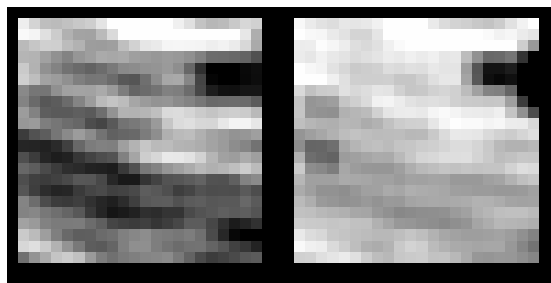


Figure 50: Sample MF metric outputs for band 20 of real HYDICE ARM image plowed field region (left) and for DIRSIG image using MBP texture model for same region (right). Notice the apparent similarity in these texture signatures.

The results of the application of the MF spatial metric to CitiPix and HYDICE ARM data are presented in Sections 5.3 and 5.4 respectively.

#### 4.5.1.2 GLCM Spatial Metric

The GLCM Spatial Texture Metric has been applied to the 19 CitiPix and 15 HYDICE ARM texture test regions of both real and synthetic imagery (representing all four texture models) in order to compare a selection of the GLCM-derived statistical features as listed in Section 3.1.2.1. Since, as mentioned previously, optimal combinations of typically 3 to 4 of these features has been proven to adequately discriminate between texture features to the level desired for most remote sensing applications, then the conjecture is that the same set of features will suffice for determining if real textures are effectively captured in DIRSIG-rendered imagery. These GLCM-derived statistical measures will in combination provide information as to whether the tested texture regions are significantly different in terms of spatial texture between the real and synthetic image, for each texture model. It was found that, in order to capture the properties of spatial textures in each of the texture test regions, three nominal GLCM features could be used. The features of Homogeneity, Contrast, and Correlation were found to be the most complete basis set that minimized redundancy, while effectively avoiding virtually unmanageable dimensions of data reported by the GLCM metric (see Section 3.1.2.1 for more details on GLCM texture features).

Due to the parametric nature of the GLCM, it is clear that the generated spatial GLCM metric for a given image region will depend on the input parameters chosen to compute the matrix. Therefore, different distance and angle parameters (or  $(\Delta x, \Delta y)$  parameters) have been used for different types of texture features so as to optimally capture the structure of the texture. This optimization has either been done by eye, based on apparent dominant scales and orientations of the particular texture being measured, or by the application of edge detection filters to identify the optimal direction vector  $(d, \alpha)$  to use for the GLCM computation. Most results in the literature also contend that typically the use of  $d = 1$  or  $d = 2$  is sufficient to capture the desired fine textural features for most aerial and satellite imagery [Clausi & Zhao, 2002]. It was thus decided that the nearest neighbors (i.e.,  $d = 1$ ) would be used to generate the GLCM texture features only, since it provides a more detailed analysis of spatial structure and correlation over the texture test regions.

An additional practical consideration is that the three main parameters (distance, angle, and window size) must be set consistently between the real and synthetic texture region under study so that the measurements provide the same meaning. By comparing the results of each of the GLCM-derived features within each band, one can surmise what aspect of the texture is or is not being captured in the synthetic version. Since the features represent slightly different theoretical and physical/visual meanings, it is sometimes possible to deduce where and how the synthetic texture may be lacking based on mismatch of the GLCM metric statistical features. This will be performed for all four texture models on various texture types and transition regions, and the analysis will in part be based on the “meanings” assigned to each of the main GLCM-derived statistical features presented by Baraldi & Parmiggiani (1995). For example, energy (f1) measures textural uniformity, while entropy (f9), contrast (f2) and variance (f4) tend to measure disorder, heterogeneity, and general differences between sets of contiguous pixels. Meanwhile, correlation (f3) is a measure of gray value linear-dependencies in the image region, where high values (i.e., close to unity) imply a linear relationship between the gray levels of pixel pairs.

While most GLCM analysis in the literature tends to quantize the number of gray levels so as to reduce the dimensionality of the matrix, this has not been performed in this work. Clearly, quantization of gray levels should be avoided for a study of this nature, since it has the potential to defeat the purpose of measuring small-scale textures within small windows. The typical reason for this quantization in most applications is because the GLCM analysis is performed image wide, and therefore each GLCM feature must be computed over the entire image, for all spectral bands. Since the windows to be used in this study will usually only contain a subset of the possible dynamic range and the GLCM features are only calculated over a certain region of an image, this quantization is deemed to be unnecessary for both homogeneous and transition region textures. As detailed in Section 4.5.3, the texture test regions to be used in this research range from 8 x 8 to 35 x 35 pixels in size. Further, the GLCMs were found to be well-populated in all of the test regions. Since

the concern of sparse GLCMs is often the primary motivation for quantization practices, we need not be concerned with this aspect in this work.

The ENVI GLCM tool was used to compute the basic GLCM features for each of the texture regions to be studied, which were then relayed to an IDL routine that compared corresponding real and synthetic GLCM texture features by using the same ideology as with the MF spatial metric. That is, both the absolute difference image and a variance-thresholded difference image were analyzed, based on repeated measurements of similar texture regions from the real imagery. The output of this GLCM utility is a collection of texture images, one for each GLCM feature selected for computation. As mentioned earlier, three Haralick GLCM features were nominally used: Homogeneity, Contrast, and Correlation. These computations were carried out on all of the corresponding texture regions for the real and DIRSIG images for all 4 texture models, for all spectral bands of the CitiPix data, and a selection of spectral bands of the HYDICE ARM data that comprises a representative sample of the spectral behavior over all wavelengths. The absolute difference images between the Homogeneity, Contrast, and Correlation output texture images were then taken in order to determine where the textures in the real and DIRSIG images differ most. The variance-threshold image (which characterizes acceptable variance of GLCM features computed for each texture region) was then applied to this difference image in order to determine where outliers (if any) are located and the magnitude of their deviation.

This threshold value is adaptive in nature, since the acceptable variance level will depend on the specific material and type of texture being measured. For example, there is more inherent variability in grass textures than for concrete and asphalt, so the threshold values present in the variance image will accordingly be higher for a grass texture image region. The same thresholding process will be carried out with the use of the SCM metric, which will be described in Section 4.5.2.2.

Figure 51 shows a very simple sample computation of a GLCM in ENVI, in which there are only 4 possible gray levels occurring in the processing window. Note how the computational form of calculating GLCM features differs slightly from the theoretical

definition and the example presented in Section 3.1.2.1. ENVI uses a base and a shift window as prescribed by the user's choice of direction vector parameters, which in this case is a horizontal shift to the right. Further, the GLCM is calculated within a processing window of user-specified size. In order to measure the scale of textures desired within the texture test regions in this research, the minimum size of 3 x 3 pixels is the best choice (and thus this parameter was used throughout).

<u>Base Window</u>	4	3	5		<u>Shift Window</u>	3	5	6
	3	5	6			5	6	3
	6	4	3			4	3	6
 <u>GLCM</u>								
	<b>GL</b>	<b>3</b>	<b>4</b>	<b>5</b>	<b>6</b>			
	<b>3</b>	0	0	2	1			
	<b>4</b>	2	0	0	0			
	<b>5</b>	0	0	0	2			
	<b>6</b>	1	1	0	0			

Figure 51: Sample ENVI GLCM Computation with parameters  $\Delta x = 1, \Delta y = 0$ .

The resulting GLCM is also shown above, which is essentially a probability distribution function of all possible co-occurring pixel values in the image window. The ENVI GLCM computational method compares corresponding pixels in the base and shift windows (i.e., pixel (1,1) of the base window is compared with pixel (1,1) of the shift window, and so on). The left vertical column on the perimeter of the GLCM is the “list” of all possible gray level values in the base window, while the horizontal top row is the same list for the shift window. The order of the entries is important, since (for example) the (3,5) entry is not the same as the (5,3) entry in the above GLCM. The method for filling in the values of the GLCM is as follows: if a 3 occurs in the shift window where a 3 occurs in the base window, then the number of times that this occurs is filled in for the (3,3) entry of the GLCM. Since no values

of 3 occur in the shift where a value of 3 occurred in the base window in the above example, the (3,3) entry is zero (0). However, for the case of the number of times that a value of 3 occurs in the shift window where a value of 4 occurred in the base window (i.e., the (4,3) entry of the GLCM), we see that this occurs twice, and so this entry in the GLCM is 2.

The texture features for each successive GLCM calculated over the texture test region are then calculated. Figure 52 shows sample GLCM texture features calculated from a 25 x 25 pixel plowed field region of the HYDICE ARM imagery in one spectral band. The left feature is the Contrast feature and the right feature is the Correlation feature.

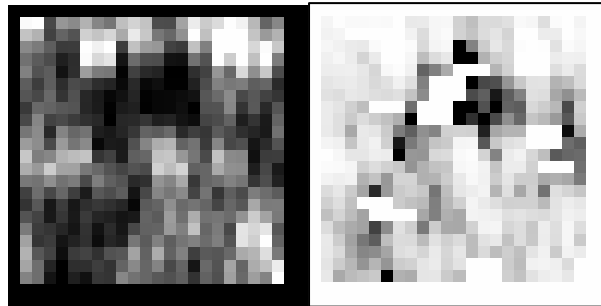


Figure 52: Sample GLCM Metric texture features. (Left): Contrast feature; (Right): Correlation feature.

Each texture test region to be investigated has its own “texture signature” based on its spatial structure. The corresponding regions for all 4 texture models and all selected texture features have been tested. Note that instead of testing all spectral bands of the HYDICE ARM imagery, a careful selection of spectral bands was used in the analysis. In particular, bands 20, 32, 65, 95, 115, 157, 184, and 195 were chosen from the 142 possible spectral bands, since this subset was deemed representative of the spectral behavior of the image. Supplemental visual analyses will also be performed for each individual band for all texture models. The results of the GLCM Metric for the CitiPix and HYDICE ARM DIRSIG imagery are presented in Section 5.3 and 5.4 respectively.

#### 4.5.2 Spectral Domain

Spatial measurements are not the only aspect involved with this validation and comparative performance analysis study. While the band-by-band GLCM analysis is able to determine how well each band performs in a spatial sense, these results cannot be simply computed separately and then combined for analysis due to the complex nature of spectral correlation between bands. Therefore, a set of spectral fidelity measures must also be invoked. In the same manner as with spatial performance measurements, spectral performance analysis will use both a simpler approach and a more detailed test method.

The first method involves a general measure of spectral clutter and overall complexity. This metric will be used to determine how well the overall background clutter statistics in the real and synthetic image compare, since this clutter is precisely what produces spatial and spectral texture. The method to be used draws from a common measure found in the hyperspectral target and anomaly detection literature called the Signal-to-Clutter Ratio (SCR). As with the spatial MF metric, this method similarly generates a simpler measure in the form of a single value indicating overall model performance when compared with the SCR value measured from the real image texture. More details of this texture model performance metric are presented in Section 4.5.2.1.

The fourth and last proposed performance measure is an entirely new concept derived from the spatial GLCM concept. Hauta-Kasari et. al. (1996, 1999) originally introduced the Generalized Spectral Co-Occurrence Matrix (GSCM) for multispectral texture analysis, segmentation, and classification applications. The motivation for this work was owing to the fact that spectral texture analysis in only RGB space was too restrictive in that spectral signatures were often very similar in all three bands (a phenomenon known as metamerism), and thus little additional information for determining texture features over monochrome methods was being obtained. Recognizing this, a method was invoked to extend GLCM analysis to accept vector-valued pixels, stacked matrices, or scalar values representing a quantized spectral domain so that the GSCM would contain information about both the spatial and spectral domains, over a much wider region of the

electromagnetic spectrum. The ideology behind this algorithm was a partial influence for the Spectral Co-Occurrence Matrix (SCM) metric that has been used in this research in order to assess the spectral fidelity of the synthetic textures compared with the real texture images.

The SCM metric follows the exact same operation as the GLCM metric, but instead measures spatial co-occurrence across user-specified (and typically uncorrelated) spectral bands. This metric provides a close approximation to a simultaneous spatial and spectral measure of texture content in an image. Thanks to the assistance of Research Systems Incorporated (RSI - the developers of ENVI), we have coordinated an implemented form of this SCM tool into the ENVI processing environment. More specific details on these methods will be presented in Section 4.5.2.2.

Although it would have been ideal to devise a single test method encompassing simultaneous spatial and spectral performance measurement, such an idyllic metric has never been achieved. This is an extremely complex problem which would be a very interesting area of future research. Therefore, this set of four performance measurements will be used in combination in order to quantify how well each of the four texture models characterize texture in the DIRSIG environment.

#### **4.5.2.1 Signal-to-Clutter Ratio (SCR) Metric**

Researchers in the field of target and anomaly detection in hyperspectral imagery (HSI) commonly employ a measure of the SCR as a threshold for reliable detection of signal patterns in Gaussian clutter [Stocker, Reed, & Yu, 1990; Manolakis et al., 2000]. This same measure will be used as a rudimentary assessment of the similarity of spectral clutter content and complexity within the selected counterpart real and synthetic texture regions in this research. The SCR metric will provide the means to determine if the overall clutter statistics are correct in the synthetic texture in relation to the real image for a given texture type sample. The advantage of this comparison is that the SCR metric generates a single numerical value that will serve as a preliminary measure of how well the overall spectral structure is characterized in the synthetic rendition of the image, before delving into much

more detailed spectral analysis involved with the SCM metric. Lastly, many HSI algorithms exploit the measure of SCR in several contexts, so it is essential that this metric is correct for synthesized texture regions if DIRSIG is to support the testing and development of these algorithms.

In its traditional form, the SCR is defined as follows:

$$SCR = [\mathbf{b}^T \mathbf{M}^{-1} \mathbf{b}]^{1/2} \quad (20)$$

where  $\mathbf{M}$  is the spectral interference (background plus noise) covariance matrix, and  $\mathbf{b}$  is the spectral signature of the “target”, which in this case will be the central pixel of the region being examined. In the case of  $L$  spectral bands,  $\mathbf{b}$  is a column vector of dimension  $(1 \times L)$ , while  $\mathbf{M}$  is given by:

$$\mathbf{M} = \sum_{n=1}^N \mathbf{x}(n) \mathbf{x}^T(n) = \mathbf{X}^T \mathbf{X} \quad (21)$$

where the matrix  $\mathbf{X}^T$  represents the set of  $N$  *de-meaned* pixels in the image window under study, and therefore has dimension  $(L \times N)$ , i.e.,

$$\mathbf{X}^T = [\mathbf{x}(1) \quad \mathbf{x}(2) \quad \mathbf{x}(3) \dots \mathbf{x}(N)] \quad (22)$$

since each entry  $\mathbf{x}(n)$  is itself a column vector representing the de-meaned spectral signature for a given pixel  $n$ . This metric will be used for each of the texture regions to be investigated, for all four texture models. In order to determine the acceptable variance for each of the texture test regions to be studied, the SCR metric will be applied to the same repeated samples from real CitiPix and HYDICE ARM imagery as was used for the MF and GLCM metrics. Incidentally, this same method of characterizing acceptable variance levels was also followed for the SCM metric.

#### 4.5.2.2 Spectral Co-Occurrence Matrix (SCM) Metric

As mentioned earlier, the concept of a GSCM has been proposed by Hauta-Kasari et al. in order to improve texture segmentation results for multispectral imagery. This algorithm generates a co-occurrence matrix that describes the spatial dependency of a quantized spectral domain. This concept of using both spatial and spectral information

simultaneously was the motivation for the SCM Metric that is to be used as the fourth synthetic texture fidelity measure in this work. The reason for not adopting the GSCM as a metric is because there were concerns with the ordering of the quantized spectral domain, and there was no guarantee that the Self-Organized Mapping (SOM) method of quantization would be carried out in the same manner in the real and synthetic corresponding imagery, since the synthetic imagery likely would not contain all of the exact same spectra as the real image. The reader is directed to the two references listed for Hauta-Kasari et al. in Section 8 for further details regarding the concerns of uniqueness in ordering of the quantization and labeling of the spectral domain that is involved in their algorithm.

In order to avoid ordering and quantization problems, a simpler approach was then conceptualized, which has never been used before in the literature on co-occurrence matrices for classification and feature extraction models. Referring back to the GLCM computation example in Figure 51 in Section 4.5.1.2, consider the exact same process with the shift window in a certain *user-specified* spectral band. In this case, the resulting co-occurrence matrix contains both spatial and spectral information, since the SCM allows for the specification of an additional parameter termed the “comparison band.” In the ENVI-implemented form of this algorithm, the user can choose a base spectral band, and a comparison spectral band which is used as the shift window. The parameters of direction vector orientation and processing window are also still available to the user for the SCM. The result is a matrix containing *cross-band* spatial and spectral co-occurrence information. The usual Haralick texture features can be computed from the SCM just as they are for the GLCM utility.

For the HYDICE ARM data, four band pairs were chosen on which the SCM metric would be performed:

- a. Bands 22 and 32 (95% correlated);
- b. Bands 30 and 162 (5% correlated);
- c. Bands 30 and 193 (-10% correlated); and
- d. Bands 65 and 185(-40% correlated).

This choice of band pairs was used in order to determine if the spectral correlation in the DIRSIG imagery was preserved compared with the corresponding real imagery. This sampling of band pairs is considered to be representative, since it encompasses well-correlated, ill-correlated, negatively ill-correlated, and negatively “well”-correlated spectral structure. The same testing methodology was used for the SCM as for the GLCM metric. That is, the same texture test regions as tested for the other 3 metrics were used, and the absolute and variance-thresholded difference images were investigated for the Homogeneity, Contrast, and Correlation features. The comparative performance analysis process is thus parallel with that of the GLCM metric, so there is no need for repetition here. An example of the SCM metric output features is presented in Figure 53.

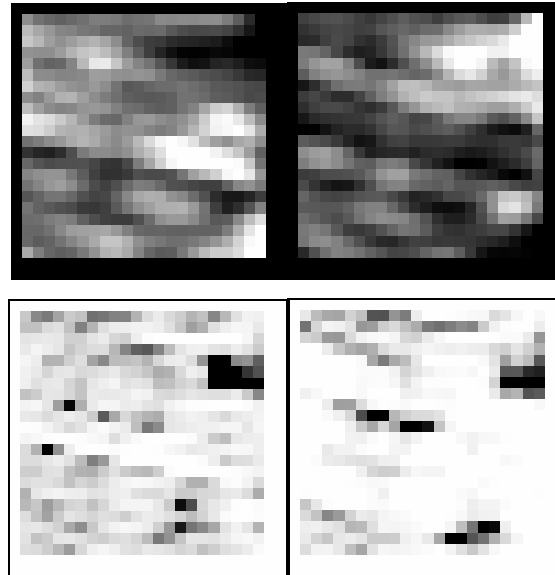


Figure 53(a): Sample SCM metric features for real HYDICE ARM image plowed field region. Top: Contrast feature for band pair 30-162 (left) and band pair 65-185 (right). Bottom: Correlation feature for band pair 30-162 (left) and band pair 65-185 (right).

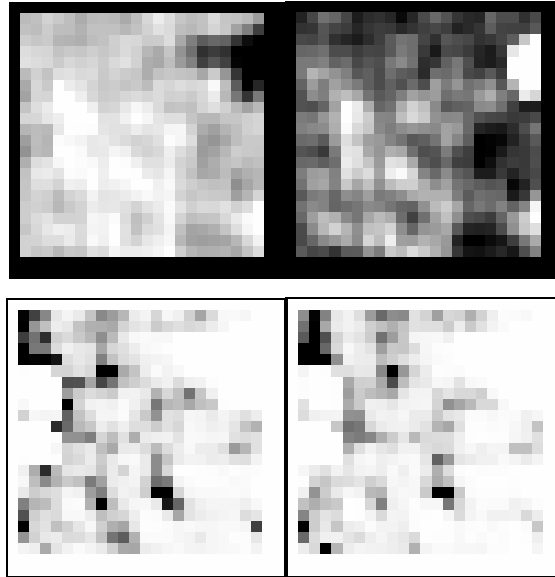


Figure 53(b): Sample SCM metric features for DIRSIG HYDICE ARM image using MBP texture model on plowed field region. Top: Contrast feature for band pair 30-162 (left) and band pair 65-185 (right). Bottom: Correlation feature for band pair 30-162 (left) and band pair 65-185 (right).

The results from the SCM metric on the CitiPix and HYDICE ARM imagery are presented in Section 5.3 and 5.4 respectively.

### 4.5.3 Detailed Methodology

This section has been included so that the reader is familiar with the texture test regions that have been selected for the comparative performance analysis of the SBP, MBP, Texture Synthesis, and FM texture characterization models. It will also list how many repeated samples were taken from real imagery in order to construct the variance threshold image for each test region.

#### 4.5.3.1 CitiPix Texture Test Regions

In order to systematically analyze the results of the synthetic imagery produced using each of the 4 texture models, 19 texture test regions were chosen from the 437 x 437 pixel CitiPix image. The regions were subdivided into “homogeneous” and “transition” regions,

where the former represents textural features within a single material class, and the latter refers to transitions between 2 or more different material classes. The four performance metrics were applied to each of these regions for all of the real and DIRSIG imagery for consistency purposes. The following table details the size and location of each of the nominal texture test regions that were used for the CitiPix imagery, as well as the number of repeated measurements that were obtained from the real CitiPix image in order to generate the acceptable variance image.

REGION NAME	SIZE (PIXELS)	NUMBER OF MEASUREMENTS
1. Asphalt	25 x 25	4
2. Left Field Healthy Grass	25 x 25	4
3. Left Field Stressed Grass	25 x 25	3
4. Right Field Healthy Grass	25 x 25	4
5. Upper Endzone	25 x 25	3
6. Lower Endzone	15 x 15	3
7. Running Track	15 x 15	4
8. Trees	15 x 15	4
9. Perimeter Grass	25 x 25	4
10. Building	15 x 15	4
11. Right Field-Stressed-Track	35 x 35	3
12. Left Field-Stressed-Track	35 x 35	4
13. Field-Track	25 x 25	4
14. Stressed-Healthy Strip, Right Field	25 x 25	4
15. Field-Yard Line, Left Field	25 x 25	4
16. Endzone-Track	25 x 25	3

17. Field-Asphalt	25 x 25	4
18. Field-Endzone	15 x 15	3
19. Grass-Baseball Dirt	15 x 15	3

Table 1: Texture Test Regions for CitiPix Data.

The first ten entries listed in Table 1 are homogeneous regions, while the last 9 are transition regions. Also, the number of measurements listed in the rightmost column includes both the nominal region that was used for comparison using the performance metrics, as well as samples from the immediate vicinity of the nominal region. As discussed in the previous sections, the repeated samples were obtained in order to construct a variance threshold image to be applied to the absolute difference images generated through the application of the performance metrics. These regions are illustrated in Figure 54. The results and analysis of the absolute and variance thresholded metrics for all 19 CitiPix texture test regions are presented in Section 5.3.

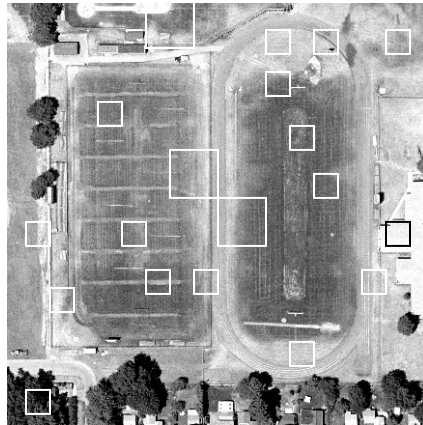


Figure 54: CitiPix texture test regions corresponding to Table 1.

#### 4.5.3.2 HYDICE ARM Texture Test Regions

A completely analogous methodology was followed for the 320 x 320 pixel HYDICE ARM image. Table 2 lists the 15 nominal test regions that were analyzed, where the first 9 are homogeneous textures, and the last 6 are transition regions.

REGION NAME	SIZE (PIXELS)	NUMBER OF MEASUREMENTS
1. Upper Plowed Field	25 x 25	4
2. Upper Wheat	25 x 25	4
3. Lower Wheat	25 x 25	4
4. Lower Plowed	25 x 25	4
5. Uncut Pasture (outside of calibration site)	25 x 25	4
6. Cut Pasture (within calibration site)	15 x 15	3
7. Parking Lot (beside trailers)	25 x 25	4
8. Trees	8 x 8	4
9. Trailers	10 x 10	4
10. Cut-Uncut Pasture	15 x 15	3
11. Uncut Pasture-Dirt	15 x 15	3
12. Uncut Pasture-Road	15 x 15	3
13. Uncut Pasture-Plowed Field	15 x 15	3
14. Wheat-Road-Uncut Pasture	25 x 25	3
15. Wheat-Road-Plowed Field	25 x 25	3

Table 2: Texture Test Regions for HYDICE ARM data.

As with the CitiPix data, these 15 nominal test regions and the repeated measurements on the real HYDICE imagery were used for application of the MF, GLCM, SCR, and SCM performance metrics, for all four texture model DIRSIG images. The above regions are illustrated in Figure 55. The results of these metrics are presented in Section 5.4.

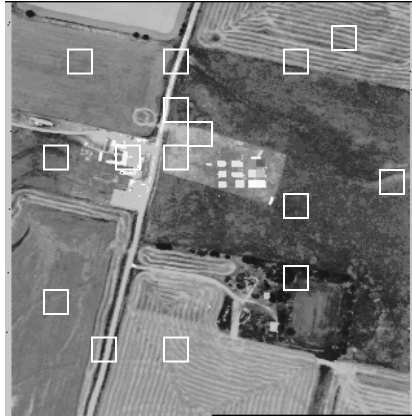
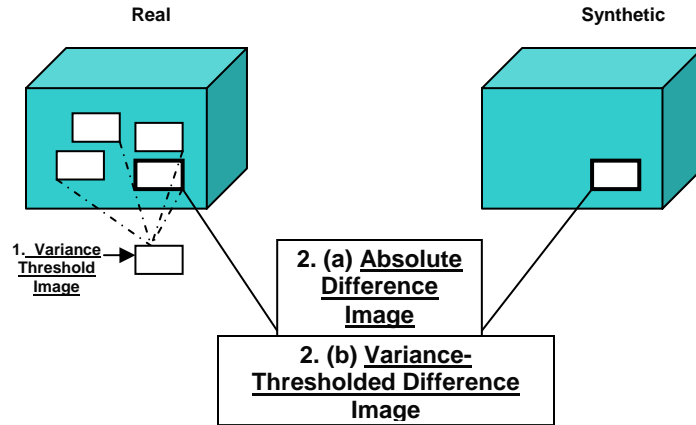


Figure 55: HYDICE ARM texture test regions corresponding to Table 2.

A synopsis of the application of performance metrics in this work is presented in Figure 56.



- For 19 CitiPix, 15 HYDICE Texture Regions
  - For MF, GLCM, SCM Metrics
  - All 3 CitiPix Bands (R-B for SCM)
- HYDICE Bands 20, 32, 65, 95, 115, 157, 184, 195 for MF, GLCM
- HYDICE Selected 4 Band Pairs for SCM Metric

Figure 56: Performance metric methodology.

## 5. Results and Analysis

This chapter will present all of the results obtained from using the SBP, MBP, Texture Synthesis, and FM texture characterization models to render the CitiPix and HYDICE ARM DIRSIG scenes. Sections 5.1 and 5.2 show numerous samples of output DIRSIG imagery that has been obtained using each of the texture models, as well as some interim results that required modifications to configuration files for improvement. Preliminary remarks regarding the qualitative physical appearance of the resultant imagery will also be provided. Sections 5.3 and 5.4 discuss the quantitative results obtained for each model after the application of the MF, GLCM, SCR, and SCM performance metrics. A thorough comparative performance analysis then follows based on the results of these metrics in section 5.5. An additional section detailing supplementary results has also been included to discuss other DIRSIG imagery that has been rendered for interest sake, and which has not been tested through the use of the four performance metrics. The results from the incorporation of a texture characterization model created by Spectral Sciences Incorporated (SSI) are also presented in section 5.6.

### 5.1 CitiPix Imagery Results

Since the CitiPix data only covers the visible region of the electromagnetic spectrum in Red, Green, and Blue channels, all three spectral bands of the output imagery results will be presented here. For comparison purposes, the real CitiPix imagery is shown below.



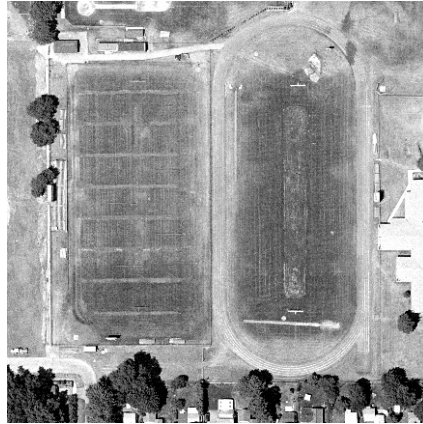


Figure 57: Real CitiPix imagery. Top left: R channel; Top right: G channel; Bottom: B channel.

The DIRSIG imagery results to be shown in the following sections follow the same order of R, G, and B channels.

### 5.1.1 SBP Model

The DIRSIG imagery obtained using the SBP Z-Score Selection texture characterization model is shown below. In this case, the Red spectral band has been used as the single bandpass texture image from which z-scores were computed and compared with ground truth reflectance curves for material types present in the scene.



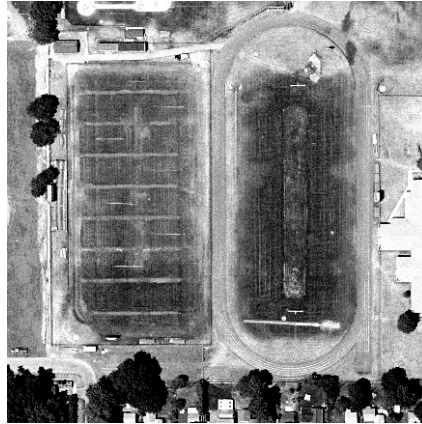


Figure 58: DIRSIG imagery (R, G, and B channels) using the SBP texture model.

A preliminary visual analysis of this synthetic imagery suggests that the spatial fidelity captured in the DIRSIG image is quite good. Since we are only dealing with three highly correlated spectral bands, it is not surprising that the DIRSIG imagery also maintains spectral structure (as much as the eye can make such a conclusion). The only apparent difference between the real and synthetic imagery is that the latter appears to be darker in the field regions, and it contains much more overall contrast and dynamic range. This would initially perhaps imply the presence of a scaling or brightness effect issue, but it actually owes to the fact that DIRSIG is able to produce an infinite dynamic range (in units of radiance) in its output imagery, and thus the difference lies only in the way in which the images are displayed, not in the actual pixel values. The effects of this are very mild, which has been further evidenced by a comparison of each corresponding spectral band after the ELM calibration process. By linking displays in ENVI, pixel reflectance values of the real and synthetic images were carefully compared. It was found that most pixel values were extremely close, and were on average within 0.5 reflectance units (where the reflectance units run from 0 – 100 nominally). The realistic-looking variability within material classes and the smooth transitions between material types in the SBP DIRSIG image has been attained largely because of the availability of very thorough and accurate ground truth reflectance curves. In some cases, DIRSIG emissivity files for different material types were merged into

one, and then the utility “expand\_emissivity\_file” was run in order to produce additional curves that would allow for non-abrupt transition regions. We call this process the generation of “transition curves”, and it has been shown to be a very useful and practical technique for the rendering of locally generated scenes such as the DIRSIG Megascene [Lentilucci & Brown, 2003]. This visual analysis will be augmented by a much more detailed quantitative analysis using the MF, GLCM, and SCM performance metrics in Section 5.3 (note: the SCR metric is only used for the HYDICE ARM imagery).

### 5.1.2 MBP Model

The DIRSIG imagery obtained using the MBP Z-Score Selection texture characterization model is shown below. In this case, all three (Red, Green, and Blue) spectral bands were used as separate texture images in the application of this model.

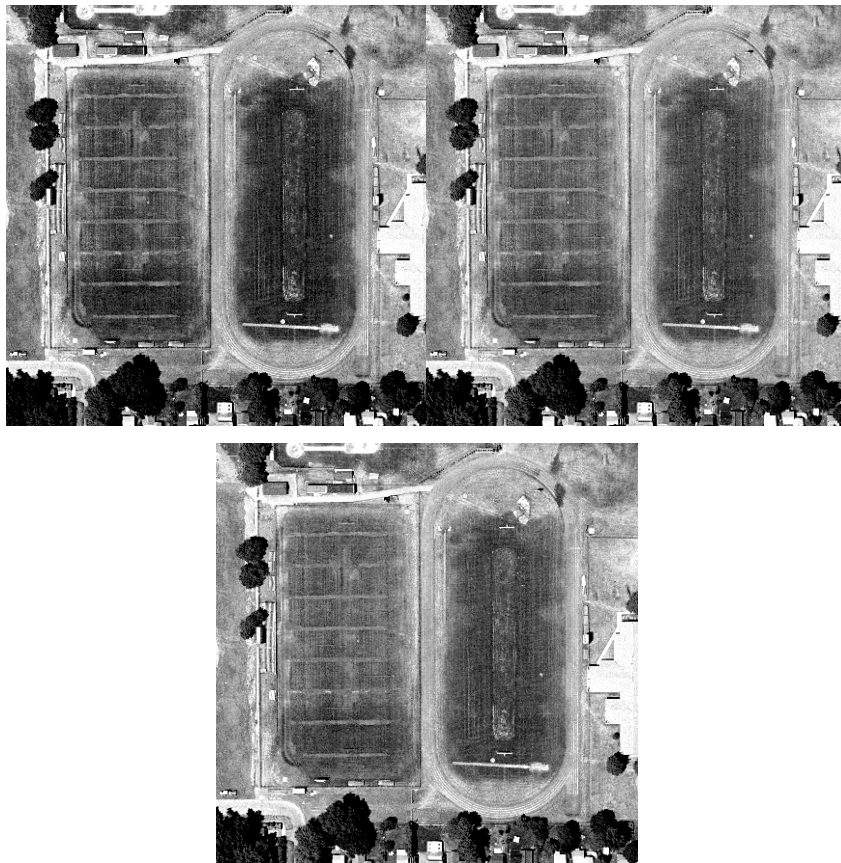


Figure 59: DIRSIG imagery (R, G, and B channels) using the MBP texture model.

By using a series of three texture image bandpasses, the curve selection for image texture application equally weights the Red, Green, and Blue regions of the spectrum. Since these three spectral bands are highly correlated, it is not surprising that the result does not differ greatly from the SBP model result, at least in terms of a preliminary visual analysis. By linking ENVI displays of the real CitiPix, the SBP, and the MBP results, it was difficult to locate any significant differences between the results of the MBP and the SBP DIRSIG imagery. The spatial and spectral structures are nearly identical in both images, as are the image-wide and local mean and variance statistics. Interestingly, it was also found that, although the pixel values of the SBP and MBP images were very close, the SBP image tended to be closer to the values of the real CitiPix image. This may at first seem disconcerting, since the MBP model is supposed to select spectral curves based on a wider sampling of the spectral domain. But once again, one must recall that we are only dealing with three well-correlated spectral bands, and that by using all three bands for z-score computations, it is possible to over-constrain the curve selection process, thereby causing the SBP model which has only used one spectral bandpass, to contain pixel values that are closer to that of the real counterpart image. The results of the rendering of the HYDICE ARM image will demonstrate the advantage of the MBP texture model much more clearly than for the CitiPix imagery, since the multiple bandpasses used for the algorithm will be derived from non-correlated spectral band regions (see Section 5.2). It is important to note that this apparent similarity between the SBP and MBP results that would cause most observers to deem them visually indistinguishable is further proof that a qualitative visual analysis must be augmented with quantitative measures that exceed the discriminative powers of the eye if one wishes to robustly measure the fidelity of synthetic imagery. The MF, GLCM, and SCM performance metric results of the CitiPix DIRSIG image using the MBP texture model are presented in Section 5.3.

### 5.1.3 Texture Synthesis Model

The DIRSIG imagery obtained using the Texture Synthesis texture characterization model is shown below. Three-band synthetic texture cubes were created for each material contained in the material map derived from the real CitiPix image, and applied using the DIRSIG “reflectance map” mode. All material class regions were synthesized using the Spectral Expansion model except for the dark rooftops, which were rendered using the Image Quilting model since only small samples were available from the real image, and it was important to avoid anomalies from mirroring processes since the dark rooftops were used for the ELM calibration process.

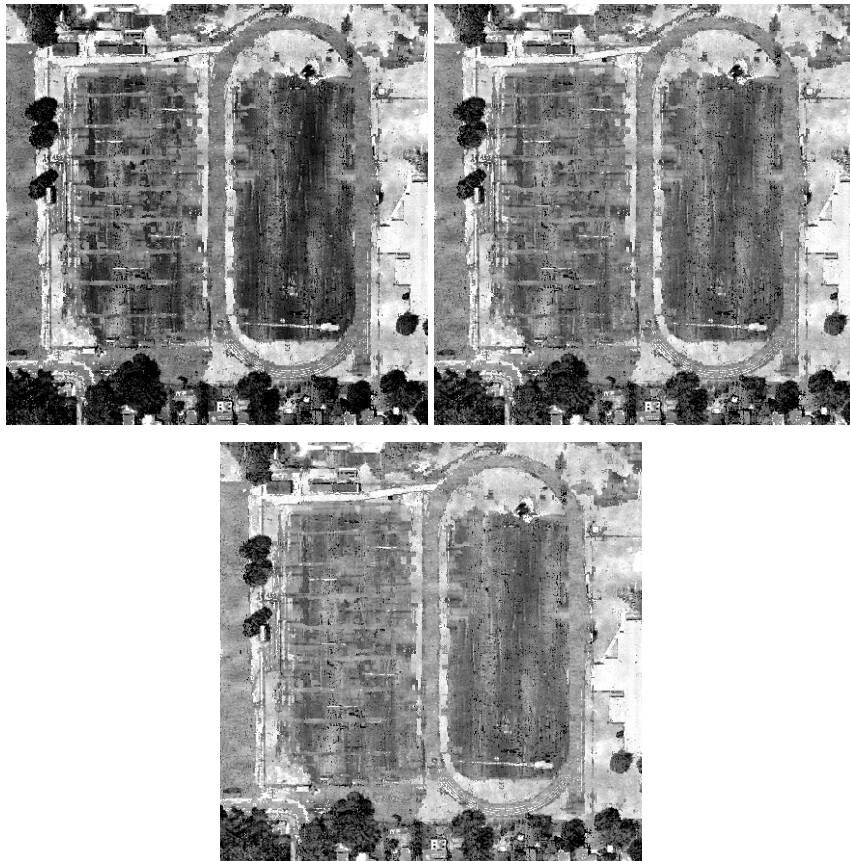


Figure 60: DIRSIG imagery (R, G, and B channels) using the Texture Synthesis model.

The GML-derived material map in Figure 41 was used in order to obtain this result. Eight synthetic texture reflectance cubes were generated using the Texture Synthesis model, and then projected onto the material map to produce both within- and between-material variability in the output DIRSIG image (as described in Figure 42 in Section 4.2.2). This model had more difficulty in capturing the exact spatial structure of the fields, since by the very nature of the Texture Synthesis model it is not able to recreate structural transitions within a given material class unless they are present in the input texture sample image (and even then, they would likely be repeated in random directions in the output synthetic texture image). Unlike the SBP and MBP models, texture is not applied on a pixel-by-pixel basis through the use of a texture map. Instead, local spatial variability is driven solely from the input sample from which the texture cube is synthesized, and thus rendering fine structures at the same size and orientation as in the real image within material classes would be virtually impossible to produce with this model. However, for more homogeneous material types such as the asphalt region on the left, the running track, and the building on the right, the appearance of the synthetic texture looks equally acceptable as that of the SBP and MBP models. In fact, even the fidelity of the tree canopy textures is impressive. Although tree leaves are not homogeneous by any means, it is the stochastic nature of these textures that allows the Texture Synthesis model to capture this variability quite well.

The transition regions between material classes are ultimately driven by the result of the material map. The overall structure present in the real counterpart image is captured in the Texture Synthesis model DIRSIG image, albeit not quite as well as with the SBP and MBP models. The transition regions are somewhat more abrupt, since the input sample textures were usually not derived from blended regions, but rather from carefully chosen regions that demonstrate the inherent variability of each material class present in the material map. These sharp transitions can be seen between the healthy and stressed grass on the fields near the endzones, as well as between the track and the fields. The transitions are generally as sharp as they are in the material map itself. The Texture Synthesis model had the most difficulty with the lines on the left field and the strip of worn grass on the right

field. This again was due to the aforementioned challenge of capturing local spatial structure within a given material class. Most of this preliminary visual analysis has been regarding the spatial appearance of this imagery. Further spatial and spectral analysis using the MF, GLCM, and SCM metrics is presented in Section 5.3.

#### 5.1.4 FM Model

The DIRSIG imagery obtained using the Fraction Map texture characterization model is shown below. As detailed in Chapter 4, four end members were extracted from the real CitiPix image, from which four corresponding fractional abundance maps were constructed. The fraction planes were then re-mixed in order to produce the following result.

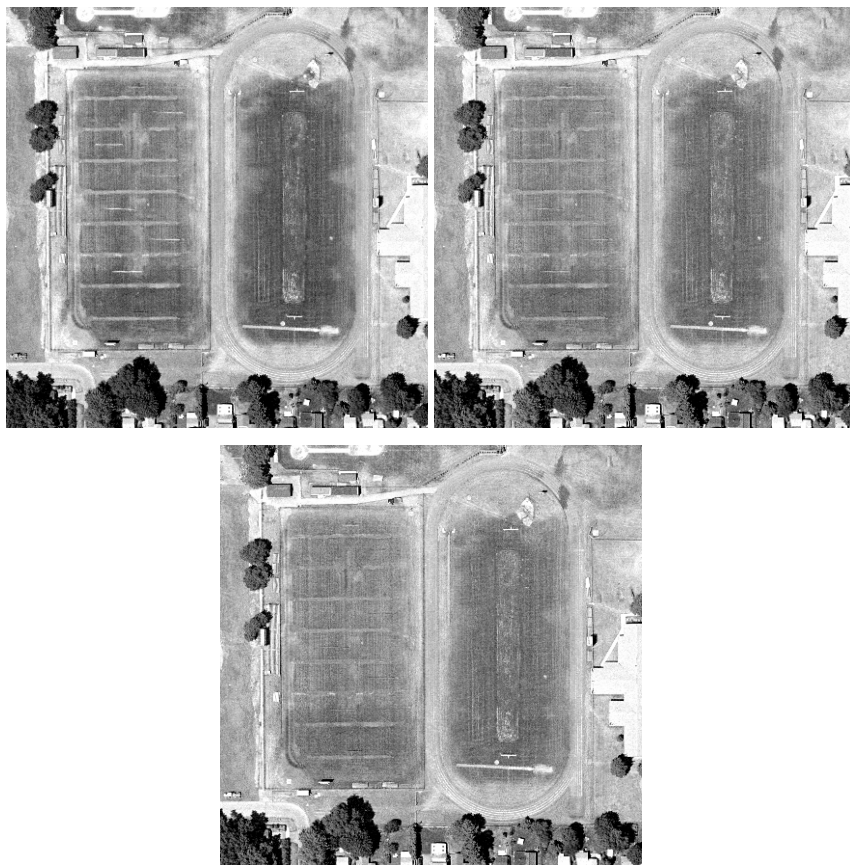


Figure 61: DIRSIG imagery (R, G, and B channels) using the FM texture model.

The FM model result for the DIRSIG CitiPix image is the most visually identical to the real CitiPix image of all four texture models being tested. Even the dynamic range and overall contrast are much closer to that of the original image. This is not surprising, since the method literally re-mixes all four of the fraction maps in order to create both spatial and spectral variability. Although the spatial structure appears to be excellent for this image, the spectral content still remains to be tested, even though the spectral extent is small for this data. Since each end member is assigned only one nominal spectral reflectance curve in order to create spectral structure in the image, it was expected that the spatial domain would be well-characterized with this model, while the spectral content had the potential to be lacking in realistic complexity. This potential is not great for the CitiPix image, since one curve may be sufficient for such a narrow spectral extent; however this potential is larger for imagery with broad coverage, such as with the HYDICE ARM data. The results of the MF, GLCM, and SCM performance metrics for the DIRSIG CitiPix image using the FM texture model are presented in Section 5.3.

## **5.2 HYDICE ARM Imagery Results**

Due to the large number of spectral bands and spectral extent of the HYDICE ARM imagery, only a representative subset of the spectral bands of the resultant DIRSIG imagery will be presented here. For comparison purposes, the spectral bands of the real HYDICE ARM imagery to be compared with the DIRSIG results are shown below.





Figure 62: Real HYDICE ARM imagery. From top left to bottom right: Bands 20, 32, 65, 95, 115, 157, 184, and 195.

Once again, the order of spectral bands presented for each of the four texture model results will be as above – from top left to bottom right: bands 20, 32, 65, 95, 115, 157, 184, and 195.

### 5.2.1 SBP Model

The results of using the SBP Z-Score Selection texture characterization model are shown below. In this case, the single bandpass used for DIRSIG rendering is band #20, which has a central wavelength value (FWHM) of 0.4661 microns. The results for 8 of the spectral bands are presented here in order to avoid tedium, to preserve space, and because these are the bands to which the performance metrics have been applied. The bands shown here and their respective FWHM values are listed in Table 3.

<u>Spectral Band Number</u>	<u>Band Centers (microns)</u>
20	0.4661
32	0.5230
65	0.8026
95	1.2297
115	1.5128
157	2.0083
184	2.2711
195	2.3690

Table 3: The 8 representative spectral bands to which the 4 performance metrics have been applied are listed above. These are also the spectral bands that will be shown for each of the DIRSIG texture model results. Note that the band center / FWHM values change with altitude for the HYDICE sensor due to its wedge spectrometer design.

Before presenting the final results obtained with the SBP model, an interim result will be shown for demonstrative purposes. As discussed in Chapters 3 and 4, the SBP and MBP models rely heavily on accurate and thorough ground truth data in order to generate realistic levels of spatial and spectral clutter. Shown below is an example of the output of the MBP model using only the MTL-supplied ground truth data (the MBP result is shown here because it better illustrates the effect of ground truth data that does not capture sufficient spatial structure of material classes). This result also used three single-band images as the texture maps (bands #20, #65, and #184) instead of masked texture maps.



Figure 63: Illustrative example of the result of using ground truth data that does not adequately represent the spatial variability of materials present in the scene to be rendered. Note the quantized and blotchy appearance especially in the plowed field, uncut pasture, and wheat regions. Left: Band 20; Right: Band 65.

The reader will notice the quantized and speckled appearance of this image compared with the real HYDICE data. This is because there was only between 6 and 8 ground truth measurements of each of the materials present in the scene, which themselves possessed a very tight distribution. Therefore, even after running the “expand\_emissivity\_file” utility to generate transition curves, the result still showed a quantized appearance. The following tables demonstrate the statistical gap between the MTL ground truth data and the real HYDICE ARM image for two sample materials (uncut pasture and wheat regions) in terms of mean reflectance and standard deviation. The standard deviation values show that the true variability of these materials is not captured in the ground truth measurements.

Band	GROUND TRUTH		IMAGE-DERIVED	
	Mean	S.D.	Mean	S.D
20	4.59	0.29	3.72	0.52
32	7.19	0.30	6.34	0.54
65	31.09	1.14	30.72	3.08
95	40.62	0.99	35.29	2.11

115	24.93	1.43	18.00	3.25
157	18.47	2.02	10.62	3.56
184	20.04	1.23	12.58	2.74
195	16.29	1.19	9.97	2.64

Table 4(a): Mean and standard deviation values for uncut pasture material class derived from MTL ground truth measurements (left) and directly from the real HYDICE ARM imagery.

	<b>GROUND TRUTH</b>		<b>IMAGE-DERIVED</b>	
<b>Band</b>	<b>Mean</b>	<b>S.D.</b>	<b>Mean</b>	<b>S.D</b>
20	4.49	0.25	4.56	0.46
32	7.16	0.29	6.97	0.60
65	24.04	0.35	22.23	3.19
95	29.79	0.39	30.78	2.65
115	18.48	0.39	22.35	1.84
157	14.20	0.35	30.78	2.25
184	14.24	0.44	22.35	2.02
195	11.35	0.35	16.94	1.89

Table 4(b): Mean and standard deviation values for wheat material class derived from MTL ground truth measurements (left) and directly from the real HYDICE ARM imagery.

Since we do not intend to test the quality of ground truth data measurements in this work, it was decided to create image-derived ground truth reflectance spectra by defining regions of interest (ROIs) in ENVI, and transforming the pixel values into emissivity curves. Another improvement was made over the former result by utilizing masked texture maps for more accurate z-score computations within the SBP algorithm. The results for the SBP model using image-derived “ground truth” and masked texture maps are shown below. The imagery is much more continuous than the result shown above. However, the shortcomings of using the SBP model for imagery with large spectral extent become more obvious for the later spectral bands.





Figure 64: DIRSIG HYDICE ARM imagery using SBP texture model (bands 20, 32, 65, 95, 115, 157, 184, and 195).

The effect of using a single bandpass texture map for rendering an image with broad spectral coverage is evident in the above imagery. The later spectral bands all tend toward random texture, while the band nearest that of the texture image (band 20, top left) has the overall best appearance. This is because the curve selections that were appropriate in the band 20 region were not the correct choices for the non-correlated IR bands. A more detailed discussion is best left until after the MBP model results are presented in the next section.



### 5.2.2 MBP Model

The results of using the MBP Z-Score Selection texture characterization model are shown below. In this case, three bandpasses were used: bands 20 (0.4661 microns), 65 (see Table 3), and 185 (2.2802 microns). Masked texture maps were used in order to optimize the z-score computations for each material class. Also, the below images were rendered using image-derived “ground truth” spectra in order to avoid the undesirable quantization effects seen in Figure 63.





Figure 65: DIRSIG HYDICE ARM imagery using MBP texture model (bands 20, 32, 65, 95, 115, 157, 184, and 195).

There is an obvious improvement made using the MBP model over the SBP model. None of the bands contain noisy structures in the MBP DIRSIG imagery. This is because the composite weighted z-score that is used in the MBP algorithm considers the spectral behavior in multiple bandpasses, and therefore tends to more correctly choose spectral reflectance curves for all pixels in the output image. A mere visual inspection of especially the later spectral bands of the SBP and MBP results reveals the powerful capabilities of the MBP model over the SBP model, and the quantitative analysis in Sections 5.3 and 5.4 will further demonstrate *how much* better the MBP model performs for imagery with larger spectral dimension. Although not much difference is observed between the CitiPix SBP and MBP results, there is a dramatic improvement for that of the HYDICE ARM imagery, just

by employing two additional texture image bandpasses. This is a very fundamental and important result that will be investigated further in the following sections. One may also notice that the calibration panels do not appear exactly the same between the real and synthetic imagery. This was advertently done, since only the 6-step grayscale panels (on the right) were used for the ELM reflectance calibration process, while the other 6 panels on the left were textured as 15% reflectance panels to avoid unnecessary tedium and potential difficulties within DIRSIG configuration files. The HYDICE ARM MBP model DIRSIG imagery will be further analyzed using the four performance metrics in Section 5.4.

### 5.2.3 Texture Synthesis Model

The results of using the Texture Synthesis texture characterization model are shown below. As described in Chapter 4, 142-band synthetic texture reflectance cubes were constructed for each of the eight materials contained in the material map derived from the real HYDICE ARM image, and applied using the DIRSIG “reflectance map” mode. All material class regions were synthesized using the Spectral Expansion model except for the trees and the road, which were rendered using the Image Quilting model.





appear. For example, the local mean and standard deviation statistics for each material class region in the real and synthetic imagery matched to within 3 %. Table 4 shows a sampling of image-wide mean and standard deviation statistics for four spectral bands extracted from the calibrated real and synthetic imagery. The same trend of agreement of first-order statistics is observed.

<b>BAND</b>	<b>REAL HYDICE</b>		<b>TEXTURE SYNTHESIS MODEL</b>	
	Mean	S.D.	Mean	S.D.
20	4.84	3.22	4.69	3.69
65	26.52	7.59	25.52	7.06
115	23.93	9.43	23.47	9.47
184	18.48	9.17	17.82	9.29

Table 5: Sample mean and standard deviation statistics of corresponding HYDICE ARM and DIRSIG Texture Synthesis model imagery.

One must also keep in mind that the very nature of the Texture Synthesis model guarantees that the spectral covariance statistics of the synthetic textures will agree with that of the real image textures. This aspect will be tested in more detail in Section 5.4 with the SCR and SCM metrics. For now however, a visual analysis will be sufficient.

The uncut pasture region is very well-represented in the DIRSIG image. There are elements of both healthy and stressed grass present in the region, but the exact spatial structure is not preserved, as with the case of the fields in the CitiPix DIRSIG Texture Synthesis model imagery. The same phenomenon was observed for the wheat regions. It was expected that the plowed field regions would be somewhat challenging for this model to capture due to its structural patterns and orientations. One will notice that the plowed patterns are indeed present; however the orientation of the patterns was not replicated as in the real HYDICE ARM image. One of the fundamental limitations of this model is evident especially in the lower road region. Recall the discussion presented in Section 4.2.2 regarding the necessity for at least 32 x 32 pixel input sample textures for the Quilting

model, and 64 x 64 pixel samples for the Spectral Expansion model. Since the road is quite narrow, it was difficult to obtain a sample of sufficient size. Therefore, the mirroring utility described in Section 4.2.2 had to be used in order to grow out this region. This caused repetitive artifacts to appear, as shown in Figure 40. These anomalies are visible in six of the above eight images in the form of repeating horizontal black bars within the lower portion of the road. As with the CitiPix DIRSIG image rendered using the Texture Synthesis model, the transition regions are well represented in this imagery, since the GML-derived material map achieved quite good separability between material class regions. Further analyses of this imagery in a more quantitative manner will be presented in Section 5.4.

#### 5.2.4 FM Model

The DIRSIG imagery obtained using the Fraction Map texture characterization model is shown below. As detailed in Chapter 4, eight end members were extracted from the real HYDICE ARM image, from which eight corresponding fractional abundance maps were constructed. The fraction planes were then re-mixed in order to produce the following result.





Figure 67: DIRSIG HYDICE ARM imagery using FM texture model (bands 20, 32, 65, 95, 115, 157, 184, and 195).

Just as with the CitiPix FM model result, this model produces the most visually pleasing imagery of all four models. In fact, the real and synthetic imagery are almost

indistinguishable if one compares Figure 64 with the real HYDICE ARM imagery at the beginning of Section 5.2. When the displays of the real and FM model HYDICE images are linked in ENVI, the calibrated pixel values are extremely close, and when overlaid there is no apparent change other than that due to the difference in the reflectance panels as described earlier. This re-mixing of fractional abundance planes has produced a very impressive result in the spatial domain. Although it appears as though the spectral correlation has been preserved based on a band-by-band visual analysis, it will be interesting to see how well the performance metrics deem this model to be in both spatial and spectral domains in Section 5.4.

### 5.3 CitiPix Metric Results

This section presents a detailed analysis of the results obtained from the application of the MF, GLCM, and SCM performance metrics for each of the 19 texture test regions of the CitiPix data set, for the Red, Green, and Blue channels. The SCR metric was not performed for the CitiPix imagery since it is designed for applications where hyperspectral imagery (HSI) data is being used. However, the SCM metric was applied across the 2 least correlated spectral bands, which are the Red and Blue bands. Both the absolute difference image and the variance-thresholded ( $\sigma^2$ ) difference image were initially examined for each texture region using these metrics in order to determine the range of values observed in the absolute difference image, the average value of the difference image entries, as well as the number of outliers in the thresholded image. Since it was found that the use of a 2-sigma threshold was much more intuitive and meaningful than sigma-squared, the following tables will present the values using the 2-sigma threshold as well as the average value for each of the absolute difference images. The analysis also included how much the entries deviated from the variance image for each model result, and the locations and features within each texture region that differed most from the corresponding real texture region. This was performed by directly comparing the variance-thresholded images for each of the features.

### 5.3.1 MF Metric

The MF Spatial Metric was applied to all three spectral bands of the DIRSIG imagery using the SBP, MBP, Texture Synthesis, and FM texture models in 19 texture test regions. The metric was also applied to the same nominal regions of the original CitiPix data, as well as sample regions in the vicinity of each nominal region in order to construct a variance image for thresholding purposes. The following synopsis tables present the relevant statistical data extracted from the absolute and thresholded MF output imagery. For all of the tables presented in Section 5.3, the texture test regions have been designated with the same numbering convention as used in Table 1 of Section 4.5.3.1, where regions 1 – 10 are homogeneous textures and regions 11 – 19 are transition region textures. The format of the synopsis tables will be the same for all metrics, for both the CitiPix and HYDICE ARM imagery. The first set of tables indicates the percentage of pixels that exceeded the 2-sigma variance threshold for the given region and texture model. This can also be thought of as the number of non-zero entries in each of the variance thresholded images. The second set of tables represents the average value of the pixels in the absolute difference image. The range of values observed in the absolute difference image for each of the regions was also investigated as a tertiary check of model performance, but the results have not been presented here in order to conserve space since the values of outliers and averages are sufficiently demonstrative. All values are in units of reflectance unless otherwise specified.

<b>R Channel – MF Metric – Avg Value of Absolute Difference Image</b>				
<b>Region</b>	<b>SBP</b>	<b>MBP</b>	<b>TS</b>	<b>FM</b>
1	0.55	2.16	2.25	0.15
2	0.13	2.3	6.85	0.10
3	0.35	2.35	3.5	0.29
4	0.10	2.85	4.2	0.09
5	0.95	2.2	3.65	0.10
6	1.1	2.1	3.9	0.14

7	0.9	2.2	1.45	0.06
8	0.3	3.5	6.6	0.20
9	1.2	2.2	3.1	0.16
10	1.25	2.1	1.55	0.07
11	0.8	2.8	3.2	0.10
12	0.7	2.95	3.65	0.095
13	0.65	2.9	3.55	0.49
14	0.1	2.6	6.5	0.08
15	0.4	2.7	4.55	0.29
16	0.69	3.7	8.95	0.10
17	0.95	2.65	3.57	0.17
18	0.4	2.4	3.97	0.34
19	0.6	2.3	2.92	0.42
<b>AVERAGE:</b>	<b>0.64</b>	<b>2.58</b>	<b>4.10</b>	<b>0.18</b>

Table 6: R Channel – MF Metric – Average Value of Absolute Difference Image

<b>G Channel – MF Metric – Avg Value of Absolute Difference Image</b>				
<b>Region</b>	<b>SBP</b>	<b>MBP</b>	<b>TS</b>	<b>FM</b>
1	0.1	1.2	1.15	0.09
2	0.78	0.84	3.65	0.55
3	0.90	0.92	0.75	0.56
4	0.99	1.05	1.3	0.89
5	1.1	1.45	2.75	0.16
6	0.90	1.42	3.5	0.164
7	0.20	1.6	0.95	0.07
8	1.3	1.34	4.4	0.81
9	1.2	1.65	2.44	0.21
10	0.70	2.25	1.66	0.08
11	0.65	1.05	1.5	0.22

12	0.70	1.65	1.75	0.16
13	0.8	0.87	1.35	0.56
14	1.5	1.51	3.7	0.72
15	1.5	1.53	2.3	0.65
16	0.75	1.7	2.2	0.16
17	0.8	1.6	1.98	0.18
18	1.3	1.37	1.45	0.54
19	1.1	1.35	1.46	0.44
<b>AVERAGE:</b>	<b>0.91</b>	<b>1.39</b>	<b>2.12</b>	<b>0.38</b>

Table 7: G Channel – MF Metric – Average Value of Absolute Difference Image

<b>B Channel – MF Metric – Avg Value of Absolute Difference Image</b>				
<b>Region</b>	<b>SBP</b>	<b>MBP</b>	<b>TS</b>	<b>FM</b>
1	0.14	0.33	0.31	0.04
2	0.10	0.55	1.65	0.08
3	0.10	0.52	0.71	0.06
4	0.05	0.54	1.70	0.032
5	0.50	0.61	1.25	0.15
6	0.55	0.60	1.35	0.05
7	0.10	0.42	0.3	0.04
8	0.25	0.62	2.45	0.22
9	0.5	0.52	0.95	0.13
10	0.01	0.42	0.41	0.009
11	0.35	0.44	1.15	0.18
12	0.30	0.57	0.95	0.14
13	0.10	0.52	0.85	0.07
14	0.10	0.55	1.35	0.08
15	0.50	0.52	1.56	0.28
16	0.40	0.56	0.70	0.09

17	0.45	0.49	0.75	0.08
18	0.10	0.59	1.48	0.065
19	0.15	0.51	1.37	0.11
<b>AVERAGE:</b>	<b>0.25</b>	<b>0.52</b>	<b>1.12</b>	<b>0.10</b>

Table 8: B Channel – MF Metric – Average Value of Absolute Difference Image

<b>R Channel – MF Metric – % Outliers</b>				
<b>Region</b>	<b>SBP</b>	<b>MBP</b>	<b>TS</b>	<b>FM</b>
1	9	15	18	5
2	8	14	22	6
3	10	16	21	6
4	9	18	24	5
5	11	15	26	5
6	12	18	22	6
7	9	14	18	6
8	8	13	23	5
9	10	16	20	5
10	12	18	18	5
11	12	19	26	6
12	9	13	28	7
13	10	15	31	5
14	12	17	28	5
15	11	16	32	6
16	12	16	24	6
17	13	18	27	6
18	10	17	25	5
19	11	19	23	5
<b>AVERAGE:</b>	<b>10.42</b>	<b>16.16</b>	<b>24.0</b>	<b>5.52</b>

Table 9: R Channel – MF Metric – % Outliers

<b>G Channel – MF Metric – % Outliers</b>				
<b>Region</b>	<b>SBP</b>	<b>MBP</b>	<b>TS</b>	<b>FM</b>
1	9	14	19	5
2	8	14	21	5
3	8	14	24	5
4	8	15	28	6
5	10	17	26	6
6	12	19	22	5
7	12	18	18	7

8	11	17	26	6
9	14	19	28	5
10	10	16	19	5
11	11	16	27	5
12	12	15	27	6
13	14	20	25	6
14	11	17	28	7
15	12	18	29	5
16	10	16	28	5
17	9	16	27	7
18	12	19	26	6
19	11	17	28	6
<b>AVERAGE:</b>	<b>10.74</b>	<b>16.68</b>	<b>25.05</b>	<b>5.68</b>

Table 10: G Channel – MF Metric – % Outliers

<b>B Channel – MF Metric – % Outliers</b>				
<b>Region</b>	<b>SBP</b>	<b>MBP</b>	<b>TS</b>	<b>FM</b>
1	8	13	17	6
2	9	13	21	5
3	9	15	20	5
4	8	14	22	5
5	10	16	20	6
6	8	13	19	5
7	11	17	18	7
8	9	16	25	5
9	10	16	23	5
10	12	19	17	5
11	11	19	24	6
12	10	16	27	5
13	10	17	28	5
14	11	18	28	7
15	9	15	26	5
16	8	15	27	5
17	8	15	29	7
18	11	17	28	6
19	12	18	29	5
<b>AVERAGE:</b>	<b>9.68</b>	<b>15.89</b>	<b>23.56</b>	<b>6.05</b>

Table 11: B Channel – MF Metric – % Outliers

The analysis using the spatial MF metric for each of the models demonstrates a few noticeable trends. First, when the range of values and average value observed in the absolute

difference images is compared between texture models, the smallest values occur for the FM model for all texture regions. This indicates that the DIRSIG imagery using the FM texture model contains the smallest deviation from the real image for each of the three spectral channels in terms of its spatial structure in each 3x3 neighborhood and between each adjoining neighborhood. The next lowest values occur for the SBP model, which agrees with the visual analysis performed in the previous section. This quantitatively proves that for the three-band case, using the MBP model tends to over-constrain the reflectance curve selection process within the z-score selection algorithm. The differences between the performance of the SBP and MBP models in terms of the MF metric is quite small in many cases. When comparing the average values of the absolute difference images and the percentage of outliers from the variance threshold for these two models, it is evident that the values are always lower for the SBP model. There are cases in which the values for the MBP model are nearly the same as the SBP model, but there are no instances in which the MBP produces lower values than the SBP models. In general, the MBP model has produced much better results for the MF metric than for the TS model. The only exception to this is for more homogeneous material classes such as the running track (region #7), asphalt (region #1), and the building (region #10). For these regions, the numerical results of the MF metric are sometimes very close between the MBP and TS models. Otherwise, however, the remaining homogeneous and transition region textures indicate better performance by the MBP model. This once again is in accordance with the visual results, since the TS model DIRSIG image appears to capture the spatial structure for the track, asphalt, and rooftop regions approximately as well as the SBP and MBP results. There was no observed distinction between performances of the models for homogeneous and transition region textures, since the same trend was present regardless of texture region type. Based on this metric alone, the preliminary performance ranking would be:

- a. FM Model;
- b. SBP Model;
- c. MBP Model; and

d. TS Model

The percentage of outliers indicated in the above tables was supplemented by the investigation of *how much* the pixel values deviated from the threshold image. This was carried out by directly comparing the thresholded images for each feature and texture model. It was found that for all cases that the value of the deviation from the threshold was considerably lower for higher-ranked models than for the lower ranked models from the average and outlier analysis. This confirms the rankings prescribed above. A similar analysis using the more complex spatial GLCM metric is performed in the following section, and many of the observations cited above are equally valid for the rest of the texture performance metrics.

### 5.3.2 GLCM Metric

A parallel analysis is now presented using the GLCM metric for the CitiPix DIRSIG imagery. The GLCM features of Contrast and Correlation were examined for this metric, and each feature was treated slightly differently. For the Contrast feature, synopsis tables are presented just as they were for the MF metric in Section 5.3.1. Also, the two supplementary steps that proved useful in the previous section will be followed in order to further investigate the behavior near the variance threshold. These are:

- a. Taking the difference of the threshold images between pairs of texture model results in order to determine the magnitude of deviation from the threshold value for each texture region; and
- b. Taking the difference of the absolute difference images between pairs of texture model results in order to determine if corresponding pixels are above or below each other.

The results of the GLCM Correlation feature will also be presented, but only based on the percentage of outliers, followed by an analysis using steps (a) and (b) outlined above. The reason for this slightly different treatment of the Correlation feature is because the ranges and absolute values of pixels contained in these texture images is quite large, and thus

the difference image values are accordingly unpalatably large to list in summation tables. A comparison of these numbers in a tabular format between models would not be demonstrative of model performance and thus is not useful. As discussed earlier, the inclusion of the Homogeneity feature was considered to be unnecessary due to its redundancy with the Contrast feature already being analyzed, and due to the inverse relationship the features possess. Theoretically, the Correlation feature should exhibit the same trends as that observed in the GLCM Contrast metric analysis, therefore serving as a “sanity check” for the results.

<b>R Channel – GLCM Con Metric – Avg Value of Absolute Difference Image</b>				
<b>Region</b>	<b>SBP</b>	<b>MBP</b>	<b>TS</b>	<b>FM</b>
1	0.52	2.92	4.69	0.08
2	0.89	3.27	12.32	0.31
3	1.1	5.24	14.92	0.605
4	1.15	4.49	10.37	0.41
5	0.69	3.66	21.93	0.12
6	0.68	3.87	7.24	0.34
7	0.82	3.05	3.95	0.058
8	7.6	16.52	18.19	0.92
9	0.63	2.95	4.29	0.094
10	0.09	1.89	3.97	0.081
11	0.64	3.21	22.37	0.37
12	1.27	6.98	16.31	0.47
13	1.19	4.86	7.36	0.19
14	1.82	4.79	15.62	0.67
15	1.58	3.91	16.1	1.38
16	0.79	3.61	4.32	0.133
17	1.48	3.12	10.43	0.248
18	1.31	2.65	14.53	0.37

19	5.43	4.11	13.51	1.67
<b>AVERAGE:</b>	<b>1.56</b>	<b>4.48</b>	<b>11.71</b>	<b>0.45</b>

Table 12: R Channel – GLCM Contrast Metric – Average Value of Absolute Difference Image

<b>G Channel – GLCM Con Metric – Avg Value of Absolute Difference Image</b>				
<b>Region</b>	<b>SBP</b>	<b>MBP</b>	<b>TS</b>	<b>FM</b>
1	0.27	0.51	1.12	0.07
2	0.38	1.12	5.41	0.142
3	0.76	1.19	8.11	0.11
4	0.93	0.937	4.26	0.18
5	0.21	0.74	5.80	0.115
6	0.13	0.96	2.97	0.123
7	0.10	0.80	0.695	0.072
8	6.21	5.41	10.1	1.02
9	0.23	1.01	1.91	0.069
10	0.10	0.127	1.01	0.06
11	0.36	0.91	5.79	0.22
12	1.34	1.79	3.73	0.31
13	0.23	0.97	4.92	0.12
14	0.10	1.32	6.25	0.047
15	1.89	1.91	8.73	0.823
16	0.14	1.02	2.21	0.126
17	0.39	0.96	3.92	0.145
18	0.72	0.92	3.954	0.107
19	2.54	3.97	4.01	1.39
<b>AVERAGE:</b>	<b>0.90</b>	<b>1.40</b>	<b>4.47</b>	<b>0.28</b>

Table 13: G Channel – GLCM Contrast Metric – Average Value of Absolute Difference Image

<b>B Channel – GLCM Con Metric – Avg Value of Absolute Difference Image</b>				
<b>Region</b>	<b>SBP</b>	<b>MBP</b>	<b>TS</b>	<b>FM</b>
1	0.07	0.075	0.085	0.045
2	0.12	0.14	0.41	0.059
3	0.10	0.117	0.97	0.06
4	0.07	0.07	0.679	0.047
5	0.08	0.09	0.71	0.04
6	0.045	0.091	0.24	0.032
7	0.08	0.099	0.12	0.073
8	0.92	0.932	1.38	0.19
9	0.05	0.07	0.11	0.04
10	0.095	0.099	0.105	0.03
11	0.089	0.096	0.83	0.048
12	0.11	0.11	0.623	0.10
13	0.105	0.151	0.412	0.076
14	0.125	0.137	0.89	0.11
15	0.195	0.20	1.21	0.105
16	0.07	0.081	0.16	0.042
17	0.41	0.27	0.31	0.114
18	0.089	0.092	0.376	0.056
19	0.25	0.24	0.746	0.289
<b>AVERAGE:</b>	<b>0.16</b>	<b>0.17</b>	<b>0.55</b>	<b>0.08</b>

Table 14: B Channel – GLCM Contrast Metric – Average Value of Absolute Difference Image

<b>R Channel – GLCM Con Metric – % Outliers</b>				
<b>Region</b>	<b>SBP</b>	<b>MBP</b>	<b>TS</b>	<b>FM</b>
1	9	19	36	6
2	12	17	38	8
3	15	19	34	8

4	14	21	37	5
5	10	18	38	7
6	11	21	39	7
7	8	20	39	8
8	9	17	36	9
9	14	16	40	6
10	12	18	36	5
11	15	18	42	4
12	12	20	44	7
13	11	22	39	6
14	9	17	37	8
15	11	16	46	9
16	10	18	35	6
17	13	18	34	6
18	12	19	39	7
19	14	20	41	6
<b>AVERAGE:</b>	<b>11.63</b>	<b>18.63</b>	<b>38.42</b>	<b>6.73</b>

Table 15: R Channel – GLCM Contrast Metric – % Outliers

<b>G Channel – GLCM Con Metric – % Outliers</b>				
<b>Region</b>	<b>SBP</b>	<b>MBP</b>	<b>TS</b>	<b>FM</b>
1	9	16	34	5
2	8	19	37	7
3	13	16	34	6
4	11	17	42	6
5	9	19	44	9
6	12	22	41	8
7	15	20	35	6
8	14	28	38	7
9	13	17	36	5
10	16	20	36	5
11	11	21	42	7
12	9	23	39	5
13	7	21	43	9
14	8	18	37	7
15	8	19	43	9
16	11	19	41	8
17	10	21	38	7
18	9	20	37	9

19	11	18	41	7
<b>AVERAGE:</b>	<b>10.26</b>	<b>19.68</b>	<b>38.84</b>	<b>6.95</b>

Table 16: G Channel – GLCM Contrast Metric – % Outliers

<b>B Channel – GLCM Con Metric – % Outliers</b>				
<b>Region</b>	<b>SBP</b>	<b>MBP</b>	<b>TS</b>	<b>FM</b>
1	10	19	34	5
2	8	17	41	5
3	11	17	40	6
4	14	19	38	6
5	12	18	41	8
6	14	21	39	7
7	10	23	35	9
8	11	22	32	9
9	9	20	42	8
10	7	18	34	5
11	10	16	40	6
12	9	16	39	6
13	12	18	37	8
14	8	22	43	5
15	10	23	38	9
16	11	18	44	9
17	9	19	42	8
18	8	17	39	6
19	11	20	42	8
<b>AVERAGE:</b>	<b>10.21</b>	<b>19.11</b>	<b>38.95</b>	<b>7.0</b>

Table 17: B Channel – GLCM Contrast Metric – % Outliers

The above GLCM Contrast metric tables show the same trends as the MF metric in terms of performance of each of the texture models. However, there is more distinct separation between performance metric values for this metric, since it is more detailed in that it describes spatial structure in a more thorough and intelligent manner. The average values of the absolute difference images for each of the texture regions always followed the ranking prescribed above using the MF metric. That is, the values were always lowest (and thus better in terms of performance) for the FM model. The second-best performance was

by the SBP model, which itself performed just as well or better than the MBP model for all regions, although the values were quite close in some cases. Once again, the GLCM Contrast metric indicated that the TS model performed the poorest of the four models. In order to fully verify that the same rank ordering should be maintained based on the GLCM Contrast metric, the variance-thresholded images had to be compared for each region and each model. By following the same process of subtracting corresponding threshold images as outlined in Section 5.3.1, it was confirmed that the magnitudes of the deviation of higher ranked models were often negligibly small for many features. In fact, if an additional threshold was set to eliminate pixel values of less than 0.1 for this new difference image, then the effective percentage of outliers for the FM model was drastically reduced (usually with maxima of approximately 2%), while that for the SBP and MBP models was approximately 5% to 8% respectively. The comparison of the absolute difference images for each texture region also confirmed that this ranking was correct, since all corresponding pixel values of the metric images followed this trend (i.e., the FM model contained the lowest values in the difference image, followed by the SBP, MBP, and TS models). The only exceptions to this were the same as that found with the MF metric; that is, the difference between the SBP and MBP models was sometimes negligibly small, and the TS models performed just as well as the MBP (and sometimes the SBP model as well) for the asphalt, track, and building rooftop test regions.

The results for each model using the GLCM Correlation feature are presented next. The mathematical formula for the GLCM Correlation feature tends to produce very large numbers. Therefore, the variance threshold will be much larger for the Correlation feature than it was for the Contrast GLCM feature. For this reason (as well as those stated above), the following synopsis tables will consist solely of the percentage of outliers for each region and each texture model.

<b>R Channel – GLCM Cor Metric – % Outliers</b>				
<b>Region</b>	<b>SBP</b>	<b>MBP</b>	<b>TS</b>	<b>FM</b>
1	11	24	44	7
2	15	22	48	7
3	12	20	46	9
4	10	19	46	10
5	12	22	47	9
6	10	26	45	7
7	9	23	43	6
8	10	25	44	6
9	11	22	44	9
10	14	20	42	7
11	16	24	47	8
12	13	26	48	7
13	11	23	48	9
14	10	26	49	7
15	9	22	46	6
16	9	19	50	6
17	10	21	47	9
18	13	20	46	8
19	11	24	49	6
<b>AVERAGE:</b>	<b>11.37</b>	<b>22.53</b>	<b>46.26</b>	<b>7.53</b>

Table 18: R Channel – GLCM Correlation Metric – % Outliers

<b>G Channel – GLCM Cor Metric – % Outliers</b>				
<b>Region</b>	<b>SBP</b>	<b>MBP</b>	<b>TS</b>	<b>FM</b>
1	12	26	39	8
2	10	25	41	8
3	13	21	44	6
4	13	26	42	8
5	15	20	42	7
6	12	27	40	8
7	10	26	38	8
8	10	22	41	6
9	14	24	44	8
10	11	23	38	9
11	12	27	47	8
12	10	29	47	9
13	12	24	49	9
14	14	28	45	7

15	14	27	48	6
16	13	24	47	6
17	10	28	49	5
18	13	22	46	8
19	12	23	48	8
<b>AVERAGE:</b>	<b>12.11</b>	<b>24.84</b>	<b>43.95</b>	<b>7.47</b>

Table 19: G Channel – GLCM Correlation Metric – % Outliers

<b>B Channel – GLCM Cor Metric – % Outliers</b>				
<b>Region</b>	<b>SBP</b>	<b>MBP</b>	<b>TS</b>	<b>FM</b>
1	13	25	38	7
2	15	24	44	7
3	10	28	42	9
4	14	26	45	7
5	16	24	41	7
6	12	26	39	6
7	17	29	37	6
8	14	30	38	9
9	12	22	42	7
10	17	24	37	7
11	14	22	44	9
12	12	25	45	6
13	11	26	48	8
14	10	26	48	8
15	14	28	49	6
16	12	24	46	9
17	15	25	50	5
18	17	29	45	8
19	11	23	48	9
<b>AVERAGE:</b>	<b>13.47</b>	<b>25.58</b>	<b>43.47</b>	<b>7.37</b>

Table 20: B Channel – GLCM Correlation Metric – % Outliers

The Correlation feature of the GLCM metric exhibits the same discriminative power as the Contrast feature based on the analysis of percentage of outliers from the threshold. Although the number of outliers is slightly higher for the Correlation feature than the Contrast feature, the same trend of performance ranking is seen as with the GLCM Contrast and MF metrics. This metric also indicates much better performance for the asphalt, track,

and rooftop materials for the TS model, since the values for these regions (#1, #7, and #10) are closer to those of the three other models. It was originally intended to present a sampling of output GLCM Contrast and Correlation features within this document. However, due to the extremely large number of texture test regions for both the CitiPix and HYDICE ARM imagery, and considering that a sampling of each real image, each texture model, each spectral band and corresponding feature would have to be shown, the image results have not been included here. These metric images have been stored electronically and they can be accessed upon request to the author. The synopsis tables and subsequent analysis are much more diagnostic and indicative of texture model performance than a visual analysis of the metric imagery, and thus their inclusion was deemed unnecessary.

### 5.3.3 SCM Metric

Although the spatial-spectral SCM metric has been designed for use with imagery of larger spectral dimension, it can be applied nonetheless even on imagery consisting of only a few spectral bands, such as the CitiPix data. In this case, the least correlated band pair (Red-Blue) was used for the analysis. The following table is a synopsis of the results observed for each texture region using all four texture models.

<b>R-B Channels – SCM Con Metric – Avg Value of Absolute Difference Image</b>				
<b>Region</b>	<b>SBP</b>	<b>MBP</b>	<b>TS</b>	<b>FM</b>
1	11.3	33.25	26.7	1.05
2	0.74	11.95	42.67	0.21
3	3.31	23.76	39.86	4.42
4	1.54	17.68	31.29	2.97
5	11.38	42.33	53.92	1.39
6	9.41	34.06	54.31	1.1
7	16.39	52.70	12.12	0.97
8	11.23	23.95	24.69	4.53

9	12.74	43.17	48.29	1.61
10	35.46	101.15	39.26	4.67
11	10.76	42.6	56.41	3.20
12	14.79	48.12	57.76	3.36
13	10.92	43.31	56.59	5.05
14	4.24	12.20	37.27	3.98
15	2.02	15.40	25.54	1.97
16	14.91	67.30	76.77	1.01
17	19.87	52.91	26.98	3.83
18	4.27	23.70	43.74	4.02
19	19.79	37.98	68.79	10.92
<b>AVERAGE:</b>	<b>11.32</b>	<b>38.29</b>	<b>43.31</b>	<b>3.17</b>

Table 21: R-B Channels – SCM Contrast Metric – Average Value of Absolute Difference Image

<b>R-B Channels – SCM Con Metric – % Outliers</b>				
<b>Region</b>	<b>SBP</b>	<b>MBP</b>	<b>TS</b>	<b>FM</b>
1	11	19	42	6
2	15	22	47	8
3	14	24	49	5
4	16	22	44	7
5	13	21	47	9
6	13	20	49	6
7	15	25	41	8
8	18	19	45	7
9	13	16	46	9
10	12	19	40	5
11	11	22	49	8
12	14	23	53	10
13	18	19	51	9
14	13	21	49	9
15	16	20	48	7
16	14	25	46	9
17	17	23	49	8
18	15	27	47	10

19	14	23	48	7
<b>AVERAGE:</b>	<b>17.89</b>	<b>21.58</b>	<b>51.89</b>	<b>7.74</b>

Table 22: R-B Channels – SCM Contrast Metric – % Outliers

This metric performs the exact same operation as the GLCM metric, except the base and shift processing windows are in different user-specified spectral bands. The values are therefore indicative of both spatial and spectral fidelity, since spatial structure and spectral correlation across the Red and Blue channels are being measured. It was not expected to obtain much new information with the SCM metric for the CitiPix data, since the spectral bands are very well correlated across the visible region. It will however specify that the spatial-spectral structure is not well represented if the metric produces a large value for a given test region. Observing the range and average values of the absolute difference image values once again indicates that the ranking used above should be maintained, since the lowest values belong to the FM model image, while the SBP, MBP, and TS models follow respectively. An important note is that, since this metric emphasizes spectral structure as well as spatial structure, we see that there is a larger gap between metric values of the SBP and MBP models. This owes to the same phenomenon of over-constraining the z-score selection algorithm within the MBP model, which in effect causes the SBP model to perform better than the MBP model, which may initially appear to be a counter-intuitive result since the concept of the MBP model was designed in order to improve spatial-spectral fidelity across the entire spectral dimension. It will be interesting to see if this result is reversed for the metrics to be run on the HYDICE ARM imagery.

The comparison of absolute difference and thresholded images for each texture test region produced the same general result as obtained with the GLCM Contrast metric and thus suggested the same rank ordering of the models. The only significant difference in the results between the GLCM and SCM Contrast metrics is that there was more separation between the SBP and MBP models using the SCM metric. One will also notice that regions 1, 7, and 10 (asphalt, track, and building rooftop) are sometimes characterized just as well as the MBP model due to the lack of within-material class transitions and/or large-scale structures that typically produce challenges for the TS model.

As discussed earlier, the FM texture model assigns only one spectral reflectance curve to each end member and then re-mixes the fractional abundance planes into a synthetic image. For this reason, the spatial fidelity was expected to be quite good, while the spectral dimension had the potential to suffer. This is not true for the CitiPix data, since the choice of an adequate spectral reflectance curve to fully characterize the end member is less crucial over such a well-correlated spectral bandpass. As such, the reflectance curve to be coupled with each fractional abundance map becomes more sensitive to errors as the spectral dimension increases. Therefore, the rendering of the HYDICE ARM image will present much more of a challenge to the FM model.

The SCM Correlation metric results are presented below, which again only shows the percentage of outliers from the threshold image for each texture test region.

<b>R-B Channels – SCM Cor Metric – % Outliers</b>				
<b>Region</b>	<b>SBP</b>	<b>MBP</b>	<b>TS</b>	<b>FM</b>
1	14	25	44	8
2	17	27	45	10
3	15	28	49	7
4	16	24	43	9
5	16	22	41	10
6	14	21	42	11
7	18	23	47	8
8	17	29	46	7
9	19	26	47	9
10	12	28	49	7
11	14	25	48	6
12	11	27	48	8
13	16	21	44	10
14	18	25	45	7
15	10	28	48	6
16	15	26	42	6
17	18	29	41	8
18	16	23	45	9
19	19	29	46	10
<b>AVERAGE:</b>	<b>15.52</b>	<b>25.58</b>	<b>45.26</b>	<b>8.21</b>

Table 23: R-B Channels – SCM Correlation Metric – % Outliers

As anticipated, these results reinforce the ranking of the texture characterization models once more. The TS model once again shows similarly good performance for the same three regions as indicated with the other metric results. For all of the above metrics, the behavior for the tree test region (#8) has been somewhat more volatile than for the other regions. This is because of the high level of inherent variability for the tree leaves in the scene. This is the only transmissive material in the image, and extinction files have been included for the SBP, MBP, and FM models in order to characterize the shadows and brighter leaves within the tree canopies. The TS model simply treated the trees as it would any other material, and thus does not exhibit transmissive properties. Also, the abrupt transition regions in the TS image have been evident especially for the GLCM and SCM metrics. This is most noticeable in the Correlation tables, where the number of outliers for the transition region textures (regions #11 - #19) is much greater than for the other three models. The final rankings of each model are presented in Section 5.5 so that the HYDICE ARM imagery results can also be accounted for when assessing overall performance. However, an interim summary table is presented below which provides the average of the averages tallied in each of the above tables. That is, the average values of the % outliers and the average value of the absolute difference images have been averaged over all metrics and all three spectral bands and reported in Table 24. The rankings for each measure are included beside the entries. The final rankings for the CitiPix data is then: 1. FM model; 2. SBP model; 3. MBP model; and 4. TS model.

<b>Texture Model</b>	<b>AVG % Outliers</b>	<b>AVG Average Value</b>
<b>SBP</b>	12.12 (2)	2.25 (2)
<b>MBP</b>	20.57 (3)	6.98 (3)
<b>TS</b>	38.15 (4)	9.63 (4)
<b>FM</b>	6.93 (1)	0.66 (1)

Table 24: Averaged values of all metrics and spectral bands for CitiPix data based on percentage of outliers from threshold and average value of absolute difference images. The rankings for each measure are included beside each entry.



## 5.4 HYDICE ARM Metric Results

This section presents a detailed analysis of the results obtained from the application of the MF, GLCM, SCR, and SCM performance metrics for each of the 15 texture test regions of the HYDICE ARM data set, for the eight representative spectral bands listed earlier (bands 20, 32, 65, 95, 115, 157, 184, and 195). All four metrics have been applied to all 15 regions of the eight spectral bands for the output DIRSIG imagery from the four tested texture models. The methodology for analyzing the metric results is completely analogous to that of the CitiPix data presented in Section 5.3. The percentage of outliers from the variance threshold images and the average values of the absolute difference images for each texture region, as well as the average value of each of the absolute difference images will be presented in the following tables. In parentheses, the ranking for each texture test region has also been included. The last row of each table indicates the average value and ranking for the particular feature being investigated.

### 5.4.1 MF Metric

The following tables provide a summary of the results obtained using the spatial MF metric on the rendered HYDICE ARM DIRSIG imagery for all four texture characterization models.

Band 20 – MF Metric – Avg Value of Absolute Difference Image				
Region	SBP	MBP	TS	FM
1	0.90 (3)	0.87 (2)	1.4 (4)	0.21 (1)
2	0.43 (3)	0.19 (2)	0.51 (4)	0.16 (1)
3	0.41 (3)	0.042 (1)	0.49 (4)	0.06 (2)
4	0.37 (3)	0.17 (2)	0.46 (4)	0.11 (1)
5	0.076 (1)	0.12 (3)	0.51 (4)	0.09 (2)
6	0.67 (3)	0.42 (2)	0.70 (4)	0.08 (1)
7	0.89 (3)	0.78 (2)	0.92 (4)	0.36 (1)
8	0.29 (4)	0.14 (2)	0.26 (3)	0.12 (1)
9	8.70 (2)	8.85 (3)	9.2 (4)	0.46 (1)
10	0.42 (2)	0.48 (3)	1.1 (4)	0.11 (1)
11	1.20 (3)	1.02 (2)	1.31 (4)	0.36 (1)

12	2.31 (3)	1.27 (2)	3.27 (4)	0.19 (1)
13	0.66 (3)	0.305 (2)	1.1 (4)	0.22 (1)
14	2.84 (3)	1.91 (2)	3.01 (4)	0.52 (1)
15	1.21 (2)	1.46 (3)	3.6 (4)	1.02 (1)
<b>AVERAGE:</b>	<b>1.43 (2.73)</b>	<b>1.20 (2.2)</b>	<b>1.86 (3.93)</b>	<b>0.27 (1.13)</b>

<b>Band 32 – MF Metric – Avg Value of Absolute Difference Image</b>				
<b>Region</b>	<b>SBP</b>	<b>MBP</b>	<b>TS</b>	<b>FM</b>
1	0.7 (3)	0.32 (2)	0.81 (4)	0.22 (1)
2	1.2 (4)	0.51 (2)	1.19 (3)	0.21 (1)
3	0.24 (3)	0.14 (2)	0.26 (4)	0.13 (1)
4	0.62 (4)	0.23 (2)	0.47 (3)	0.18 (1)
5	0.27 (2)	0.3 (3)	0.49 (4)	0.21 (1)
6	1.08 (3)	0.48 (2)	1.12 (4)	0.28 (1)
7	1.01 (3)	0.71 (2)	1.31 (4)	0.20 (1)
8	0.72 (4)	0.37 (2)	0.38 (3)	0.15 (1)
9	10.7 (4)	6.4 (2)	9.1 (3)	0.81 (1)
10	0.9 (3)	0.86 (2)	1.02 (4)	0.20 (1)
11	1.56 (3)	0.99 (2)	1.6 (4)	0.32 (1)
12	2.23 (3)	1.31 (2)	3.46 (4)	0.29 (1)
13	1.01 (3)	0.74 (2)	1.15 (4)	0.21 (1)
14	3.64 (3)	1.65 (2)	3.71 (4)	0.42 (1)
15	4.1 (3)	1.52 (2)	4.9 (4)	1.21 (1)
<b>AVERAGE:</b>	<b>2.0 (3.2)</b>	<b>1.10 (2.07)</b>	<b>2.06 (3.73)</b>	<b>0.34 (1)</b>

<b>Band 65 – MF Metric – Avg Value of Absolute Difference Image</b>				
<b>Region</b>	<b>SBP</b>	<b>MBP</b>	<b>TS</b>	<b>FM</b>
1	5.46 (3)	4.31 (2)	5.6 (4)	0.51 (1)
2	5.1 (4)	3.29 (2)	4.02 (3)	0.41 (1)
3	1.84 (4)	1.1 (2)	1.767 (3)	0.46 (1)
4	1.47 (4)	0.67 (2)	1.38 (3)	0.34 (1)
5	4.12 (4)	1.47 (2)	3.87 (3)	0.26 (1)
6	2.23 (4)	1.1 (2)	2.1 (3)	0.32 (1)
7	6.72 (4)	2.01 (2)	3.89 (3)	0.61 (1)

8	2.79 (4)	2.37 (2)	2.64 (3)	0.32 (1)
9	7.07 (4)	1.06 (2)	4.4 (3)	0.28 (1)
10	10.13 (4)	2.98 (2)	5.82 (3)	0.46 (1)
11	2.22 (3)	1.0 (2)	3.4 (4)	0.21 (1)
12	6.89 (3)	2.11 (2)	9.1 (4)	0.33 (1)
13	5.78 (4)	1.69 (2)	3.1 (3)	0.37 (1)
14	5.28 (3)	3.1 (2)	9.6 (4)	1.2 (1)
15	3.98 (3)	2.52 (2)	8.6 (4)	0.76 (1)
<b>AVERAGE:</b>	<b>4.74 (3.67)</b>	<b>2.05 (2)</b>	<b>4.62 (3.33)</b>	<b>0.46 (1)</b>

<b>Band 95 – MF Metric – Avg Value of Absolute Difference Image</b>				
<b>Region</b>	<b>SBP</b>	<b>MBP</b>	<b>TS</b>	<b>FM</b>
1	5.83 (4)	3.72 (2)	5.79 (3)	0.37 (1)
2	3.89 (4)	2.72 (2)	3.71 (3)	0.37 (1)
3	1.91 (4)	1.41 (2)	1.9 (3)	0.26 (1)
4	1.62 (4)	0.93 (2)	1.48 (3)	0.91 (1)
5	2.35 (4)	0.72 (2)	1.67 (3)	0.14 (1)
6	1.75 (3)	1.71 (2)	2.15 (4)	0.59 (1)
7	2.35 (4)	1.63 (2)	2.29 (3)	0.92 (1)
8	1.98 (4)	1.41 (2)	1.89 (3)	0.13 (1)
9	7.2 (4)	1.22 (2)	4.2 (3)	0.56 (1)
10	4.82 (4)	2.56 (2)	4.59 (3)	0.67 (1)
11	3.38 (3)	3.03 (2)	3.39 (4)	0.66 (1)
12	6.56 (3)	2.16 (2)	7.02 (4)	0.36 (1)
13	3.42 (4)	2.02 (2)	3.14 (3)	0.39 (1)
14	7.36 (3)	2.77 (2)	7.5 (4)	0.43 (1)
15	4.91 (3)	1.98 (2)	5.13 (4)	1.1 (1)
<b>AVERAGE:</b>	<b>3.96 (3.67)</b>	<b>2.0 (2)</b>	<b>3.72 (3.33)</b>	<b>0.52 (1)</b>

<b>Band 115 – MF Metric – Avg Value of Absolute Difference Image</b>				
<b>Region</b>	<b>SBP</b>	<b>MBP</b>	<b>TS</b>	<b>FM</b>
1	4.98 (4)	2.76 (2)	3.96 (3)	0.27 (1)
2	1.43 (3)	0.27 (2)	2.9 (4)	0.24 (1)
3	1.86 (4)	0.83 (2)	1.79 (3)	0.31 (1)

4	1.43 (3)	0.64 (2)	1.52 (4)	0.17 (1)
5	1.48 (4)	1.26 (2)	1.46 (3)	0.29 (1)
6	1.97 (4)	0.889 (2)	1.93 (3)	0.09 (1)
7	9.26 (4)	6.4 (2)	9.03 (3)	0.69 (1)
8	0.97 (3)	0.96 (2)	1.04 (4)	0.17 (1)
9	6.13 (3)	4.01 (2)	6.84 (4)	0.53 (1)
10	6.1 (4)	2.45 (2)	4.67 (3)	0.59 (1)
11	9.4 (4)	4.74 (2)	8.7 (3)	0.22 (1)
12	5.58 (3)	2.97 (2)	5.7 (4)	0.44 (1)
13	3.53 (4)	2.11 (2)	3.3 (3)	0.20 (1)
14	6.07 (3)	2.45 (2)	6.1 (4)	0.66 (1)
15	3.47 (3)	2.04 (2)	3.9 (4)	0.28 (1)
<b>AVERAGE:</b>	<b>4.24 (3.53)</b>	<b>2.32 (2)</b>	<b>4.19 (3.47)</b>	<b>0.34 (1)</b>

<b>Band 157 – MF Metric – Avg Value of Absolute Difference Image</b>				
<b>Region</b>	<b>SBP</b>	<b>MBP</b>	<b>TS</b>	<b>FM</b>
1	10.6 (4)	4.95 (2)	9.7 (3)	1.07 (1)
2	2.29 (4)	1.02 (2)	2.21 (3)	0.98 (1)
3	2.76 (4)	1.46 (2)	2.6 (3)	0.92 (1)
4	2.09 (3)	0.9 (2)	2.3 (4)	0.87 (1)
5	2.74 (3)	1.58 (2)	2.91 (4)	0.59 (1)
6	4.47 (4)	1.24 (2)	3.93 (3)	1.14 (1)
7	10.2 (3)	9.13 (2)	10.27 (4)	0.76 (1)
8	1.15 (2)	1.18 (3)	1.19 (4)	0.52 (1)
9	5.94 (2)	7.02 (3)	11.3 (4)	0.83 (1)
10	8.8 (4)	2.97 (2)	6.44 (3)	1.12 (1)
11	8.4 (4)	3.98 (2)	7.6 (3)	1.5 (1)
12	7.03 (4)	3.12 (2)	6.91 (3)	0.61 (1)
13	5.45 (4)	3.97 (2)	5.2 (3)	0.68 (1)
14	7.43 (4)	5.31 (2)	6.98 (3)	1.64 (1)
15	5.56 (3)	2.11 (2)	9.2 (4)	1.2 (1)
<b>AVERAGE:</b>	<b>5.66 (3.47)</b>	<b>3.33 (2.13)</b>	<b>5.92 (3.4)</b>	<b>0.96 (1)</b>

<b>Band 184 – MF Metric – Avg Value of Absolute Difference Image</b>				
<b>Region</b>	<b>SBP</b>	<b>MBP</b>	<b>TS</b>	<b>FM</b>
1	7.45 (4)	5.61 (2)	7.27 (3)	0.29 (1)
2	1.77 (4)	0.21 (2)	1.54 (3)	0.2 (1)
3	1.98 (4)	0.41 (2)	1.91 (3)	0.37 (1)
4	2.1 (3)	1.72 (2)	2.7 (4)	0.98 (1)
5	1.69 (4)	1.09 (2)	1.6 (3)	0.18 (1)
6	2.4 (4)	1.04 (2)	2.1 (3)	0.76 (1)
7	12.47 (4)	8.07 (2)	10.98 (3)	0.63 (1)
8	1.23 (4)	1.12 (2)	1.21 (3)	0.14 (1)
9	10.2 (2)	10.92 (3)	11.8 (4)	0.56 (1)
10	4.73 (4)	2.33 (2)	4.3 (3)	0.81 (1)
11	7.97 (4)	4.2 (2)	7.3 (3)	0.34 (1)
12	3.92 (3)	1.56 (2)	4.2 (4)	0.43 (1)
13	6.25 (4)	2.01 (2)	5.5 (3)	0.54 (1)
14	8.6 (4)	4.4 (2)	8.4 (3)	1.61 (1)
15	5.34 (3)	2.96 (2)	10.2 (4)	1.01 (1)
<b>AVERAGE:</b>	<b>5.21 (3.67)</b>	<b>3.18 (2.07)</b>	<b>5.40 (3.27)</b>	<b>0.59 (1)</b>

<b>Band 195 – MF Metric – Avg Value of Absolute Difference Image</b>				
<b>Region</b>	<b>SBP</b>	<b>MBP</b>	<b>TS</b>	<b>FM</b>
1	8.92 (4)	5.93 (2)	8.2 (3)	0.31 (1)
2	1.97 (4)	0.38 (2)	1.72 (3)	0.23 (1)
3	2.86 (4)	1.21 (2)	2.41 (3)	0.54 (1)
4	3.93 (3)	0.98 (2)	3.97 (4)	0.30 (1)
5	1.99 (4)	1.42 (2)	1.89 (3)	0.16 (1)
6	2.7 (4)	0.91 (2)	2.3 (3)	0.62 (1)
7	10.85 (4)	7.26 (2)	9.67 (3)	0.18 (1)
8	1.13 (3)	1.54 (4)	1.09 (2)	0.27 (1)
9	9.7 (3)	9.1 (2)	12.2 (4)	1.49 (1)
10	6.2 (4)	3.61 (2)	5.1 (3)	0.76 (1)
11	7.79 (4)	3.26 (2)	6.93 (3)	0.17 (1)
12	5.94 (4)	1.99 (2)	5.6 (3)	0.71 (1)
13	6.99 (4)	3.57 (2)	6.1 (3)	0.42 (1)

14	7.14 (4)	3.73 (2)	6.89 (3)	2.31 (1)
15	5.77 (3)	2.32 (2)	6.2 (4)	0.42 (1)
<b>AVERAGE:</b>	<b>5.59 (3.73)</b>	<b>3.15 (2.13)</b>	<b>5.35 (3.13)</b>	<b>0.59 (1)</b>
Table 25: Average value of absolute difference images for MF Metric.				
<b>Band 20 – MF Metric – % Outliers</b>				
<b>Region</b>	<b>SBP</b>	<b>MBP</b>	<b>TS</b>	<b>FM</b>
1	16 (3)	9 (2)	29 (4)	5 (1)
2	17 (3)	11 (2)	31 (4)	5 (1)
3	17 (3)	10 (2)	36 (4)	7 (1)
4	15 (3)	8 (2)	35 (4)	6 (1)
5	19 (3)	9 (2)	36 (4)	7 (1)
6	21 (3)	9 (2)	28 (4)	7 (1)
7	23 (3)	10 (2)	35 (4)	8 (1)
8	18 (3)	13 (2)	39 (4)	5 (1)
9	19 (3)	12 (2)	29 (4)	5 (1)
10	24 (3)	9 (2)	33 (4)	7 (1)
11	23 (3)	11 (2)	31 (4)	5 (1)
12	22 (3)	13 (2)	37 (4)	6 (1)
13	20 (3)	12 (2)	39 (4)	8 (1)
14	21 (3)	12 (2)	36 (4)	5 (1)
15	17 (3)	9 (2)	38 (4)	5 (1)
<b>AVERAGE:</b>	<b>19.47 (3)</b>	<b>10.47 (2)</b>	<b>34.13 (4)</b>	<b>6.07 (1)</b>

<b>Band 32 – MF Metric – % Outliers</b>				
<b>Region</b>	<b>SBP</b>	<b>MBP</b>	<b>TS</b>	<b>FM</b>
1	14 (3)	12 (2)	31 (4)	6 (1)
2	18 (3)	11 (2)	33 (4)	5 (1)
3	19 (3)	10 (2)	30 (4)	5 (1)
4	17 (3)	13 (2)	29 (4)	7 (1)
5	16 (3)	11 (2)	27 (4)	5 (1)
6	19 (3)	9 (2)	32 (4)	6 (1)
7	18 (3)	9 (2)	35 (4)	6 (1)
8	22 (3)	11 (2)	34 (4)	5 (1)
9	23 (3)	9 (2)	34 (4)	7 (1)

10	21 (3)	8 (2)	31 (4)	7 (1)
11	20 (3)	10 (2)	30 (4)	6 (1)
12	18 (3)	11 (2)	28 (4)	7 (1)
13	21 (3)	10 (2)	29 (4)	5 (1)
14	23 (3)	9 (2)	31 (4)	5 (1)
15	19 (3)	11 (2)	34 (4)	5 (1)
<b>AVERAGE:</b>	<b>19.2 (3)</b>	<b>10.27 (2)</b>	<b>31.2 (4)</b>	<b>5.8 (1)</b>

<b>Band 65 – MF Metric – % Outliers</b>				
<b>Region</b>	<b>SBP</b>	<b>MBP</b>	<b>TS</b>	<b>FM</b>
1	25 (3)	10 (2)	29 (4)	6 (1)
2	27 (3)	11 (2)	35 (4)	5 (1)
3	29 (3)	9 (2)	31 (4)	5 (1)
4	24 (3)	9 (2)	33 (4)	5 (1)
5	26 (3)	10 (2)	35 (4)	7 (1)
6	25 (3)	13 (2)	27 (4)	8 (1)
7	28 (3)	14 (2)	31 (4)	6 (1)
8	31 (3)	12 (2)	33 (4)	6 (1)
9	35 (4)	10 (2)	34 (3)	5 (1)
10	36 (3)	11 (2)	38 (4)	5 (1)
11	35 (3)	13 (2)	39 (4)	5 (1)
12	34 (3)	11 (2)	35 (4)	5 (1)
13	38 (4)	10 (2)	35 (3)	6 (1)
14	39 (3)	9 (2)	39 (4)	6 (1)
15	33 (3)	11 (2)	41 (4)	5 (1)
<b>AVERAGE:</b>	<b>31 (3.13)</b>	<b>10.87 (2)</b>	<b>34.33 (3.87)</b>	<b>5.67 (1)</b>

<b>Band 95 – MF Metric – % Outliers</b>				
<b>Region</b>	<b>SBP</b>	<b>MBP</b>	<b>TS</b>	<b>FM</b>
1	29 (3)	12 (2)	30 (4)	5 (1)
2	34 (3)	12 (2)	36 (4)	6 (1)
3	33 (3)	11 (2)	35 (4)	6 (1)
4	36 (4)	10 (2)	34 (3)	6 (1)
5	34 (3)	12 (2)	38 (4)	7 (1)

6	32 (3)	9 (2)	39 (4)	6 (1)
7	31 (3)	9 (2)	33 (4)	6 (1)
8	29 (3)	10 (2)	36 (4)	5 (1)
9	33 (4)	12 (2)	32 (3)	5 (1)
10	39 (4)	12 (2)	36 (3)	6 (1)
11	36 (4)	13 (2)	34 (3)	5 (1)
12	38 (4)	13 (2)	37 (3)	5 (1)
13	37 (3)	11 (2)	39 (4)	6 (1)
14	39 (3)	10 (2)	41 (4)	6 (1)
15	40 (4)	9 (2)	39 (3)	5 (1)
<b>AVERAGE:</b>	<b>34.67 (3.4)</b>	<b>11 (2)</b>	<b>35.93 (3.6)</b>	<b>5.67 (1)</b>

<b>Band 115 – MF Metric – % Outliers</b>				
<b>Region</b>	<b>SBP</b>	<b>MBP</b>	<b>TS</b>	<b>FM</b>
1	29 (3)	12 (2)	34 (4)	6 (1)
2	33 (4)	11 (2)	31 (3)	5 (1)
3	36 (4)	9 (2)	32 (3)	5 (1)
4	39 (4)	10 (2)	36 (3)	5 (1)
5	41 (4)	10 (2)	38 (3)	5 (1)
6	44 (4)	11 (2)	37 (3)	7 (1)
7	43 (4)	13 (2)	39 (3)	5 (1)
8	47 (4)	12 (2)	40 (3)	5 (1)
9	48 (4)	12 (2)	44 (3)	7 (1)
10	43 (4)	12 (2)	41 (3)	5 (1)
11	41 (3)	11 (2)	41 (3)	6 (1)
12	40 (4)	10 (2)	37 (3)	6 (1)
13	44 (4)	9 (2)	38 (3)	5 (1)
14	42 (4)	10 (2)	39 (3)	5 (1)
15	46 (4)	9 (2)	39 (3)	6 (1)
<b>AVERAGE:</b>	<b>41.07 (3.87)</b>	<b>10.73 (2)</b>	<b>37.73 (3.07)</b>	<b>5.67 (1)</b>

<b>Band 157 – MF Metric – % Outliers</b>				
<b>Region</b>	<b>SBP</b>	<b>MBP</b>	<b>TS</b>	<b>FM</b>
1	39 (4)	10 (2)	37 (3)	5 (1)

2	34 (3)	9 (2)	36 (4)	5 (1)
3	36 (4)	9 (2)	33 (3)	5 (1)
4	36 (4)	11 (2)	31 (3)	6 (1)
5	38 (4)	10 (2)	31 (3)	6 (1)
6	33 (4)	12 (2)	32 (3)	5 (1)
7	39 (4)	12 (2)	32 (3)	5 (1)
8	38 (4)	13 (2)	31 (3)	7 (1)
9	41 (4)	10 (2)	35 (3)	7 (1)
10	40 (4)	9 (2)	34 (3)	5 (1)
11	42 (4)	9 (2)	33 (3)	5 (1)
12	46 (4)	12 (2)	33 (3)	6 (1)
13	44 (4)	10 (2)	38 (3)	5 (1)
14	43 (4)	11 (2)	39 (3)	5 (1)
15	41 (4)	11 (2)	37 (3)	5 (1)
<b>AVERAGE:</b>	<b>39.33 (3.93)</b>	<b>10.53 (2)</b>	<b>34.13 (3.07)</b>	<b>5.47 (1)</b>

<b>Band 184 – MF Metric – % Outliers</b>				
<b>Region</b>	<b>SBP</b>	<b>MBP</b>	<b>TS</b>	<b>FM</b>
1	38 (3)	11 (2)	39 (4)	6 (1)
2	35 (4)	10 (2)	34 (3)	6 (1)
3	39 (4)	10 (2)	34 (3)	5 (1)
4	41 (4)	10 (2)	36 (3)	5 (1)
5	45 (4)	13 (2)	37 (3)	5 (1)
6	46 (4)	12 (2)	33 (3)	5 (1)
7	41 (4)	11 (2)	39 (3)	7 (1)
8	42 (4)	12 (2)	40 (3)	6 (1)
9	39 (4)	9 (2)	37 (3)	7 (1)
10	44 (4)	10 (2)	39 (3)	5 (1)
11	42 (3)	10 (2)	42 (3)	5 (1)
12	45 (4)	9 (2)	42 (3)	5 (1)
13	42 (4)	12 (2)	40 (3)	5 (1)
14	41 (4)	10 (2)	40 (3)	6 (1)
15	47 (4)	11 (2)	44 (3)	5 (1)
<b>AVERAGE:</b>	<b>41.8 (3.87)</b>	<b>10.67 (2)</b>	<b>38.4 (3.07)</b>	<b>5.53 (1)</b>

<b>Band 195 – MF Metric – % Outliers</b>				
<b>Region</b>	<b>SBP</b>	<b>MBP</b>	<b>TS</b>	<b>FM</b>
1	41 (3)	11 (2)	41 (3)	7 (1)
2	44 (4)	9 (2)	40 (3)	6 (1)
3	46 (4)	9 (2)	43 (3)	5 (1)
4	48 (4)	11 (2)	38 (3)	5 (1)
5	48 (4)	10 (2)	37 (3)	5 (1)
6	47 (4)	9 (2)	37 (3)	5 (1)
7	49 (4)	12 (2)	39 (3)	5 (1)
8	44 (4)	12 (2)	40 (3)	6 (1)
9	46 (4)	11 (2)	42 (3)	6 (1)
10	48 (4)	13 (2)	42 (3)	5 (1)
11	49 (4)	11 (2)	43 (3)	7 (1)
12	44 (4)	13 (2)	41 (3)	6 (1)
13	45 (4)	12 (2)	38 (3)	5 (1)
14	45 (4)	11 (2)	39 (3)	6 (1)
15	49 (4)	9 (2)	44 (3)	5 (1)
<b>AVERAGE:</b>	<b>46.2 (3.93)</b>	<b>10.87 (2)</b>	<b>40.27 (3)</b>	<b>5.53 (1)</b>

Table 26: Percentage of outliers from variance threshold for MF metric.

The above synopsis tables exhibit some very noticeable trends. The first and most obvious result is that the FM model contains the lowest values for the average value (and range of values) within the absolute difference images, thereby indicating the best overall performance. This was verified by analyzing the corresponding absolute difference images for each region and model, and subtracting the FM model result from the results of the SBP, MBP, and TS models. All pixel values in the TS and SBP models were larger than the FM model values, while the MBP model contained the closest values to that of the FM model. In general, the values of the MBP model images were all greater than or equal to the values of the FM model metric images, with the exception of eleven pixels (out of all fifteen regions) for which the MBP value was negligibly smaller than that of the corresponding FM model pixel, where the difference value was less than  $10^{-5}$ .

The magnitude of the deviation from the threshold image for each region was also investigated for all texture model results. This provided a confirmation of the results of the percentage of outliers from the threshold. Both the average values of the absolute difference images and the percentage of outliers suggest the same ranking of texture models based on the MF metric alone.

Although it was clear that the FM model contained values indicating the best overall performance, the results were not always as clear for the remaining models. For example, the reader will notice that the absolute difference image average values for the MBP and SBP models do not show a completely consistent trend since the earlier bands (such as bands 20 and 32) contain very similar values, while the performance tends to diverge for the remaining spectral bands. In a few rare cases the average values and corresponding pixel values in the absolute difference images were slightly lower in the SBP than the MBP results, but in general the values of the MBP images were less than or equal to those of the SBP model. This is an intuitively expected result, since the single texture image bandpass used for texturing the SBP model scene was band 20, and thus the performance is quite good in bands 20 and 32 which are relatively well-correlated. For bands 65, 95, 115, 157, 184, and 195, there is a much more significant gap between the metric values for the MBP and SBP models, indicating superior performance by the MBP model. This is due to the noisy later spectral bands of the SBP image (shown in Section 5.2) due to incorrect spectral reflectance curve selection for non-correlated spectral bands.

As for the TS model, it generally contained the largest numbers in the range and average of the absolute difference images. Its MF metric image pixel values were all greater than that of the FM and MBP models, while they were sometimes comparable to that of the SBP model. For the earlier bands (20 and 32), the SBP model contained mostly lower values than the TS model, while in the later spectral bands the performance metric values oscillated between the models. It is therefore difficult to assign a clear relative ranking of the SBP and TS models using the MF metric alone for these later spectral bands. However, by assigning a weight to the SBP model for its superior performance in the earlier region of the spectrum,

a preliminary ranking based on the MF metric can be assigned for reference purposes. It is expected that the use of the other texture performance metrics will be able to further discriminate the performance of the models. The tentative ranking based on the MF metric results is:

- a. FM model;
- b. MBP model;
- c. SBP model; and
- d. TS model.

The following section will present the results of the more detailed spatial GLCM metric on the same texture test regions for all four texture models.

#### 5.4.2 GLCM Metric

The following tables provide a synopsis of the values obtained through the application of the GLCM Contrast metric on the rendered HYDICE ARM DIRSIG imagery:

<b>Band 20 – GLCM Con Metric – Avg Value of Absolute Difference Image</b>				
<b>Region</b>	<b>SBP</b>	<b>MBP</b>	<b>TS</b>	<b>FM</b>
1	0.72 (3)	1.1 (2)	1.98 (4)	0.66 (1)
2	0.042 (3)	0.02 (1)	1.6 (4)	0.02 (1)
3	0.05 (2)	0.06 (3)	0.32 (4)	0.035 (1)
4	0.31 (3)	0.21 (2)	0.74 (4)	0.16 (1)
5	0.063 (2)	0.07 (3)	0.15 (4)	0.03 (1)
6	0.39 (4)	0.24 (2)	0.36 (3)	0.03 (1)
7	0.61 (3)	0.22 (2)	3.1 (4)	0.05 (1)
8	0.051 (3)	0.05 (2)	0.11 (4)	0.03 (1)
9	21.92 (3)	6.2 (2)	102.7 (4)	4.2 (1)
10	1.32 (3)	0.42 (2)	1.92 (4)	0.17 (1)
11	1.9 (3)	1.1 (2)	2.36 (4)	0.39 (1)
12	50.2 (3)	32.4 (2)	67.3 (4)	1.1 (1)
13	0.47 (3)	0.31 (2)	1.98 (4)	0.20 (1)
14	47.2 (3)	32.1 (2)	89.3 (4)	2.1 (1)

15	6.67 (3)	6.01 (2)	13.1 (4)	2.7 (1)
<b>AVERAGE:</b>	<b>8.79 (2.93)</b>	<b>5.37 (2.07)</b>	<b>19.13 (3.93)</b>	<b>0.79 (1)</b>

<b>Band 32 – GLCM Con Metric – Avg Value of Absolute Difference Image</b>				
<b>Region</b>	<b>SBP</b>	<b>MBP</b>	<b>TS</b>	<b>FM</b>
1	1.64 (3)	1.62 (2)	2.07 (4)	1.34 (1)
2	0.07 (3)	0.04 (2)	2.2 (4)	0.03 (1)
3	0.21 (3)	0.08 (2)	1.1 (4)	0.05 (1)
4	1.62 (4)	0.87 (2)	1.19 (3)	0.37 (1)
5	0.10 (3)	0.09 (2)	0.98 (4)	0.02 (1)
6	0.74 (4)	0.49 (2)	0.52 (3)	0.18 (1)
7	0.92 (2)	0.95 (3)	1.57 (4)	0.04 (1)
8	0.13 (2)	0.14 (3)	0.16 (4)	0.09 (1)
9	29.6 (3)	8.9 (2)	99.6 (4)	7.1 (1)
10	1.4 (3)	1.1 (2)	2.6 (4)	0.28 (1)
11	1.89 (4)	0.83 (2)	1.79 (3)	0.13 (1)
12	32.3 (3)	21.3 (2)	68.4 (4)	2.7 (1)
13	0.52 (3)	0.29 (2)	1.76 (4)	0.18 (1)
14	49.96 (3)	33.1 (2)	96.1 (4)	2.0 (1)
15	13.1 (3)	5.92 (2)	14.7 (4)	3.2 (1)
<b>AVERAGE:</b>	<b>8.95 (3.07)</b>	<b>5.05 (2.13)</b>	<b>19.65 (3.8)</b>	<b>1.18 (1)</b>

<b>Band 65 – GLCM Con Metric – Avg Value of Absolute Difference Image</b>				
<b>Region</b>	<b>SBP</b>	<b>MBP</b>	<b>TS</b>	<b>FM</b>
1	12.12 (4)	4.73 (2)	10.3 (3)	3.8 (1)
2	4.74 (3)	3.23 (2)	9.6 (4)	0.8 (1)
3	3.74 (3)	1.32 (2)	10.2 (4)	0.59 (1)
4	3.91 (4)	2.12 (2)	3.49 (3)	0.19 (1)
5	15.54 (4)	3.76 (2)	13.3 (3)	1.1 (1)
6	2.26 (4)	1.84 (2)	2.2 (3)	0.76 (1)
7	27.4 (3)	9.63 (2)	46.3 (4)	0.43 (1)
8	103.4 (4)	7.1 (2)	13.1 (3)	2.6 (1)
9	66.7 (3)	25.2 (2)	79.2 (4)	19.6 (1)
10	5.51 (3)	3.92 (2)	9.82 (4)	1.67 (1)

11	24.8 (4)	5.16 (2)	19.7 (3)	2.01 (1)
12	25.2 (3)	8.37 (2)	82.1 (4)	2.9 (1)
13	15.7 (4)	8.1 (2)	14.3 (3)	2.2 (1)
14	47.9 (3)	13.2 (2)	103.4 (4)	6.6 (1)
15	56.3 (3)	27.9 (2)	65.6 (4)	6.1 (1)
<b>AVERAGE:</b>	<b>27.68 (3.47)</b>	<b>8.37 (2)</b>	<b>32.17 (3.53)</b>	<b>3.42 (1)</b>

<b>Band 95 – GLCM Con Metric – Avg Value of Absolute Difference Image</b>				
<b>Region</b>	<b>SBP</b>	<b>MBP</b>	<b>TS</b>	<b>FM</b>
1	14.78 (3)	12.4 (2)	14.9 (4)	3.91 (1)
2	3.13 (3)	1.64 (2)	7.7 (4)	0.32 (1)
3	3.42 (3)	1.12 (2)	7.9 (4)	0.62 (1)
4	4.12 (3)	1.6 (2)	6.5 (4)	1.32 (1)
5	2.08 (3)	1.1 (2)	2.2 (4)	0.12 (1)
6	3.02 (3)	2.04 (2)	3.04 (4)	0.93 (1)
7	13.9 (3)	8.2 (2)	49.6 (4)	0.96 (1)
8	52.3 (4)	5.28 (2)	6.3 (3)	1.78 (1)
9	78.3 (3)	32.1 (2)	82.1 (4)	27.4 (1)
10	6.44 (3)	3.42 (2)	7.1 (4)	1.98 (1)
11	9.33 (4)	6.47 (2)	8.99 (3)	1.6 (1)
12	27.7 (3)	7.08 (2)	77.3 (4)	3.2 (1)
13	7.37 (4)	5.34 (2)	6.2 (3)	2.1 (1)
14	33.7 (3)	12.1 (2)	64.8 (4)	9.2 (1)
15	19.8 (3)	13.4 (2)	49.7 (4)	9.4 (1)
<b>AVERAGE:</b>	<b>18.63 (3.2)</b>	<b>7.55 (2)</b>	<b>26.29 (3.8)</b>	<b>4.32 (1)</b>

<b>Band 115 – GLCM Con Metric – Avg Value of Absolute Difference Image</b>				
<b>Region</b>	<b>SBP</b>	<b>MBP</b>	<b>TS</b>	<b>FM</b>
1	29.8 (3)	20.4 (2)	69.6 (4)	1.36 (1)
2	3.81 (3)	1.12 (2)	12.2 (4)	0.39 (1)
3	6.18 (4)	0.68 (2)	6.1 (3)	0.30 (1)
4	2.49 (3)	1.01 (2)	9.6 (4)	0.10 (1)
5	3.39 (3)	1.37 (2)	4.4 (4)	0.19 (1)
6	5.12 (4)	2.03 (2)	4.1 (3)	0.89 (1)

7	17.21 (3)	10.2 (2)	34.9 (4)	0.92 (1)
8	2.97 (4)	0.98 (2)	2.4 (3)	0.32 (1)
9	119.7 (2)	313.2 (4)	137.6 (3)	15.2 (1)
10	17.19 (3)	11.1 (2)	32.3 (4)	1.93 (1)
11	67.61 (3)	23.8 (2)	71.2 (4)	2.2 (1)
12	78.8 (3)	36.4 (2)	103.2 (4)	4.6 (1)
13	24.7 (3)	17.6 (2)	25.2 (4)	1.1 (1)
14	98.3 (3)	42.7 (2)	107.6 (4)	14.1 (1)
15	104.7 (3)	71.2 (2)	106.4 (4)	3.1 (1)
<b>AVERAGE:</b>	<b>38.80 (3.2)</b>	<b>36.92 (2.13)</b>	<b>48.45 (3.73)</b>	<b>3.11 (1)</b>

<b>Band 157 – GLCM Con Metric – Avg Value of Absolute Difference Image</b>				
<b>Region</b>	<b>SBP</b>	<b>MBP</b>	<b>TS</b>	<b>FM</b>
1	58.1 (3)	40.2 (2)	98.7 (4)	6.7 (1)
2	5.82 (3)	1.96 (2)	11.1 (4)	1.1 (1)
3	10.13 (3)	1.2 (2)	13.3 (4)	0.76 (1)
4	4.32 (3)	1.3 (2)	12.9 (4)	0.93 (1)
5	3.79 (3)	2.21 (2)	6.7 (4)	0.47 (1)
6	5.36 (2)	5.93 (3)	6.41 (4)	1.62 (1)
7	26.1 (3)	11.3 (2)	41.3 (4)	1.01 (1)
8	7.19 (4)	0.78 (2)	1.61 (3)	0.45 (1)
9	132.4 (3)	78.1 (2)	266.7 (4)	30.1 (1)
10	23.8 (3)	19.2 (2)	42.6 (4)	5.1 (1)
11	106.4 (4)	48.2 (2)	97.4 (3)	3.8 (1)
12	149.4 (3)	97.4 (2)	176.2 (4)	6.2 (1)
13	57.4 (4)	29.5 (2)	55.4 (3)	3.2 (1)
14	122.4 (3)	67.9 (2)	124.6 (4)	11.4 (1)
15	182.7 (4)	102.3 (2)	143.4 (3)	11.7 (1)
<b>AVERAGE:</b>	<b>59.69 (3.2)</b>	<b>33.83 (2.07)</b>	<b>73.22 (3.73)</b>	<b>5.64 (1)</b>

<b>Band 184 – GLCM Con Metric – Avg Value of Absolute Difference Image</b>				
<b>Region</b>	<b>SBP</b>	<b>MBP</b>	<b>TS</b>	<b>FM</b>
1	72.3 (3)	29.7 (2)	74.3 (4)	3.2 (1)
2	3.92 (3)	0.6 (2)	5.97 (4)	0.37 (1)

3	6.2 (4)	1.4 (3)	1.39 (2)	0.12 (1)
4	8.86 (3)	6.68 (2)	9.7 (4)	0.76 (1)
5	2.76 (3)	1.23 (2)	5.9 (4)	0.27 (1)
6	2.72 (4)	1.64 (2)	2.4 (3)	0.38 (1)
7	19.1 (3)	12.1 (2)	47.2 (4)	1.54 (1)
8	1.84 (4)	0.83 (2)	1.63 (3)	0.36 (1)
9	140.8 (3)	39.1 (2)	247.1 (4)	22.7 (1)
10	18.09 (3)	16.1 (2)	27.5 (4)	2.0 (1)
11	76.67 (4)	37.9 (2)	69.8 (3)	1.79 (1)
12	90.2 (3)	61.02 (2)	92.3 (4)	5.6 (1)
13	54.5 (4)	13.2 (2)	50.3 (3)	2.3 (1)
14	92.9 (3)	42.6 (2)	97.2 (4)	20.1 (1)
15	74.6 (3)	53.7 (2)	79.2 (4)	7.2 (1)
<b>AVERAGE:</b>	<b>44.36 (3.33)</b>	<b>21.19 (2.07)</b>	<b>54.13 (3.6)</b>	<b>4.58 (1)</b>

<b>Band 195 – GLCM Con Metric – Avg Value of Absolute Difference Image</b>				
<b>Region</b>	<b>SBP</b>	<b>MBP</b>	<b>TS</b>	<b>FM</b>
1	65.39 (4)	27.6 (3)	19.7 (2)	5.8 (1)
2	2.98 (3)	0.89 (2)	5.9 (4)	0.41 (1)
3	6.46 (3)	1.97 (2)	6.6 (4)	0.56 (1)
4	10.23 (3)	7.2 (2)	11.6 (4)	1.73 (1)
5	1.69 (3)	1.12 (2)	3.7 (4)	0.38 (1)
6	3.12 (4)	2.01 (2)	2.6 (3)	0.91 (1)
7	21.4 (3)	12.02 (2)	36.8 (4)	0.73 (1)
8	1.45 (4)	0.99 (2)	1.32 (3)	0.76 (1)
9	92.3 (3)	24.1 (2)	202.3 (4)	14.6 (1)
10	24.5 (3)	10.4 (2)	32.4 (4)	0.84 (1)
11	49.8 (4)	40.7 (2)	47.8 (3)	2.1 (1)
12	77.1 (3)	32.6 (2)	81.2 (4)	9.2 (1)
13	49.4 (4)	31.2 (2)	46.7 (3)	4.4 (1)
14	141.2 (4)	47.8 (2)	131.3 (3)	7.2 (1)
15	103.1 (4)	67.6 (2)	98.7 (3)	7.8 (1)
<b>AVERAGE:</b>	<b>43.34 (3.47)</b>	<b>20.55 (2.07)</b>	<b>48.57 (3.47)</b>	<b>3.83 (1)</b>

Table 27: Average values of absolute difference images for GLCM Contrast metric.

<b>Band 20 – GLCM Con Metric – % Outliers</b>				
<b>Region</b>	<b>SBP</b>	<b>MBP</b>	<b>TS</b>	<b>FM</b>
1	19 (3)	11 (2)	26 (4)	6 (1)
2	17 (3)	12 (2)	28 (4)	6 (1)
3	22 (3)	10 (2)	29 (4)	5 (1)
4	21 (3)	10 (2)	29 (4)	6 (1)
5	24 (3)	10 (2)	33 (4)	6 (1)
6	22 (3)	9( 2)	32 94)	5 (1)
7	23 (3)	10 (2)	35 (4)	5 91)
8	20 (3)	11 (2)	36 (4)	6 (1)
9	22 (3)	14 (2)	32 (4)	7 (1)
10	19 (3)	12 (2)	33 (4)	6 (1)
11	24 (3)	13 (2)	36 (4)	5 (1)
12	25(3)	11 (2)	37 (4)	5 (1)
13	23(3)	14 (2)	32 (4)	6 (1)
14	22(3)	11 (2)	34 (4)	7 (1)
15	25 (3)	10 (2)	31 (4)	7 (1)
<b>AVERAGE:</b>	<b>21.87 (3)</b>	<b>11.2 (2)</b>	<b>32.2 (4)</b>	<b>5.87 (1)</b>

<b>Band 32 – GLCM Con Metric – % Outliers</b>				
<b>Region</b>	<b>SBP</b>	<b>MBP</b>	<b>TS</b>	<b>FM</b>
1	19 (3)	11 (2)	27 (4)	6 (1)
2	18 (3)	10 (2)	26 (4)	6 (1)
3	20 (3)	10 (2)	29 (4)	7 (1)
4	20 (3)	21 (2)	30 (4)	6 (1)
5	19 (3)	9 (2)	31 (4)	6 (1)
6	23 (3)	10 (2)	34 (4)	5 (1)
7	25 (3)	12 (2)	27 (4)	5 (1)
8	25 (3)	13 (2)	35 (4)	6 (1)
9	23 (3)	13 (2)	38 (4)	7 (1)
10	24 (3)	15 (2)	37 (4)	7 (1)

11	29 (3)	14 (2)	39 (4)	6 (1)
12	28 (3)	11 (2)	33 (4)	8 (1)
13	25 (3)	10 (2)	34 (4)	8 (1)
14	27 (3)	12 (2)	38 (4)	6 (1)
15	24 (3)	13 (2)	32 (4)	7 (1)
<b>AVERAGE:</b>	<b>23.27 (3)</b>	<b>11.6 (2)</b>	<b>32.67 (4)</b>	<b>6.4 (1)</b>
<b>Band 65 – GLCM Con Metric – % Outliers</b>				
<b>Region</b>	<b>SBP</b>	<b>MBP</b>	<b>TS</b>	<b>FM</b>
1	31 (3)	11 (2)	33 (4)	7 (1)
2	34 (4)	10 (2)	33 (3)	6 (1)
3	36 (3)	10 (2)	37 (4)	6 (1)
4	37 (3)	13 (2)	39 (4)	7 (1)
5	38 (3)	12 (2)	41 (4)	5 (1)
6	38 (3)	13 (2)	39 (4)	7 (1)
7	36 (3)	14 (2)	37 (4)	8 (1)
8	39 (4)	11 (2)	37 (3)	6 (1)
9	41 (4)	14 (2)	39 (3)	6 (1)
10	43 (4)	9 (2)	41 (3)	7 (1)
11	39 (3)	11 (2)	40 (4)	6 (1)
12	38 (4)	13 (2)	37 (3)	8 (1)
13	41 (4)	14 (2)	39 (3)	6 (1)
14	44 (4)	12 (2)	42 (3)	6 (1)
15	43 (4)	10 (2)	41 (3)	7 (1)
<b>AVERAGE:</b>	<b>38.53 (3.53)</b>	<b>11.8 (2)</b>	<b>38.33 (3.47)</b>	<b>6.53 (1)</b>

<b>Band 95 – GLCM Con Metric – % Outliers</b>				
<b>Region</b>	<b>SBP</b>	<b>MBP</b>	<b>TS</b>	<b>FM</b>
1	39 (4)	12 (2)	38 (3)	6 (1)
2	41 (4)	10 (2)	37 (3)	6 (1)
3	45 (4)	13 (2)	36 (3)	7 (1)
4	42 (4)	12 (2)	36 (3)	5 (1)
5	42 (4)	11 (2)	35 (3)	7 (1)
6	41 (4)	9 (2)	39 (3)	8 (1)
7	47 (4)	10 (2)	40 (3)	8 (1)

8	48 (4)	10 (2)	42 (3)	6 (1)
9	43 (4)	11 (2)	38 (3)	7 (1)
10	46 (4)	9 (2)	38 (3)	7 (1)
11	49 (4)	12 (2)	36 (3)	5 (1)
12	44 (4)	14 (2)	39 (3)	6 (1)
13	45 (4)	12 (2)	41 (3)	6 (1)
14	41 (4)	14 (2)	30 (3)	7 (1)
15	46 (4)	12 (2)	40 (3)	6 (1)
<b>AVERAGE:</b>	<b>43.93 (4)</b>	<b>11.4 (2)</b>	<b>37.67 (3)</b>	<b>6.47 (1)</b>

<b>Band 115 – GLCM Con Metric – % Outliers</b>				
<b>Region</b>	<b>SBP</b>	<b>MBP</b>	<b>TS</b>	<b>FM</b>
1	39 (4)	14 (2)	38 (3)	6 (1)
2	44 (4)	12 (2)	38 (3)	6 (1)
3	48 (4)	10 (2)	37 (3)	6 (1)
4	46 (4)	12 (2)	40 (3)	7 (1)
5	42 (4)	12 (2)	41 (3)	6 (1)
6	44 (4)	14 (2)	38 (3)	5 (1)
7	46 (4)	15 (2)	36 (3)	6 (1)
8	46 (4)	11 (2)	34 (3)	8 (1)
9	48 (4)	13 (2)	39 (3)	6 (1)
10	41 (4)	9 (2)	36 (3)	7 (1)
11	39 (4)	10 (2)	38 (3)	5 (1)
12	37 (3)	14 (2)	39 (4)	8 (1)
13	41 (4)	10 (2)	35 (3)	6 (1)
14	46 (4)	12 (2)	33 (3)	6 (1)
15	48 (4)	11 (2)	39 (3)	7 (1)
<b>AVERAGE:</b>	<b>43.67 (3.93)</b>	<b>11.93 (2)</b>	<b>37.4 (3.07)</b>	<b>6.33 (1)</b>

<b>Band 157 – GLCM Con Metric – % Outliers</b>				
<b>Region</b>	<b>SBP</b>	<b>MBP</b>	<b>TS</b>	<b>FM</b>
1	47 (4)	10 (2)	41 (3)	6 (1)
2	46 (4)	13 (2)	39 (3)	6 (1)
3	42 (4)	11 (2)	40 (3)	7 (1)

4	43 (4)	14 (2)	40 (3)	7 (1)
5	41 (3)	12 (2)	41 (3)	6 (1)
6	39 (4)	15 (2)	35 (3)	6 (1)
7	45 (4)	10 (2)	36 (3)	5 (1)
8	42 (4)	13 (2)	41 (3)	8 (1)
9	38 (4)	9 (2)	36 (3)	7 (1)
10	44 (4)	10 (2)	34 (3)	7 (1)
11	49 (4)	12 (2)	34 (3)	6 (1)
12	46 (4)	9 (2)	37 (3)	6 (1)
13	48 (4)	13 (2)	40 (3)	8 (1)
14	49 (4)	11 (2)	42 (3)	6 (10)
15	47 (4)	10 (2)	39 (3)	7 (1)
<b>AVERAGE:</b>	<b>44.4 (3.93)</b>	<b>11.47 (2)</b>	<b>38.33 (3)</b>	<b>6.53 (1)</b>

<b>Band 184 – GLCM Con Metric – % Outliers</b>				
<b>Region</b>	<b>SBP</b>	<b>MBP</b>	<b>TS</b>	<b>FM</b>
1	49 (4)	11 (2)	41 (3)	7 (1)
2	46 (4)	14 (2)	40 (3)	7 (1)
3	44 (4)	15 (2)	36 (3)	5 (1)
4	49 (4)	13 (2)	36 (3)	7 (1)
5	48 (4)	9 (2)	39 (3)	7 (1)
6	46 (4)	10 (2)	38 (3)	6 (1)
7	45 (4)	9 (2)	36 (3)	6 (1)
8	49 (4)	9 (2)	36 (3)	8 (1)
9	50 (4)	12 (2)	37 (3)	6 (1)
10	45 (4)	15 (2)	40 (3)	5 (1)
11	42 (4)	15 (2)	39 (3)	5 (1)
12	47 (4)	13 (2)	38 (3)	8 (1)
13	47 (4)	13 (2)	38 (3)	7 (1)
14	49 (4)	10 (2)	36 (3)	7 (1)
15	48 (4)	14 (2)	38 (3)	6 (1)
<b>AVERAGE:</b>	<b>46.93 (4)</b>	<b>12.13 (2)</b>	<b>37.87 (3)</b>	<b>6.47 (1)</b>

<b>Band 195 – GLCM Con Metric – % Outliers</b>				
<b>Region</b>	<b>SBP</b>	<b>MBP</b>	<b>TS</b>	<b>FM</b>
1	47 (4)	12 (2)	43(3)	6 (1)
2	48 (4)	10 (2)	41 (3)	7 (1)
3	44 (4)	9 (2)	38 (3)	7 (1)
4	47 (4)	10 (2)	36 (3)	6 (1)
5	42 (4)	14 (2)	36 (3)	8 (1)
6	44 (4)	14 (2)	36 (3)	6 (1)
7	45 (4)	12 (2)	39 (3)	7 (1)
8	45 (4)	11 (2)	41 (3)	5 (1)
9	50 (4)	15 (2)	45 (3)	7 (1)
10	49 (4)	14 (2)	40 (3)	5 (1)
11	45 (4)	10 (2)	38 93)	5 (1)
12	47 (4)	13 (2)	38 (3)	8 91)
13	48 (4)	9 (2)	36 (3)	8 (1)
14	46 (4)	10 (2)	45 (3)	6 91)
15	49 (4)	14 (2)	43 (3)	7 (1)
<b>AVERAGE:</b>	<b>46.4 (4)</b>	<b>12.47 (2)</b>	<b>39.67 (3)</b>	<b>6.53 (1)</b>

Table 28: Percentage of outliers from threshold for GLCM Contrast metric.

The same general trends are evident with the GLCM Contrast metric as for the MF metric. Once again, the FM model contains the lowest percentage outliers from the threshold and the lowest average values within the absolute difference images. The corresponding pixel values of the absolute difference images are all lower than those of the MBP, SBP, and TS models. This result makes sense intuitively since the spatial appearance of the FM model result is the most visually identical to the real HYDICE ARM image, for all spectral bands. It is therefore clear that the FM model out-performs all of the other models in the spatial domain, for all fifteen of the texture test regions, across all spectral regions. The MBP model results of the GLCM Contrast metric indicate the second best performance spatially. Although the SBP model shows comparable performance for spectral bands 20 and 32, the spatial structure begins to deteriorate for the later spectral bands of the SBP

image. This is the same result as observed with the MF metric, but the divergence is much more emphasized using the more detailed GLCM metric. Therefore, the MBP model performs much better overall, which is also not a surprising result since the MBP model attained the second best ranking through a visual analysis.

The oscillating behavior of the SBP and TS models is still present in the GLCM Contrast metric result. Although there is a wider gap between the values with the GLCM metric than with the MF metric, there is no clear pattern within these results regarding relative performance for the later spectral bands. This is evident even through a visual analysis of the resultant imagery; the earlier spectral bands of the SBP model appear comparable to the result of the MBP model, while the TS model appears to lack the spatial structure present in the real HYDICE imagery. However, the spatial structure is similarly lacking in both the TS and SBP models from bands 65 onward. The road region in the TS image tends to suffer spatially due to the artifacts discussed earlier, while that of the SBP model performs somewhat better. The plowed region of the TS model does not capture the oriented structure of the plowed patterns, but nonetheless contains more patterns than the SBP model for the later spectral bands. These results are reflected in the above average absolute difference image value tables for regions 1 and 4 (plowed fields) and for regions 12, 14 and 15, which are transition regions including the road. At this point it is suitable to maintain the ranking as presented in the previous section, since the analysis has only been based on spatial performance, and because the SBP model image does not contain as many spatial artifacts as the TS model image does. Further, the earlier region of the spectrum is much better in terms of its spatial texture characterization in the SBP model image. Since the results are very similar in terms of spatial content, the spectral texture analysis of the SCR and SCM metrics will prove to be crucial in distinguishing between the overall performance of the TS and SBP models. First, the percentage of outliers for each of the models using the GLCM Correlation metric will also be presented as it was for the CitiPix data in the previous section.

<b>Band 20 – GLCM Cor Metric – % Outliers</b>				
<b>Region</b>	<b>SBP</b>	<b>MBP</b>	<b>TS</b>	<b>FM</b>
1	28 (3)	15 (2)	35 (4)	7 (1)
2	29 (3)	16 (2)	36 (4)	8 (1)
3	27 (3)	14 (2)	34 (4)	8 (1)
4	26 (3)	17 (2)	36 (4)	7 (1)
5	33 (3)	16 (2)	38 (4)	7 (1)
6	32 (3)	14 (2)	39 (4)	8 (1)
7	31 (3)	15 (2)	35 (4)	6 (1)
8	30 (3)	15 (2)	36 (4)	8 (1)
9	29 (3)	13 (2)	36 (4)	7 (1)
10	28 (3)	17 (2)	38 (4)	7 (1)
11	33 (3)	15 (2)	36 (4)	6 (1)
12	32 (3)	14 (2)	36 (4)	8 (1)
13	30 (3)	17 (2)	39 (4)	9 (1)
14	29 (3)	15 (2)	36 (4)	8 (1)
15	31 (3)	14 (2)	35 (4)	8 (1)
<b>AVERAGE:</b>	<b>29.87 (3)</b>	<b>15.13 (2)</b>	<b>36.33 (4)</b>	<b>7.47 (1)</b>

<b>Band 32 – GLCM Cor Metric – % Outliers</b>				
<b>Region</b>	<b>SBP</b>	<b>MBP</b>	<b>TS</b>	<b>FM</b>
1	29 (3)	16 (2)	36 (4)	7 (1)
2	27 (3)	14 (2)	36 (4)	8 (1)
3	30 (3)	13 (2)	38 (4)	8 (1)
4	33 (3)	17 (2)	39 (4)	7 (1)
5	29 (3)	15 (2)	41 (4)	9 (1)
6	31 (3)	15 (2)	36 (4)	6 (1)
7	33 (3)	11 (2)	39 (4)	7 (1)
8	28 (3)	10 (2)	37 (4)	7 (1)
9	30 (3)	14 (2)	39 (4)	8 (1)
10	31 (3)	12 (2)	41 (4)	5 (1)
11	34 (3)	16 (2)	39 (4)	8 (1)
12	33 (3)	17 (2)	42 (4)	6 (1)
13	29 (3)	13 (2)	39 (4)	7 (1)

14	32 (3)	15 (2)	40 (4)	9 (1)
15	35 (3)	16 (2)	37 (4)	7 (1)
<b>AVERAGE:</b>	<b>30.93 (3)</b>	<b>14.27 (2)</b>	<b>38.6 (4)</b>	<b>7.27 (1)</b>

<b>Band 65 – GLCM Cor Metric – % Outliers</b>				
<b>Region</b>	<b>SBP</b>	<b>MBP</b>	<b>TS</b>	<b>FM</b>
1	37 (3)	15 (2)	40 (4)	7 (1)
2	34 (3)	14 (2)	37 (4)	7 (1)
3	31 (3)	18 (2)	36 (4)	8 (1)
4	39 (4)	15 (2)	36 (3)	6 (1)
5	31 (3)	14 (2)	35 (4)	8 (1)
6	29 (3)	16 (2)	38 (4)	8 (1)
7	39 (4)	15 (2)	38 (3)	9 (1)
8	34 (3)	13 (2)	36 (4)	7 (1)
9	36 (3)	16 (2)	41 (4)	8 (1)
10	38 (4)	12 (2)	38 (3)	6 (1)
11	30 (3)	15 (2)	34 (4)	8 (1)
12	29 (3)	13 (2)	37 (4)	6 (1)
13	38 (4)	16 (2)	34 (3)	7 (1)
14	31 (3)	15 (2)	38 (4)	7 (1)
15	33 (3)	15 (2)	34 (4)	8 (1)
<b>AVERAGE:</b>	<b>33.93 (3.2)</b>	<b>14.8 (2)</b>	<b>36.8 (3.73)</b>	<b>7.33 (1)</b>

<b>Band 95 – GLCM Cor Metric – % Outliers</b>				
<b>Region</b>	<b>SBP</b>	<b>MBP</b>	<b>TS</b>	<b>FM</b>
1	38 (4)	13 (2)	34 (3)	6 (1)
2	36 (4)	10 (2)	34 (3)	6 (1)
3	36 (4)	12 (2)	31 (3)	8 (1)
4	36 (4)	15 (2)	33 (3)	6 (1)
5	39 (4)	13 (2)	29 (3)	7 (1)
6	41 (4)	11 (2)	33 (3)	7 (1)
7	35 (4)	15 (2)	36 (4)	6 (1)
8	37 (4)	14 (2)	36 (3)	8 (1)
9	36 (4)	10 (2)	34 (3)	5 (1)
10	36 (4)	12 (2)	33 (3)	7 (1)

11	39 (4)	9 (2)	36 (3)	7 (1)
12	38 (3)	13 (2)	38 (3)	6 91)
13	34 (3)	15 (2)	36 (4)	5 (1)
14	35 (3)	16 (2)	35 (3)	9 (1)
15	36 (3)	13 (2)	37 (4)	7 91)
<b>AVERAGE:</b>	<b>36.8 (3.73)</b>	<b>12.73 (2)</b>	<b>34.33 (3.2)</b>	<b>6.67 (1)</b>

<b>Band 115 – GLCM Cor Metric – % Outliers</b>				
<b>Region</b>	<b>SBP</b>	<b>MBP</b>	<b>TS</b>	<b>FM</b>
1	42 (4)	13 (2)	34 (3)	7 (1)
2	44 (4)	15 (2)	36 (3)	7 (1)
3	41 (4)	15 (2)	36 (3)	6 (1)
4	39 (4)	17 (2)	38 (3)	7 (1)
5	43 (4)	14 (2)	36 (3)	8 (1)
6	40 (4)	15 (2)	39 (3)	5 (1)
7	42 (4)	15 (2)	37 (3)	7 (1)
8	42 (4)	13 (2)	30 (3)	7 (1)
9	44 (4)	17 (2)	36 (3)	8 (1)
10	45 (4)	16 (2)	42 (3)	7 (1)
11	48 (4)	15 (2)	44 (3)	9 (1)
12	43 (3)	15 (2)	47 (4)	8 (1)
13	43 (4)	16 (2)	34 (3)	6 (1)
14	41 (4)	13 (2)	36 (3)	8 (1)
15	45 (4)	16 (2)	38 (3)	8 (1)
<b>AVERAGE:</b>	<b>42.8 (3.93)</b>	<b>15.0 (2)</b>	<b>37.53 (3.07)</b>	<b>7.2 (1)</b>

<b>Band 157 – GLCM Cor Metric – % Outliers</b>				
<b>Region</b>	<b>SBP</b>	<b>MBP</b>	<b>TS</b>	<b>FM</b>
1	41 (4)	16 (2)	36 (3)	7 (1)
2	42 (4)	13 92)	36 (3)	7 (1)
3	44 (4)	12 (2)	34 (3)	8 91)
4	41 (4)	15 (2)	38 (3)	6 (1)
5	40 (4)	11 (2)	39 (3)	9 (1)
6	39 (3)	16 (2)	41 (4)	7 (1)
7	37 (4)	18 (2)	36 (3)	6 (1)

8	42 (4)	12 (2)	35 (3)	5 (1)
9	42 (4)	11 (2)	37 (3)	9 (1)
10	44 (4)	14 92)	32 (3)	8 (1)
11	41 (4)	16 (2)	36 (3)	8 (1)
12	43 (4)	15 (2)	38 (3)	7 (1)
13	47 (4)	15 (2)	37 (3)	9 (1)
14	42 (4)	14 (2)	39 (3)	7 (1)
15	45 (4)	17 (2)	40 (3)	8 (1)
<b>AVERAGE:</b>	<b>42.0 (3.93)</b>	<b>14.33 (2)</b>	<b>36.93 (3.07)</b>	<b>7.4 (1)</b>

<b>Band 184 – GLCM Cor Metric – % Outliers</b>				
<b>Region</b>	<b>SBP</b>	<b>MBP</b>	<b>TS</b>	<b>FM</b>
1	44 (3)	14 (2)	46 (4)	7 (1)
2	42 (3)	12 (2)	46 (4)	7 (1)
3	41 (3)	14 (2)	49 (4)	9 (1)
4	47 (4)	11 (2)	38 (3)	7 (1)
5	48 (4)	15 (2)	41 (3)	8 (1)
6	43 (4)	17 (2)	38 (3)	7 (1)
7	46 (4)	13 (2)	41 (3)	9 91)
8	47 (4)	12 (2)	46 (3)	9 (1)
9	41 (4)	14 92)	39 (3)	7 (1)
10	44 (4)	16 (2)	38 (3)	6 (1)
11	45 (4)	13 (2)	33 (3)	8 (1)
12	47 (4)	11 (2)	38 (3)	5 (1)
13	48 (4)	10 (2)	34 (3)	9 (1)
14	43 (4)	14 (2)	36 (3)	8 (1)
15	46 (4)	16 (2)	38 (3)	8 (1)
<b>AVERAGE:</b>	<b>44.8 (3.8)</b>	<b>13.47 (2)</b>	<b>40.07 (3.2)</b>	<b>7.47 (1)</b>

<b>Band 195 – GLCM Cor Metric – % Outliers</b>				
<b>Region</b>	<b>SBP</b>	<b>MBP</b>	<b>TS</b>	<b>FM</b>
1	43 (4)	16 (2)	36 (3)	8 (1)
2	41 (4)	13 (2)	34 (3)	7 (1)
3	44 (4)	11 (2)	34 (3)	7 (1)
4	47 (4)	15 (2)	34 (3)	8 (1)

5	48 (4)	12 (2)	37 (3)	7 (1)
6	43 (4)	14 (2)	36 (3)	9 (1)
7	41 (4)	10 (2)	39 (3)	6 (1)
8	46 (4)	14 (2)	40 (3)	8 (1)
9	45 (4)	13 (2)	39 (3)	8 (1)
10	47 (4)	16 (2)	36 (3)	7 (1)
11	49 (4)	13 (2)	34 (3)	8 (1)
12	44 (4)	15 (2)	38 (3)	7 (1)
13	48 (4)	14 (2)	35 (3)	7 (1)
14	44 (4)	16 (2)	36 (3)	8 (1)
15	47 (4)	15 (2)	40 (3)	9 (1)
<b>AVERAGE:</b>	<b>45.13 (4)</b>	<b>14.73 (2)</b>	<b>36.53 (3)</b>	<b>7.6 (1)</b>

Table 29: Percentage of outliers from threshold for GLCM Correlation metric.

As with the CitiPix data analysis, the number of outliers from the variance threshold image for each texture test region serves as a “sanity check”, since it confirms the results found with the MF metric and the GLCM Contrast metric. It therefore provides a convenient synopsis of the relative performance of the texture characterization models. This table further supports the ranking of the models based on their spatial domain performance indicated by the results of the GLCM Contrast and MF metrics, since the FM model has the lowest percentage of outliers, while the MBP model contains the second lowest. As observed previously, the SBP model performs virtually the same as the MBP model in band 20, and even in most cases in band 32, but the values tend to diverge increasingly for the later bands due to the poorer spatial performance of the SBP model. The oscillatory behavior between the SBP and MBP models in these later bands is still present, and the problems with the road transition regions in the TS model imagery is obvious for regions 12, 14, and 15. Therefore, the samew rank order as found for the MF and GLCM Contrast metric will be maintained. The next sections will present the results of applying the spectral SCR metric and the spatial-spectral SCM metric on the exact same texture test regions of the rendered DIRSIG imagery.

### 5.4.3 SCR Metric

As discussed in Section 4.5.2.1, the SCR metric has been included in order to assess the overall spectral content and complexity of the background clutter present in each of the rendered DIRSIG images as compared with the real HYDICE ARM imagery. The advantage of using this metric is that it provides a single numeric value indicative of spectral performance, without any consideration of the spatial domain. If the spectral structure and complexity is captured in the synthetic image, then its SCR value (for the given region being tested) should theoretically be within an acceptable variance threshold of the corresponding value for the real HYDICE ARM image. The same fifteen texture test regions have been used to obtain SCR values from the SBP, MBP, TS, and FM model DIRSIG images. These values were then compared with the corresponding real image SCR values. The threshold was defined by taking repeated measurements of the SCR from the same regions of the real image that were used to construct acceptable variance threshold images for the MF, GLCM, and SCM metrics. This threshold value is the rightmost column of the below table, which indicates the (1 sigma) standard deviation of the repeated SCR measurements from the real image. It was found that the use of a 1-sigma threshold separated texture model performance much better than a 2-sigma threshold did for the SCR metric.

<b>Region</b>	<b>SBP</b>	<b>MBP</b>	<b>TS</b>	<b>FM</b>	<b>Real</b>	<b>S.D.</b>
1	56.95 (4)	85.36* (2)	91.58* (1)	97.78* (3)	<b>90.50</b>	25.94
2	58.28 (4)	82.12 (2)	95.97* (1)	139.66 (3)	<b>104.74</b>	15.19
3	76.90 (4)	188.47 (3)	276.90* (1)	225.29 (2)	<b>411.95</b>	176.03
4	26.25 (4)	68.05* (2)	81.79* (1)	117.19 (3)	<b>77.21</b>	16.15
5	198.09 (4)	106.49* (2)	119.04* (1)	158.92* (3)	<b>120.25</b>	39.16
6	464.34 (4)	254.69* (3)	200.91* (1)	235.27* (2)	<b>196.06</b>	72.86

7	33.19 (4)	163.71 (3)	297.16* (1)	176.39 (2)	<b>504.28</b>	237.99
8	773.24 (4)	897.42 (3)	4,469.35* (1)	943.44 (2)	<b>6,222.54</b>	2,258.74
9	192.91 (4)	274.19 (3)	663.82* (1)	297.29 (2)	<b>1,004.99</b>	486.53
10	103.53 (4)	145.25* (2)	147.31* (1)	126.60 (3)	<b>172.51</b>	43.30
11	110.23 (4)	133.75* (2)	142.37* (1)	118.99* (3)	<b>153.82</b>	35.32
12	34.48 (4)	90.85* (2)	142.68* (1)	162.67 (3)	<b>123.61</b>	35.86
13	28.94 (4)	86.95* (2)	123.45* (1)	195.37* (3)	<b>119.29</b>	74.10
14	32.14 (4)	73.85* (2)	60.43* (1)	75.01* (3)	<b>58.90</b>	18.96
15	145.97 (4)	103.46 (2)	62.94* (1)	110.35 (3)	<b>72.74</b>	12.47
<b>Average:</b>	<b>155.70</b> <b>(4.0)</b>	<b>183.64</b> <b>(2.33)</b>	<b>465.05</b> <b>(1.0)</b>	<b>212.01</b> <b>(2.67)</b>	<b>628.89</b>	<b>236.57</b>

Table 30: SCR metric values and ranking for each test region for SBP, MBP, TS, and FM models for HYDICE ARM imagery (\* = value is within +/- 1 sigma S.D). The average SCR value is tallied in the bottom row, as well as the average rank value for each model.

The above table exhibits some clear trends. First, the TS model has the closest SCR values to the SCR values of the real HYDICE ARM image. In each case, the TS model image regions have an SCR value within 1 sigma standard deviation of the real corresponding value. This is an intuitive result, since the very nature of the TS model guarantees that the spectral statistics will be correct due to its spectral covariance enforcement methodology in creating synthetic texture. Another consistent observation is that the SBP model has SCR values farthest from the corresponding real image SCR values.

In fact, none of its SCR values lie within the standard deviation threshold, although some values are quite close to the threshold. This result is not surprising since the single-bandpass z-score curve selection algorithm has only utilized a single narrow band in the visible region of the spectrum, and thus it has tended to select curves from the ground truth measurement database that were not optimal for each of the materials in the scene for non-correlated spectral bands.

The MBP and FM models both perform quite well for this metric; however their relative performance is not consistent. Despite this oscillatory behavior, it is possible to rank one over the other if the results are carefully analyzed. For instance, the MBP model has 9 of its 15 values within the threshold value, while the FM model has 6. It is also worthy to note that for the three cases in which the FM model SCR values lie outside of the threshold, they were extremely close to the threshold value, as one can infer from the above table. Further, the MBP model attained the second-best performance metric value (next to the TS model) for 10 of the 15 regions, while the FM model did so for the other 5 regions, which incidentally are all homogeneous texture regions. Therefore, since the rankings of each region for the SCR metric are consistent 66.6% of the time, and because the SCR values are so close between the FM and MBP models, the following ranking based solely on the SCR metric result can be concluded (which is further confirmed by the average rankings listed in the above table):

- a. TS model;
- b. MBP model;
- c. FM model; and
- d. SBP model.

It is important to note that there is a potential for bias with the SCR values of the TS model result. Since the input texture sample images used to generate the synthetic textures for each material class region were extracted from the real HYDICE imagery in the same vicinity as the SCR texture test regions, the covariance calculations were derived from virtually identical region samples. This means that the SCR values of the TS model result are

using the exact same spectral covariance values in the statistical enforcement step of texture synthesis and for the SCR computation. It is thus not surprising that the SCR values for the TS model are extremely close to those of the real HYDICE image. At the same time, there is also much room for improvement for the MBP model. The image-derived “ground truth” spectra used in the spectral reflectance curve database for applying spectral variability to each pixel of the MBP result utilized only a subset of spectral curves in order to avoid unpalatably long run times. The initially large ( $10^3 - 10^4$  curves) DIRSIG emissivity files were randomly truncated to contain 500 curves. In effect, this did not guarantee that the same spectra were used for the SCR metric computation while further limiting the ability of the model to capture the complete nature of variability for each texture test region. Therefore, the MBP SCR values are not as close to those of the real image or the TS model. If one is willing to endure very long DIRSIG rendering run times with non-truncated reflectance curve databases, then the MBP model SCR metric results would accordingly improve to resemble the SCR values of the real image, and may even rank better than the TS model. Since the SCR metric is exclusively spectral in nature and the MF and GLCM metrics were strictly spatially oriented, the SCM metric results presented in the following section will provide a means to investigate a simultaneously weighted measure of the spatial and spectral fidelity in the HYDICE ARM synthetic imagery.

#### **5.4.4 SCM Metric**

As detailed in Section 4.5.2.2, the SCM has been implemented into the ENVI processing environment with the capability of the user specifying a basic and a comparison spectral band when applying the SCM metric. Since an exhaustive sample of all combinations of spectral band pairs would not be practical within the scope of this work, four representative spectral band pairs were selected for the HYDICE ARM data in order to assess the simultaneous spatial-spectral texture characterization for well-correlated (bands 22-32), ill-correlated (bands 30-162), negatively ill-correlated (bands 30-193), and negatively “well”-correlated (bands 65-185) spectral bands (see Chapter 4 for more details on methodology of the application of the SCM metric). If the SCM metric values for a

particular texture model are low and within or near the acceptable variance threshold, then the model is able to maintain both the spatial and spectral correlation and structure in the output DIRSIG image. This is because the SCM metric works just as the GLCM spatial metric does, except it performs the operation across two specified spectral bands. It therefore represents a parameterized description of spatial and spectral texture through the use of the familiar co-occurrence matrix features introduced earlier. In order to be consistent in the application of all performance metrics, the Contrast and Correlation features were investigated for each texture test region for each of the DIRSIG images and compared with the corresponding regions of the real HYDICE ARM image. The analysis will be completely analogous to that of the GLCM metric. It is expected that this metric will be much more significant for this data set than for the CitiPix imagery, simply due to the larger spectral dimension of the HYDICE ARM data. The following synopsis tables present the SCM metric Contrast and Correlation features for each region and texture model:

<b>Bands 22-32 – SCM Con Metric – Avg Value of Absolute Difference Image</b>				
<b>Region</b>	<b>SBP</b>	<b>MBP</b>	<b>TS</b>	<b>FM</b>
1	5.65 (4)	4.4 (2)	5.4 (3)	1.4 (1)
2	3.69 (4)	2.29 (2)	3.49 (3)	1.78 (1)
3	0.89 (4)	0.67 (2)	0.86 (3)	0.44 (1)
4	1.09 (3)	0.72 (2)	1.17 (4)	0.34 (1)
5	0.56 (1)	1.31 (3)	0.77 (2)	1.6 (4)
6	1.58 (3)	1.38 (2)	1.59 (3)	1.1 (1)
7	3.5 (3)	2.1 (2)	3.58 (4)	0.89 (1)
8	0.87 (4)	0.57 (2)	0.60 (3)	0.41 (1)
9	15.1 (3)	12.6 (2)	84.9 (4)	5.4 (1)
10	3.72 (3)	2.9 (2)	4.61 (4)	1.69 (1)
11	4.32 (3)	3.2 (2)	4.79 (4)	1.67 (1)
12	41.6 (3)	5.4 (2)	42.4 (4)	1.34 (1)
13	1.71 (3)	1.46 (2)	1.79 (4)	1.22 (1)
14	47.3 (3)	9.31 (2)	48.6 (4)	3.96 (1)
15	14.8 (3)	9.56 (2)	17.6 (4)	6.9 (1)
<b>AVERAGE:</b>	<b>9.76 (3.13)</b>	<b>3.86 (2)</b>	<b>14.81 (3.53)</b>	<b>2.01 (1.2)</b>

<b>Bands 30-162 – SCM Con Metric – Avg Value of Absolute Difference Image</b>				
<b>Region</b>	<b>SBP</b>	<b>MBP</b>	<b>TS</b>	<b>FM</b>
1	310.2 (4)	31.1 (2)	256.6 (3)	21.2 (1)
2	79.7 (4)	15.6 (2)	39.2 (3)	9.4 (1)
3	48.9 (4)	38.1 (2)	41.9 (3)	36.2 (1)
4	123.4 (4)	87.3 (2)	120.6 (3)	69.6 (1)
5	18.9 (4)	6.08 (2)	17.9 (3)	1.94 (1)
6	93.2 (4)	51.2 (2)	81.3 (3)	28.5 (1)
7	297.6 (4)	113.3 (2)	272.1 (3)	12.5 (1)
8	5.13 (4)	4.66 (2)	4.97 (3)	3.4 (1)
9	182.8 (4)	97.2 (2)	121.6 (3)	6.2 (1)
10	120.6 (4)	59.8 (2)	113.1 (3)	54.1 (1)
11	169.7 (4)	44.7 (2)	157.4 (3)	32.2 (1)
12	327.1 (4)	16.45 (2)	189.7 (3)	9.6 (1)
13	147.3 (4)	30.5 (2)	140.2 (3)	17.2 (1)
14	392.6 (4)	27.2 (2)	379.8 (3)	14.3 (1)
15	162.3 (4)	54.4 (2)	145.6 (3)	50.2 (1)
<b>AVERAGE:</b>	<b>165.30 (4)</b>	<b>45.17 (2)</b>	<b>138.80 (3)</b>	<b>24.44 (1)</b>

<b>Bands 30-193 – SCM Con Metric – Avg Value of Absolute Difference Image</b>				
<b>Region</b>	<b>SBP</b>	<b>MBP</b>	<b>TS</b>	<b>FM</b>
1	272.9 (4)	33.7 (2)	251.6 (3)	16.2 (1)
2	45.7 (4)	12.3 (2)	20.2 (3)	4.1 (1)
3	33.6 (4)	27.6 (2)	29.7 (3)	21.3 (1)
4	147.3 (4)	98.4 (2)	122.8 (3)	92.1 (1)
5	19.6 (4)	6.7 (2)	11.2 (3)	3.9 (1)
6	66.8 (4)	44.2 (2)	46.7 (3)	26.3 (1)
7	192.4 (4)	81.4 (2)	187.2 (3)	34.8 (1)
8	1.86 (4)	1.66 (2)	1.71 (3)	1.2 (1)
9	152.1 (4)	77.9 (2)	92.1 (3)	21.3 (1)
10	124.9 (4)	65.3 (2)	73.2 (3)	60.1 (1)
11	98.9 (4)	29.2 (2)	84.3 (3)	14.3 (1)
12	79.8 (4)	22.6 (2)	63.1 (3)	13.7 (1)
13	157.6 (4)	42.54 (2)	148.2 (3)	13.4 (1)

14	279.3 (4)	37.6 (2)	229.7 (3)	21.1 (1)
15	239.9 (4)	83.3 (2)	166.4 (3)	61.2 (1)
<b>AVERAGE:</b>	<b>127.51 (4)</b>	<b>44.29 (2)</b>	<b>101.87 (3)</b>	<b>27.0 (1)</b>

<b>Bands 65-185 – SCM Con Metric – Avg Value of Absolute Difference Image</b>				
<b>Region</b>	<b>SBP</b>	<b>MBP</b>	<b>TS</b>	<b>FM</b>
1	60.33 (4)	27.9 (2)	54.6 (3)	18.6 (1)
2	67.8 (4)	22.1 (2)	66.9 (3)	6.9 (1)
3	14.8 (4)	8.6 (2)	13.1 (3)	7.1 (1)
4	43.4 (4)	26.4 (2)	34.7 (3)	17.6 (1)
5	186.3 (4)	21.3 (2)	136.4 (3)	18.2 (1)
6	42.7 (4)	13.2 (2)	16.7 (3)	5.8 (1)
7	364.4 (4)	76.6 (2)	227.6 (3)	21.6 (1)
8	192.8 (4)	9.31 (2)	191.6 (3)	3.9 (1)
9	138.9 (4)	47.89 (2)	61.3 (3)	24.7 (1)
10	247.3 (4)	36.7 (2)	171.9 (3)	20.8 (1)
11	243.7 94)	42.3 (2)	170.8 (3)	24.7 (1)
12	283.9 (4)	34.3 (2)	157.6 (3)	21.6 (1)
13	256.8 (4)	50.7 (2)	113.4 (3)	30.2 (1)
14	167.4 (4)	31.4 (2)	154.7 (3)	24.1 (1)
15	123.6 (4)	64.6 (2)	112.9 (3)	23.8 (1)
<b>AVERAGE:</b>	<b>162.28 (4)</b>	<b>34.22 (2)</b>	<b>112.28 (3)</b>	<b>17.97 (1)</b>

Table 31: Average values of absolute difference images for SCM Contrast metric.

<b>Bands 22-32 – SCM Con Metric – % Outliers</b>				
<b>Region</b>	<b>SBP</b>	<b>MBP</b>	<b>TS</b>	<b>FM</b>
1	22 (3)	14 (2)	34 (4)	7 (1)
2	21 (3)	15 (2)	36 (4)	8 (1)
3	24 (3)	12 (2)	38 (4)	8 (1)
4	20 (3)	11 (2)	33 (4)	7 (1)
5	27 (3)	16 (2)	31 (4)	9 (1)
6	29 (3)	14 (2)	30 (4)	7 (1)
7	23 (3)	13 92)	36 (4)	7 (1)
8	22 (3)	13 92)	37 (4)	8 (1)
9	20 (3)	10 (2)	34 (4)	6 (1)

10	25 (3)	14 (2)	36 (4)	7 (1)
11	26 (3)	16 (2)	38 (4)	6 (1)
12	28 (3)	15 (2)	36 (4)	8 (1)
13	24 (3)	13 (2)	39 (4)	6 (1)
14	26 (3)	16 (2)	33 (4)	7 (1)
15	29 (3)	12 (2)	36 (4)	7 (1)
<b>AVERAGE:</b>	<b>24.4 (3)</b>	<b>13.6 (2)</b>	<b>37.53 (4)</b>	<b>7.2 (1)</b>

<b>Bands 30-162 – SCM Con Metric – % Outliers</b>				
<b>Region</b>	<b>SBP</b>	<b>MBP</b>	<b>TS</b>	<b>FM</b>
1	39 (4)	16 (2)	36 (3)	7 (1)
2	43 (4)	18 (2)	38 (3)	7 (1)
3	46 (4)	19 (2)	36 (3)	6 (1)
4	38 (4)	14 (2)	34 (3)	7 (1)
5	49 (4)	17 (2)	35 (3)	7 (1)
6	47 (4)	12 (2)	36 (3)	8 (1)
7	49 (4)	17 (2)	36 (3)	7 (1)
8	46 (4)	10 (2)	38 (3)	8 (1)
9	49 (4)	13 (2)	39 (3)	8 (1)
10	48 (4)	16 (2)	36 (3)	7 (1)
11	44 (4)	18 (2)	34 (3)	6 (1)
12	48 (4)	13 (2)	32 (3)	7 (1)
13	49 (4)	16 (2)	36 (3)	9 (1)
14	46 (4)	14 (2)	34 (3)	7 (1)
15	48 (4)	15 (2)	31 (3)	6 (1)
<b>AVERAGE:</b>	<b>45.93 (4)</b>	<b>15.2 (2)</b>	<b>35.4 (3)</b>	<b>7.13 (1)</b>

<b>Bands 30-193 – SCM Con Metric – % Outliers</b>				
<b>Region</b>	<b>SBP</b>	<b>MBP</b>	<b>TS</b>	<b>FM</b>
1	44 (4)	18 (2)	34 (3)	6 (1)
2	47 (4)	14 (2)	33 (3)	8 (1)
3	42 (4)	15 (2)	36 (3)	8 (1)
4	47 (4)	17 (2)	36 (3)	9 (1)
5	49 (4)	13 (2)	39 (3)	8 (1)

6	48 (4)	16 (2)	38 (3)	7 (1)
7	46 (4)	15 (2)	31 (3)	9 (1)
8	46 (4)	15 (2)	35 (3)	7 (1)
9	49 (4)	11 (2)	37 (3)	6 (1)
10	44 (4)	12 (2)	36 (3)	8 (1)
11	45 (4)	17 (2)	36 (3)	8 (1)
12	48 (4)	15 (2)	38 (3)	7 (1)
13	45 (4)	16 (2)	32 (3)	8 (1)
14	47 94)	12 (2)	34 (3)	7 (1)
15	49 (4)	15 (2)	34 (3)	9 (1)
<b>AVERAGE:</b>	<b>46.4 (4)</b>	<b>14.73 (2)</b>	<b>35.27 (3)</b>	<b>7.67 (1)</b>

<b>Bands 65-185 – SCM Con Metric – % Outliers</b>				
<b>Region</b>	<b>SBP</b>	<b>MBP</b>	<b>TS</b>	<b>FM</b>
1	47 (4)	16 (2)	36 (3)	6 (1)
2	44 (4)	18 (2)	35 (3)	8 (1)
3	49 (4)	13 (2)	33 (3)	8 (1)
4	47 (4)	13 (2)	31 (3)	8 (1)
5	48 (4)	16 (2)	34 (3)	9 (1)
6	50 (4)	15 (2)	36 (3)	7 (1)
7	49 (4)	12 92)	38 (3)	8 (1)
8	48 (4)	15 (2)	35 (3)	8 (1)
9	46 (4)	10 (2)	37 (3)	7 (1)
10	48 (4)	17 (2)	36 (3)	8 (1)
11	46 (4)	13 (2)	36 (3)	9 (1)
12	49 (4)	17 (2)	34 (3)	6 (1)
13	47 (4)	13 (2)	36 (3)	7 (1)
14	49 (4)	17 (2)	36 (3)	9 (1)
15	48 (4)	13 (2)	38 (3)	8 (1)
<b>AVERAGE:</b>	<b>47.67 (4)</b>	<b>14.53 (2)</b>	<b>35.4 (3)</b>	<b>7.73 (1)</b>

Table 32: Percentage of outliers from threshold for SCM Contrast metric.

<b>Bands 22-32 – SCM Cor Metric – % Outliers</b>				
<b>Region</b>	<b>SBP</b>	<b>MBP</b>	<b>TS</b>	<b>FM</b>
1	32 (3)	17 (2)	34 (4)	8 (1)
2	39 (4)	17 (2)	36 (3)	8 (1)
3	28 (3)	16 (2)	36 (4)	9 (1)
4	29 (3)	14 (2)	39 (4)	8 (1)
5	26 (3)	16 (2)	40 (4)	8 (1)
6	29 (3)	19 (2)	36 (4)	9 (1)
7	30 (3)	15 (2)	39 (4)	7 (1)
8	28 (3)	15 (2)	38 (4)	9 (1)
9	26 (3)	12 (2)	35 (4)	9 (1)
10	25 (3)	11 (2)	34 (4)	7 (1)
11	28 (3)	17 (2)	37 (4)	8 (1)
12	29 (3)	11 (2)	39 (4)	8 (1)
13	26 (3)	18 (2)	33 (4)	9 (1)
14	29 (3)	15 (2)	38 (4)	7 (1)
15	26 (3)	17 (2)	36 (4)	9 (1)
<b>AVERAGE:</b>	<b>28.67 (3.07)</b>	<b>16.07 (2)</b>	<b>36.67 (3.93)</b>	<b>8.2 (1)</b>

<b>Bands 30-162 – SCM Cor Metric – % Outliers</b>				
<b>Region</b>	<b>SBP</b>	<b>MBP</b>	<b>TS</b>	<b>FM</b>
1	41 (4)	17 (2)	34 (3)	9 (1)
2	44 (4)	18 (2)	32 (3)	8 (1)
3	45 (4)	15 (2)	30 (3)	8 91)
4	42 94)	14 (2)	33 (3)	8 (1)
5	43 (4)	12 (2)	39 (3)	9 (1)
6	41 (4)	17 (2)	36 (3)	7 (1)
7	39 (4)	11 (2)	36 (3)	9 (1)
8	40 (4)	18 (2)	34 (3)	8 (1)
9	44 (4)	13 (2)	36 (3)	8 (1)
10	48 (4)	10 (2)	37 (3)	9 (1)
11	49 (4)	15 (2)	36 (3)	9 (1)
12	46 (4)	18 (2)	34 (3)	7 (1)

13	48 (4)	19 (2)	36 (3)	8 (1)
14	45 (4)	14 (2)	38 (3)	8 (1)
15	49 (4)	17 (2)	35 (3)	7 (1)
<b>AVERAGE:</b>	<b>44.27 (4)</b>	<b>15.2 (2)</b>	<b>35.07 (3)</b>	<b>8.13 (1)</b>

<b>Bands 30-193 – SCM Cor Metric – % Outliers</b>				
<b>Region</b>	<b>SBP</b>	<b>MBP</b>	<b>TS</b>	<b>FM</b>
1	47 (4)	16 (2)	34 (3)	8 (1)
2	44 (4)	13 (2)	36 (3)	8 (1)
3	46 (4)	16 (2)	36 (3)	9 (1)
4	49 (4)	17 (2)	38 (3)	9 (1)
5	48 (4)	14 (2)	34 (3)	9 (1)
6	46 (4)	15 (2)	32 (3)	7 (1)
7	44 (4)	15 (2)	34 (3)	9 (1)
8	48 (4)	18 (2)	32 (3)	9 (1)
9	48 (4)	19 (2)	36 (3)	8 (1)
10	49 (4)	14 (2)	38 (3)	7 (1)
11	44 (4)	16 (2)	32 (3)	9 (1)
12	43 (4)	11 (2)	30 (3)	8 (1)
13	48 (4)	17 (2)	36 (3)	7 (1)
14	46 (4)	19 (2)	34 (3)	6 (1)
15	45 (4)	18 (2)	33 (3)	9 (1)
<b>AVERAGE:</b>	<b>46.33 (4)</b>	<b>15.87 (2)</b>	<b>34.33 (3)</b>	<b>8.13 (1)</b>

<b>Bands 65-185 – SCM Cor Metric – % Outliers</b>				
<b>Region</b>	<b>SBP</b>	<b>MBP</b>	<b>TS</b>	<b>FM</b>
1	47 (4)	13 (2)	36 (3)	8 (1)
2	44 (4)	21 (2)	38 (3)	8 (1)
3	49 (4)	16 (2)	36 (3)	9 (1)
4	48 (4)	17 (2)	36 (3)	8 (1)
5	49 (4)	15 (2)	38 (3)	8 (1)
6	46 (4)	13 (2)	36 (3)	7 (1)
7	44 (4)	12 (2)	33 (3)	9 (1)
8	48 (4)	17 (2)	34 (3)	8 (1)

9	49 (4)	15 (2)	32 (3)	8 (1)
10	46 (4)	17 (2)	34 (3)	9 (1)
11	49 (4)	14 (2)	36 (3)	7 (1)
12	50 (4)	16 (2)	31 (3)	9 (1)
13	49 (4)	13 (2)	32 (3)	8 (1)
14	48 (4)	10 (2)	36 (3)	8 (1)
15	50 (4)	16 (2)	38 (3)	9 (1)
<b>AVERAGE:</b>	<b>47.73 (4)</b>	<b>15.0 (2)</b>	<b>35.07 (3)</b>	<b>8.2 (1)</b>

Table 33: Percentage of outliers from threshold for SCM Correlation metric.

Both the Contrast and Correlation features of the SCM metric are able to distinguish the performance of each of the texture models quite well in terms of both spatial and spectral structure. As with the other metrics, the best performance values belong to the FM model. This is evident by the average (and range) of values of each region's absolute difference image, since the entries are much lower than those of the other three models (see the above tables). In order to verify this result (since the average and range are not always themselves sufficient to confirm that overall performance is better for this metric), the absolute difference images were compared directly for each model result, and for each texture test region for the Contrast feature of the SCM metric. In all cases, when the FM model metric images were subtracted from the corresponding images of the other models, the result was greater than zero. This indicates that all pixel values were smaller for the FM model, and thus performed the best of all models. Further, the magnitude of the deviation from the threshold was also investigated in order to supplement the information provided by the percentage of outliers for each texture region. The deviation from the threshold was smallest for the FM model, and second to smallest for the MBP model, despite the fact the actual percentage of outliers for the FM and MBP models were very close for all 4 spectral band pairs. This indicates that the best overall spatial-spectral performance was achieved by the FM model for the rendering of the HYDICE ARM imagery. It has been shown already that the FM model performs quite well spatially through the application of the MF and GLCM metrics. However, since the SCR metric indicated that the spectral performance of

the FM model was not as good as for the TS model, and extremely close to the performance of the MBP model, its spatial-spectral overall performance had the potential to suffer. The results of the SCM metric clearly show that by weighting both spatial and spectral dimensions, the FM model performs better than the other models. This means that what the FM models lacks spectrally (compared to the TS model), it makes up for in the spatial domain. Further, the very good results of the SCM metric also shows that the weighting of the end member spectra according to their fractional abundance maps generally creates an adequate level of spectral structure and clutter that is comparable to the real counterpart image. That is, despite the fact that the spectral covariance statistics are not as close to the real image as the TS model is, the spectral correlation is preserved in the FM model image for this sampling of spectral band pairs, and it is reasonable to infer that this correlation is maintained throughout the spectral extent of the image. This means that the various linear combinations of end member spectra assigned to each mixed pixel is sufficient to represent the spectral clutter present in the real HYDICE ARM image. The number of outliers in the SCM Correlation metric further substantiates the best overall performance of the FM model. One must keep in mind however that there is a stricter requirement on the availability of multi-band input image data in order to have the FM model perform optimally.

The SCM performance metric values that come closest to the FM model belong to the MBP model. There is very clear separation between the MBP model and the FM model, as well as between the MBP model and the SBP and TS models. The range and average values for the MBP imagery are all greater than that of the FM model, but less than those of the TS and SBP models. This is also true for the corresponding pixel values of the absolute difference images; that is, there is no oscillatory behavior between the MBP model and any other model. The percentage of outliers and the magnitude of the deviation from the acceptable variance threshold of the SCM Contrast metric is much smaller for the regions of the MBP image than for the SBP and TS models. Therefore, the MBP model has secured the second-best ranking for the SCM metric alone, which is reinforced by the number of outliers for the SCM Correlation metric in the above table.

The relative performance of the TS and SBP models was the most difficult to discern. For the 95%-correlated band pair (bands 22 and 32), the SBP model performs better than the TS model in general, although the difference tended to be subtle, since the values were lower for the SBP model for 60% of the regions, of which all but one were homogeneous texture regions. However, for the remaining three band pairs, the TS model achieved better performance values. This is an intuitive result since the SBP and TS models shared similar spatial performance metric values for the later spectral bands, while the SBP model performed better spatially for band 20 and often for band 32. Since the SBP model uses only one bandpass for spectral reflectance curve selection, it was able to choose spectra for each pixel that were optimized for that region of the spectrum. It therefore was able to maintain the spatial-spectral correlation between bands 22 and 32 better than the TS model because these bands are so well correlated. This broke down for the band pairs that involved later spectral bands due to the lack of adequate spatial structure in those bands (as observed with the MF and GLCM metrics), and due to the poor spectral performance in those bands (as evidenced by the performance of the SBP model with the SCR metric). Since the spectral performance is much better for the TS model than the SBP model, and because the spatial performance for the later spectral bands of the SBP and TS models are comparable, the SCM metric is able to account for both of these aspects and provide metric values that weight spatial and spectral performance simultaneously. In general then, it is reasonable to rank the overall performance of the TS model higher than the SBP model for the HYDICE ARM imagery despite the fact that the SBP model performs slightly better for bands well-correlated with the visible region of the spectrum. Further, for the SCM metric alone (both Contrast and Correlation features), the TS model out-performs the SBP model for 75% of the tested band pairs. Therefore, the ranking based on the SCM metric alone is:

- a. FM model;
- b. MBP model;
- c. TS model; and
- d. SBP model.

The SCM metric is therefore successful as a simultaneous measure of spatial and spectral fidelity of synthetic image texture. Determining how much the SCM metric differentially weights the spatial and spectral domains is difficult. However, since only two spectral bands are used in its computation and it otherwise follows the process of the GLCM spatial metric, it is reasonable to estimate that this metric weights the spatial domain more than the spectral domain. See Sections 5.5.5 and 5.5.6 for more discussion regarding weighting of each performance metric and spatial-spectral weighting of the SCM metric. This is an important result since this metric provides the initial mechanics for summarizing the relative performance of all four models for the HYDICE ARM imagery. This is true because the separate analyses of the MF, GLCM, and SCR metrics suggested that the FM model always performed the best spatially, and the MBP model performed second-best. Also, the oscillatory behavior observed with the spatial metrics made it very difficult to conclusively rank the relative performance of the SBP and TS models. This was designed to be alleviated by considering the spectral domain as well in order to diagnose the overall performance of each model. The SCR metric verified that the TS model performed extremely well spectrally, while the SBP model performed the worst of all four models. The result was two quite different rank orders from separate spatial and spectral analyses. The question then became, “how much does one weight the spatial and spectral performance metrics?” This aspect will be discussed in Section 5.5.6.

### **5.5 Comparative Performance Analysis of Texture Models**

The above analysis contained in the previous two sections has provided separate analyses of each model using each of the four performance metrics, for both the CitiPix and the HYDICE ARM imagery. The following section will summarize the results achieved by each of the texture models, as well as provide a final overall ranking based on a list of conditions that must be satisfied and/or limitations that must be overcome for each model to perform reasonably well. The following table represents a summary of the above synopsis tables for the rendered HYDICE ARM imagery. It contains the “average of the averages” for the average value of the absolute difference images and the percentage of outliers from

the threshold for all eight sample spectral bands, and for the MF, GLCM, and SCM performance metrics.

<b>Texture Model</b>	<b>AVERAGE % Outliers</b>	<b>AVERAGE Avg Value</b>
<b>SBP</b>	38.11 (3.87)	37.40 (3.43)
<b>MBP</b>	12.94 (2.0)	14.24 (2.06)
<b>TS</b>	36.32 (3.36)	36.12 (3.39)
<b>FM</b>	6.79 (1)	5.12 (1.02)

Table 34: Summary table indicating overall performance of texture models for all eight sample spectral bands and MF, GLCM, and SCM performance metrics. The average ranking using these metrics is also included in parentheses.

The above table suggests a preliminary ranking of texture models based only on the HYDICE imagery of: 1. FM model; 2. MBP model; 3. TS model; and 4. SBP model. This rank order will be verified in Section 5.5.6 through the application of weights for each performance metric.

### **5.5.1 SBP Model**

The performance of the SBP z-score selection texture characterization model depends significantly upon the spectral extent of the image to be rendered, as well as the availability of accurate and thorough ground truth measurements. This is evidenced by its bipolar performance between the results of the rendered CitiPix and HYDICE ARM DIRSIG imagery. For the CitiPix data, the SBP model performed second-best, next only to the FM model. The reason it performed so well is because the use of only one bandpass for selecting material spectra on a pixel-by-pixel basis for a scene consisting only of well-correlated spectral bands is reasonable and thus preservation of spectral correlation is not a significant concern. There was also a very large and well maintained database of material spectra present in the CitiPix scene, due to ongoing efforts at RIT in constructing the DIRSIG Megascene, from which the CitiPix image used in this work has been derived. This thorough sampling of material spectra permitted the excellent modeling of both homogeneous and transition region textures.

The SBP model performed worst overall of all four texture models for the HYDICE ARM DIRSIG scene (see the final ranking charts in Section 5.5.6). The reasons for its poor performance are just the contrary to those cited above; that is, the MTL-supplied ground truth measurements did not adequately capture the true spatial-spectral variability of the materials present in the HYDICE ARM scene. The spatial-spectral performance lacked especially in the later spectral bands because the z-score curve selection algorithm only uses one narrow bandpass to assign spectra to all pixels in the scene for all wavelengths, which resulted in incorrect choices for non-correlated spectral regions. This was quantitatively verified by its poor performance spatially in the later spectral bands through the application of the MF and GLCM metric, as well as its inability to perform within the standard deviation threshold for the SCR metric. The SCM metric further corroborated this analysis by demonstrating that while the spatial-spectral structure was maintained in spectral bands well-correlated with the visible region, it broke down for non-correlated band pairs.

### **5.5.2 MBP Model**

The MBP model performed quite well for both the CitiPix and the HYDICE ARM rendered DIRSIG imagery. Although it was ranked third overall for the CitiPix image, it nonetheless performed almost exactly as well as the SBP model did, and far better than the TS model performed. The reason for the poorer performance by the MBP model is that the use of three separate bandpasses for the z-score selection algorithm tended to over-constrain the choice of spectra for each pixel in the resultant DIRSIG image. This was an interesting result, since the motivation for the MBP texture model concept was to improve on the SBP model results. This result, of course, is only the case when rendering imagery with only well-correlated spectral bands (i.e, for images with small spectral dimension). For cases where the spectral dimension is large and thus contains several uncorrelated spectral band regions, the distinct advantages of the use of the MBP texture model are obvious. This was the case for the rendered HYDICE ARM imagery using the MBP texture model, in which the spatial-spectral structure was preserved throughout the entire spectral range, and it was ranked second-best, next only to the FM model. The results shown in Section 5.2 demonstrate this

effect of the deterioration of the spatial-spectral structure of the SBP image in the later bands, while the MBP image does not exhibit this phenomenon whatsoever. It is interesting to note that for the CitiPix imagery, both the SBP and MBP texture models utilized the same database of ground truth measurements for the application of image texture. However, for the HYDICE ARM imagery, the ground truth data was demonstrated to be lacking and thus image-derived spectra were used in place of the actual measurements obtained at the collection site. This drastically improved the results for both the SBP and MBP models, but the most significant improvement was observed in the MBP imagery. This is yet another instance that suggests that both the SBP and MBP models depend greatly on the availability of thorough and accurate ground truth spectral measurements. In order to avoid testing of ground truth practices, the best-case scenario of image-derived spectra was used as the final result to which the texture performance metrics were applied. If the entire set of image-derived spectral reflectance curves had been used for the z-score selection algorithm, then the SCR metric values would accordingly improve to the level of the TS model or better, thereby closer resembling the SCR values of the real HYDICE image.

### **5.5.3 Texture Synthesis Model**

The TS model consists of an entirely new methodology of creating synthetic texture in DIRSIG imagery. It does not have the dependence upon ground truth spectra since texture is created directly by sample texture image inputs from which spatial and spectral statistics are derived (unless, of course, one wants to extend the spectral extent of the output DIRSIG image. In this case, ground truth curves would be used to calculate the spectral covariance statistics of each material in the scene for input into the Spectral Expansion TS model). It does, however have other limitations that are evident in the results of both the rendered CitiPix and HYDICE ARM DIRSIG imagery. One of these is that there is a minimum input sample texture image size required, which must be in increments of powers of two for this model. This places restrictions on the types of materials in a scene that can be rendered, since any narrow features which are not at least 64 x 64 pixels in dimension will require some pre-processing (such as the mirroring routine that was used in this work) in

order to grow regions out to the minimum size required by the TS model. Another associated problem then arises in that this tends to introduce artifacts in the output DIRSIG image, such as those observed in the road region of the HYDICE ARM image, and the baseball dirt of the CitiPix image.

Another limitation is that within- and between-material class transitions are not well-modeled, such as the transitions between healthy and stressed grass and the lines on the football field in the CitiPix image. Also, structural patterns are very difficult to capture in the TS model synthetic textures, such as the plowed field regions of the HYDICE ARM image. This is due to the fact that there is a finite input sample texture size from which the TS model extracts statistics to construct synthetic texture. This method tends to work better for materials with repeating structural primitives on a much smaller scale than that observed for the plowed field regions. Lastly, the between-material transition regions are more abrupt than the other models, since their smoothness depends on the transitions in the associated material class map for scene construction. Since transition regions of a given material class would seldom be used as an input sample texture image for this model, the homogeneous properties will be repeated in the output synthetic texture until the transition edge occurs to another material class region. This is the case for the *reflectance map* implementation of the TS model into DIRSIG; it is possible that future efforts can concentrate on a more complex incorporation of this model into the DIRSIG environment. The TS model approach has the attractive feature of forcing a solution that matches the desired spectral covariance and spatial correlation statistics in one spectral band. However it cannot assure that the areal spatial patterns within a texture region are reproduced in the output SIG image.

These limitations were evident in the CitiPix and HYDICE ARM DIRSIG imagery especially in the spatial domain, since neither data set possessed the aesthetically pleasing spatial appearance that the other three models were able to produce. As such, the TS model was ranked last in terms of performance for the CitiPix imagery, even though certain material types that demonstrated relatively little within-material class variability (such as asphalt, rooftops, etc.) were characterized just as well as the MBP model was able to

produce. However, the advantage of the TS model was more obvious upon the application of spatial and spectral metrics on the HYDICE ARM data. Although the TS model produced the worst spatial results in the earlier spectral bands, it performed comparably with the SBP model for the later spectral bands. Further, since the TS model guarantees that the spectral covariance statistics will be correct in the output synthetic textures (due to the nature of the constraint enforcement of the model), it performed better than any of the models for the purely spectral SCR metric. After the application of the weighted spatial-spectral SCM metric, it was clear that the TS model was able to out-perform the SBP model overall for the HYDICE ARM imagery due to its ability to maintain spectral fidelity in its synthetic textures. The TS model was not able to perform as well as the MBP or FM models.

#### **5.5.4 FM Model**

The FM texture model was ranked as the best overall model for both the CitiPix and HYDICE ARM imagery. It was expected that, given reasonably well-separated and noise-free fractional abundance planes coupled with accurate representative end member spectra, the FM model would perform very well in the spatial domain, since it literally re-mixes spectra on a pixel-by-pixel basis into an output DIRSIG image. The concern with this model was more significant for the spectral domain, since the current DIRSIG implementation of this model only accepts one “averaged” end member spectrum for each fraction plane, and the spatial-spectral texture is thereby created by re-mixing combinations of each constituent end member according to the weights of their corresponding fraction maps.

For the CitiPix data, the FM model performed exceptionally well, which was not a surprising result since only well correlated spectral bands were present in the image and thus the potential problems associated with the assignment of a single end member reflectance spectrum is not as crucial as it was for the HYDICE ARM data. Therefore, the MF, GLCM, and SCM metrics all indicated that the FM model performed much better than the other three models both spatially and spectrally for the CitiPix DIRSIG image.

For the HYDICE ARM data, the MF and GLCM metrics both indicated that the FM model once again performed best in the spatial domain. However, the spectral SCR metric ranked the FM model third out of the four models (although it performed almost exactly as well as the MBP model for this metric). It therefore performed comparably with the MBP model in a spectral sense, but not nearly as well as the TS model. The SCM metric confirmed that the FM model performed best overall in a spatial-spectral sense, which implied that the re-mixing of different combinations of the eight end member spectra was able to produce the same amount (or even better) of spatial-spectral complexity and clutter as the MBP model, while maintaining the spectral correlation between selected spectral band pairs.

Although this model was deemed to perform best for both the CitiPix and the HYDICE ARM data sets, it does not necessarily imply that it is always going to be the best model to use. The relative performance of the models depends on what data is available to the user as well as the nature of the imagery to be rendered. In order to create adequate spatial and spectral mixing in the output DIRSIG imagery, one must have a sufficient number of input spectral bands of imagery available to produce the necessary fraction maps. In the case tested here, the entire real HYDICE image was used to select end members and subsequently to unmix to create fraction planes. Also, there are certain conditions that must be met in order to ensure that the FM model performs optimally. First, one must be sure to utilize a spectral unmixing algorithm that will produce distinct, noise-free fractional abundance maps. Second, the results are very sensitive to the number of end members used for the unmixing process. In order to capture the same spatial and spectral complexity of real imagery, one must use an appropriate number of end members. A certain degree of trial and error may be involved with this process. Also, one must be careful when assigning an “average” spectrum to each of the end member fraction maps. In order to maintain the spectral structure and correlation, a truly representative spectrum must be used; otherwise the results of the SCR and SCM metric will not achieve the excellent results that have been shown in this work. It is clear that with accurate end member spectra allocated to each

fraction plane, the spectral clutter present in real imagery can be replicated through their various fractional contributions.

### **5.5.5 Sources of Error**

Every possible effort was made in this research to be consistent in the incorporation and application of the image texture characterization models, the texture model performance metrics, and the resulting analyses. By doing so, the sensitivity of error propagation on the comparative performance analysis of each of the texture models could often be minimized and/or “cancelled out.” However, the appearance of anomalies and subtle errors are virtually unavoidable in any research effort and as such they will be discussed here.

The most eminent potential for error is in the choice of image calibration methodology used in this work. The Empirical Line Method (ELM), although a robust technique for calibration of imagery to the desired units of measurement and for the removal of the worst of atmospheric effects, is sensitive to errors if not treated carefully. Since the process involves the fitting of ground truth and image-derived values to a straight-line relationship, the line can be easily skewed if the “bright points” used for calibration are incorrect. This can adversely affect the slope of the calibration line, thereby causing the introduction of erroneous reflectance (or whichever unit of measurement is preferred) values of scene materials. The simplicity of this model often causes it to be the target of much criticism, but it can also work to the user’s advantage. For example, the ELM calibration of the HYDICE ARM scene (and of the corresponding DIRSIG rendered scenes) was very straight-forward since the scene contains calibration panels for the purpose of calibrating the image to reflectance units. With the assistance of a very detailed ground truth report by MTL, the ELM calibration could be carried out with high confidence. The only potential problem encountered was the fact that the brighter panels tended to be saturated in the image subset used for this research. In order to alleviate concerns with how this might affect the calibration results, the HYDICE ARM image was calibrated using all 6 panels of the 6-step grayscale, and then with only 5 panels (the 64% reflectance panel was not used), and finally with only 4 panels (in which the 32% reflectance panel was also not used). Image

wide and material-specific local statistics were extracted from each of these three calibrated images, including mean, standard deviation, and variance values. The results were remarkably similar for all three cases, which implied that the two brightest panels did not add much information for the calibration process. The mean and standard deviation values were all well within less than 0.5% of each other in each case. It was decided that the image calibrated using all six panels would be used thereafter for the real and DIRSIG imagery.

The calibration of the CitiPix imagery was slightly more challenging due to the fact that there were no calibration panels present in the scene. However, as mentioned previously, there has been extensive ground truth collection efforts in the vicinity and within the boundaries of the CitiPix image used in this work. Both the dark and bright points used in the calibration were very reliable measurements, consisting of many repeated measurements with tight distributions. This was crucial for an accurate calibration, since ideally the dark and bright points should be inherently low in variability, such as rooftops, asphalt, and concrete. Fortunately, thorough ground truth data was available for all three of these types of materials as well as others present in the scene. In order to test the calibration results, a second line was fit using other spectra with moderate nominal reflectance values (i.e., neither considered “bright” nor “dark”). The results of the two calibrated images were analyzed in the same manner as the three HYDICE ARM calibrated images. In this case, the results were within 1% of each other for local and global statistics. The original calibration was then used on all subsequent DIRSIG-rendered CitiPix imagery for consistency sake. As discussed in Sections 4.4, 5.1, and 5.2, a visual inspection of the corresponding real and DIRSIG images within linked ENVI displays demonstrated that all calibrations appeared to be equally successful. This is particularly important since it was the reflectance values that were ultimately compared using the texture model performance metrics. Therefore, each of the calibrated images were produced with a high level of confidence, especially since the exact same bright and dark control points were used to calibrate the real and DIRSIG imagery thereby avoiding any variations introduced due to inconsistent calibration processes. The results for samples of performance metrics using the alternately-calibrated images were

also analyzed and compared with the results using the nominally calibrated imagery in order to determine if there was any suspected error propagation when applying the performance metrics. For all cases, the observed differences between the metric image results were at the same 0.5% and 1% values as indicated above, thus indicating negligible error propagation from the calibration step to the metric analysis step.

Another potential factor for variability within the results is the edge effects resulting from performance metric application to the corresponding real and DIRSIG imagery. Since the MF, GLCM, and SCM metrics all act as filters within 3x3 processing windows, these edge effects are unavoidable. Although this phenomenon has the potential to introduce edge artifacts, it is not considered to be a significant concern since the edge effects occur consistently to all corresponding texture test regions being investigated. That is, the edge truncation and/or wrapping algorithm within the ENVI filtering feature is always performed in the same manner and thus any artifacts appearing in a particular texture test region metric image for one texture model would appear in the corresponding metric image for another texture model.

The fundamental limitations involved with the use of the TS texture characterization model also provide a potential for errors in the form of artifacts that should not be present in the output synthetic texture image. Although this is not really considered to be an “error” per se, it is worthwhile to discuss its implications once again. The best illustrative example of such an instance is for the road region of the HYDICE ARM image, which is a narrow feature from which it is impossible to extract a pure square input material texture sample image for the algorithm. For this and other non-square regions not exceeding 64x64 pixels in dimension, this becomes a problem. The method invoked to address this dilemma was to grow out the sample region through the use of a mirroring code. As discussed earlier, this introduced repetitive artifacts in the road region of the TS model DIRSIG image that clearly did not exist in the real HYDICE ARM imagery. Perhaps with a more complex and versatile DIRSIG implementation of the TS model, or even through the modification of the TS model source code this restriction can be improved, but the fact nonetheless remains that an

outside process other than the TS model code has created such artifacts, despite the fact that the root cause is the limitation imposed by the model itself.

There is some uncertainty associated with the overall texture model performance ranking process (see Section 5.5.6). There are numerous alternate methods that can be used to differentially weight the performance based on each metric result, since both spatial and spectral metrics have been used. Further, it is difficult to quantitatively determine how much to fractionally weight the SCM metric in terms of its spatial/spectral emphasis in its result. Since the SCM metric only compares two spectral bands per computation but otherwise follows the same process as the GLCM metric, one could surmise that this metric is more spatially weighted than spectral. Therefore, the accuracy of the application a differential spatial-spectral weighting to this metric of 0.5-0.5, 0.7-0.3, or 0.85-0.15 is impossible to robustly determine. Although this uncertainty exists, it does not significantly affect the results of overall ranking since using each of the above rankings still provides identical overall model rankings. This is because there is enough separation between model performance for each of the metrics that variability in SCM metric weighting does not affect the overall rank order.

As previously mentioned, there is a concern with biased SCR metric values for the TS model since the same regions were used to enforce spectral covariance statistics in synthesizing the texture as used for the covariance for computation of the SCR value of each region. This has the potential to produce overly optimistic SCR metric values in relation to the results of the other models. In order to reduce run times, the reflectance curve database had to be truncated for the MBP model. This caused the corresponding real and MBP SCR metric values to diverge somewhat. If the entire sampling of curves had been used, then the SCR metric values for the MBP model would likely be comparable to those of the TS model and the real image. This dilemma suggests the potential for biased results based on methodology such as the choice of texture regions to be tested, sampling of spectral reflectance curves in the database for the MBP and SBP models, and the choice of input regions to extract for the TS model.

The sources of error discussed above have been presented for completeness sake and for consideration of future research efforts intending to improve upon the results obtained in this research. The following section provides a summarized view of the performance metric results for each of the texture characterization models that have been tested, as well as an overall performance ranking, and the conditions and/or limitations that must be overcome for optimal model performance.

### 5.5.6 Comparative Performance Analysis Synopsis

In the above analysis we have observed somewhat variable texture model performance between the CitiPix and HYDICE ARM data, as well as between the different performance metrics. For convenience, the rankings for each metric are shown in the following tables.

#### CitiPix Imagery

<b>MF Metric</b>	<b>GLCM Metric</b>	<b>SCM Metric</b>
1. FM Model	1. FM Model	1. FM Model
2. SBP Model	2. SBP Model	2. SBP Model
3. MBP Model	3. MBP Model	3. MBP Model
4. TS Model	4. TS Model	4. TS Model

Table 35: Texture model rankings for each of the three performance metrics applied to the CitiPix DIRSIG output imagery.

#### HYDICE ARM Imagery

<b>MF Metric</b>	<b>GLCM Metric</b>	<b>SCR Metric</b>	<b>SCM Metric</b>
1. FM Model	1. FM Model	1. TS Model	1. FM Model
2. MBP Model	2. MBP Model	2. MBP Model	2. MBP Model
3. SBP Model	3. SBP Model	3. FM Model	3. TS Model
4. TS Model	4. TS Model	4. SBP Model	4. SBP Model

Table 36: Texture model rankings for each of the three performance metrics applied to the HYDICE ARM DIRSIG output imagery.

In order to postulate what the final overall rankings of the texture characterization models would be, it is necessary to distinguish between the types of imagery being rendered

in DIRSIG. For the CitiPix data, all of the metrics suggest the same rank ordering of the models. Therefore the final ranking for imagery to be rendered with small spectral dimension (i.e., consisting only of well-correlated spectral bands, such as the visible region of the CitiPix data) would be exactly that listed in Table 35. This of course is dependent upon the availability of thorough and accurate ground truth data so that the spatial variations of the materials in the scene can be adequately modeled using the SBP and MBP models. Also, the MBP model listed here uses three spectral bandpasses, covering the entire bandpass of the CitiPix image. It would be interesting to see how well the MBP model would work using just 2 bandpasses, such as the Red and Blue channels only. Since the TS model has been shown to be more spectrally oriented in its approach, it would not be the best choice of model for this situation, since spatial texture is more crucial for imagery of very limited spectral extent. This is summarized once again in Table 38.

If the imagery to be rendered is a multi- or hyperspectral image consisting of non-correlated spectral bands, then the rankings using each of the metrics for the HYDICE ARM data in Table 36 should be considered. The spatial metrics (MF and GLCM) both suggest the same rank ordering of the models. However, for the later spectral bands the TS and SBP models performed very similarly, as evidenced by their oscillatory behavior of their respective metric values. The SCM metric indicated a ranking very comparable to the rankings of the spatial metrics, except the TS and SBP models are reversed. The margin of improvement between the models is larger for the SCM metric, which indicates a better overall performance by the TS model. This is further corroborated by the exceptional spectral performance of the TS model indicated by the SCR metric. Since most hyperspectral algorithms exploit spectral structure much more than spatial patterns, the superior spectral clutter captured in the TS model DIRSIG imagery makes this model a more intelligent choice in order to achieve an optimal trade-off of spatial and spectral texture characterization. This suggests another consideration that causes overall rankings to be more difficult to obtain for hyperspectral data. That is, the choice of model can also depend on the nature of algorithms that are planned to be used on the output synthetic image. For

instance, if SCR is an important measure in its processing, then choosing a texture model that performs well for the spectral SCR metric only may be a viable choice. This of course is still subject to the availability of input image data for each model.

There are numerous techniques that can be employed in producing an overall ranking of the texture models. The following discussion will outline only a few possibilities. First, since the MF and GLCM metrics provide identical model performance rankings, and since each is a measure of spatial fidelity, only one needs to be used. The GLCM metric has been chosen here since it achieves better discrimination between texture features. The ideology behind obtaining an overall spatial-spectral ranking of texture model performance involves the weighting of each metric and its associated result. Unfortunately, this step inevitably involves some degree of subjectivity. One simple method is to apply a weight of unity to the GLCM and SCR metrics and 0.5 to the SCM metric. The ranking achieved by a given model using each metric is then weighted by the associated metric ranking. The following table illustrates this scenario:

		<b>Ranking</b>			
	<b>Weight</b>	<b>1</b>	<b>2</b>	<b>3</b>	<b>4</b>
<b>GLCM</b>	1	FM	MBP	SBP	TS
<b>SCR</b>	1	TS	MBP	FM	SBP
<b>SCM</b>	0.5	FM	MBP	TS	SBP

Table 37: The use of metric weights in order to determine overall spatial-spectral texture model performance.

For each model, the ranking for each metric is multiplied by its corresponding weight and summed. As such, the model with the lowest value indicates the best overall performance. In this case, the results are as follows: 1. FM model (4.5); 2. MBP model (5); 3. TS model (6.5); and 4. SBP model (9). This ranking coincides with the ranking provided by the SCM metric and with the preliminary ranking prescribed in Table 34. Also, this analysis further shows how close the performance of the MBP and FM models is for the HYDICE imagery in terms of overall spatial-spectral performance. There is clear separation between the

FM/MBP models and the TS/SBP models, as well as between the TS and SBP models in this ranking method. An alternative to this method is to assign weights of unity to all three metrics. In this case, the ranking result is: 1. FM model (5); 2. MBP model (6); 3. TS model (8); and 4. SBP model (11). This weighting technique produces the same rank order as with the other weighting combination, and also exhibits the same separation trends between relative model performance. This simple ranking method provides an intuitive summary of spatial/spectral overall performance of each model based on the combination of each separate metric result. Although there are several other ranking techniques that can be invoked for this process, the above results are considered sufficient to objectively rate the performance of each texture model.

The final rankings based on the HYDICE ARM data (and thus for most scenarios in which the spectral dimension is large) are presented in Table 38. Table 39 provides a synopsis of the limitations that must be overcome and other conditions required for optimal texture model performance.

<b>Small Spectral Dimension</b>	<b>Hyperspectral Imagery</b>
1. FM Model	1. FM Model
2. SBP Model	2. MBP Model
3. MBP Model	3. TS Model
4. TS Model	4. SBP Model

Table 38: Final ranking of texture characterization models based on nature of imagery to be rendered in DIRSIG.

<b>Texture Model</b>	<b>Conditions / Limitations</b>
SBP Model	Ground truth data required for adequate spatial-spectral structure / Does not optimally characterize spectral band regions that are non-correlated with texture image bandpass
MBP Model	Ground truth data required for adequate spatial-spectral structure / Multiple non-correlated texture maps required
TS Model	Minimum size required for input sample texture image / difficulty modeling within- and between-material class transition regions spatially
FM Model	Adequate ground truth data required in order to confidently assign averaged spectrum to each end member's fraction map / Production of noise-free, distinct fraction planes required / Stricter requirement for multi-band input image data

Table 39: Synopsis of the conditions that must be met and limitations that must be overcome for optimal texture model performance.

An assessment of how well each of the four texture metrics is able to determine model performance is also appropriate. In particular, it is useful to investigate which of the metrics is most meaningful on its own, or if a reduced combination of metrics would be recommended. In the spatial domain, the MF and GLCM metrics have been used. One will notice that the rankings produced by the MF and GLCM metrics were identical for both the CitiPix and HYDICE ARM data. This suggests the possibility that the MF metric is redundant with respect to the GLCM metric analysis. If a choice of the two metrics was necessary, then the GLCM metric would be recommended since it is a more detailed measure of spatial texture properties. It has also produced larger gaps between model performance, and thus has greater discriminative powers between texture features. This is not surprising, since the GLCM is an often used mathematical description of texture features used for classification and segmentation applications. There is also much more versatility offered with the GLCM metric, since one can alter the size of the processing window, the orientation at which one desires to measure the GLCM on a given region, not to mention the fact that there are several choices for GLCM-derived texture features that can be calculated to suit the types of textures present in the scene being measured. Although there are much more analyses and parameters involved with this metric than for the MF metric, it

nonetheless provides a more rigorous and detailed texture description than the MF metric. If one opts for a simpler, more general measure of spatial texture then the MF metric is a viable option. The MF metric offers the advantage of simpler implementation, less parameters to decide upon, and a simpler post-analysis stage, with the trade-off being less flexibility and less discriminative power between visually similar texture features.

The only purely spectral metric used in this analysis was the SCR metric. It is relatively simple to implement, and it is the only metric used that conveniently indicates performance with a single numeric value, thereby negating any requirement for post-analysis. This metric is important as a measure of spectral clutter and complexity in a synthetic image since it ignores the spatial structure, and provides an independent measure of spectral structure in relation to the real counterpart image. Since spectral structure is used almost exclusively in most HSI applications, it is important to be able to assess whether the synthetic spectral behavior is benign or realistically variable as observed in real imagery. The only concern with its use in this analysis is that it has the potential to be biased as a metric towards models that enforce spectral covariance statistics in generating synthetic texture (such as with the TS model). The TS model has therefore exhibited the best performance of all models for this metric on the HYDICE ARM imagery. The concern for such a bias is alleviated if one considers how relevant the SCR measure is in many practical situations. For instance, the SCR is often used in the literature for various target and anomaly detection algorithms. Thus if the spectral clutter in a synthetic image is comparable to that of a real image (as indicated by the SCR value), then such HSI algorithms will tend to behave as they would for real imagery, which is the exact result that is desired for DIRSIG and other SIG models.

The Spectral Co-Occurrence Matrix (SCM) is a new concept that has not been presented in any earlier work. It is a simple extension of the GLCM methodology that considers both spatial and spectral structures in a compact mathematical form by performing cross-band co-occurrence computations. Its ENVI-integrated version offers the potential for new research in texture feature extraction, classification, segmentation, synthetic imagery

texture fidelity measurements, as well as several other applications that can be explored with this tool. Perhaps future research efforts can focus on making the SCM into a more elegant and potentially more complex measure of simultaneous spatial-spectral structure. For the purposes of this research, the SCM metric has provided an effective and convenient measure of spatial-spectral texture for user-defined spectral band pairs. Although the analysis was only performed on a sampling of band pairs, it is considered to be sufficiently thorough for this work to determine whether spatial and spectral correlation and structure are maintained in the tested synthetic imagery. One will notice that the rankings provided by the SCM metric alone coincide with the final overall rankings of the models based on both the spatial and spectral domains. Therefore, the SCM metric is the most intriguing and perhaps most useful metric used in this work in the assessment of the fidelity of overall spatial-spectral variability in synthetic imagery.

The use of the GLCM and SCM metrics will inevitably require decisions to be made regarding the types of texture features to calculate, the size of the processing window to be used, and the orientation at which to calculate the GLCM/SCM features. For the most rigorous testing, and to distinguish between fine texture features, a 3x3 processing window is the best option, used in conjunction with GLCM orientation vectors in horizontal, vertical, or diagonal directions of one pixel in length (i.e.,  $(\Delta x, \Delta y) = (1,0), (0,1),$  or  $(1,1)$ ). In fact, the computational form of the GLCM and SCM deliver extremely similar results for all three of these nearest-neighbor orientations. It was also noticed that certain co-occurrence-derived features are redundant with respect to other features. As mentioned previously, most GLCM studies have found that the use of 2-4 of these features is sufficient for texture feature discrimination to the desired level for remotely sensed imagery. Although the original plan was to use the Contrast, Correlation, and Homogeneity features in combination, it was found that the use of both the Contrast and Homogeneity measures was redundant, due to their inverse relationship. Contrast was found to be a more descriptive measure of texture, and thus it was used as the primary feature for the GLCM and SCM metric analysis. It was also found that the use of the number of outliers for the Correlation

feature was effective to use as reinforcement of performance indicated by the Contrast feature alone. This was due to the large absolute values and ranges of values observed in the Correlation feature texture images. There are many other features to work with, and the choice is dependent upon the particular application and the nature of the imagery upon which the GLCM/SCM measures will be applied.

This concludes the comparative performance analysis that was originally intended to be completed in this research. The following section will discuss supplementary results that were completed for interest sake or for contractual reasons. First, the results of DIRSIG imagery rendered using the FM, SBP, and MBP models of the CitiPix scene simulated with the HYDICE imaging spectrometer platform are presented in Section 5.6.1. This effectively extends the spectral coverage of the image. Secondly, the imagery and performance metric results of the incorporation of an additional texture characterization model are presented in Section 5.6.2.

## **5.6 Supplementary Results**

### **5.6.1 CitiPix Scene Rendered Using HYDICE Imaging Spectrometer**

The above analysis required the existence of counterpart real imagery at the same spectral resolution and extent in order to assess the spatial and spectral fidelity of the rendered DIRSIG imagery. However, in most practical situations one seeks to simulate imagery at varying resolutions and with different sensor platforms so that the versatility of synthetic image generation can be fully realized. This section has been included in order to show additional results of certain texture models under a different sensor configuration than for which truth imagery exists. Since this work has focused on CitiPix and HYDICE ARM imagery, the combination of the two data sets was the next logical step. The following set of imagery represents the simulation of the same CitiPix scene as used in the above comparative performance analysis, but with the HYDICE imaging spectrometer used as the sensor platform instead of the Kodak CitiPix framing array camera. This required some careful alterations of several associated DIRSIG configuration files in order to obtain the correct spatial and spectral resolution, sensor response, atmospheric and flight parameters, as

well as many other details. Note that this effectively extends the spectral coverage from a three-band CitiPix image to a 210-band hyperspectral image, at the same spectral resolution as seen in the Lamont HYDICE ARM scene used above. The GSD was kept at 0.45 m, and thus the CitiPix-HYDICE synthetic imagery is the exact same size as the original CitiPix data (437 x 437 pixels). DIRSIG scenes using the SBP, MBP, and FM texture models were used in the following simulations. The most significant modification for constructing these scenes was the inclusion of ground truth data for material classes present in the real CitiPix image. This required much larger emissivity files in order to capture the spectral character that should be observed in the near and far infrared spectral regions. Since there is no corresponding real imagery with which to apply the performance metrics, the results are shown only for interest sake and to demonstrate how flexible and powerful synthetic image generation using the DIRSIG environment can be.

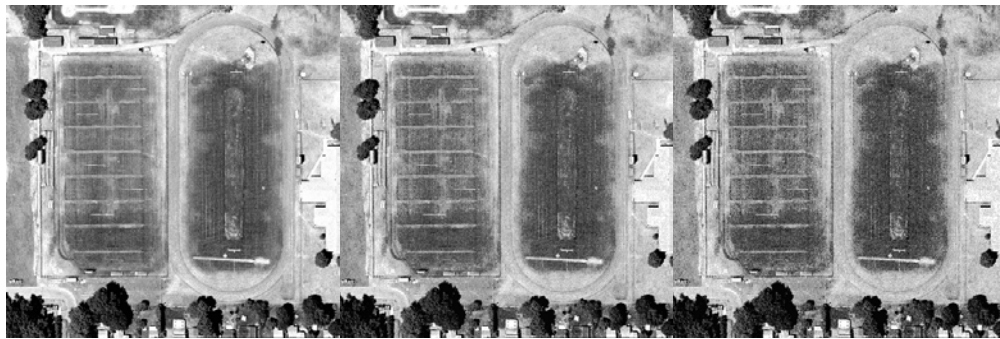


Figure 68: CitiPix scene simulation using HYDICE imaging spectrometer and SBP texture model. Bands 51, 105, and 184 are shown here.



Figure 69: CitiPix scene simulation using HYDICE imaging spectrometer and MBP texture model. Bands 51, 105, and 184 are shown here.

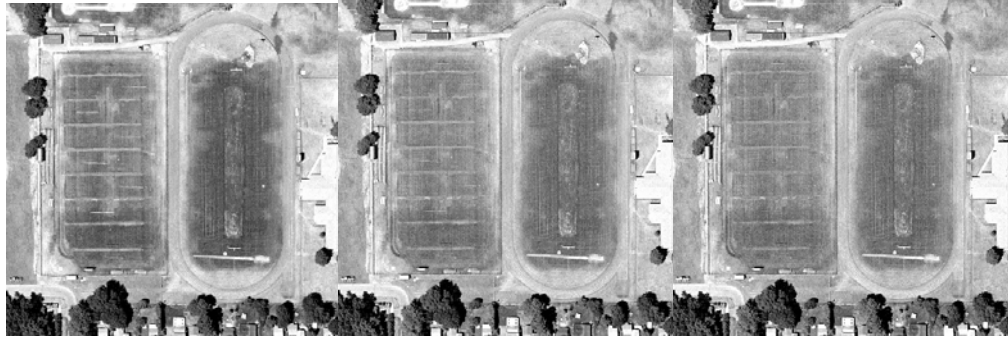


Figure 70: CitiPix scene simulation using HYDICE imaging spectrometer and FM texture model. Bands 51, 105, and 184 are shown here.

Based on a visual analysis alone, the spatial fidelity of all three models appears to be quite good for most of spectral bands, including the three bands shown above. One very subtle point is that the SBP model imagery tends to begin looking slightly noisy in the later bands, such as in band 184 above. The onset of this phenomenon is earlier than for the MBP model imagery, which also begins to appear noisy in the later bands. This effect is not surprising since the texture maps used for rendering this imagery were all from the visible region of the electromagnetic spectrum. Therefore, although there was adequate ground truth data to cover this spectral range, the z-score selection algorithm applied spectra to pixels based on statistics in the visible region only. This produced a somewhat flat spectral response in the output imagery, since most of the spectral bands look nearly identical to each other instead of exhibiting the expected spectral behavior of materials such as grass. The same effect was observed for the FM model imagery. Since this image was constructed using the same four fraction maps as used with the CitiPix FM model DIRSIG image, there does not appear to be as much spectral complexity as in the real image. In this image, each pixel contains a mixture of four end member spectra in weighted amounts according to their respective fractional abundance maps. The selection of a valid representative curve for each end member is more crucial for an image of larger spectral dimension, which is evident in the fact that most of the spectral bands appear very similar once again. In fact, it resembles

the 3-channel CitiPix FM DIRSIG image throughout the spectrum. It does not exhibit the same noise phenomenon as in the SBP and MBP images shown above.

Performing this process for the Texture Synthesis model is somewhat more complicated, and would require some modifications to Tyrrell's source code. This would not be possible using either the S/P or Quilting models due to the fact that these algorithms require input sample textures at the same or better spectral resolution than the imagery to be rendered, and the spectral coverage cannot be expanded as it has using the SBP, MBP, and FM models. The Spectral Expansion model was conceptualized in order to address this limitation, and in this work, synthetic textures have been generated only as far spectrally as the real imagery extended, since the input curves used for spectral covariance statistical enforcement was derived directly from the input image. Some careful pre-processing would also be necessary for this in order to ensure that the curves are sampled at the exact intervals as the desired output spectral resolution. The largest challenge for expanding spectral coverage using the Texture Synthesis model is to obtain and manage a very thorough database of ground truth reflectance curves for all materials present in the scene (i.e., even though the ground truth we currently have for this scene is quite good, it would not be adequate for the Texture Synthesis model). An extremely careful ground truth collection process that accounts for the complete variability of materials, transition regions, and spatial structure would be required in order to maintain any sense of spatial correlation and structure in the output image. Measurements taken at regular intervals in grid patterns are likely the best method to achieve this. Since the images rendered using the Texture Synthesis model in this work used the input image directly, this demonstrates the best case scenario, since the curves effectively are derived from a grid sampling in the form of image pixels, and the curves are ordered in a spatial sense as dictated by the spatial structure of the image in each spectral band. This would be an interesting area of future research if the Texture Synthesis model was to be investigated further and/or improved.

## **5.6.2 SSI Texture Characterization Model Results**

As part of an ongoing contract between the Rochester Institute of Technology (RIT), Spectral Sciences, Inc. (SSI), Kodak, and Air Force Research Laboratories (AFRL) to investigate an improved method for the incorporation of spatial-spectral variability in synthetic hyperspectral imagery (HSI), SSI has submitted sample synthetic texture results to be tested within the scope of this research. The following sections detail the background theory used for the SSI approach to creating synthetic textures, as well as the results of incorporating these textures into the HYDICE ARM DIRSIG scene. The four performance metrics were run on a subset of the texture test regions in order to quantitatively assess the spatial and spectral fidelity of the output synthetic imagery.

### **5.6.2.1 Background Theory**

The paper detailing the latest version of the SSI texturing tool is not yet published. This texture model is based on the extraction of hyperspectral scene statistics through the use of an end member selection algorithm called Sequential Maximum Angle Convex Cone (SMACC) which uses a convex cone matrix factorization to find a hierarchy of end members and simultaneously computes the fractional contribution to intensity maps of each material represented [Sundberg, Gruninger, Haren, 2002]. The SSI texture model is largely driven by spectral statistics in its production of synthetic texture cubes representing each constituent end member of the scene to be rendered. SSI is currently working on improved methodology for characterizing spatial texture as well as spectral texture within their model.

### **5.6.2.2 Texture Model Results and Performance Analysis**

SSI has submitted synthetic texture cubes representing the plowed field, wheat, and uncut pasture regions of the HYDICE ARM imagery. These textures have been incorporated into DIRSIG in a manner very similar to the implementation of the Texture Synthesis model since the format of input textures make the “reflectance map” mode of DIRSIG texture application the obvious choice. Although the SSI textures cover three



material class regions according to the material map used for the rendering process of the DIRSIG scene, there were six synthetic texture cubes provided. These textures distinguished between the upper and lower plowed fields (regions F3 and F5), the upper and lower wheat regions (regions F1 and F2), and for two distinct material classes within the uncut pasture region (regions F4 and F7). Due to time constraints and the lack of a more versatile method to incorporate all of the textures separately, only three of the textures could be used in constructing the DIRSIG scene. This is because the material map does not make such distinctions between the upper and lower plowed and wheat fields and thus only one texture belonging to each material class could be selected. Although this method of incorporation of textures into DIRSIG is completely valid, perhaps future efforts will attempt a more rigorous implementation of the SSI textures.

Since SSI did not provide textures for the road, buildings, cut pasture, and trees, these regions were “filled in” by using the original image as the remaining reflectance map. The DIRSIG image results are presented below.



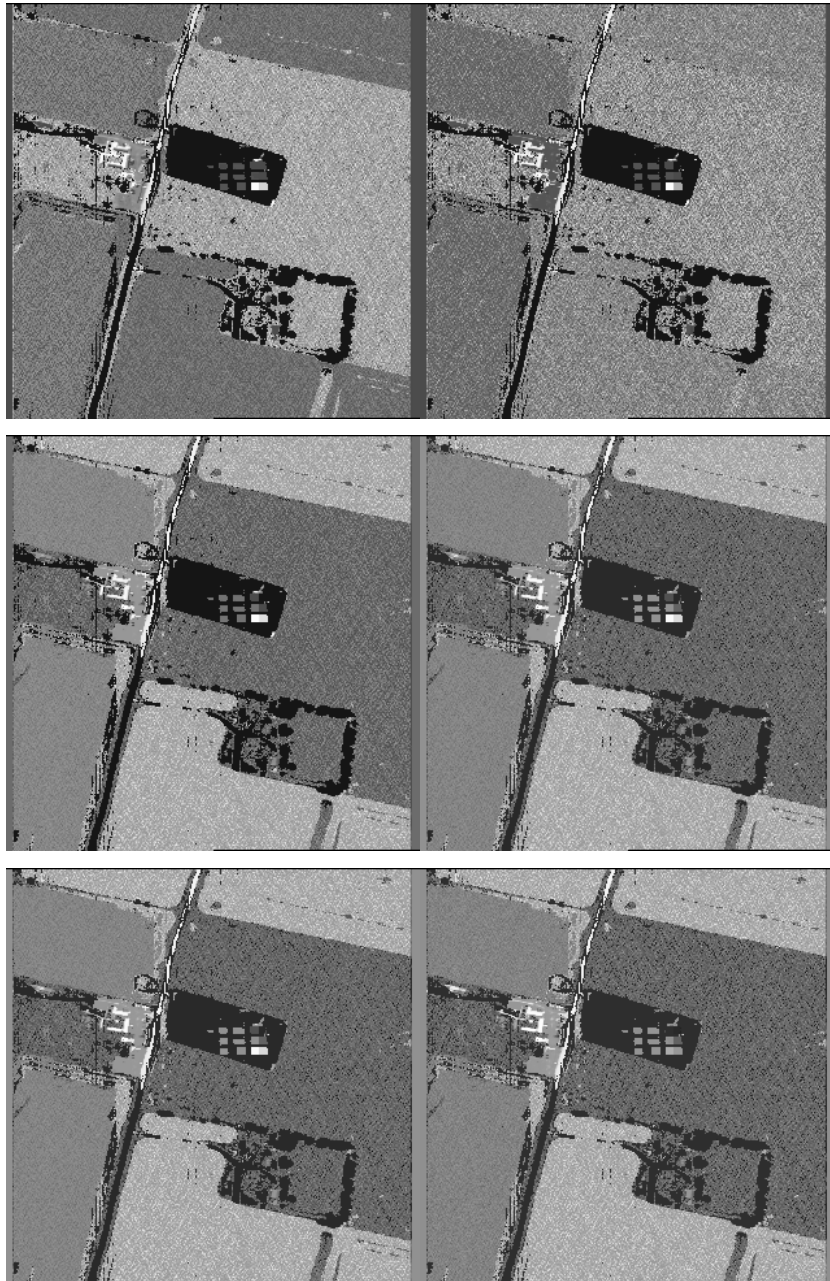


Figure 71: Sampling of SSI texture characterization model results for rendering of HYDICE ARM imagery. Spectral bands 20, 32, 65, 95, 115, 157, 184, and 195 are shown.

Since the SSI model is admittedly spectrally driven in its production of synthetic textures, the spatial structure was expected to be lacking in comparison to the FM and MBP model results shown in the previous sections. In the spatial domain, the results look similar to that of the TS model, except the artifacts are not present in the road region for the SSI imagery since the SSI model did not attempt to render this region. It is important not to focus on the uncut pasture region (at the calibration site), the trees, the road, and the buildings for this imagery since these regions were not rendered using the SSI texture model. The wheat fields appear to have achieved the visually closest result to that of the real HYDICE ARM image, since it is spatially more homogeneous in nature than the plowed fields and uncut pasture regions. The plowed fields do not exhibit the spatial structure observed in the real imagery, since the oriented structural patterns have been lost in the synthesis process. The uncut pasture region is visually similar to the result of the TS model, since both models were able to achieve the large inherent variability of the region. However, the transitions to the dirt and stressed grass regions on the right edge of the image are not present, which was also observed with the TS model result. This is due to the nature of the model itself somewhat, but also due to the method of incorporation of the textures. That is, if another more complex technique other than the “cookie-cutter” reflectance map method was to be used so that the F7 region could be incorporated in to the scene, then this transition region would be replicated with much better fidelity. The transition region between the plowed field and uncut pasture regions is virtually indistinguishable in band 95, so it should be interesting to see if this is evident in the results of the spatial MF and GLCM metrics. It is suspected that the most significant testing of the SSI texture model will be for the spectral domain. The SCR metric will be applied in order to determine how well the spectral clutter and complexity is represented in the synthetic texture. The SCM metric will also be employed in order to assess the simultaneous weighted spatial-spectral texture of the scene.

Since not all regions of this imagery were rendered using the SSI texture model, only a subset of texture test regions have been used for the application of the performance

metrics. Five of the fifteen test regions were considered to be applicable, where three of the regions are homogeneous and the remaining two are transition region textures. The regions to be tested are listed below with the same numbering convention as used in the previous metric tables:

- a. Region 4 (Plowed Field);
- b. Region 2 (Wheat Field);
- c. Region 5 (Uncut Pasture);
- d. Region 11 (Uncut Pasture – Dirt/Stressed Grass); and
- e. Region 13 (Plowed Field – Uncut Pasture).

The results of each performance metric are presented in the following synopsis tables:

	MF Metric – Band 20			MF Metric – Band 32		
Region	Outliers	Range	Average	Outliers	Range	Average
4	44	0.04 – 1.04	0.56	48	0.0006 – 1.5	0.84
2	46	0.004 – 0.64	0.52	47	0.02 – 0.74	0.63
5	49	0.3 – 1.13	0.70	49	0.007 – 1.09	0.73
11	48	0.01 – 2.78	1.62	50	0.003 – 3.05	1.99
13	50	0.3 – 1.69	1.39	49	0.05 – 1.8	1.36
	MF Metric – Band 65			MF Metric – Band 95		
Region	Outliers	Range	Average	Outliers	Range	Average
4	48	0.08 – 4.70	2.98	48	3.1 – 6.82	4.21
2	49	0.03 – 5.98	3.97	46	1.2 – 6.61	3.86
5	47	0.04 – 7.65	5.3	44	0.4 – 4.93	2.59
11	49	0.5 – 10.33	5.93	49	5.1 – 13.1	7.82
13	50	0.1 – 7.1	6.02	50	0.5 – 11.03	8.13

	MF Metric – Band 115			MF Metric – Band 157		
Region	Outliers	Range	Average	Outliers	Range	Average
4	48	3.0 – 7.53	4.66	48	2.3 – 9.15	5.82
2	46	0.001 – 4.39	2.41	49	0.0009 – 3.57	2.32
5	49	0.006 – 4.4	2.84	47	0.02 – 5.3	3.41
11	50	0.05 – 18.61	11.56	50	0.03 – 17.6	11.03
13	48	0.01 – 5.23	3.92	50	0.02 – 6.93	5.63

	MF Metric – Band 184			MF Metric – Band 195		
Region	Outliers	Range	Average	Outliers	Range	Average
4	48	10.0 – 25.27	21.6	49	11.4 – 25.2	19.3
2	49	7.1 – 13.16	11.2	47	4.2 – 10.10	7.72
5	46	3.1 – 12.15	9.8	50	0.03 – 8.47	5.46
11	49	0.06 – 11.3	8.7	49	0.1 – 13.8	9.5
13	50	4.1 – 30.94	20.9	50	0.28 – 32.3	18.4

Table 40: MF Metric results for sampling of bands of SSI DIRSIG HYDICE ARM imagery.

	GLCM Con Metric – Band 20			GLCM Con Metric – Band 32		
Region	Outliers	Range	Average	Outliers	Range	Average
4	49	0.001 – 1.44	0.86	50	0.01 – 1.87	1.64
2	50	0.002 – 0.28	0.192	52	0.001 – 0.36	0.26
5	52	0.04 – 1.05	0.59	49	0.01 – 2.1	1.43
11	49	0.0005 – 4.61	3.56	48	0.01 – 2.97	2.26
13	51	0.02 – 3.58	2.17	50	0.01 – 2.23	2.12

	GLCM Con Metric – Band 65			GLCM Con Metric – Band 95		
Region	Outliers	Range	Average	Outliers	Range	Average
4	50	0.007 – 7.35	4.36	52	7.3	0.003 – 9.92
2	52	0.02 – 28.6	10.1	49	8.2	0.0005 – 14.66
5	51	0.04 – 43.12	24.7	48	19.6	0.005 – 27.63
11	49	0.40 – 48.1	31.7	51	10.23	0.004 – 14.4
13	52	0.05 – 42.3	28.4	50	10.5	0.04 – 13.8

	GLCM Con Metric – Band 115			GLCM Con Metric – Band 157		
Region	Outliers	Range	Average	Outliers	Range	Average
4	53	0.09 – 12.51	10.4	50	0.002 – 31.17	19.43
2	51	0.008 – 7.47	5.19	48	0.09 – 19.25	14.2
5	49	0.79 – 54.9	17.97	53	2.6 – 74.23	31.3
11	52	0.26 – 130.0	94.5	49	0.43 – 320.1	196.3
13	50	0.02 – 52.7	32.4	52	0.47 – 140.1	102.1

	GLCM Con Metric – Band 184			GLCM Con Metric – Band 195		
Region	Outliers	Range	Average	Outliers	Range	Average
4	49	0.2 – 241.7	46.2	49	3.0 – 317.5	98.3
2	53	3.1 – 57.78	33.7	52	3.4 – 68.81	39.6
5	51	9.2 – 270.8	137.6	50	26.1 – 257.7	159.2
11	49	0.02 – 876.6	576.8	51	0.07 – 1121.03	982.8
13	50	0.17 – 505.3	393.7	53	1.0 – 617.8	411.2

Table 41: GLCM Contrast Metric results for sampling of bands of SSI DIRSIG HYDICE ARM imagery.

<b>GLCM Correlation Feature Metric – Number of Outliers – SSI Model</b>								
<b>Region</b>	<b>20</b>	<b>32</b>	<b>65</b>	<b>95</b>	<b>115</b>	<b>157</b>	<b>184</b>	<b>195</b>
4	51	50	49	51	49	52	50	52
2	53	52	48	50	55	54	49	49
5	54	54	52	53	51	49	54	49
11	46	51	54	55	49	53	51	52
13	49	54	53	51	52	51	52	53

Table 42: GLCM Correlation Metric (number of outliers) for SSI model results.

The spatial MF and GLCM metrics each exhibit the same trends, although they are more pronounced in the GLCM metric upon the comparison of the absolute difference images and the deviations from the variance threshold images for each region. The ranges of values and averages listed in the above tables are also indicative of the overall spatial performance of the SSI model relative to the other texture models. There is some oscillatory behavior present between the SBP, TS, and SSI models in much the same manner as observed in Section 5.4. The SBP model once again performs better than both the TS and SSI models in bands 22 and 32, while in the later spectral bands, the performance of the SBP model declines, and the SSI model begins to produce values that are comparable with those of the SBP model, but the SBP model tends to more frequently produce lower metric values than the SSI model. Meanwhile, the TS model still performs better than both the SSI and SBP models for the later bands, which is clear even through a visual analysis. The MF and GLCM metric indicate that the SSI model has characterized the wheat region better than any of the other regions that have been tested, which also agrees with the qualitative results discussed earlier. In fact, the average values and absolute difference images for the wheat texture (region #2) tend to have lower values than for the SBP and TS models in many cases. However, the spatial performance of the SSI model is not nearly as good (for any of the five test regions) as the MBP and FM texture models. Despite the somewhat better results for the wheat texture region, the remaining four test regions were not characterized as

well as any of the other four texture models. In particular, the transition region of uncut pasture-dirt/stressed grass (region #11) is not even visually evident, and as such the spatial metrics have shown that the SSI model contains the highest values of any model for this region. Note that this is in part due to the incorporation method of the SSI model, and that a more complex approach other than the reflectance map mode of DIRSIG may produce better spatial results for this region. The MF, GLCM Contrast, and GLCM Correlation metric values all suggest that an appropriate ranking based on spatial performance alone is:

- a. FM Model;
- b. MBP Model;
- c. SBP Model;
- d. TS Model; and
- e. SSI Model.

The above spatial metric analysis will now be supplemented with a spectral analysis through the application of the SCR metric. The results are presented below:

<b>Region</b>	<b>SCR Value (SSI Model)</b>	<b>SCR Value (Real Image)</b>
4	73.48*	77.21
2	107.67*	119.29
5	131.99*	120.25
11	134.89*	153.82
13	123.92*	104.74

Table 43: SCR values for five texture test regions of SSI DIRSIG HYDICE ARM imagery. (\* = within 1-sigma standard deviation threshold).

Upon comparison with the SCR table for the other four texture models, it is clear that the SSI model performs extremely well in a purely spectral sense, as evidenced by the fact that its SCR values for each of the five test regions are within the standard deviation threshold value. The SCR metric values are very close to those of the TS model, but the TS model achieved values closer to those of the real image for 4 of the 5 regions – and the

difference between the deviations from the threshold for the region in which the SSI model performed better was only on the order of  $10^{-2}$ . The region for which the SSI model performed worst for the SCR metric is the uncut pasture-dirt/stressed grass transition region texture (region 11) since this transition region was not well-modeled due to the reflectance map incorporation method of the model. The poorer performance for this test region was also evident in the spatial MF and GLCM metric results. With more careful implementation and the use of the F7 region that SSI has provided, this region would have the potential to be modeled nearly as well as with the other models. The ranking of the models including the SSI model based on the SCR results alone is:

- a. TS Model;
- b. SSI Model;
- c. MBP Model;
- d. FM Model; and
- e. SBP Model.

The results of the application of the SCM Contrast and Correlation features are presented in the synopsis tables below:

Region	SCM Con Metric – Bands 22-32			SCM Con Metric – Bands 30-162		
	Outliers	Range	Average	Outliers	Range	Average
4	44	0.009 – 6.62	2.49	43	15.1 – 256.6	132.9
2	43	0.07 – 2.55	1.87	46	0.6 – 80.31	43.6
5	46	0.002 – 3.2	1.67	42	0.08 – 51.8	20.1
11	45	0.001 – 10.7	5.6	41	0.67 – 339.4	163.2
13	42	0.007 – 3.26	1.93	45	0.29 – 189.8	151.2

Region	SCM Con Metric – Bands 30-193			SCM Con Metric – Bands 65-185		
	Outliers	Range	Average	Outliers	Range	Average
4	44	23.9 – 192.2	138.7	41	8.1 – 188.6	41.6

2	42	6.7 – 140.5	37.5	43	26.2 – 156.51	59.4
5	41	1.4 – 31.6	17.9	46	3.4 – 231.6	153.8
11	42	0.13 – 311.8	89.6	42	3.0 – 497.3	223.2
13	44	33.1 – 277.3	153.3	40	22.3 – 410.16	198.7

Table 44: SCM Contrast Metric for SSI model results.

<b>SCM Correlation Feature Metric – Number of Outliers – SSI Model</b>				
<b>Region</b>	<b>22-32</b>	<b>30-162</b>	<b>30-193</b>	<b>65-185</b>
4	43	44	44	45
2	41	45	45	45
5	40	41	45	46
11	43	40	42	42
13	45	42	41	43

Table 45: SCM Correlation Metric (number of outliers) for SSI model results.

The results of the SCM Contrast metric once again show that the region that was best characterized by the SSI model was the wheat region. On a few occasions in the above chart, the average value and range of its absolute difference image was lower than both the SBP and TS model corresponding values. For most entries for all of the other test regions, the metric values were typically in between the TS and SBP values for the three later band pairs. The SBP model still shows the best performance in the 22-32 band pair, while the TS and SSI models perform similarly for this band pair. For the later band pairs, the SSI model's metric values begin to drop lower than the corresponding values for the SBP model, but typically do not exceed those of the TS model. Observation of the average value and range of values of the absolute difference image is not sufficient to determine the relative performance, since the average values are quite close, and it does not guarantee that all corresponding pixel entries of the metric images will exhibit the same trend. Therefore, direct comparisons of the absolute difference images were carried out. In general, between

90% – 97% of the values for the SSI model were between the SBP and TS model values for the later three band pairs, indicating that the SSI model performed better overall in the later bands than the SBP model based in its superior spectral performance. However, the SSI model did not perform quite as well as the TS model for most test regions, since as we saw with the SCR metric, its spectral performance was similar but not quite as good, while the spatial structure was typically poorer than that of the TS model. Therefore, the results found with the SCM metric make intuitive sense, and the rankings for the SCM metric are once again suitable to employ as the final overall rankings. The results of the SCM Correlation feature listed above reinforce the validity of this rank ordering. The rankings, including the SSI model are:

- a. FM Model;
- b. MBP Model;
- c. TS Model;
- d. SSI Model; and
- e. SBP Model.

## **6. Conclusions and Recommendations**

The objectives sated at the outset of this report have been achieved in a two-phase process. The first phase consisted of the implementation and/or incorporation of the SBP, MBP, TS, and FM texture characterization models into the DIRSIG environment. Synthetic imagery was then generated using each of these models within DIRSIG for a 3-channel visible region Kodak CitiPix scene, as well as for a 210-spectral band HYDICE ARM hyperspectral image spanning from 0.4 – 2.5 microns. The synthetic texture cubes derived from the SSI texture characterization model were also incorporated into a DIRSIG HYDICE ARM scene. A quantitative comparative performance analysis of each of the texture characterization models then followed as part of the second phase, through the application of a series of four performance metrics. The metrics were designed to assess both the spatial and spectral fidelity, complexity, and variability of synthetic texture

representations for the rendered CitiPix and HYDICE ARM imagery produced using each texture model. The metrics were applied through a very detailed comparison with the corresponding registered real imagery, after which the metric results were compared in order to evaluate how well the texture models performed relative to one another.

It was found that model performance depended upon the nature of the imagery to be rendered, as evidenced by the different rankings obtained for the CitiPix and HYDICE ARM data. Although the spatial and spectral resolutions were not found to be significant, it was the spectral dimensionality of the data that was a crucial factor that governed texture model performance. The rankings are repeated below for convenience.

<b>Small Spectral Dimension</b>	<b>Hyperspectral Imagery</b>
1. FM Model	1. FM Model
2. SBP Model	2. MBP Model
3. MBP Model	3. TS Model
4. TS Model	4. SBP Model

Table 46: Final rankings of texture characterization models based on nature of imagery to be rendered.

The results of the DIRSIG imagery examples shown, as well as the metric results clearly demonstrate the conditions that must be met and the limitations that must be overcome in order to achieve optimal model performance. The SBP and MBP models require accurate and thorough ground truth data in order to realistically capture the spatial and spectral variability of scene material classes. The FM model also requires adequate ground truth measurements, distinct fraction maps, and robust end member selection processes in order to assign single end member spectra to each fraction plane. Further, the FM model requires multi-band image data in order to produce adequate fraction planes, while the MBP model requires the availability of multiple, ideally non-correlated texture map images for optimal performance. These requirements were met in this research, thereby demonstrating that the simple mixing of end member spectra in accordance with their pixel-

by-pixel fractional abundances is able to adequately represent realistic levels of spatial and spectral clutter. Although the TS model did not perform as well as the FM and SBP models in the spatial domain, its spectral texture was extremely well characterized, due simply to the nature of constraint enforcement of the model. The TS model performed worst overall for the CitiPix data, while its performance improved for the HYDICE ARM HSI data, since spectral structure is accordingly more significant for such data sets. Several other reasons for the differential performance results were discussed in the main body of this report.

The relative merits of the performance metrics were also presented. It was found that there was a degree of redundancy between the spatial MF and GLCM metrics, where the latter provides a more rigorous and flexible measurement of texture features. The SCR metric was valuable in terms of its independent analysis of spectral clutter and simplicity, while the SCM metric made use of a new concept in order to simultaneously measure spatial and spectral synthetic texture fidelity. A significant finding is that the rankings produced by the SCM metric coincided with the overall ranking of the models for both the CitiPix and HYDICE ARM data using the other three metrics combined, thereby providing a convenient and effective measure of spatial-spectral texture within one metric. However, it is not recommended that this metric be used alone. A more objective overall ranking can be obtained through the application of weights to each performance metric as carried out in Section 5.5.6.

Supplementary results were also presented to demonstrate the behavior of expanding the spectral coverage of the synthetic image beyond the extents of the input corresponding real image. Although the metrics were not applied to this data, similar trends were apparent. The SSI texture model results were also analyzed. The spatial performance was very similar to that of the TS model for the rendering of the HYDICE ARM scene. The model performed better than the FM, SBP, and MBP models in the spectral domain, although not quite as well as the TS model did for the regions tested. However its overall ranking provided by the consideration of the SCM metric and all four of the metrics combined was

fourth. This is because of the influence of the very good spectral fidelity coupled with its poor spatial performance.

There are several recommended paths for future research efforts in order to augment and/or improve upon the results presented in this work. First, the analysis presented herein has focused solely on the reflective region of the electromagnetic spectrum. It would be interesting to determine how well each of the texture characterization models performs in the thermal region, and to assess whether texture modeling becomes increasingly complex in this regime. Although many of the methods appear to be equally applicable regardless of whether we are working in the reflective or thermal regions, there is always the potential for more challenges when trying to model thermal variability in synthetic imagery.

It has been mentioned several times in this report that a more careful and complex implementation of the TS model could improve the spatial performance of the model, in particular for within- and between-material class transition regions. An alternative method to the reflectance map mode of DIRSIG may be cumbersome, but it can nonetheless be investigated so as to potentially improve the overall spatial-spectral performance of the TS model. The same can be said about the SSI texture model, since it has also been incorporated using the reflectance map mode of DIRSIG texture application. Another possibility with the TS model is that the source code can be modified to accommodate smaller input texture sample sizes. Although this would likely be a very complicated task for the user who is unfamiliar with Tyrrell's code, it is an option for future work. If this is pursued, one must also be careful that the smaller samples do not compromise the integrity of the synthesized texture, since the input sample is required in a large enough dimension so as to provide sufficient statistics for constraint enforcement of the synthesis step. Perhaps a less overwhelming option would be to seek an alternative to the mirroring routine that was used to grow out smaller, non-square input sample texture regions so that the concerns with artifacts appearing in the output DIRSIG image can be eliminated.

The rendering of the CitiPix scene using a simulation of the HYDICE sensor platform (see Section 5.6.1) suggested the acquisition of very thorough and organized

ground truth data in order to allow the TS model to expand its spectral coverage beyond that available in the input sample texture imagery, while maintaining adequate spatial structure. This would require the use of the Spectral Expansion code, and would not be possible using the S/P or Quilting texture synthesis models. If a very methodical and thorough ground truth collection effort is invoked to better capture the spatial structure (e.g, in grid patterns, for example) it could be possible to both extend spectral coverage and improve the spatial aspect of the TS model by reading in reliable ground truth data instead of having to use the actual image. In fact, such a grid-like ground truth collection effort would be beneficial for other models, such as the SBP, MBP, and FM models, for a wide variety of scenes.

The MBP DIRSIG imagery of the CitiPix scene used the Red, Green, and Blue channels as the multiple (3) bandpass regions used for calculating z-scores of the spectral reflectance curves and the corresponding texture maps. As a result, the curve selection process was over-constrained and thus the MBP model showed a slightly worse overall performance than the SBP model, which initially was a counter-intuitive outcome. It would be interesting for this same scene to be simulated using the MBP model, but with only two bandpasses (i.e., the Red and Blue channels only, since they are the least correlated band pair) and compare with the results of the one- and three-texture image bandpass model results.

In order to determine the sensitivity to different end member selection routines and the resultant quality of fraction planes, an interesting study would be to render scenes using the FM model using various end member selection algorithms and unmixing tools. Since the FM model has performed superior to all other models in this work, further improvement of its methodology would be a worthwhile task. Also, as an optimization step to the FM model it would be worthwhile to investigate the effectiveness of the use of the residual error fraction plane produced by the unmixing algorithm being used. This usually takes the form of a RMS error image that could potentially be sampled in some manner and forced into the re-mixed SIG image solution. This additional fraction plane could improve the spatial and

spectral variability significantly as long as there is adequate input multi-band image data available to construct the fractional abundance maps.

It has been shown in this research that the use of the SCM metric offered an effective and convenient simultaneous measure of spatial and spectral texture in synthetic imagery. The SCM concept should be investigated for use in other applications in which GLCM spatial texture analysis is typically performed, such as for classification, segmentation, and texture feature extraction tasks. The SCM tool presents the opportunity to exploit both spatial and spectral properties within an extension of a well-known and proven-effective tool that has been used in numerous applications, and thus it has great potential for future research efforts.

The comparative performance analysis conducted in this work consisted of the combinatorial application of a series of four performance metrics. An additional method of testing the spatial and spectral variability and complexity of background clutter that would have been pursued if time had permitted is through the use of target detection algorithms. For instance, if realistic levels of modeled clutter are present, it will likely take the form of confusion and produce false alarms within the detection results, instead of the usual case in which benign, flat backgrounds tend to make detection algorithms appear as though they are more effective than they would actually be if tested on real imagery. Analysis of ROC curves for corresponding real and synthetic imagery would be another less abstract and practical method of performance analysis than those used in this study. Another improvement that is recommended to the existing metric analysis is to be more consistent with the application of the variance threshold images. The threshold used for the SCR metric was 1-sigma standard deviation, while the acceptable variance threshold images for the MF, GLCM, and SCM metrics used the measure of variance (sigma-squared). Since it was found that this value is not as intuitive as the 1-sigma threshold, it is recommended that a 2-sigma standard deviation would have been more appropriate for the analysis. In that case, the number and percentage of outliers from the threshold would have been a more valuable measure of performance for each texture test region for the MF, GLCM, and SCM metrics. This did

not affect the comparative performance analysis of the texture models significantly since the absolute difference images were directly inspected for each region and the deviation from the threshold proved to be more important than the actual number or percentage of outliers.

Lastly, it is suggested that any alternative texture characterization models that have demonstrated good spatial and spectral variability should also be tested within the DIRSIG environment. If certain advantages are found with such other models, then it is possible to employ one texture model that has shown excellent results for a given material class, while modeling other materials with another texture model that tends to perform well for other types of texture. Such optimized spatial and spectral texture characterization is what is strived for in the production of synthetic imagery, and even if the solution is combinatorial between various algorithms, or even if a new texture model is implemented that possesses the strongest traits of these models, we will be improving our understanding of the underlying processes that create natural image texture and thus we will be better suited in our ability to model such processes.

## 7. References

L. Baraldi and P. Parmiggiani (1995). An Investigation of the Textural Characteristics Associated With Gray Level Cooccurrence Matrix Statistical Parameters, IEEE Transactions on Geoscience and Remote Sensing, Vol. 33, No. 2, March 1995.

M. Becker (1999). *Rhino: Nurbs 3D Modeling*, Robert McNeel and Associates.

M. Berger (1998). Texture Vector Analysis Using Regular Synthetic Texture Patterns, Proceedings of IEEE International Geoscience and Remote Sensing Symposium, IGARSS '98, Vol. 2, pp. 1071 -1075.

J.W. Boardman, F.A. Kruse, R.O. Green (1995). Mapping Target Signatures via Partial Unmixing of AVIRIS Data, Fifth Annual JPL Airborne Earth Science Workshop, Vol. 1, AAVIRIS Workshop, pp. 23-26.

Brodatz Database, <http://www.ux.his.no/~tranden/brodatz>.

P. Brodatz (1966). *Textures – A Photographic Album for Artists and Designers*, New York: Dover.

S.D. Brown (2001). DIRSIG Users' Manual – Release 3.4. Digital Imaging and Remote Sensing Laboratory, RIT.

S.D. Brown & E.J. Tentilucci (2003). Advances in Wide Area Hyperspectral Image Simulation, Proceedings of the SPIE conference on Targets and Backgrounds IX: Characterization and Representation, Vol. 5075, ISBN, April (2003).

C. J. Burtner (2001). Texture Characterization in DIRSIG, Bachelors' Degree Thesis, Rochester Institute of Technology.

J-F. Cardoso (1998). Blind Signal Separation: Statistical Principles, Proceedings of the IEEE, Vol. 86, No. 10, October 1998.

D.A. Clausi and M.E. Jernigan (1998). A Fast Method to Determine Co-Occurrence Texture Features, IEEE Transactions on Geoscience and Remote Sensing, Vol. 36, No. 1, January 1998.

D.A. Clausi & Y. Zhao (2002). Rapid Extraction of Image Texture by Co-Occurrence Using a Hybrid Data Structure, Computers & Geosciences, Vol. 28, pp. 763-774.

G. R. Cross & A. K. Jain (1983). Markov Random Field Texture Models, IEEE-PAMI-5, p. 25-39, January 1983.

J. De Bonet & P. Viola (1998). Texture Recognition Using a Non-Parametric Multi-Scale Statistical Model, IEEE Computer Society Conference on Computer Vision and Pattern Recognition Proceedings, pp. 641 -647.

DIRSIG Homepage. <http://www.cis.rit.edu/~dirsig.html>

DIRS Research: Modular Imaging Spectrometer Instrument (MISI). Center for Imaging Science, RIT. Web page: <http://www.cis.rit.edu/research/dirs/research.misi.html>

D. Dunn, W.E. Higgins, & J. Wakeley (1994). Texture Segmentation Using 2-D Gabor Elementary Functions, IEEE Pattern Analysis and Machine Intelligence, Vol. 16, No. 2.

- A. Efros & W. Freeman (2001). Image Quilting for Texture Synthesis and Transfer, Proceedings of the 28th annual conference on Computer Graphics and Interactive Techniques, 12-17 August 2001, ACM SIGGRAPH, pp. 341-346.
- L. Ganesan and P. Bhattacharyya (1995). A Statistical Design of Experiments Approach for Texture Description, Pattern Recognition, Vol. 28, No. 1, pp. 99-105.
- C. Gotlieb & H. Kreyszig (1990). Texture Descriptors Based on Co-Occurrence Matrices, Computer Vision, Graphics, and Image Processing, Vol. 51, pp. 70-86.
- R.M. Haralick (1973). Textural Features for Image Classification, IEEE Transactions on Systems, Man, and Cybernetics, Vol. SMC-3, pp. 610-621, Nov. 1973.
- M. Hassner & J. Sklansky (1980). The Use of Markov Random Fields as Models of Texture, Computer Graphics and Image Processing, Vol. 12, pp. 357-370.
- M. Hauta-Kasari, J. Parkkinen, T. Jaaskelainen, and R. Lenz (1996). Generalized Co-occurrence Matrix for Multispectral Texture Analysis, Proceedings of the 13<sup>th</sup> International Conference on Pattern Recognition, December 1996, Vol. 2, pp. 785-789.
- M. Hauta-Kasari, J. Parkkinen, T. Jaaskelainen, and R. Lenz (1999). Multispectral Texture Segmentation Based on the Spectral Co-Occurrence Matrix, Pattern Analysis & Applications, Vol. 2, pp. 275-284.
- R.M. Haralick (1979). Statistical and Structural Approaches to Texture, Proceedings of IEEE, Vol. 67, No. 5, May 1979, pp. 786-804.

D. Heeger & J. Bergen (1995). Pyramid-Based texture Analysis/Synthesis, Proceedings of ACM SIGGRAPH, August 1995.

B. Julesz (1962). Visual Pattern Discrimination. IRE Transactions on Information Theory, IT-8, 1962.

J.M. Keller & S. Chen (1989). Texture Description and Segmentation Through Fractal Geometry, Computer Vision, Graphics, and Image Processing, Vol. 45, pp. 150-166.

C.S. Kennedy (2002). The Testing and Assessment of Texturing Tools Used to Build Scenes in DIRSIG, Bachelors' Degree Thesis, Rochester Institute of Technology.

K.I. Laws (1985). Goal-Directed Textures-Image Segmentation, Applications of AI II, SPIE Vol. 548, pp. 19-26.

K. Lee (2002). A Subpixel Scale Target Detection Algorithm for Hyperspectral Imagery, Ph.D. Dissertation, Center for Imaging Science, Rochester Institute of Technology.

Y. Liang, E. Simoncelli, & Z. Lei (2000). Color Channels Decorrelation By ICA Transformation in the Wavelet Domain for Color Texture Analysis and Synthesis, Proceedings of the IEEE Conference on Computer Vision and Pattern Recognition, Vol. 1, pp. 606-611.

G. Lohmann (1995). Analysis and Synthesis of textures: A Co-Occurrence-Based Approach, Computers & Graphics, Vol. 19, No. 1, pp. 29-36.

S.Y. Lu & K.S. Fu (1978). A Syntactic Approach to Texture Analysis, Computer Graphics and Image Processing, Vol. 7, pp. 303-330.

R. Manduchi & J. Portilla (1999). Independent Component Analysis of Textures, Proceedings of the Seventh IEEE International Conference on Computer Vision, Vol. 2 , pp. 1054 -1060.

D. Manolakis, G. Shaw, & N. Keshava (2000). Comparative Analysis of Hyperspectral Adaptive Matched Filter Detectors, Algorithms for Multispectral and Hyperspectral Imagery VI, S.S. Chen and M.R. Descour eds., Vol. 4049, pp. 2-17, SPIE Orlando, FL, April 2000.

MTL Systems, Incorporated (1997). Atmospheric Compensation Investigation – ARM Site – Ground Truth Collection Report MTR-97-011. Submitted to Lockheed-Martin Missiles & Space Co., Inc., August 1997.

J. Portilla, R. Navarro, O. Nestares, and A. Taberbero (1996). Texture Synthesis-by-Analysis Based on a Multiscale Early-Vision Model, Optical Engineering, Vol. 35, No. 8.

W.I. Rosenblum, C. Salvaggio, J.R. Schott (1990). Selection of Optimal Textural Features for Maximum Likelihood Image Classification, RIT/DIRS Report #89/90-66-131, January 1990. Prepared for the United States Department of Energy.

J.R. Schott (1997). *Remote Sensing: The Image Chain Approach*. Oxford University Press, Inc., Oxford, New York.

J.R. Schott, C.N. Salvaggio, S.D. Brown, R.A. Rose (1995). Incorporation of Texture in Multispectral Synthetic Image Generation Tools, Presented at the SPIE Aerosense, Targets and Backgrounds: Characterization and Representation, Vol. 2469, No. 23, Orlando, FL.

- J.R. Schott, S.D. Brown (1998). Incorporation of Enhanced Texture/Transition Modeling Tools Into a Synthetic Image Generation Model, Proceedings of the International Geoscience and Remote Sensing Symposium (IGARSS '98), Vol. 3 pp. 1508 -1511.
- E. Simoncelli and J. Portilla (1998). Texture Characterization via Joint Statistics of Wavelet Coefficient Magnitudes, Fifth IEEE International Conference on Image Processing, Chicago, October 4-7, Vol. 1, IEEE Computer Society.
- A.D. Stocker, I.S. Reed, & X. Yu (1990). Multi-Dimensional Signal Processing for Electro-Optical Target Detection, Signal and Data Processing of Small Targets, SPIE Vol. 1305 pp. 218-231.
- W.D. Stromberg & T.G Farr (1986). A Fourier-Based Textural Feature Extraction Procedure, IEEE Transactions on Geoscience and Remote Sensing, Vol. GE-24, No. 5, pp. 722-731.
- R. Sundberg, J. Gruninger, & R. Haren (2002). Extraction of Hyperspectral Scene Statistics and Scene Realization, Proceedings of the SPIE, Vol. 4725, No. 25.
- A. Teuner O. Pichler, and B.J. Hosticka (1995). Unsupervised Texture Segmentation of Images Using Tuned Matched Gabor Filters, IEEE transactions on Image Processing, Vol. 4, No. 6.
- A. Tyrrell (2002). Multi/Hyperspectral Texture Synthesis, Masters' Degree Thesis, Rochester Institute of Technology, Rochester, NY, USA.
- G. Van de Wouwer et al. (1999). Statistical texture Characterization from Discrete Wavelet Representations, IEEE Transactions on Image Processing, Vol. 8, No. 4, April 1999.

VisTex Database. <http://www.white.media.mit.edu/vismod/imagery/VisionTexture/vistex.html>.

L. Wang and D. He (1990). A New Statistical Approach for Texture Analysis, Photogrammetric Engineering and Remote Sensing, Vol. 56, No. 1, January 1990, pp. 61-66.

Webster's Dictionary (1986). Allan Publishers, New York, USA.

K. Wikantika et al. (2000). An Investigation of Textural Characteristics Associated With Spectral Information for Land Use Classification, Proceedings of International Geoscience and Remote Sensing Symposium (IGARSS) 2000, Vol. 7, pp. 2915-2917.

M.E. Winter (1999). N-FINDR: An Algorithm for Fast Autonomous Spectral End Member Determination in Hyperspectral Data, Proceedings of the SPIE, Vol. 3753, pp. 266-675.

A. Witkin & M. Kass (1991). Reaction-Diffusion Textures, Proceedings SIGGRAPH July 1991, in Computer Graphics, T.W. Sederberg, ed., Vol. 25, pp. 299-308.

S. Yang & C. Hung (2002). Texture Classification in Remotely sensed Images, Proceedings of the IEEE Southeast Conference 2002, pp. 62-66.

S. Zucker & D. Terzopoulos (1980). Finding Structure in Co-Occurrence Matrices for Texture Analysis, Computer Graphics and Image Processing, Vol. 12, pp. 286-308.

